Ravinder S. Dahiya
Maurizio Valle

Robotic Tactile Sensing

Technologies and System

Springer

Robotic Tactile Sensing

Ravinder S. Dahiya • Maurizio Valle

Robotic Tactile Sensing

Technologies and System

Springer

Ravinder S. Dahiya
Istituto Italiano di Tecnologia (IIT)
Genova, Italy
and
Present address:
Center for Materials and Microsystems
Fondazione Bruno Kessler
Trento, Italy

Maurizio Valle
Department of Biophysical & Electronic Engineering
University of Genova
Genova, Italy

ISBN 978-94-007-0578-4 ISBN 978-94-007-0579-1 (eBook)
DOI 10.1007/978-94-007-0579-1
Springer Dordrecht Heidelberg New York London

Library of Congress Control Number: 2012943859

To my Teachers, Friends, and Family
To Beatrice, Margherita, Benedetta and to my parents

Foreword

Human intelligence is a multi-technological achievement. The way we move, perceive and learn depends just as much on the physical structure, texture and shape of our muscles and bones as it does on our "mind".

If we want to understand and, to some extent, replicate human intelligence we need to understand the technological solutions supporting the biological functions and discover the technologies which allow such functions to be implemented artificially. Interesting results and technologies have been produced by "merely" concentrating on technologies of the mind (e.g. reasoning, learning, recognition, etc.) and by inventing new materials and devices mimicking natural solutions; however—at least so far—efforts have been disjointed and, consequently, the development of 'intelligent systems' is, to some extent, still un-chartered territory.

After many years in this field, I still firmly believe that the way ahead lies in multidisciplinary team-work: on one side, scientists, analyze the multi-technological bases of human intelligence and cognition and, on the other, they synthesize artificial systems as "living" proof-of-concept. The challenge lies in reproducing the functions rather than the shape while accepting the fact that the shape (morphology), at the micro and macro levels, affects the functions.

What humans do is inescapably shaped by the body; in order to understand human intelligence and implement intelligent artifacts, it is necessary to consider systems with some degree of anthropomorphism—with the proviso, that I see anthropomorphism as a starting point not as a goal.

This book is a good example of such approach applied to the sense of touch. Touch, among senses used by humans to support and develop intelligent behavior, is the sense that puts us "in touch" with the world, is the sense guiding the safe interaction with the objects and with others, is the source of sensations that guides us in learning to reach a goal. In spite of its fundamental contribution to learning and executing intelligent behaviors in humans the technology available to provide artificial systems with the sense of touch is still very far from the accuracy, robustness and softness found in natural system. The main reason being the fact that a good touch sensor must exhibit much diversified processing abilities embedded in a soft substrate. The sensor of a TV camera does not enter into physical contact with

the world and, as such, its substrate could be rigid and planar. On the contrary tactile sensing measures the parameters related to physical contact with world (spatial position, roughness, stress, temperature, slippage, shape etc.) and, as such, must be mediated by a soft, compliant substrate. It is the combination of measuring features and soft substrates that represents, with respect to current technologies, the main challenge to realizing tactile sensors.

This book is an excellent example of how current knowledge about human sensory systems can be investigated and exploited to provide suggestions on how to build artificial sensors. Every chapter abounds with the enthusiasm of the authors. The investigation, from an engineering perspective, of the multifaceted components of human "sense of touch" will help readers to understand that touch provides a much richer set of sensations than it is usually thought and that tactile perception is based as much in the processing capabilities as it is on the supporting material (a good tactile sensor embedded in a rigid substrate is bound to fail). Next to the bases of human touch, this book presents and discusses for first time an exhaustive set of system issues (related to tasks, mechanical and electrical hardware, and software) which should be considered while developing robotic tactile sensing system. The discussion on system issues is followed by an up-to-date state of the art of the technologies that have been proposed to implement artificial tactile sensors including, the materials and the methods for miniaturized sensors. The "material" properties of "artificial skin" that are flexible, conformable and stretchable and, as such, suitable to cover large areas of artificial systems, are critically discussed. After a very exhaustive, critically discussed and up-to-date state of the art, the realization of a high resolution tactile sensor is presented based on a POSFET device. This part of the book is a very good example of how available technology can be engineered into an effective device by merging smart material properties and microelectronics. Many interesting historical details and an abundance of colorful illustrations have been provided.

The book is a very good example of how a mix of multidisciplinary knowledge coming from neuroscience, robotics and microelectronics, can form the basis of a sound engineering process and how this process can produce a state-of-the-art device. It is also a unique tribute to the many scientists who were involved in understanding and developing artificial tactile sensing systems. I think that the authors can be confident that there will be readers who will have gained a broader perspective of the disciplines of robotic tactile sensing as a result of their efforts. The book is destined to play a major role in exciting, motivating, and educating the next generation of researchers in the area of sensors and robotics, from all over the world.

Italian Institute of Technology Giulio Sandini
Robotics, Brain and Cognitive Sciences
Genoa, Italy

Foreword

Robotics has undergone major transformations in scope and dimension. From a largely industrial focus, it has rapidly expanded into the challenging dynamics of the human world—owing to the maturation of the field and the advances in technology. Nonetheless, new challenges are to be overcome to make the transition to robots that share the space with humans, which safely interact with them, providing services in manufacturing, entertainment, education, healthcare and assistance.

One major challenge is the physical interaction of robots with real world objects, which requires handling of environmental uncertainties. The sensory data from multiple sense modalities such as vision, touch, and audio is needed and, in this context, the sense of touch is particularly important as it enables body awareness—the presence and occupancy of space. Unlike other senses (e.g. vision, audio), touch is distributed (not centralized), involves complex physical interaction, and plays a fundamental role in estimating contact properties such as shape, texture, hardness, material type and many more. From historical perspective, the 'sense of touch' has been a component of robotics for roughly as long as artificial vision and auditory sense modalities. Yet, as important as sense of touch has been, the present day robotics largely misses this sensory modality. Among others, the distributed nature of touch sensing and large number of sensors needed to cover the robot's body and associated practical issues like large number of wires to connect the sensing elements, have been attributed as the reasons for the slow development of touch. Above all, a system approach has been missing. This is precisely what makes this book so interesting. This book presents a unique in-depth discussion on the very issues that have been hurting the development of tactile sensing systems and their effective usage in robotics. Every chapter is filled with the enthusiasm of the authors.

In the first part, the book begins by providing suggestions on how to build artificial sensors based on our current knowledge about human sensory systems. The human sensory system is a sound example as it flawlessly exploits various sensory modalities toward achieving system goals. The articulated engineering perspective of the multifaceted components of human "sense of touch" will help readers to understand that tactile perception is based as much in the processing capabilities as it is on the supporting hardware such as tactile sensors. The book presents an exhaus-

tive set of system issues (related to tasks, mechanical and electrical hardware, and software) which should be considered while developing robotic tactile sensing system. An up-to-date state of the art of the tactile sensor technologies, including the materials and the methods for miniaturized sensors as well as those suitable for large area coverage, has been presented. The second part of the book presents the research toward novel high resolution POSFET tactile sensing device and chips. This part of the book presents how the marriage of transducers (piezoelectric polymer) and electronic devices (MOS transistor) can be exploited to obtain improved tactile sensing technology. The authors finally conclude this part by discussing future extensions toward tactile sensing system on chip and the mechanically flexible POSFET like chips, able to bend around and conform to e.g. the fingertips of robots. The intellectual fascination of robotic tactile sensing, its depth and breadth, and its importance as core interaction technology, is conveyed in an intriguing and visually appealing way. I believe this book will become a cornerstone of tactile sensing research and education.

Italian Institute of Technology Giorgio Metta
Genoa, Italy

Preface

Future robots will be expected to work closely and interact safely with humans as well as the environment. Among various sensing modalities needed to perceive and react to the events of the real world, the sense of touch is particularly important as it enables awareness of the body and differentiating "me" from "not me". Unlike other senses (e.g. vision, audio), it involves complex physical interaction, and plays a fundamental role in estimating contact properties such as shape, texture, hardness, material type and many more. The sense of touch provides action related information, such as slip, and helps in carrying out actions, such as rolling an object between fingers without dropping it. Touch sense modality also helps in understanding the rich interaction behaviors of real world objects—which depend on their weight and stiffness; on how their surface feels when touched; how they deform on contact and how they move when pushed.

From historical perspective, the robotics community has emphasized the need for touch/tactile sensing in robots for a long time and 'sense of touch' has been a component of robotics for roughly as long as artificial vision and auditory sense modalities. Touch sensing began to develop in the 1970s—albeit at a slower pace, when compared with the development of other sensory modalities. The extent to which the 'sense of touch' was utilized largely remained restricted to joint force/torques or simply 'intrinsic touch sensing'—which can probably be attributed to the focus largely on the industrial robotics during the initial era of automation. Both, from safety and operational point of view, intrinsic touch and vision are considered to be more convenient and suitable for an industrial set up. For this reason, until the end of last decade, research on sensors and sensors based robotics was biased toward using vision and intrinsic touch sensing. This is evident from large number of articles, published in various robotic related journals and conferences, where vision and joint force/torque sensors have been employed in various robotic tasks. The first special issue on 'sense of touch' in robotics, published by IEEE Transactions on Robotics (TRO) appeared only in 2011.

As far as tactile sensing (or extrinsic sensing) in robotics is concerned, early surveys show that a wide diversity in the types of tactile sensing devices emerged in the 1980s. Early works on tactile sensing focused on the creation of sensor devices

using new transduction techniques and a large number of experimental devices and prototypes were built and reported in the literature. Particular attention was given to the development of tactile sensing arrays for object recognition. The creation of multifingered robotic hands during 1980s increased the interest in tactile sensing for robotic manipulation and thus started appearing the works utilizing tactile sensing in real-time control of manipulation. The new applications demand features such as mechanical flexibility and conformability and accordingly new designs and materials for tactile sensing started receiving attention. While the development of tactile sensors for robotic fingertips and hands continued, the application areas such as motion planning in unstructured environment brought whole body sensing to the fore. As a result, many sensitive skin design projects were undertaken in the late 1980s and 1990s. Over a period of time, robotics itself has undergone paradigm shift. In addition to the manipulation and exploration tasks, the new generation robots are also expected to interact safely. As a result, there is an increased interest in developing large area or whole body tactile sensing structures that allow a robot to carry out a task while maintaining physical contact. The discussion on 'sense of touch' in robots is now not restricted to the sensing hardware and related issues only. The whole body skin concept in robotics has also brought up challenging issues related to data handling, data representation, effective utilization of the tactile data and overall system integration. This book presents many such issues and discusses them with an aim to push forward the research toward "effective" utilization of tactile sensing in robotics.

This book contains eight chapters, divided into two parts: Part I and Part II. Part I (Chaps. 1–5) explains the WHY, WHERE, WHAT and HOW components of tactile sensing and summarizes the current knowledge about the sense of touch. We begin with a discussion on the role and importance of tactile sensing (in humans and robots). Various terms associated with the sense of touch are then defined to present a clear picture about the scope of this book within 'sense of touch'. Then we discuss more on human touch sensing, the ability of humans to perceive the world through sense of touch, and how human touch sensing can be a reference for the robotic tactile sensing. We then explore the expectations and requirements of a robotic tactile sensing system, considering issues related to task, electronics, mechanics and engineering, with an aim to understand how tactile sensing can be made an effective component of robotic devices. In the last chapter of Part I, we present a detailed discussion on the state of the art in the field of tactile sensing. The various chapters have been selected to provide insight into the mechanisms and issues that underlie the development of effective tactile sensing system. The first part therefore contains most of the general information that a reader would like to know about tactile sensing in robotics and also the issues that one would face while trying to make tactile sensing an effective component of robots. Part II (Chaps. 6–8) of the book is about integrated tactile sensing systems on silicon chip. In particular, various stages of development of POSFET (Piezoelectric Oxide Semiconductor Field Effect Transistor) devices based tactile sensing chips are presented in these three chapters. Part II of this book presents the research that Dr. Ravinder S. Dahiya conducted during his doctoral studies at the University of Genova and Italian Institute of Technology,

Genova, Italy. The fabrication of tactile sensing chips and further extensions in this directions have been carried out at Fondazione Bruno Kessler (FBK), Trento, Italy. The chapter-wise detailed information is given in following paragraphs.

Chapter 1 provides an answer to the questions—'WHY' and 'WHERE' the tactile sensing is needed. The role and importance of tactile sensing, first in humans and then in robotics, is explained with a number of examples. Some new application areas (e.g. biomedical, human–robot interaction, rehabilitation, and prosthetics etc.) where tactile sensing plays key role are also presented.

Often, robotic tactile sensing has been associated with detection and measurement of (only) forces in a predetermined area, which is only partly true. A real world interaction involves contact parameters which can be a mechanical stimulation (force, stress, roughness etc.) or other parameters like temperature, hardness, moistness etc. Thus, Chap. 2 attempts to answer the 'WHAT' component of tactile sensing by defining various terms related to 'sense of touch'. First, the terms related to 'sense of touch' in humans, and then analogous terms for robotic tactile sensing are presented. Finally, a classification of robotic tactile sensors, on the basis of transduction method, task to be done, location of sensors on robot's body and their mechanical/physical nature, has been presented.

A large number of studies on human touch sensory modality have addressed many problems that are challenging to roboticists as well. In this sense scientific studies on human sense of touch can throw some light on the development of a tactile sensing system that can be effectively integrated and used in various robotic tasks. With this aim, a discussion on the physiology of human 'sense of touch' its role and perceptual importance in humans, supported by a number of studies, are presented in Chap. 3. Based on these studies, various design hints for robotic tactile sensing are derived.

The overall performance of any system is dictated not only by the isolated quality of the individual components, but also by how these components integrate to achieve the goal. With this aim, Chap. 4 provides an in-depth discussion on the development of robotic tactile sensing system, keeping in view the application and system related expectations and requirements. The application requirements such as measurement of a specific contact parameter, the hardware (electrical/mechanical) requirement such as compatibility of new sensor with existing hardware, physical requirements such as conformability, and practical requirements such as cost-effectiveness etc., all together place many constraints on the development of a tactile sensing system. The design of tactile sensors and finally their integration of the robot, are a result of many trade-offs. For the first time, this book presents a discussion on such requirements and expectations and, wherever possible, alternative solutions are suggested. The effective integration of such sensors and structures on various robotic platforms will allow researchers to develop new cognitive algorithms involving touch information from large areas. In addition to robotics, such structures will also help to understand human interaction with the environment. Chapter 4, together with Chap. 5, provides an answer to the question—'HOW' robotic tactile sensing should be developed or has been developed? The discussion in this chapter can serve as a reference for the design of tactile sensing systems.

Chapter 5 provides a state of the art of robotic tactile sensing including, the tactile sensor technologies, the materials and the methods, for miniaturized sensors and schemes for large area skin like coverage. The discussion in this chapter is supported with selected examples of tactile sensors/sensing arrays reported in literature. Relative advantages and disadvantages of various methods and the recent trend for developing tactile sensing system are presented. Touch sensing structures such as electronic skin, that are flexible, conformable, stretchable and thus suitable for covering large body parts of robots, are being increasingly investigated nowadays. A critical evaluation of various tactile sensors or sensing arrays is presented, keeping in view the tactile sensing system and associated issues, presented in Chap. 4.

Chapter 6 presents the first phase of the development of tactile sensing chip and the experimental characterization of these tactile sensing chips. In the first phase, 32 elements MEA, epoxy-adhered with thin piezoelectric polymer films, are developed as tactile sensing arrays. Design aspects like spatial resolution, capability of recording dynamic contact events, multifunctionality etc. of these tactile sensing arrays are inspired from discussion presented in Chaps. 3 and 4. The development of MEA based tactile sensor arrays provides a feasibility study for the POSFET (Piezoelectric Oxide Semiconductor Field Effect Transistor) based tactile sensing chips presented in Chaps. 7 and 8.

Chapters 7 and 8 present high performance and high resolution POSFET devices based tactile sensing chips. The tactile sensing arrays and chips presented in Chaps. 6–8 have been fabricated at FBK, Trento, Italy. The novel aspect of a POSFET device is that it presents an integral sensor unit comprising of transducer (i.e. piezoelectric polymer) and the first electronic unit (i.e. transistor): in this way, the sensor and conditioning electronics are brought closer and hence the overall response is better than that of conventional approach, in which, the sensor and conditioning electronics are placed at a distance. The 'integral sensor unit' thus conforms very well with the 'Sense and Process at same place' concept, presented in Chap. 4. The POSFET based tactile sensing chips, presented in simplest form, can be easily extended to accommodate interface and local processing circuitry. In fact, such advances have been presented in Chap. 8, where CMOS implementation of POSFET chip (having sensors and conditioning electronics on chip) has also been discussed. Design aspects like spatial resolution, capability of recording dynamic contact events, multifunctionality etc. of these tactile sensing chips are inspired from discussion presented in Chaps. 3 and 4. The 5×5 and 4×4 POSFET devices based tactile sensing chips, presented in Chap. 8, have high density, good spatial resolution and a linear response over a large range of dynamic forces. The capability of tactile sensing chips to detect dynamic stimulus (varying, both in space and time) is demonstrated. In addition to the high performance, a tactile sensing solution must also possess properties such as mechanical flexibility. The current research on mechanically flexible POSFET tactile sensing chips is presented at the end of Chap. 8.

"Smart materials" like piezoelectric polymers (e.g. PVDF-TrFE) are of interest as transducers in rapidly expanding range of applications. They are capable of sensing dynamic forces and temperature. They are key components of the tactile sensing chips presented in Part II. The basic theory behind their use as sensors and actuators is given in Appendix A. It is valuable to use some form of theoretical model

to assess, the performance of a transducer; the effects of design changes; constructional flaws and electronics modifications etc. Instead of evaluating the transducer and conditioning electronics independently, it is advantageous to develop and implement the theoretical model of transducer in such a way that overall sensor (i.e. transducer + conditioning electronics) performance can be optimized. To this end, the electrical model of piezoelectric polymers and its implementation in SPICE are presented in Appendix B. The model can be used to evaluate the performance of polymers over a wide range of frequencies and same is true for the POSFET tactile sensing devices presented in Chaps. 7 and 8. Using the SPICE model, a discussion on various design issues associated with polymers, is also presented. Finally, the design of charge and voltage amplifiers, used to measure the piezoelectric polymer response, is described in Appendix C.

With its multidisciplinary scope, this book is suitable for graduate students and researchers coming from diverse areas such as robotics, material science, humans sense of touch, electronics, microsystems, and instrumentation. To better explain the concepts the text is supported by large number of figures. The technological trends and other applications of tactile sensing are presented in the book. We hope that this book will provide a valuable resource to students encountering this subject for the first time, as well as to the experts who have contributed so much to our understanding of the robotic sense of touch.

Lastly, we would like to thank all the colleagues whom we worked with in making this book a reality.

Ravinder expresses gratitude to his Ph.D. supervisors Prof. Maurizio Valle (also co-author of this book), Prof. Giulio Sandini and Prof. Giorgio Metta, who have strongly supported this endeavor right from beginning. Ravinder looks forward to their continuous support in his future endeavors also.

Ravinder is very grateful to his wife Reena and son Shreyan, for their great support. Reena also helped in drawing some of the figures presented in this book. Ravinder is also thankful to his family and friends for their unequivocal support throughout and for which mere expression of thanks likewise does not suffice.

Maurizio is deeply indebted to Ravinder S. Dahiya for proposing novel approaches and ideas, which have fueled most of his research group's major achievements. He started to work in the fascinating area of robotic tactile sensing with the supervision of the Ph.D. activity of Ravinder some years ago. He appreciates a lot Ravinder's genuine attitude toward scientific research and his very valuable skills. Maurizio is very grateful to Ravinder for the fruitful and exciting discussions on scientific issues such as robotic tactile sensing and many others.

We are thankful to Dr. Leandro Lorenzelli, head of the Bio-MEMS group at FBK, for his support and commitment to the work presented in this book—especially the work presented in Part II. We thank him for his continuous support, friendly advice, generously sharing the ideas and expertise on fabrication technology and much more. Our gratitude also goes to all members of Bio-MEMS group at FBK for their support in realizing the POSFET related work. Likewise, we acknowledge the help received from the members of RBCS, Italian Institute of Technology, Genova and DIBE, University of Genova, Italy. We are thankful to Andrea Adami, Lucia Seminara and Luigi Pinna for helping us in proof reading. We also acknowledge the

contributions of graduate students, doctoral students, and collaborators who contributed in shaping up the ideas. We are also grateful to Italian Institute of Technology, Fondazione Bruno Kessler and University of Genova for providing support of the project. Finally, we thank many colleagues in the scientific community for contributing to the field of robotic tactile sensing and making it exciting and challenging.

Trento/Genova, Italy

Ravinder S. Dahiya
Maurizio Valle

Contents

Part I
Technologies and System

This part of the book comprises of five chapters (Chaps. 1–5) and explains the WHY, WHERE, WHAT and HOW components of tactile sensing and summarizes the current knowledge about the sense of touch. This part begins with a discussion on the role and importance of tactile sensing (in humans and robots). Various terms associated with the sense of touch are then defined to present a clear picture about the scope of this book within 'sense of touch'. This is followed by more discussion on human touch sensing, the ability of humans to perceive the world through sense of touch, and how human touch sensing can be a reference for the robotic tactile sensing. The expectations and requirements of a robotic tactile sensing system are then explored, considering issues related to task, electronics, mechanics and engineering etc., with an aim to understand how tactile sensing can be made an effective component of robotic devices. In the last chapter of this part, a detailed discussion is presented on the state of the art in the field of tactile sensing. The various chapters have been selected to provide insight into the mechanisms and issues that underlie the development of effective tactile sensing system. The first part therefore contains most of the general information that a reader would like to know about tactile sensing in robotics and also the issues that one would face while trying to make tactile sensing an effective component of robots. It is hoped that this part of the book will provide a valuable resource to students encountering this subject for the first time, as well as to the experts who have contributed so much to our understanding of the robotic sense of touch.

Chapter 1
Touch Sensing—Why and Where?

Abstract Sensory information from several sensory modalities (e.g. touch, vision, hearing etc.) is needed to interact and perceive the environment. The sensory modality discussed in this book is the 'sense of touch'—more specifically the 'tactile sensing'. The touch sensing is different from sensory modalities such as vision, and hearing, as it is distributed over the body and involves physical contacts with the objects. This chapter present few examples that highlight the importance of the 'sense of touch' and the impact its 'effective' introduction will have on the overall robotics research.

Keywords Touch sensing · Tactile sensing · Manipulation · Grasping · Biomedical · Safe interaction · Perception · Human robot interaction · Rehabilitation · Prosthetics

1.1 Introduction

Rapid technological advances and increasing expectations from machines have changed the face of Robotics. The concept of a robot as an industrial tool operating in no-humans zone (yet controlled by humans) is fading, and new generation robots such as humanoids, bio-robots, social robots, assisting and medical robots etc. are making way in to our lives. As humanoids they simulate the human structure and behavior; as bio-robots they help gain insight into working of biological systems; as social robots they allow human–robot interaction; as exoskeletons and artificial limbs they assist humans; and as medical robots they help carry out surgical interventions more accurately and less invasively. These robots will learn autonomously; interact safely (causing no harm to themselves or to the objects with which they interact); possess qualities like self maintenance, and more. Attaining these features would have been relatively easier if a complete model of the environment was available, and if the robot actuators could execute motion commands perfectly relative to this model. Unfortunately, a complete world model is not available in most cases of interest and robots have to plan and successfully execute the tasks in presence of environmental uncertainties—which makes sensing an important component of new generation robotics. For this reason, today's new generation robots are equipped

R.S. Dahiya, M. Valle, *Robotic Tactile Sensing*,
DOI 10.1007/978-94-007-0579-1_1,

with more and more sensing components and consequently they are (to some extent) able to deal with high complexity and dynamics of real world.

The sensors based robotics came up when the traditional motion strategies proved to be insufficient in reducing the uncertainties in relative locations of objects. As an example, if a robot is to place a book on a table, then moving the book within a reasonable height above the table and then simply dropping it was a motion strategy. Though simple and faster, the outcome of such strategies is, however, erroneous due to unavoidable control and model errors. The insufficiency of such strategies for ever changing robotics paved way to the sensor-based strategies. Sensors provide information about the state of the environment and the state of the robotic system, which act as a basis for control, decision making, and interaction with other agents/objects in the environment. Sensors are therefore the important means of compensating for the incomplete information.

In general, sensory information from several sensory modalities (e.g. touch, vision, hearing etc.) is needed to interact and perceive the environment. The information could come from single sensory modality or simultaneously from multiple sensory modalities to obtain a robust percept. This is to say that multiple sensory modalities may interact, calibrate or combine with each other in optimal ways to obtain a robust percept—as in humans [1]. As an example, force, visual and tactile feedback have been proposed to open a sliding door [2]. The sensory modality discussed in this book is the 'sense of touch'—more specifically the 'tactile sensing'. For the general discussion presented in this chapter, these term carry same meaning. However, distinction is made starting from the next chapter, where the terms have been defined. The touch sensing is different from sensory modalities such as vision, and hearing, as it is distributed over the body and involves physical contacts with the objects. This chapter present few examples that highlight the importance of the 'sense of touch' and the impact its 'effective' introduction will have on the overall robotics research.

1.2 Touch Sensing—Why?

1.2.1 Touch Sensing in Humans

Touch means contact between our body and another person, object, plant, or animal. What happens if we have all sensory modalities other than the 'sense of touch'? Can we still touch and handle the objects the way we normally do? To find out the answer, and to get a glimpse of the importance of 'sense of touch', one may perform a simple experiment of exploring the objects after putting hands on an ice block for a while. In one such experiment, presented in [3], the skin on volunteers' hand was anesthetized, making the hand numb and ensuring that the mechanoreceptors[1] activity was no longer available to the brain. It was observed that even though volunteers'

[1]Mechanoreceptors are the specialized nerve endings that respond to mechanical stimulation. For details, refer to Chap. 3.

could see what they were doing, they could no longer maintain a stable grasp of objects. The movements become inaccurate and unstable when 'sense of touch' is lost. In another, rather unusual, experiment performed on astronauts in the International Space Station (ISS), the vibrotactile cues provided via 'sense of touch' were found to be highly indicative of the direction and spatial disorientation [4]. In daily life, our brain determines up and down orientation by integrating the cues from visual, vestibular and proprioceptive senses and our body reference frame or the idiotropic vector. But, in microgravity environment such as that of ISS, astronauts need to adjust the integration of these orientation cues. In this experiment in microgravity—that has no real life equivalent, the capability of orienting oneself with cues from 'sense of touch' was found to be much better than that from visual cues. A daily life example underlining the importance of touch sensing is the presence of 'Do Not Touch' signboards in museums. The presence of such signboards point towards the fact that humans', especially children, do not just rely on 'vision' while interacting with environment and they tend to explore by touching. The importance of tactile sensing is seen in the damage that patients with peripheral neuropathy accidentally do to themselves.

A well-documented example of loss of sense of touch described by Cole [5] is that of Mr. Ian Waterman, who suffered loss of most of his touch sensation (all kinesthetic capabilities and most cutaneous sensations except temperature and pain sensation) below the neck due to rare neurological illness. Immediately after the loss of touch sensation, Mr. Waterman fell on the floor in a heap and could not walk or stand upright. He could move his limbs, but could not control them in a precise way. He could not tell the position of his limbs or whether they were moving, without looking at them. When not looking at them, his fingers and, particularly, his arms would move uncontrollably and sometimes they would unwittingly hit him. When lying in bed, he could not feel his body or the bed itself. Contact deforms the skin in ways that convey information to the brain about the identity of external entities; their size, shape, compliance, texture, and temperature. But, in case of Mr. Waterman all this is not possible, as he can not feel objects properties, such as shape or texture, by haptically exploring them. To a large extent, he can not use force-feedback information about the environment to control his body or perceive the world. The loss of touch sensation thus gave Mr. Waterman the terrifying sensation of floating. The sense of touch is therefore unique in that it is not merely receptive, but it is crucial for guiding motor behavior. We interact with the environment to acquire tactile information, and use that knowledge to modify the world.

1.2.2 Touch Sensing in Robots

What a robot can or can not do without 'sense of touch' can be gauged from many of the difficulties that humans could face in its absence. The interaction behaviors of real world objects can be better understood when robots physically interact with them—as humans do. Considering humanoid robots, for instance, the 'sense of

touch' will help them in knowing the interaction behaviors of real world objects—which depends on weight and stiffness of the object; on how their surfaces feel when touched; how they deform on contact and how they move when pushed etc. In biomedical robotics, the tactile and force feedbacks together may improve the lump (or hard tissue) detection capability of robots during a minimal invasive surgery (MIS). Similarly, in human–robot interaction, the tactile sensing is required for safe interaction, and for teaching the robots. Certain properties of objects like mechanical compliance can be realized only through touch. Touch information is needed to measure material properties such as hardness [6], temperature [7], etc. Without adequate touch feedback, achieving normal tasks that require high levels of dexterity is extremely difficult, if not impossible. From above it is clear that touch sensing is critical at many different levels, from controlling the body to perceiving the environment, as well as learning about and interacting with it. All these strongly argue for the importance of providing adequate touch sensory information when using robots to interact with real environments. Therefore, robotic platforms with integrated (skin-like) touch sensing capability are of large interest.

The 'sense of touch' is an essential modality that allows us to assess the contact parameters such as shape, surface texture, stiffness, and temperature etc. It helps in developing awareness of the body, enables differentiating "me" from "not me", and helps us roll an object between fingers without dropping. The information obtained via 'sense of touch' is used in reflexes and automatic responses (e.g., grasp force regulation) without expending cognitive effort. In daily life we use tactile sensor to feel objects, to measure comfort of shoes through touch receptors in foot, and many more where sensory modalities like vision would be of little help. The tasks mediated via 'sense of touch' can be grouped under three categories: manipulation (perception for action), exploration (action for perception) and Reaction or Haptics [8]. It may be noted that all these tasks are dynamic in nature where relative movement of sensors is involved. Some of the tasks under these categories are shown in Fig. 1.1 and discussed in following paragraphs.

Grasping is essential skill for a general purpose robot, working in an industrial or home-like environment. It is a manipulation task where touch data is used as a control parameter or for grasp stability. Using tactile sensors to maximize the contact surface for removing a book from a bookshelf is an example where tactile sensing is used for closed loop control [9]. Similarly, the touch sensing can enable prevention of slippage while holding an object, thus helping in attaining stable grasp. The information of interest during grasping typically includes contact point estimation, surface normal and curvature measurement, pose, shape, weight, slip detection and/or material properties [10, 11]. Many times the environment is unstructured which makes it difficult to estimate the parameters of interest and hence poses challenge for the traditional approaches in obtaining stable grasp. For instance, vision sensory modality has traditionally been employed to determine the touch information such as shape and pose of an object. However, the accuracy of vision is limited and small errors in object pose are common even for known objects and even small errors can cause failures in grasping. The uncertainties such as those arising out of the softness or deformability of an object also lead to grasp failures, as most of

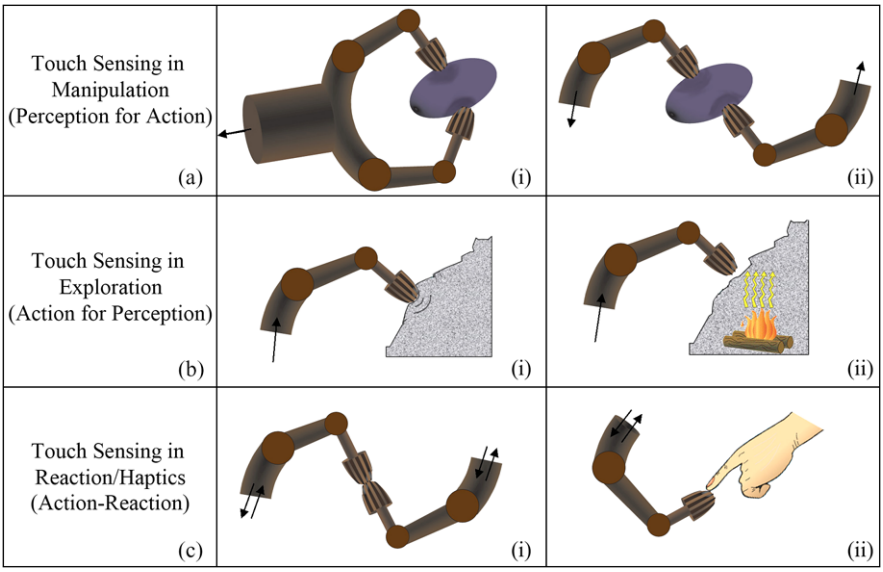

Fig. 1.1 The three principle robotic tasks where tactile sensing is used (adapted with permission from [8], Springer Science+Business Media). (**a**) Manipulation of objects by a robot or by multiple robots. The perception of object leads to the action by the robot. The action related information is unidirectional i.e. from manipulated object towards the controller; (**b**) Exploring the contact properties such as hardness, temperature, and texture etc. In case of exploration, the action precedes perception, with action related information flowing from controller towards the contact; (**c**) The reaction tasks where a robot reacts to a stimuli coming from another robot or human or any other external agent. The action–reaction cycle involves bi-directional flow of signal, as shown in the figure

the analytical methods used for grasp stability focus on rigid objects. Investigations into the kinematics and dynamics during dexterous manipulation with robotic hands also suggest that the equations of motion of the combined hand and object system are quite sensitive to the contact conditions or events between the fingers and the object. This is to say that stable grasp requires detection of the changes in the state of the contacts (between the fingertips and the object, and between the grasped object and the external environment) and tactile feedback can be very useful for this purpose. Equipping robot hands with suitable touch sensors (i.e. tactile and joint force sensors) is therefore much needed to extend the possibilities beyond those resulting from using other sensor modalities only.

Touch sensing plays an important role in exploring the objects and differentiating them from one another. In robotics, this is done by touching the objects, or grasping them multiple times or manipulating them in different ways through the haptic inputs. For instance, by moving the finger over surface or on an object, the robot can extract data/features from several points to obtain the tactile image, which can be used to create or enhance a model using learning techniques. From the contact information it is possible to derive information regarding the object's inherent prop-

erties such as: Is the object stiff or is it compliant? Is there any texture? What is the friction coefficient? etc.

Tactile sensing is also important for safe interaction of robots with humans, objects, and possibly in unstructured environments. The robotic interaction with environment has mainly come through visual sensing techniques [12–15]—thanks to the availability of high performance video cameras, CMOS imagers and also significant research in the area of computer vision. Vision based interaction does not involve direct physical interaction with the environment and, at times, the results may be misleading. Like humans, some of the information about real world objects, like the shapes of objects, can be deciphered with vision cameras located on the robot [16, 17] and further finer details can be obtained by moving the cameras/robot around the object. But, such a movement around the object may not always be feasible, as happens with humans also. Even if such a movement is possible, the presence of visual inaccuracies due to large distance between robot cameras and the object can make it difficult to explore and manipulate a given object. Of course, such inaccuracies can be reduced by keeping the cameras close to the object, or in other words, somewhere close to fingers on the robot hand e.g. Eye-in-Hand Configuration [13]. With such a mechanism, the robot can no more be called a humanoid. More importantly, the Eye-in-Hand configuration seriously prevent vision of the object during the last stages of grasping and during manipulation. Using a large number of cameras—which is impractical anyway—cannot solve completely the problems in such situations. Processing of visual information in such scenarios becomes quickly computationally very expensive. Involvement of the 'sense of touch' information, in such situations, can provide complimentary solutions and improve the cognitive capabilities of humanoid robots.

The classical robot interaction tasks such as peg-in-hole problem, involve specific robot parts (typically, the end-effector tip) during interaction and force/torque sensors have been widely and successfully adopted for this. However, physical interaction of a robot with the real world does not necessarily come through touching by fingers or hands. Other body parts such as the arms, are also involved many times. For instance, a robot lifting an elderly or disabled person and moving him/her from wheelchair to the bed. Advanced robot systems such as humanoids, will require the capability of controlling more complex forms of interaction (e.g. whole hand or whole arm grasping and manipulation, gait stability control etc.). These tasks will require the monitoring of the contacts of the robot with the environment—which may happen at unpredictable positions and unpredictable ways. Therefore, skin-like sensors, not only on the fingers and hands, but also over the whole body, are needed for such complex forms of interactions to enable the implementation of safe interaction strategies.

1.3 Touch Sensing—Where?

Over the years, the application domain of robots has shifted away from the arena of industry to unstructured environments. The application areas of robotics where

tactile sensing is likely to play key role include: biomedical applications, such as non-invasive or minimal invasive surgery; human–robot interaction, such as during assisting elderly people; rehabilitation, such as enabling development of advanced prosthetic limbs; humanoids and more [8, 17–21]. Some of these application areas are described in following sections.

1.3.1 Biomedical Applications

One of the most exciting and relatively new application areas for tactile sensing is the biomedical robotics, especially the robotic minimal invasive surgery. Modern surgical procedures are far more intricate than those of the past and the surgeon's knowledge and skillful hands may not guarantee the success of operation. Many times surgeons do not have physical access to the damaged tissues or the internal body organ under observation. For instance, in MIS such as laparoscopy, a long and slender tool is inserted in the abdominal wall through small puncture openings and surgeon uses a range of tip-mounted instruments guided by video feedback images [22]. In such cases, the physical access through touch sensing, which can provide information like stiffness of tissues, is not available to the surgeon. The palpation of tissues and organs is an essential procedure that surgeons follow. Using an interface tool that provides no or poor tactile feedback is analogous to a surgeon experiencing some of the consequences of Mr. Waterman's illness, discussed in previous section. The surgical instruments equipped with tactile sensors to remotely measure tactile sensations from inside the patient's body and display this information to the surgeon are therefore of large interest.

Similarly, many surgical operations demand precision in terms of position and of the force applied by the surgeon. In this context, robots can be useful assisting tools for surgeons as they are very precise in position (with error tolerance in the order of few microns) and the application of accurate force. Robotic surgery can thus accomplish what doctors cannot because of precision and repeatability of robotic systems. The force and tactile feedback is helpful in attaining the desired precision. With tactile sensors equipped robots it may be possible to operate the patients remotely, and advance the concept of telemedicine and teleoperation.

1.3.2 Human–Robot Interaction

Human–Robot interaction (HRI) is an important area where investigation include development of new techniques for knowledge transfer from human to robot or teaching the robots by humans for the completion of a task, and development of human-friendly interfaces for robot control [23]. The research in human–robot interaction is also in anticipation of the growing presence of robots within general society. From the standpoint of robots in HRI, the tactile sensing is important due

to requirements of safe robot operation around humans and safe interaction with humans, for instance in a robot-assisted touch therapy or while assisting elderly people. The manipulation with hands as well as large body parts like arms will be needed in these areas. During HRI, tactile sensing also enables behavior development as robots depend on tactile contact from a human while building, refining or adapting a behavior. The human centered environment is pretty much unstructured with objects of different kinds of shapes, softness, textures and composition. The involvement of tactile sensing is crucial for such tasks due to safety concerns and user friendliness.

1.3.3 Rehabilitation and Prosthetics

Rehabilitation is another major area of application where robotic technology is applied to the rehabilitative needs of people with disabilities and as aid to the elderly. The use of robots in rehabilitation is often associated with: (a) replacement (or rehabilitation therapy) of the handicapped function of physically disabled, and (b) assisting the elderly to carry out necessary daily tasks. For user's convenience and safety, the human–robot interaction technology is important in rehabilitation robotics. This underlines the importance of sense of touch. For instance, when a robot contacts human skin, it applies mechanical forces on the surface of soft tissues. The applied force must be restricted for the safety of the person using the rehabilitation robotic devices and the effective control needed to do so requires the tactile, force, and torque sensors. The sensorized beds, consisting of embedded pressure sensors such as Force Sensing Resistors (FSRs), is another example of rehabilitation tools which can monitor the patient's posture and motion on the bed. Using the feedback from sensorized bed, a robot can assist the patient [24].

The prosthetics and orthotics have been closely associated with rehabilitation robotics. The terms prosthesis and orthosis are associated with the artificial limbs (although the term can also be used for an internal organ or joint) and the devices that support or control part of the body respectively. With technological advances, the prosthetic devices have evolved from just cosmetic artificial limbs to present day prosthetic limbs (e.g. dexterous hands) where movements are controlled via motors or actuators. The touch sensors are the important feedback elements of the prosthetic devices, which help control the movements in tasks like grasping. Further advances will allow future prosthetics to carry out human-like movements. The tactile sensing will again be an important component of future prosthetic devices, with tactile sensory components embedded all over their surface, to warn the user about the contacted object being too warm (or cold) and if the pressures exerted on the 'skin' of the prosthetic hand are excessive.

1.4 Summary

The discussion in this chapter underlines the importance and role of touch sensing, especially in the new generation robots and future robotics. Besides serving the applications discussed in this chapter, the tactile sensing is likely to significantly impact the overall robotics research. For instance, incorporation of tactile information would require revisiting conventional data processing techniques and algorithms. In this context, whole body tactile sensing will be of particular interest as most of the existing tactile data handling techniques take into account tactile information from the fingers and hands or end-effectors of a robot. There are many tasks that humans perform with ease with feedback from receptors all over the body. For instance, an adult person lifting an elderly or disabled person and moving him/her from wheelchair to the bed. During such a task, the adult person gets tactile feedback from large contact areas. How humans utilize the tactile information from large contact areas is another interesting area of investigation. The successful execution of similar tasks by robots will require tactile sensors all over the body (or robot skin) and new methods of analyzing and using the data. Education is another area where robotic technology (e.g. robotic toys) has been applied and where touch sensing might play important role.

References

1. M.O. Ernst, M.S. Banks, Humans integrate visual and haptic information in a statistically optimal fashion. Nature **415**, 429–433 (2002)
2. M. Prats, P. Sanz, A. del Pobil, Vision–tactile–force integration and robot physical interaction, in *IEEE International Conference on Robotics and Automation*, Kobe, Japan (2009), pp. 3975–3980
3. G. Westling, R.S. Johannson, Factors influencing the force control during precision grip. Exp. Brain Res. **53**, 277–284 (1984)
4. J.B.F. Van Erp, A.H.C. Van Veen Hendrik, Touch down: the effect of artificial touch cues on orientation in microgravity. Neurosci. Lett. **404**, 78–82 (2006)
5. J. Cole, *Pride and a Daily Marathon* (MIT Press, Cambridge, 1995)
6. M. Shikida, T. Shimizu, K. Sato, K. Itoigawa, Active tactile sensor for detecting contact force and hardness of an object. Sens. Actuators A, Phys. **103**, 213–218 (2003)
7. J.-i. Yuji, C. Sonoda, A PVDF tactile sensor for static contact force and contact temperature, in *IEEE Sensors*, Korea (2006), pp. 738–741
8. M.R. Cutkosky, R.D. Howe, W. Provancher, Force and tactile sensors, in *Springer Handbook of Robotics*, ed. by B. Siciliano, O. Khatib (Springer, Berlin, 2008), pp. 455–476
9. A. Morales, M. Prats, P. Sanz, A.P. Pobil, An experiment in the use of manipulation primitives and tactile perception for reactive grasping, in *Robotics Science and Systems, Workshop on Robot Manipulation Sensing and Adapting to the Real World*, Atlanta, USA (2007)
10. D. Prattichizzo, J.C. Trinkle, Grasping, in *Springer Handbook of Robotics*, ed. by B. Siciliano, O. Khatib (Springer, Berlin, 2008), pp. 671–698
11. R.S. Fearing, Tactile sensing mechanisms. Int. J. Robot. Res. **9**(3), 3–23 (1990)
12. P. Martinet, J. Gallice, Position based visual servoing using a non-linear approach, in *IEEE/RSJ International Conference on Intelligent Robots & Systems* (1999), pp. 531–535
13. M. Saedan, M.H. Ang Jr., 3D vision-based control on an industrial robot, in *IASTED International Conference on Robotics & Applications*, Florida, USA (2001), pp. 152–157

14. A. Clerentin, C. Pegard, C. Drocourt, Environment exploration using an active vision sensor, in *IEEE/RSJ International Conference on Intelligent Robots & Systems*, vol. 3 (1999), pp. 1525–1530
15. E. Cheung, V.L. Lumelsky, Proximity sensing in robot manipulation motion planning: system & implementation issues. IEEE Trans. Robot. Autom. **5**(6), 740–751 (1989)
16. M.J. Schlemmer, G. Biegelbauer, M. Vincze, Rethinking robot vision—combining shape and appearance. Int. J. Adv. Robot. Syst. **4**(3), 259–270 (2007)
17. T. Mukai, M. Onishi, T. Odashima, S. Hirano, Z. Luo, Development of the tactile sensor system of a human-interactive robot "RI-MAN". IEEE Trans. Robot. **24**(2), 505–512 (2008)
18. M.H. Lee, H.R. Nicholls, Tactile sensing for mechatronics—a state of the art survey. Mechatronics **9**, 1–31 (1999)
19. P. Puangmali, K. Althoefer, L.D. Seneviratne, D. Murphy, P. Dasgupta, State-of-the-art in force and tactile sensing for minimally invasive surgery. IEEE Sens. J. **8**, 371–381 (2008)
20. J. Dargahi, S. Najarian, Advances in tactile sensors design/manufacturing and its impact on robotics applications—a review. Ind. Robot **32**, 268–281 (2005)
21. R.S. Dahiya, G. Metta, M. Valle, G. Sandini, Tactile sensing—from humans to humanoids. IEEE Trans. Robot. **26**, 1–20 (2010)
22. U. Voges, Technology in laparoscopy—what to expect in the future. Urologe Ausgabe (a) **35**, 208–214 (1996)
23. B.D. Argall, A.G. Billard, A survey of tactile human–robot interactions. Robot. Auton. Syst. **58**, 1159–1176 (2010)
24. J.W. Jung, C.Y. Lee, J.J. Lee, Z.Z. Bien, User intention recognition for intelligent bed robot system, in *The 8th International Conference on Rehabilitation Robotics*, Daejeon, Korea (2003), pp. 100–103

Chapter 2
Tactile Sensing: Definitions and Classification

Abstract The 'sense of touch has been used as a layman term in Chap. 1. However, 'sense of touch' and 'tactile sensing' are not same. This chapter provides the definitions of various terms associated with the touch sense modality. Generally, the 'sense of touch' in robotics gets inspiration from humans. Thus, various terms associated with human sense of touch are presented first. Following this, the analogous terms for robotic applications are defined.

Keywords Sense of touch · Tactile sensing · Classification · Definitions · Extrinsic tactile sensing · Intrinsic tactile sensing · Cutaneous · Kinesthetic · Haptics · Perception

2.1 Definitions

The 'sense of touch' in humans comprises of two main submodalities—cutaneous and kinesthetic—characterized on the basis of their sensory inputs. Cutaneous sense receives sensory inputs from the receptors embedded in the skin and kinesthetic sense receives sensory inputs from the receptors within muscles, tendons and joints [1, 2]. It should be noted that the sensory inputs are not only mechanical stimulations but also heat, cooling and various stimuli that produce pain.

In context with the submodalities mentioned above, most researchers have distinguished among three sensory systems—cutaneous; kinesthetic and haptic. According to Loomis and Lederman [1, 3], cutaneous system involves physical contact with the stimuli and provides the awareness of the stimulation of the outer surface of body by means of receptors in the skin and associated somatosensory area of Central Nervous System CNS. The *kinesthetic system* provides information about the static and dynamic body postures (relative positioning of the head, torso, limbs and end effectors) on the basis of: (a) Afferent information originating from the muscles, joints and skin, and (b) Efference copy, which is the correlate of muscle efference available to the higher brain. It should be noted that the involvement of the afferent information from skin, in kinesthetic sensing, indicates its dependence on cutaneous sensing. The haptic system uses significant information about objects and events both from cutaneous and kinesthetic systems [1, 3].

R.S. Dahiya, M. Valle, *Robotic Tactile Sensing*,
DOI 10.1007/978-94-007-0579-1_2,

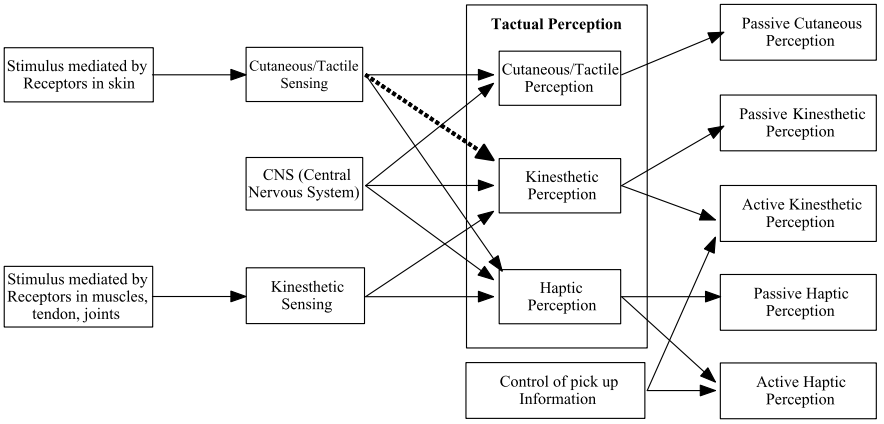

Fig. 2.1 The components of tactual perception. *Dotted line* represents the partial dependence of kinesthetic perception on stimulus mediated by receptors in the skin, or in other words, on cutaneous sense. (With permission from [10], ©IEEE [2010])

The perception of a stimulus can be categorized as cutaneous perception, kinesthetic perception and haptic perception—on the basis of three sensory systems discussed above. The perception of stimulus coming from cutaneous part is called cutaneous or tactile perception. In terms of Loomis and Lederman [1], the 'tactile' perception refers to the perception mediated solely by variations in cutaneous stimulation. Kinesthetic perception is mediated exclusively or nearly so (as kinesthetic sense partly depends on the cutaneous sense as well) by the variations in kinesthetic stimulation e.g. the perception of stimulus when cutaneous sensibility is disabled by anesthesia. Kinesthetic perception may include contact or lack thereof, between skin surface and external stimuli without providing any spatial or textural information e.g. discriminating length of objects—whether touched or not the perception of length comes from the kinesthetic part. All perceptions mediated by cutaneous sensibility and/or kinesthesis are referred as tactual perception. The haptic perception is the tactual perception in which both cutaneous and kinesthetic systems convey significant information.

Investigation of the properties of peripheral nervous system is done in two ways: first, in which observer is touched by moving objects and second, which involves the purposive exploration of objects by observer. Accordingly, the 'sense of touch' is classified as passive and active touch. Loomis and Lederman [1] made distinction between passive and active touch by adding the motor control inputs to the afferent information, as shown in Fig. 2.1. In everyday context, the touch is active as the sensory apparatus is present on the body structures that produce movements.

The above classification is suitable to define tactile sensing and associated terms for robotics applications. Most of the times, the robotic tactile sensing has been associated with detection and measurement of forces in a predetermined area. Jayawant [4] defined it as the continuous detection of forces in an array and further made a distinction between tactile sensing and force sensing, on the basis that the tactile

sensing involves force sensitive surfaces that are capable of generating continuous graded signals as well as parallel processing. Crowder [5] defined tactile sensing as detection and measurement of perpendicular forces in a predetermined area and subsequent interpretation of the spatial information. Following human sense of touch, this definition of tactile sensing is narrow for not including contact parameters other than perpendicular forces, and it is broad for including the 'interpretation' of spatial information—which is basically 'perception', that includes the role of both cutaneous sensing and the corresponding area of analysis in somatosensory cortex in CNS. The tactile or cutaneous sensing is associated with the detection and measurement of contact parameters which can be a mechanical stimulation (force, stress, roughness etc.), temperature, moistness etc. In this context, definition of tactile sensor by Lee [6] is more complete as the tactile sensor is defined as a device or system that can measure a given property of an object through contact in the world. As discussed later in the next chapter, the studies on cutaneous sensing has shown the presence of some coding or pre-processing of the stimulus information at the receptor level i.e. before transmitting the stimulus information to higher levels [7–9].

In view of these facts, tactile sensing is defined as the process of detecting and measuring a given property of a contact event in a predetermined area and subsequent pre-processing of the signals—before sending them to higher levels for perceptual interpretation [10]. On similar lines, touch sensing can be termed as tactile sensing at single contact point. These definitions of tactile and touch sensing, are used in this book. The analogous terms, for cutaneous and kinesthetic sensing, in robotics are termed as extrinsic (or external) and intrinsic (or internal) sensing respectively. In robotic applications, extrinsic or tactile sensing is achieved through tactile sensing arrays or a coordinated group of touch sensors.

At the system level, tactile sensing system can be said to be made of various components that lead to the perception of a contact event. For example, the extrinsic or tactile sensing and the computational processing unit in robots can be termed as extrinsic or tactile sensing system—analogous to the cutaneous sensing system in which each receptive field is associated with a specific area of analysis in the somatosensory cortex of CNS (Fig. 2.1). On similar arguments intrinsic sensing system and haptic system can also be defined for robotic applications.

2.2 Classification

A broad classification of robotic tactile sensing is given in Fig. 2.2. Based on the function or the task to be accomplished, the robotic tactile sensing may be grouped into two categories—first, 'Perception for Action' as in grasp control and dexterous manipulation and second, 'Action for Perception' as in object recognition, modeling and exploration. In addition to these two functional categories, a third category—not shown in Fig. 2.2—could be haptics, which involves action and reaction or in other words, two way transfer of touch information.

Based on the site where a sensor is located, the robotic touch sensing can be categorized as extrinsic and intrinsic sensing. While intrinsic sensors are placed within

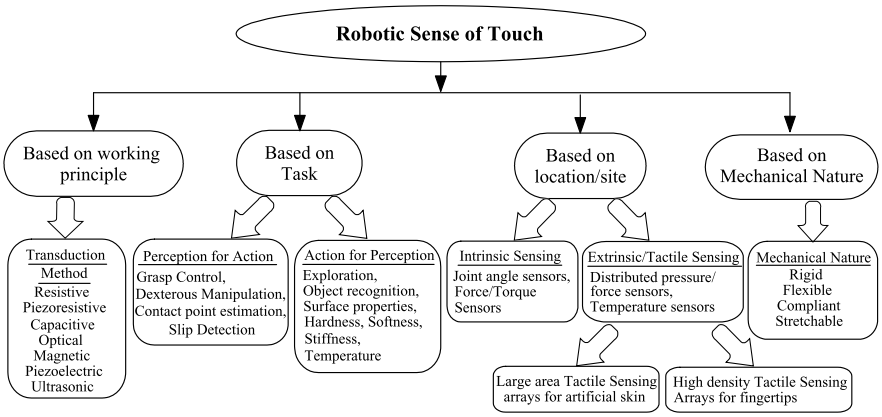

Fig. 2.2 The classification of touch sensing in robotics. (With permission from [10], ©IEEE [2010])

the mechanical structure of the system and derive the contact data like magnitude of force using force sensors; the extrinsic or tactile sensors/sensing arrays are mounted at or near the contact interface and deal with the data from localized regions. Like cutaneous sensing in humans, discussed in next chapter, the spatial resolution of touch sensors need not be uniform throughout the body/structure. As an example, in humans the spatial discrimination is finest in the fingertips, where the touch receptors are plentiful and the receptive fields are small. In other regions such as trunk, the spatial information is less precise because the receptors are fewer and thus have large receptive fields. Following this argument, the extrinsic or tactile sensing can be further categorized in two parts—first, for highly sensitive parts (e.g. fingertips) and second, for less sensitive parts (e.g. palm or large area skin). Whereas former requires a high density tactile sensing arrays or a large number of touch sensors in a small space ($\sim$1 mm spatial resolution) and fast response (of the order of few milliseconds); such constraints, especially one related to spatial resolution, can be relaxed for the latter.

Both, extrinsic/tactile and intrinsic sensing can also be classified—not shown in Fig. 2.2—on the basis of the working principle of sensors and on the basis of physical nature of the sensors. On the basis of working principle, tactile sensors can be resistive, capacitive, inductive, optical, magnetic, piezoelectric, ultrasonic, magneto-electric etc. On the basis of the mechanical nature, the sensors can be flexible, compliant, stiff and rigid etc. A detailed discussion on sensors, based on these classifications, is present in Chap. 5.

The discussion in this book is primarily focused on the extrinsic/tactile sensing. Hereafter, for simplicity, the term ‘tactile sensing’ is used for ‘extrinsic/tactile sensing’ in robotic applications.

References

1. J.M. Loomis, S.J. Lederman, Tactual perception, in *Handbook of Perception and Human Performances*, vol. 2 (Wiley, New York, 1986)
2. M.S.A. Graziano, M.M. Botvinick, in *How the Brain Represents the Body: Insights from Neurophysiology and Psychology* (Oxford University Press, London, 2002), pp. 136–157
3. R.L. Klatzky, S.J. Lederman, Touch, in *Experimental Psychology*, ed. by A.F. Healy, R.W. Proctor. Handbook of Psychology, vol. 4 (Wiley, New York, 2003), pp. 147–176
4. B.V. Jayawant, Tactile sensing in robotics. J. Phys. E, Sci. Instrum. **22**, 684–692 (1989)
5. R.M. Crowder, Automation and robotics (1998), http://www.soton.ac.uk/~rmc1/robotics/artactile.htm
6. M.H. Lee, H.R. Nicholls, Tactile sensing for mechatronics—a state of the art survey. Mechatronics **9**, 1–31 (1999)
7. R.S. Johannson, I. Birznieks, First spikes in ensembles of human tactile afferents code complex spatial fingertip events. Nat. Neurosci. **7**(2), 170–177 (2004)
8. I. Birznieks, P. Jenmalm, A.W. Goodwin, R.S. Johannson, Encoding of direction of fingertip forces by human tactile afferents. J. Neurosci. **21**(20), 8222–8237 (2001)
9. P. Jenmalm, I. Birznieks, A.W. Goodwin, R.S. Johannson, Influence of object shape on responses of human tactile afferents under conditions characteristics of manipulation. Eur. J. Neurosci. **18**, 164–176 (2003)
10. R.S. Dahiya, G. Metta, M. Valle, G. Sandini, Tactile sensing—from humans to humanoids. IEEE Trans. Robot. **26**(1), 1–20 (2010)

Chapter 3
Human Tactile Sensing

Abstract Designing a meaningful robotic tactile sensing system requires a broad, but integrated, knowledge of how tactile information is encoded and transmitted at various stages of interaction via touch. In this context, various scientific studies on human sense of touch can provide a good starting point. The sense of touch in humans comprises of two main submodalities, i.e. "cutaneous" and "kinesthetic", characterized on the basis of the site of sensory inputs. Much of the real world interactions involve both cutaneous/tactile and kinesthetic submodalities. This chapter focuses on the cutaneous/tactile component of human sense of touch. A brief discussion on the spatial properties of the human skin and its receptors is presented. The discussion is followed by the role and perceptual importance of the cutaneous/tactile sense in humans. This chapter has been included with an aim to understand if (and how) human tactile sensing can be the basis for the robotic tactile sensing. The chapter concludes with a set of design criteria, derived from the discussion on human cutaneous sensing, for robotic tactile system.

Keywords Human sense of touch · Neurophysiology · Cutaneous · Kinesthetic · Haptics · Perception · Tactile encoding · Skin mechanics · Artificial tactile sensing

3.1 Introduction

Designing a meaningful robotic tactile sensing system requires a broad, but integrated, knowledge of how tactile information is encoded and transmitted at various stages of interaction via touch. In this context, various scientific studies on human sense of touch can provide a good starting point. The observations of natural systems have inspired engineers for centuries [1] and often served as inspiration or starting point in robotics [2–5]. Many studies on human sense of touch have addressed the sensing problems that are challenging to roboticists as well. These studies include sensor performance, sensor fusion, object recognition, feature extraction, movements for optimum exploration of material properties, active and passive perception, selective attention, sensory guided motor control etc. In the absence of any rigorous robotic tactile sensing theory such studies can help define the important parameters like tactile sensor density, resolution, location, and bandwidth etc. They

R.S. Dahiya, M. Valle, *Robotic Tactile Sensing*,
DOI 10.1007/978-94-007-0579-1_3,

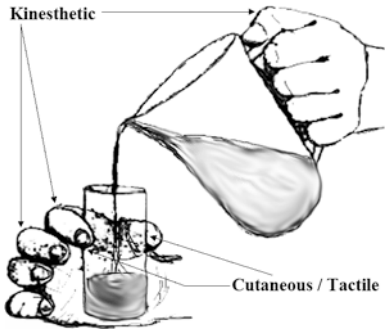

Fig. 3.1 The kinesthetic and cutaneous/tactile components of human sense of touch

may also bring up new ideas resulting in an increase in the level of tactile sensitivity and acuity of robots to the human range.

The sense of touch in humans comprises of two main submodalities, i.e. "cutaneous" and "kinesthetic", characterized on the basis of the site of sensory inputs. The cutaneous or tactile sense receives sensory inputs from the receptors embedded in the skin, and the kinesthetic sense receives sensory inputs from the receptors (or proprioceptors) within muscles, tendons, and joints [6–8]. Considering the example of pouring water in a glass, as illustrated in Fig. 3.1, the sensory inputs from finger joints belong to kinesthetic submodality and the sensory inputs from skin parts in contact with jug and glass belong to cutaneous/tactile submodality. This chapter primarily focuses on the cutaneous/tactile component of human sense of touch. For detailed study on touch sense modality in humans one may refer to the standard literature on human sense modalities [6–8].

3.2 Neurophysiology of Human Tactile System

The human cutaneous/tactile sense modality is distributed and housed in the largest and heaviest sense organ—the skin, and deals with the spatiotemporal perception of external stimuli through a large number of receptors. Inside the skin, these receptors are embedded at various levels—in both the outer layer called epidermis and the underlying layer known as dermis. The receptors can be classified according to the type of stimulation they respond to—mechanoreceptors for mechanical stimuli (e.g. pressure, vibration, light touch etc.), thermoceptors for temperature or thermal stimuli, and nociceptors for pain/damage [9, 10]. The nociceptor units in the skin also respond to extremes in temperature and sometimes to mechanical stimulation [8]. The discussion in this chapter is primarily about the mechanoreceptors which mediate the response to mechanical stimuli. The four major types of mechanoreceptors, shown in Fig. 3.2, are: Meissner's corpuscles, Pacinian corpuscles, Merkel cells, and Ruffini corpuscles. Meissner and Merkel receptors located at the junction of the epidermis are the enlarged endings of nerve fibers. The Meissner's corpuscles are the most common mechanoreceptors of glabrous (smooth, hairless) skin (fingertips, for instance), and their afferent fibers account for about 40% of the sensory

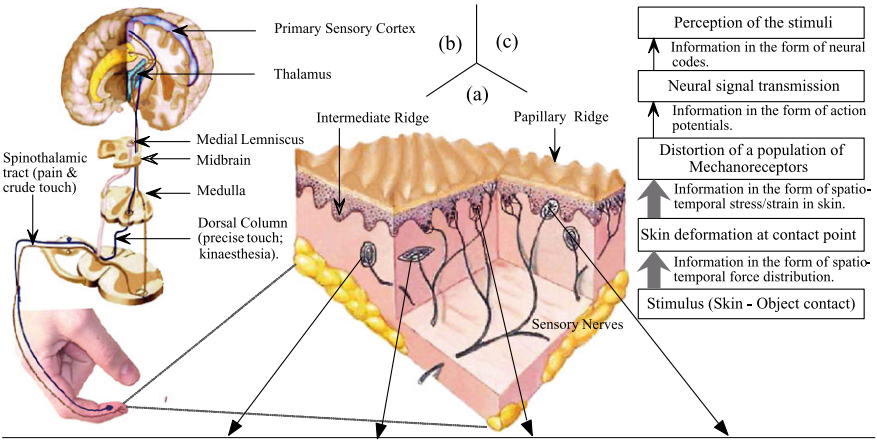

Classification Basis		Pacinian Corpuscle	Ruffini Corpuscle	Merkel Cells	Meissner's Corpuscle
Type		FA II	SA II	SA I	FA I
Adaptation Rate Property		Fast	Slow	Slow	Fast
Fiber Innervation Density (per cm2)					
Fingertip		21	49	70	140
Distal Phalax (not tip)		15	28	42	77
Proximal & Middle Phalanx		10	14	30	37
Spatial Acuity (mm)		10+	7+	0.5	3-4
Vibration/rapid indent threshold	Best (μm)	0.01	40	8	2
	Mean (μm)	0.08	300	30	6
Stimuli Frequency (Hz)		40-500+	100-500+	0.4-3	3-40
Percentage in human hand		10-15 %	20 %	25 %	40 %
Conduction Velocity (m/s)		35-70	35-70	40-65	35-70
Effective Stimuli		Temporal changes in the skin deformation	Sustained downward Pressure; Lateral skin stretch; Skin slip.	Spatial deformation; Sustained pressure; Curvature, edge, corners.	Temporal changes in skin deformation
Sensory Function		High frequency vibration detection; Tool use.	Finger position; Stable grasp; Tangential Force; Motion direction	Pattern/form detection; texture perception; Tactile flow perception.	Low frequency vibration & motion detection; Grip control; Tactile flow perception

Fig. 3.2 Human Cutaneous/Tactile Sensing. (**a**) Section of glabrous skin showing physical location and classification of various mechanoreceptors [6, 7, 10, 15–17]. The small limiting ridges that exist between two intermediate ridges are not shown in the figure; (**b**) Tactile signal Transmission—from fingertips to somatosensory area of brain; (**c**) Functional events during tactile signal transmission from contact point to the brain. For simplicity, the signal flow is unidirectional. In general, the information transfer is bidirectional as same path is used by motor signals. (With permission from [18], ©[2010] IEEE)

innervation of the human hand [10]. The Merkel cell complex—a group of 5–10 Merkel cells grouped in tree like structure—lies on the tip of epidermal part of the intermediate ridges, as shown in Fig. 3.2. Intermediate ridges are the undulating epidermal tissues that descend into the epidermal–dermal junction and play a positive role in improving the tactile spatial acuity [11–13]. The Merkel cells account for about 25% of the mechanoreceptors of the hand. The Pacinian corpuscles and Ruffini endings, on other hand, are embedded more deeply in the dermis and underlying subcutaneous tissue. Pacinian corpuscles make up 10–15% of the cutaneous receptors in human hand. The number of mechanoreceptors varies across the body per cm^2 area have been estimated to be 241 in the fingertips and 58 in the palm of

adult humans [14]. Because the hand is the most densely innervated part of the human body, it is not surprising that we use the hand more than any other body part to glean information beyond ourselves that allows us to interact with our surroundings in meaningful ways. The two main attributes that are used to classify mechanoreceptors are: (a) the rate of adaptation; and (b) the size of the receptive field. These are described in following paragraphs. Further classification, functions and the location of various mechanoreceptors in the glabrous skin are given in Fig. 3.2.

The strength of the stimulus is conveyed by the rate of action potential[1] discharge, which depends on the how mechanoreceptor fire or respond when exposed to stimulus. Meissner corpuscles and Pacinian corpuscles are called fast adapting (FA) as they respond with bursts of action potentials when their preferred stimulus is first applied and when it is removed, but they fall silent during the steady state between stimulus onset and offset (which is to say they "adapt fast" to the stimulus). On other hand, Merkel cells and Ruffini corpuscles remain active throughout the period during which the stimulus is in contact with its receptive field, as shown in Fig. 3.3(b). In other words, they adapt slowly to the stimulus and hence they are termed as slow adapting[2] (SA). Consider the task, given in Fig. 3.3(a), where a person grasps and lifts an instrumented test object from a table, holds it in air, and then places it back. Dividing the complete task into sub-tasks or action phases (reach, load, lift, hold, replace, unload) and observing the response of receptors, shown in Fig. 3.3(b), one may notice that FA receptors respond during start and end of the task and the transition of sub-tasks only. On other hand, the SA receptors continue to respond during whole task period. Therefore, the receptors (Pacinian corpuscles and Meissner's corpuscles) that initially fire in the presence of a stimulus and then become quiescent (e.g. during action-phase transition only) are particularly effective in conveying information about changes (dynamic) in the information the receptor reports; conversely, receptors (Ruffini corpuscles and Merkel cells) that continue to fire convey information about the persistence of a stimulus (static). The usefulness of having some receptors that adapt quickly and others that do not is to provide information about both the *dynamic* and *static* features of a stimulus. This is an important observation from robotics point of view, as most of the tasks involve both dynamic and static features.

Receptive field is another important attribute of receptors in the skin. It is the region of skin directly innervated by the terminals of receptor neurons. In other words, it is the region of the skin within which a tactile stimulus evokes a sensory response or the extent of body area to which the receptor will respond. The receptive fields of mechanosensory neurons in humans are smaller in fingertip (1–2 mm diameter) and larger in palm (5–10 mm diameter) and still larger in parts like arm. The mechanoreceptors closer to the skin surface (i.e. Meissner and Merkel receptors) have a smaller and more finely tuned receptive fields. The deep layer mechanoreceptors (i.e. Pacinian corpuscles and Ruffini endings), on the other hand, have a larger

[1] The voltage pulses generated when the stimulus is greater than a threshold.

[2] Both FA and SA are further classified as type I (FA-I, SA-I) and type II (FA-II, SA-II).

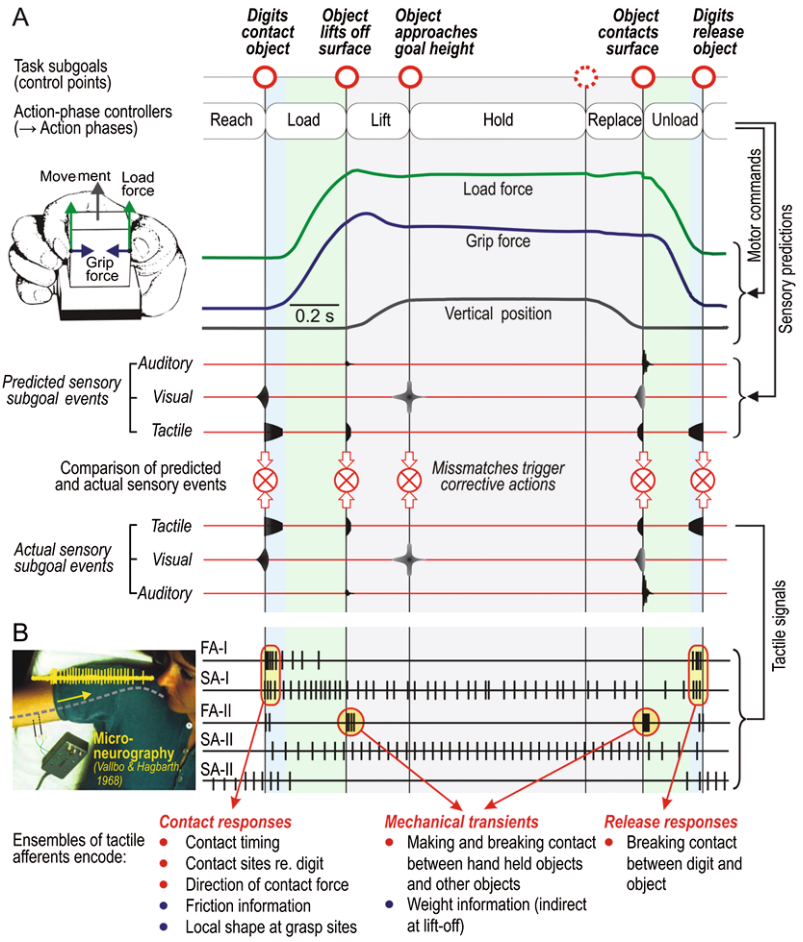

Fig. 3.3 (**a**) The contact events (at the *top*) defining action-phases or sub-tasks of a task where person lifts an instrumented object, hold it in air, and place is back; (**b**) Signals of peripheral tactile sensory neurons during the task. (With permission from [19], ©(2008) Elsevier)

receptive field with much less defined boundaries. To envision the importance of receptive field, one may, for instance, think what if all cutaneous receptor neurons covered the entire digital pad. Under such a circumstance, wouldn't it be impossible to discriminate two spatially separate stimuli applied to the fingertip (since all the receptive fields would be returning the same spatial information)? The adjacent receptive field however may overlap because of the multiple ways in which receptors innervate sensory neurons. Such overlapping provides an intrinsic mechanism for fault tolerance and improves robustness.

3.3 Spatio-Temporal Properties of Human Tactile Sensing

The accuracy with which stimuli can be sensed varies from one region of body to another. The tactile sensitivity, acuity and various threshold (in time as well as space) are some of the important aspects of human tactile sensing that influence the outcome of various tasks. For instance, the pattern sensing capability of cutaneous sense is limited by both its spatial and temporal sensitivities, as these sensitivities quantify the information loss or blurring of stimulus by spatio-temporal filtering effect of cutaneous sense at early stage of cutaneous processing [20]. Such unwanted blurring effects are of concern in robotics as well, since adjacent tactile sensing elements may be passively triggered. Such effects can be used to define the "cross-talk" limits of robotic tactile sensors.

The spatial acuity—the smallest separation at which one can tell that he/she has been touched at two points—gives information about the spatial resolution. It is related to receptive fields, discussed earlier, in an inverse fashion—smaller the receptive field better the tactile acuity. Studies using two points threshold or compass method[3] [21, 22] and grating orientation method[4] [23], show that the spatial acuity varies across the body. It is highest at fingertips, face and toes and lowest at thigh, shoulders and belly. Using orientation grating method, it is found that the spatial resolution in the palm is about seven times smaller than that of the fingertips [24]. Similarly, with the two point threshold method it has been shown that one can resolve two points as close as 3 mm on the fingertips and this goes up to approximately 30 mm on the belly [6]. More sensitive psychophysical methods show that, on the fingertips, the spatial resolution is about 1 mm [25, 26]. These results place the tactile acuity somewhere between vision and audition—being worse than vision, but better than auditory spatial resolution [6]. The ability to perceive a fine spatial structures of a stimulus also depends on its temporal properties (namely, its vibration frequency). The spatial acuity decreases if vibration frequency is increased [27]. The spatial acuity of torso measured with vibro-tactile stimuli has been reported to be 20–30 mm [28]. Skin microstructures such as intermediate ridges (Fig. 3.2) are known to enhance the tactile spatial acuity by transmitting magnified signals from surface of skin to the mechanoreceptors underneath [29, 30] and their involvement in texture perception has also been suggested [31].

The studies on finding the limits of human perception of the temporal aspects of the tactile stimuli show that humans are capable of detecting vibrations up to 700 Hz, i.e. they can detect a single temporal interval of about 1.4 ms [8]. Some

[3]Two points threshold method involves measurement of the minimal interstimulus distance required to perceive two simultaneously applied stimuli as distinct (the indentations of the points of a pair of caliper, for example).

[4]In orientation grating method, subjects are presented with a grating in one of two orientations on the skin. For example, on the fingerpad the gratings are presented in either a proximal–distal orientation or at right angles to that in the lateral–medial orientation. The subject indicates the orientation. The grating orientation task relies on devising stimuli that are identical except for the orientation in which they are presented to the skin.

other studies suggest a higher value (about 5 ms or more) of the interval of perceiving two tactile stimuli as separate events [32]. If the separation is less, they are perceived as one. Comparing it with temporal acuity of vision (upper limit of 50 Hz for a flickering light) and audition (20 kHz), one can see that touch again lies between vision and audition, but this time audition is the best and vision is the worst[5] [6]. The ability to count the number of stimuli also indicate that tactile sense is better for counting than vision but not as good as hearing [34]. Temporal separation of two contact events at different locations is also important in order to detect the presence of multiple events. The critical temporal separation for two events at different locations on fingertips has been found to be in the order of 30–50 ms [35].

The pressure threshold and skin deformation are other common intensive measures of absolute tactile sensitivity. The higher the pressure threshold, the lower the sensitivity of the body part. Controlled pressure sensitive studies show that pressure thresholds vary with body site. Whereas normal mean threshold values average about 0.158 gm on the palm and about 0.055 gm on the fingertips of men, the corresponding values for women are 0.032 gm and 0.019 gm, respectively [36]. Johansson and Vallbo [37] estimated that 90% of the SA-I and the FA-I mechanoreceptors get excited to a stimulus of 5 mN. This force stimulus applied through a Von Frey hair with a diameter of 0.27 mm corresponds to 87 mN/mm^2 [37, 38]. With these values, one could infer the level of resolutions that a robotic tactile sensor should have.

The temperature sensitivity also varies with the body parts. For example, from a baseline temperature of 33 discharge, changes as small as 0.16 and 0.12°C for warm and cold, respectively, can be detected at the fingertips [39]. Corresponding values at volar base of thumb are 0.11 and 0.07°C.

3.4 Tactile Information Transfer and Encoding

One may wonder how the information is transferred to the brain from a large number of receptors that are distributed all over the body with variable density. Transmission of afferent mechanosensory information from the periphery to the brain begins with a variety of receptors types, discussed in previous sections. From the moment the skin is stimulated by an external medium (e.g., by a pointed object) to the resulting touch perception that is experienced (e.g., a localized prickly sensation), a variety of complex mechanical, perceptual and cognitive phenomena take place, as shown in Fig. 3.2(c). Despite their variety, all receptors transduce or convert stimulus in to an electrical signal in the sensory neuron in fundamentally the same way. On contact with an object, the skin conforms to its surface and maintains the same local contour. The same deformation is projected to a large number of receptors in the skin—each representing a small portion of the object. The peripheral sensory

[5]For hearing the threshold is about 0.01 ms and for vision it is about 25 ms [33].

apparatus thus deconstructs the object into tiny segments and encodes the tactile information as spikes of action potentials. This means, no single sensory axon, or even class of sensory axons, signals all of the relevant information. Spatial properties are processed by populations of receptors that form many parallel pathways to the brain. The amplitude or strength of the stimulus is transformed by mechanoreceptors in the form of a train of action potentials [7]—somewhat similar to digitizing and coding of analog signals in an analog to digital (A/D) converter.

The sensory information of the external world is then transmitted from peripheral receptors toward the CNS for higher level processing and interpretation. The CNS does not always get the raw touch information as some pre-processing of the signals is done at various data transfer stages. For instance, during natural manipulations humans are able to perceive independently the curvature and direction of force from the first spikes of the signals originating from an ensemble of receptors in the terminal phalanx [40]. And if this is so, then CNS must only perform some higher level processing to disentangle the interactions between such information and other parameters (like magnitude and rate of change of contact force, temperature, change in viscoelastic properties of fingertip etc.) of stimuli on the fingertip [41]. Besides these, the tactile information transfer to brain is also subjected to an intense process of selection [42]. For example, the tactile information is transferred when attention is paid to 'which part of the body is being stroked'.

The sensory information from peripheral receptors is transmitted toward the CNS via multiple nerves up to the spinal cord and via two major pathways: spinothalamic and dorsal-column-medial-lemniscal (DCML) thereafter, as shown in Fig. 3.2. The 'Spinothalamic Pathway' is slower and carries temperature and pain related information. The 'DCML Pathway', on other hand, is faster and conveys the pressure/vibration related tactile information more quickly to brain. DCML pathway carries information from only the upper and lower body and from the posterior third of the head. Tactile (and proprioception) information from the face is transmitted to CNS via different route called trigeminal somatic sensory systems. DCML pathway is important for the spatial and temporal comparisons of the stimuli. Neural circuits in the DCML and somatosensory areas of the cerebral cortex integrate the fragmented information obtained from populations of receptors in the neighboring areas of skin and construct a coherent percept of the object [7]. It should be noted that the nerves from each receptor or group of receptors do not synapse until the spinal column, which indicates that there is one data channel per receptor. Such an arrangement works well for biological systems but is less suitable for human-made artificial systems such as the robotic tactile systems where too many wires, originating from large number of tactile sensors, are not desirable (see Fig. 3.6).

An important feature of human sensory system is the representation of various body parts as 'somatotopic maps' in the somatic sensory cortex [7, 10]. The tactile information from the peripheral receptors to the brain travels in a somatotopic grouping i.e. nerve fibers from population of receptors in the different regions of the body tend to group together. The set of active neural pathways leading to the specific cortical areas of the somatotopic map can thus encode the information such as the location of the stimulus [43]. By analyzing which nerve fibers have been

excited, the brain thus reconstructs a coherent image of the contacted object from fragmented information conveyed in multiple pathways. It is to be noted that the somatotopic representations do not reflect the body in actual proportion. Instead, the amount of cortical and subcortical space allocated to various body parts is proportional to the density of peripheral receptors. For instance, compared to the torso and proximal limbs, the face and hands are grossly enlarged in the somatotopic maps. The anomalies arise because task performed by hands and face, such as manipulation and facial expression are more important for humans and hence more central circuitry is needed to govern them.

It may be noticed that there is a distinct functional hierarchy within the constituent pathways of the somatosensory system i.e. primary afferent fibers converge onto second-order neurons, located in the central nervous system, and then onto third- and higher-order neurons [7]. Like peripheral receptors, the neurons at each hierarchical level have a receptive field, which is defined by the population of neurons (from previous level) that converge on them. The receptive fields of second and higher-order sensory neurons are larger as they receive convergent input from hundreds of receptors, each with a slightly different but overlapping receptive field. For example, the receptive fields of sensory neurons innervating a finger cover tiny spots on the skin, while those of the cortical cells receiving these inputs are large areas covering an entire fingertip, or several adjacent fingers. receptive fields in higher cortical areas are even larger. The receptive fields of higher-order sensory neurons are also more complex[6] than those of receptor neurons because they are sensitive to specific stimulus features, such as motion, direction or the orientation. Further, the size and position of the receptive fields of higher-order sensory neurons (cortical neurons) on the skin are not fixed permanently but can be modified by experience or by injury to sensory nerves. In spite of having larger receptive fields, covering a larger area of skin, the cortical neurons are able to discriminate fine detail because they respond best to excitation in the middle of their receptive fields [7]. For a detailed understanding of how CNS combines the information from the large number of receptors to get a coherent image of the contacted object one can refer to [6, 7, 44].

The representation of robot's body in a way similar to the somatotopic maps (in other words, artificial somatotopic maps) shall help in utilizing the tactile data and locating the position of stimuli in 3-dimensional space, which may otherwise be labor intensive and error prone because of changing robot's postures.

3.5 Tactile Sensing and Perception

Humans are excellent at recognizing common objects by touch alone and cues like material properties, shape etc. are critical to this endeavor. Both cutaneous and

[6]The early processed tactile signals are directly related to stimuli, whereas later processing stages are progressively more abstract.

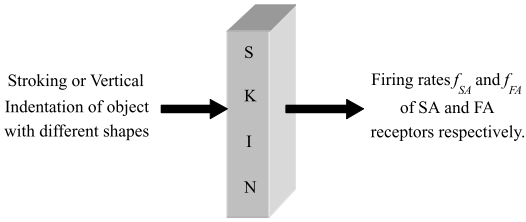

Fig. 3.4 Model of skin for coding of shape and orientation by the mechanoreceptors

kinesthetic sensing contribute to the perception of such cues. Tactile sensing in humans is better adapted to feel the material properties of objects than is to feel their shapes, particularly when the object is large enough to extend beyond the fingertip [6]. Perhaps this is the reason why most of the studies on tactile sensibility in humans and other primates have reported sensory perception in the context of exploratory tasks [45].

shape detection of the objects small enough to be within the contact area (7–12 mm) of fingertips, is an important function of the mechanoreceptors. The experiments involving stroking and vertical indentation of the skin, with the force equal to that exerted by humans during natural manipulation (15–90 gm wt.), indicate that the object shape and orientation are signaled by the spatio-temporal responses of the afferent fiber populations, particularly those of the SAs [46–50]. Further, humans are able to perceive independently curvature and force direction from these signals [41]. These experiments reveal that the firing rate of an SA is a function of the vertical displacement, vertical velocity, and the amount and the rate of change of curvature of the skin. However, SAs become silent in the event of negative rate of change of curvature. In case of FA, the firing rate is a function of the vertical velocity and the rate of change of curvature at the most sensitive part of the receptive field. These studies give a direct relation between the stimuli and neural signals that code them (irrespective of the intervening mechanisms such as the stresses and strain at the receptor site). Thus, assuming skin to be a "blackbox" (Fig. 3.4), the relation between the stimuli (e.g. the shape) and the output (e.g. the firing rate of afferent fibers) can be written as:

$$f_{SA} = a_1 R^{-1} + a_2 \frac{\mathrm{d}R^{-1}}{\mathrm{d}t} + a_3 \Delta Z + a_4 \frac{\mathrm{d}Z}{\mathrm{d}t} \tag{3.1}$$

$$f_{FA} = b_2 \frac{\mathrm{d}R^{-1}}{\mathrm{d}t} + b_4 \frac{\mathrm{d}Z}{\mathrm{d}t} \tag{3.2}$$

where, f_{SA} and f_{FA} are the firing rates of SA and FA receptors respectively; R^{-1} is the skin curvature at contact point; ΔZ is the vertical displacement and a_1, a_2, a_3, a_4, b_2, and b_4 are the constants. Firing rates given above are zero in case of negative rate of change of the curvature. The *edge* sensitivity is a special case of the general property of sensitivity to changes in skin curvatures. As can be noticed from (3.1)–(3.2), the FA and SA receptors respond simultaneously at edges and boundaries. At other points FA receptors are silent. The response of SA receptors is higher at edges than at uniform surface because of high compressive strain at such points. The edge

detection sensitivity of SA-I receptors has also been attributed to the presence of Merkel cells on the tips of epidermal part of intermediate ridges that are believed to magnify the tactile signals from the surface of the skin to the mechanoreceptors below by way of micro-lever action [11, 51]. The role of intermediate ridges is further discussed later in the section on skin mechanics. The sensitivity to the rate of change of curvature, in addition to the curvature, also enhances the contrast at the edges of objects, where curvature changes abruptly. From a robotics point of view, these results highlight the importance of having sensors that respond to both static and dynamic stimuli. For instance, a combination of capacitive/resistive and piezoelectric transduction could be one of the many possible solutions.

Information about *surface texture* plays a major role in tactile object recognition (e.g., baseball vs. an orange) and can be important when manipulating objects. For example, a ball made of foam is manipulated very differently than a ball made of steel. The three main dimensions of texture perception are roughness/smoothness, hardness/softness, and stickiness/slipperiness. Neurophysiological studies suggest that the tactile *roughness* perception is accurately predicted by spatial variations of discharge of SA afferents instead of their mean firing rates, which means the roughness is a function of multiple tactile elements. Besides this, experiments also show that roughness varies with the spatial distribution, height and diameter of elements [52–54]. The form and shape of the elements (e.g. pointed, round or flat) and material properties of the surface (e.g. stiffness, elasticity) can also contribute to roughness [54]. Textured surfaces with widely spaced elements that lead to higher penetration in skin are perceived rougher than those with closely spaced elements. Contrary to the general belief that the temporal parameters have little effect on roughness perception [54], recent studies show that temporal cues do indeed contribute [55]. Fingerprints or papillary ridges, shown in Fig. 3.2, also enhance the tactile sensitivity of Pacinian corpuscles and, hence, help in feeling fine textures [29]. Discrimination of surface roughness is also enhanced when there is tangential movement between the surface and skin [56] and this is independent of the mode (active or passive) of touch [57]. In other words, this property is salient to cutaneous/tactile sensing. Roughness of objects has also been found to be significantly correlated with friction. The correlation is much stronger when the variations and rate of change of the tangential forces are considered. This is evident from the experiments where subjects maintained a steady normal force rather than reducing it, to allow the tangential force to initiate and maintain sliding while scanning a surface with higher friction [58, 59]. These facts underline the importance of tangential forces and that its knowledge, in addition to the normal forces, can be useful in robotic applications.

hardness/softness is associated with the compliance of an object. As the hand is pressed against a compliant object, it conforms to the contour of the skin in proportion to the contact force. The compliance (and the softness) of the object appears to be signaled by the rate of growth of the area over which the skin contacts the object as the contact force increases, as well as the increase in the reaction force exerted by the object on the skin across the contact area. Softness perception has been shown to rely primarily on cutaneous cues (eliminating kinesthetic information has no effect on subjects' ability to discriminate softness)—most likely relying on the signals from SA-I afferents [60].

Detection of *slip* can be viewed as the coding of motion by the receptors in the skin. Slip or relative movement between a surface and the skin is important for perception of roughness [54, 59, 61], hardness [60] and shape [62, 63]. slip plays an important role in grip force control by acting as an error signal. All these, except static contact associated with thermal sensing, involve movement of fingers and thus also highlight the importance of dynamic tactile sensing, as also suggested in [64].

Tactile feedback from the contact surface of an object influences the perception of *force* used to support it. Experiments studying the effect of tactile sensing on the perception of force demonstrate underestimation of forces produced by muscles when tactile sensory feedback from hand is constrained [65]. Interestingly, complete elimination of tactile feedback by anesthetizing skin results in an opposite perception of force i.e. increase in the perceived force or heaviness [66] and decrease in the maximum force that the fingers can produce [67]. Further, the effect of eliminating the tactile sensing from various fingers is also different. Elimination of cutaneous sensing from thumb and index finger results in an increase in perceived heaviness by 40% and 13% respectively [66].

In addition to magnitude, the *direction of force* is also critical for handling objects with irregular shapes and in dexterous manipulation for regulating the balance between normal and tangential forces—to ensure grasp stability (the so-called friction cone [68])—while maintaining the desired orientation of the objects. Tactile afferents from the terminal phalanx of finger have been shown to contribute to the encoding of direction of fingertip forces. The directionality is thought to be due to different strains produced at the receptor site by forces (equal to those used in natural manipulation) applied in different directions [45].

In context with motor control, tactile information plays an important role in the controlling the execution of *reaching to grasp* movements. The contribution of cutaneous receptors for controlling prehensile force during object manipulation has been studied extensively [9, 69, 70]. In such manipulation tasks, friction rather than texture, is an important parameter to find the grip force strength [69]. In grip force control, slip plays an important role by acting as an error signal which requires a corrective increase in the force. The role of tactile sensory information from fingers in such tasks is to ascertain the actual shear or load force and help in optimally adjusting the grip force [9, 67, 69]. During grasp, the cutaneous feedback is needed to have the actual state of the system, as the internal models (of objects) underlying anticipatory control mechanisms are no longer updated in its absence [67, 71]. Various phases of a grasping action, namely, reaching, loading, lifting, holding, replacing, and unloading (Fig. 3.3), are characterized as discrete sensory events by specific tactile afferent responses. In other words, signals from tactile afferents mark transitions between consecutive action phases. The planning and control of manipulation in the brain is centered on the mechanical events that mark transitions between consecutive action phases [72]. This means impaired tactile sensibility will make manipulation difficult as the brain lacks the information about mechanical contact. Touch information (along with kinesthetic, vision and motor-feedback signals) is needed to obtain the 'body schema', which is an internal representation of body's structure [73]. The role of touch signals in 'reaching' is evident, as movements are planned

in spatial coordinate frames that are referenced to different parts of the body or to the body schema.

The correct grasp of an object requires fine control of not only the strength of finger muscle activation, but also of its temporal course or the duration, in various phases of grasp. Lack of tactile sensing lengthens the duration of the finger-opening phase of the grasp, thereby impairing the control of grasp [74]. Thus, tactile information is possibly used in getting minimal duration for various phases, or in other words, for the time optimization of various phases of the movement. The discharge from specific receptors at the beginning and the end of a movement can be used to compute grasp time for various phases and thus, the grasp temporal parameters can be optimized [9]. In this context, taxels (i.e. touch sensing elements) that are able to record dynamic events could be helpful in robotics. Tactile information from fingertips has also been shown to contribute to the control of *timing* in sequential actions such as playing a piano or tapping in synchrony to an external signal [75]. Thus, a variety of information about real-world objects is obtained through cutaneous sensing.

However, it should be noted that humans system is complete, multi-level integrated system and 'sense of touch' is not isolated. Multiple sensory information from several sensory modalities like touch, vision, hearing, etc., is needed to perceive a stimulus. Sometimes the sensory modalities compete (for example, when attention comes into play), and at other times, the whole is an integrated combination of the different inputs. Even if a single modality is involved, the perception of an object can be due to a combined contribution of its sub modalities. As an example, human ability to discriminate differences between 2D angles depends on both cutaneous and proprioceptive feedback [76]. The combination and integration of sensory information from multiple sources is key to robust perception, as it maximizes the information derived from the different sensory modalities and improves the reliability of the sensory estimate. Examples involving multiple sensory information include, the perception of roughness and moistness of surfaces modulated by the frequency content of auditory feedback [77], and the perception of size [78] and shape [79] with improved reliability obtained by integrating visual and haptic information in a statistically optimal fashion. Similarly, both vision and proprioception provide information about position of hand in space [80]. A simple task as reaching for a glass of water requires vision for location of the glass, touch for finer details about the physical properties of the glass, proprioceptive information for the posture and so on. Haptically and visually acquired size-related information may influence the feedforward or anticipatory control of forces during loading and transitional phases of precision grip [81]. Thus, the design of any artificial tactile sensing for robots should also take into account the presence of other sensing modalities and their combined contributions in achieving a common goal.

3.6 Skin Mechanics and Tactile Sensing

Skin acts as a medium through which surface indentations are converted into stresses/strains and further coded as neural signals by various receptors. Skin is multilayered, nonlinear, nonhomogeneous, and viscoelastic. In an adult human, the skin is spread over a surface area of around $\sim$1.8 m^2 and weighs around 4.1 kg [82]. The thickness of skin in adult humans vary between 0.6–0.8 mm and the Young's modulus is around 4×10^5 N/m^2 [83]. Geometrically and structurally, it is a complex mechanical system supported on a deformable system of muscles and fat [51]. The stiffness of various skin layers significantly vary, with epidermis being considerably stiffer than the dermis (the Young's modulus of base layer i.e. epidermis is 10–10000 times that of dermis) [12]. With such properties, the skin mechanics is bound to play an important role in the tactile perception.

The role of epidermal–dermal stiffness difference, and intermediate ridges (the undulating epidermal tissues that descend into the epidermal–dermal junction, see, Fig. 3.2), studied through continuum mechanics or finite element modeling shows the concentration of stress on the ridge tips. The concentration of stress improves the capability to distinguish different test indenters and enhances the capability to differentiate their finer details [12]. Interestingly, the tactile receptors (Merkel Cells) are also located near to the points where stress is concentrated. The presence of physical interlocking between the epidermis and dermis layers of skin helps in resisting any tendency of their relative sliding over each other also creates a filtering mechanism that distributes forces and stresses from their point of application [13]. Such a filtering mechanism also has considerable impact on the spatial resolution.

The presence of intermediate ridges and their role in magnifying the tactile signals by way of micro-lever action (or Cauna's model, or lever arm mechanism) has been mentioned earlier in this chapter. The mechanism postulates that the papillary ridge and the underlying intermediate ridge operate as single unit, with the intermediate ridge acting as a lever that magnifies the indentation imposed at the papillary ridges [11, 51, 84]. Intermediate ridges should not be confused with papillary ridges or fingerprints that are basically the external parallel whorls. However, the center of each papillary ridge protuberance lies directly above the center of each intermediate ridge (see, Fig. 3.5(a)) [12]. The concept of lever arm mechanism is shown in Fig. 3.5(b)–(c). In response to the indentation applied at the papillary ridge, the intermediate ridges tilt outward as shown in Fig. 3.5(b)–(c). The direction and movement of intermediate ridges tip deep in the skin is thus controlled by the force and/or displacement applied at the papillary ridges. As a consequence, the intermediate ridges act as mechanical amplifiers and converts the small displacements at papillary ridges into larger at the tip of intermediate ridge. However, finite element studies indicate very little involvement of papillary ridges in such mechanism [84]. The ability to detect very small asperities, (e.g. 1 μm) edge), has been suggested due to the lateral deformation of papillary ridges [51, 85]. Papillary ridges improve gripping [86] and the tactile sensitivity of Pacinian corpuscles (thus, helping us feel fine texture) [29]. A number of attempts have been made to model such mechanical behaviors of the skin [12, 15, 86, 87].

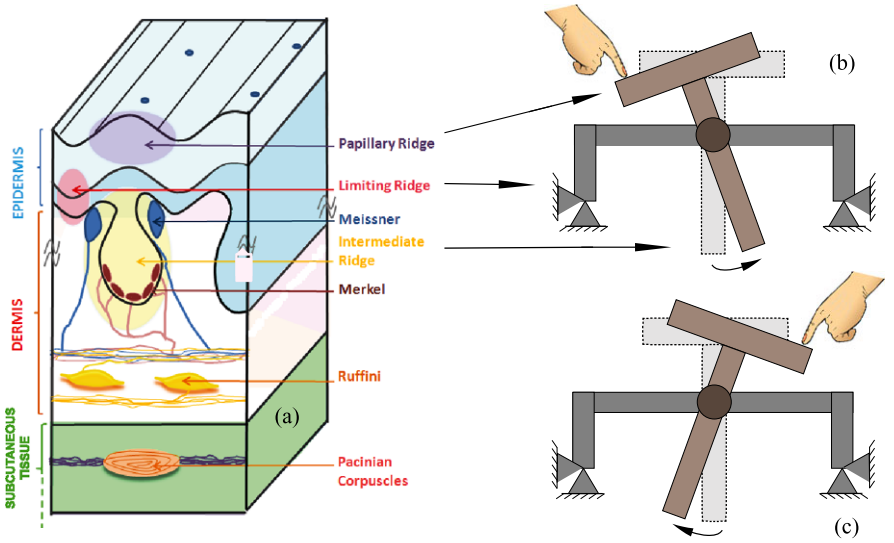

Fig. 3.5 (**a**) The glabrous skin structure showing various microstructures [30]. Though Ruffini afferents are shown here, recent studies point toward their presence in the hairy skin of human hand and not in the glabrous skin [88, 89]; (**b**)–(**c**) The lever arm mechanism showing the displacement of the tip of intermediate ridge as a result of small displacement at the papillary ridge

3.7 Design Hints for Robotic Tactile Sensing System

Following above discussion on human tactile sensing system, some basic design criteria can be formulated for tactile sensing in a general robotic system. A few such attempts have been reported in the literature [90–94], and some of their findings are also included in following design hints:

(a) *Spatial Properties:*

- The presence of varied and distributed receptors having sharp division of functions calls for using different kinds of miniaturized artificial sensors—each optimally measuring a particular contact parameter (though each may partly contribute to detection of other parameters as well). The multi-functionality i.e. ability to measure more than one contact parameter (e.g. contact force and hardness detection [95], tactile and thermal sensor [96]), is desired. The number of such sensing elements may depend on the body site where tactile sensors (or array of tactile sensors) are intended to be placed.
- The spatial resolution of the tactile sensors, distributed or arranged in an array, should be according to the body site. For a realistic contact feeling, the spatial resolution need not be higher than suggested by the two-point discrimination threshold. Thus, for body sites like fingertips, the spatial resolution should be about 1 mm—which translates to an approximately 15 × 10 element grid on a fingertip sized area—and for less sensitive sites like palm and shoulders it could be as high as 5 mm.

- Even if the spatial resolutions indicated by tests such as two-point-discrimination are sufficient for realistic contact feeling, the collective data from different mechanoreceptors makes it possible to detect fine surface textures down to 40 μm. This suggests that the overall performance can be improved by suitably handling the collective data from various sensors.

(b) *Sensor Performance:*

- The sensors should demonstrate high sensitivity and broad dynamic range. Normal manipulation involves forces in the range of 15–90 gm. wt. [46, 47] and 90% of the mechanoreceptors can detect forces as low as 85 mN applied on a 1 mm^2 area [38]. Considering involvement of tactile sensors in various exploratory tasks, a force sensitivity range of 1–1000 gm. wt. (∼0.01–10 N) and a dynamic range of 1000:1[7] are desirable [97]. However, in case of robotic applications, the sensitivity of sensors must also be such that robot does not detect its own motion.
- In addition to the magnitude, the touch sensors should be able to measure the direction of force. This is important because robots, in general, do not have a prior model of real world objects and they need to use their limbs to contact and learn about the object.
- Tactile sensors should be able to detect and measure both static and dynamic contact events so as to capture both the transient and steady state parameters of a contact event. For instance, the shape detection requires measurement of both stress and rate of change of stress. More than one mode of transduction may be required to meet such requirements.
- The robotic tactile sensors should be fast and respond quickly. This is particularly important, if the feedback from tactile sensor is involved in the robotic control loop. The need to involve tactile sensing in control loop of robotic applications has been felt greatly due to insufficient contact information available from artificial muscles or kinesthetic sense alone. The signal frequency range to which different mechanoreceptors in human skin respond (Fig. 3.2) can be used to set the response time requirements of sensors. In general, for real time contact details, each touch element should have a response time of as fast as 1 msec. The same is also true for an array of tactile sensing elements. However, such conditions can be somewhat relaxed in case of whole body skin type of distributed tactile sensors.

(c) *Data Transfer, Representation, and Processing:*

- The contact information can be transferred via different paths with different transfer rates. The signals (mechanical) that require urgent attentions (e.g., in

[7]The levels at which contact forces should be resolved can also be obtained by the knowledge of the elasticity of the fingertip skin and minimum detectable skin displacement. Given that the elasticity of fingertip skin is roughly of the order of 10^3 N/m and the detectable skin displacement is of the order of 10^{-6} m (Fig. 3.2), one could conclude that the sensor should resolve 10^{-3} N.

feedback control) can be transferred via faster path. However, such an arrangement would probably increase the number of wires—which is undesirable in robotics.

- Schemes similar to the somatotopic maps in humans can be useful in robotics for effectively handling and utilizing the tactile data. Such representations can help in locating the tactile sensors 3-dimensional space—which may otherwise be labor intensive and error prone because positions of tactile sensors change with robot's postures.
- In humans, the information collected by every mechanoreceptor is not directly sent to the brain for processing. Instead some complex pre-processing takes place to fit the limited throughput of the nervous system. Thus, to reduce the amount of information transfer to the central processing unit, it is important for large tactile arrays or modules to have some level of preprocessing (data selection, local computation, etc.) at the sensory location. Such an architecture would free up "robot's brain" for more intelligent works. Alternately, it would allow scaling up the system to practically any number of sensors.

(d) *Skin Mechanics and Properties:*

- The tactile sensors may also be embedded into or covered with elastic material just like the receptors in the skin lying under different layers of skin. Although embedding the sensors in elastic material may introduce some blurring or filtering effects; the increase in contact area, as a result of such elastic covering, is helpful in manipulation.
- The elastic covering of the sensors may be designed to have ridge structure similar to that of intermediate and papillary ridges present in the skin. The mechanical amplification with such arrangements can also help in reducing electronic components (e.g. input amplifiers may not be needed) and hence simplifying the electronic circuitry. By concentrating the stresses on the sensing elements, such structures can also compensate the blurring effect of elastic cover. A textured pattern like papillary ridges on the surface of elastic material increases detectability [98]. Further, the elastic cover can also protect the sensor from damages.
- The tactile skin should be light in weight, thin and flexible. When distributed over the body, it should not significantly increase the diameter/thickness of robot link/part. With a total weight of around 4.1 kg and thickness in the range 0.6–0.8 mm, the adult human skin is spread over a surface area of around $\sim$1.8 m^2 [82, 83]. Assuming a uniform skin thickness of 0.7 mm all over the body, the weight of skin per unit volume in humans is 3.25 g/cm^3 and weight per unit area is approximately 0.223 g/cm^2. Achieving such low values with conventional methods can be challenging for the robotic tactile system. Developing electronics and sensing components using micro-/nano-structures such as micro/nanowires over few micron thick substrates could be one potential alternative route for developing the light weight electronic skin [99].
- Biological sensors derive information like, detailed contours of objects, because the skin is compliant and conforms to object. Thus, the robotic tactile

sensing structures should be robust, flexible, conformable, stretchable and soft, so that they can withstand harsh conditions of temperature, humidity, chemical stresses, electric field, sudden force or shock etc.

(e) *Others:*

- With a simple scratch, human skin can lose hundreds of cells, yet our bodies don't fail from such a loss. Other cells carry on while repairs are made. With trillions of modules (cells) per person, human tactile system (in fact whole body) is "modular" and we enjoy its benefits (in terms of fault tolerance) every day. The modular approach for robotic tactile sensing system could be advantageous not for fault tolerance, but also in terms of scalability, flexibility, simplicity, and portability etc.
- Linearity and low hysteresis are also desired. Although non-linearity can be taken care by inverse compensation, the same is difficult for hysteresis. Output from the tactile sensor should be stable, monotonic and repeatable. It is interesting to note that the human tactile sensing is hysteric, nonlinear, time varying and slow. However, the presence of large number of these 'technologically poor' receptors enables the central nervous system to extract useful information.

The requirements mentioned above are application dependent and thus should not be considered as definitive. Some of the design cues described above seem to be technologically challenging. Thus, technological and manufacturing issues like production of sensing devices with similar performance (repeatability across different fabrications), type and number of interconnects, and repeatability of response over time, etc. should also be considered while designing robotic tactile sensors or skin.

3.8 Summary

A number of studies have been described, showing how tactile signals are acquired and then used by the brain to explore, perceive and learn about objects—which eventually helps in manipulation, exploration and control. The aim of the discussion in this chapter is not to imitate human tactile sensing. Imitating a biological system may not be feasible due to technological constraints. And, even if it is feasible there is no guarantee that the solution will be optimal and robust. Imagine, for instance, aeroplanes flapping the wings? Another example, shown in Fig. 3.6, where imitation of human sense of touch is illustrated. In humans, the nerves from each receptor or group of receptors do not synapse until the spinal column, which indicates that there is one data channel per receptor. Such an arrangement works well for biological systems but what if the same is adopted for robotic tactile sensing—only wires will be seen around the robot, making it difficult for robot to do any effective work. Therefore, the purpose of this chapter is to understand how humans tactile sensing systems works, to use the acquired knowledge for defining the limits for robot tactile

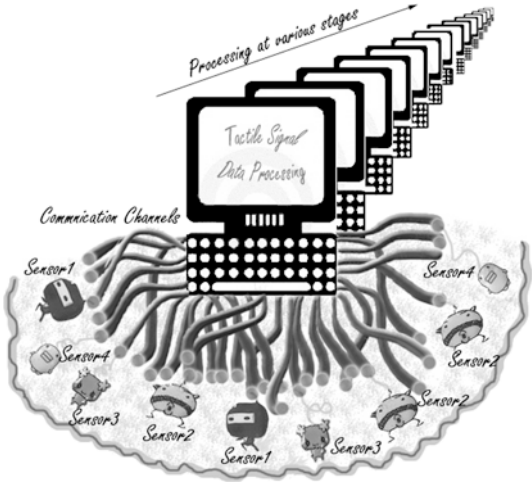

Fig. 3.6 The human sense of touch inspired tactile data processing

sensing and to see how technological solutions can be developed to obtain similar functionalities.

In summary, the ways in which biological systems acquire and process the sensory data to control behavior may not always lead to the best engineering solutions for robots. Nevertheless, they provide useful insights into how behaving organisms respond to dynamically changing environments, and also provide a comprehensive multi-level conceptual framework within which to organize the overall task of designing the sensors for robotic systems. Hence some design cues can be used as desiderata for the robotic tactile sensors, for arrays and more generally for building an electronic skin.

References

1. T.D. Crouch, *Wings: A History of Aviation from Kites to the Space Age* (Norton, New York, 2003)
2. R. Pfeifer, M. Lungarella, F. Lida, Self-organization, embodiment and biologically inspired robotics. Science **318**, 1088–1093 (2007)
3. G. Bekey, *Autonomous Robots: From Biological Inspiration to Implementation and Control* (MIT Press, Cambridge, 2005)
4. T.J. Prescott, P. Redgrave, K. Gurney, Layered control architectures in robots and vertebrates. Adapt. Behav. **7**(1), 99–127 (1999)
5. R.A. Brooks, New approaches to robotics. Science **253**, 1227–1232 (1991)
6. J.M. Wolfe, K.R. Kluender, D.M. Levi, L.M. Bartoshuk, R.S. Herz, R.L. Klatzky, S.J. Lederman, *Sensation and Perception* (Sinauer, Sunderland, 2006)
7. E.R. Kandel, J.H. Schwartz, T.M. Jessell, *Principles of Neural Science*, 4th edn. (McGraw-Hill, New York, 2000)
8. R.L. Klatzky, S.J. Lederman, Touch, in *Experimental Psychology*, ed. by A.F. Healy, R.W. Proctor. Handbook of Psychology, vol. 4 (Wiley, New York, 2003), pp. 147–176

9. R.S. Johannson, G. Westling, Roles of glabrous skin receptors and sensorimotor memory in automatic control of precision grip when lifting rougher or more slippery objects. Exp. Brain Res. **56**, 550–564 (1984)
10. D. Purves, G.J. Augustine, D. Fitzpatrick, W.C. Hall, A.-S. LaMantia, J.O. McNamara, L.E. White, *Neuroscience*, 4th edn. (Sinauer, Sunderland, 2008)
11. N. Cauna, Nature and functions of the papillary ridges of the digital skin. Anat. Rec. **119**, 449–468 (1954)
12. G.J. Gerling, G.W. Thomas, The effect of fingertip microstructures on tactile edge perception, in *First Joint Eurohaptics Conference on Haptic Interfaces for Virtual Environment and Teleoperator Systems* (2005), pp. 63–72
13. T.A. Quilliam, The structure of fingerprint skin, in *Active Touch: The Mechanisms of Recognition of Objects by Manipulation*, ed. by G. Gordon (Pergamon, Elmsdorf, 1978), pp. 1–18
14. R.S. Johannson, A.B. Vallbo, Tactile sensibility in the human hand: relative and absolute densities of four types of mechanoreceptive units in glabrous skin. J. Physiol. **286**, 283–300 (1979)
15. J.R. Phillips, K.O. Johnson, Tactile spatial resolution III—a continuum mechanics model of skin predicting mechanoreceptors responses to bars, edges and gratings. J. Neurophysiol. **46**(6), 1204–1255 (1981)
16. R.S. Johannson, U. Landstrom, R. Lundstorm, Responses of mechanoreceptors afferent units in the glabrous skin of the human hand to sinusoidal skin displacements. Brain Res. **244**, 17–25 (1982)
17. A.B. Valbo, R.S. Johannson, Properties of cutaneous mechanoreceptors in the human hand related to touch sensation. Hum. Neurobiol. **3**, 3–14 (1984)
18. R.S. Dahiya, G. Metta, M. Valle, G. Sandini, Tactile sensing—from humans to humanoids. IEEE Trans. Robot. **26**(1), 1–20 (2010)
19. R.S. Johannson, J.R. Flanagan, Tactile sensory control of object manipulation in humans, in *Somatosensation*, ed. by E. Gardner, J.H. Kaas. The Senses: A Comprehensive Reference, vol. 6 (Academic Press, San Diego, 2008), pp. 67–86
20. J.M. Loomis, S.J. Lederman, Tactual perception, in *Handbook of Perception and Human Performances*, vol. 2 (Wiley, New York, 1986), p. 2
21. S. Weinstein, Intensive and extensive aspects of tactile sensitivity as a function of body part, sex and laterality, in *The Skin Senses* (Thomas, Springfield, 1968)
22. K.O. Johanson, J.R. Phillips, Tactile spatial resolution. I. Two-point discrimination, gap detection, grating resolution, and letter recognition. J. Neurophysiol. **46**, 1177–1192 (1981)
23. J.C. Craig, Grating orientation as a measure of tactile spatial acuity. Somatosens. Motor Res. **16**(3), 197–206 (1999)
24. J.C. Craig, K.B. Lyle, A comparison of tactile spatial sensitivity on the palm and fingerpad. Percept. Psychophys. **63**(2), 337–347 (2001)
25. J.M. Loomis, On the tangibility of letters and braille. Percept. Psychophys. **29**, 37–46 (1981)
26. J.C. Craig, J.M. Kisner, Factors affecting tactile spatial acuity. Somatosens. Motor Res. **15**(1), 29–45 (1998)
27. S.J. Bensmaia, J.C. Craig, K.O. Johanson, Temporal factors in tactile spatial acuity: evidence for RA interference in fine spatial processing. J. Neurophysiol. **95**, 1783–1791 (2006)
28. J.B.F. Van Erp, Touch down: vibrotactile spatial acuity on the torso: effect of location and timing parameters, in *First Joint Eurohaptics Conference on Haptic Interfaces for Virtual Environment and Teleoperator Systems* (2005)
29. J. Scheibert, S. Leurent, A. Prevost, G. Debregeas, The role of fingerprints in the coding of tactile information probed with a biomimetic sensor. Science **323**, 1503–1506 (2009)
30. R.S. Dahiya, M. Gori, Probing with and into fingerprints. J. Neurophysiol. **104**, 1–3 (2010)
31. S.J. Lederman, Heightening tactile impressions of surface texture, in *Active Touch: The Mechanisms of Recognition of Objects by Manipulation*, ed. by G. Gordon (Pergamon, Oxford, 1978), pp. 205–214
32. G.A. Gescheider, Temporal relation in cutaneous stimulation, in *Cutaneous Communication Systems and Devices*, ed. by G. Gordon (Psychonomic Society, Austin, 1974), pp. 33–37

33. C.E. Sherrick, R.W. Cholewiak, Cutaneous sensitivity, in *Handbook of Perception and Human Performance*, ed. by K. Boff, L. Kaufman, J.L. Thomas (Wiley, New York, 1986), pp. 12-1–12-58
34. E.C. Lechelt, Temporal numerosity discrimination—intermodal comparisons revisited. Br. J. Psychol. **66**, 101–108 (1975)
35. J.C. Craig, X. Baihua, Temporal order and tactile patterns. Percept. Psychophys. **47**(1), 22–34 (1990)
36. L.A. Jones, S.J. Lederman, Tactile sensing, in *Human Hand Function* (Oxford University Press, Cambridge, 2006), pp. 44–74
37. R.S. Johannson, A.B. Vallbo, Spatial properties of the population of mechanoreceptive units in the glabrous skin of the human hand. Brain Res. **184**, 353–366 (1980)
38. R.S. Johannson, A.B. Vallbo, G. Westling, Thresholds of mechanosensitive afferents in the human hand as measured with Von Frey hairs. Brain Res. **184**, 343–351 (1980)
39. J.C. Stevens, K.K. Choo, Temperature sensitivity of the body surface over the life span. Somatosens. Motor Res. **15**, 13–28 (1998)
40. R.S. Johannson, I. Birznieks, First spikes in ensembles of human tactile afferents code complex spatial fingertip events. Nat. Neurosci. **7**(2), 170–177 (2004)
41. P. Jenmalm, I. Birznieks, A.W. Goodwin, R.S. Johannson, Influence of object shape on responses of human tactile afferents under conditions characteristics of manipulation. Eur. J. Neurosci. **18**, 164–176 (2003)
42. A. Berthoz, *The Brain's Sense of Movement* (Harvard University Press, Cambridge, 2000)
43. S.S. Hsiao, J. Lane, P. Fitzgerald, Representation of orientation in the somatosensory system. Behav. Brain Res. **135**, 93–103 (2002)
44. B.E. Stein, M.A. Meredith, *The Merging of the Senses* (MIT Press, Cambridge, 1993)
45. I. Birznieks, P. Jenmalm, A.W. Goodwin, R.S. Johannson, Encoding of direction of fingertip forces by human tactile afferents. J. Neurosci. **21**(20), 8222–8237 (2001)
46. R.H. LaMotte, M.A. Srinivasan, Tactile discrimination of shape: responses of slowly adapting mechanoreceptive afferents to a step stroked across the monkey fingerpad. J. Neurosci. **7**(6), 1655–1671 (1987)
47. R.H. LaMotte, M.A. Srinivasan, Tactile discrimination of shape: responses of rapidly adapting mechanoreceptive afferents to a step stroked across the monkey fingerpad. J. Neurosci. **7**(6), 1672–1681 (1987)
48. M.A. Srinivasan, R.H. LaMotte, Tactile discrimination of shape: responses of slowly and rapidly adapting mechanoreceptive afferents to a step indented into the monkey fingerpad. J. Neurosci. **7**(6), 1682–1697 (1987)
49. A.W. Goodwin, V.G. Macefield, J.W. Bisley, Encoding of object curvature by tactile afferents from human fingers. J. Neurophysiol. **78**(6), 2881–2888 (1997)
50. P.S. Khalsa, R.M. Friedman, M.A. Srinivasan, R.H. LaMotte, Encoding of shape and orientation of objects indented into the monkey fingerpad by populations of slowly and rapidly adapting mechanoreceptors. J. Neurophysiol. **79**, 3238–3251 (1998)
51. S.J. Lederman, D.T. Pawluk, Lessons from the study of biological touch for robotic tactile sensing, in *Advanced Tactile Sensing for Robots—Robotics and Automated Systems*, ed. by H.R. Nicholls, vol. 5 (World Scientific, Singapore, 1992), pp. 151–192
52. C.E. Connor, K.O. Johnson, Neural coding of tactile texture: comparison of spatial and temporal mechanisms for roughness perception. J. Neurosci. **12**(9), 3414–3426 (1992)
53. D.T. Blake, S.S. Hsiao, K.O. Johnson, Neural coding mechanisms in tactile pattern recognition: the relative contributions of slowly and rapidly adapting mechanoreceptors to perceived roughness. J. Neurosci. **17**(19), 7480–7489 (1997)
54. E.M. Meftah, L. Belingard, C.E. Chapman, Relative effects of the spatial and temporal characteristics of scanned surfaces on human perception of tactile roughness using passive touch. Exp. Brain Res. **132**, 351–361 (2000)
55. C.J. Cascio, K. Sathian, Temporal cues contribute to tactile perception of roughness. J. Neurosci. **21**(14), 5289–5296 (2001)

56. J.W. Morley, A.W. Goodwin, I. Darian-Smith, Tactile discrimination of gratings. Exp. Brain Res. **49**, 291–299 (1983)
57. S.J. Lederman, The perception of surface roughness by active and passive touch. Bull. Psychon. Soc. **18**, 252–255 (1983)
58. A.M. Smith, G. Gosselin, B. Houde, Deployment of fingertip forces in tactile exploration. Exp. Brain Res. **147**, 209–218 (2002)
59. A.M. Smith, C.E. Chapman, M. Deslandes, J.S. Langlais, M.P. Thibodeau, Role of friction and tangential force variation in the subjective scaling of tactile roughness. Exp. Brain Res. **144**, 211–223 (2002)
60. M.A. Srinivasan, R.H. LaMotte, Tactual discrimination of softness. J. Neurophysiol. **73**, 88–101 (1995)
61. K.O. Johanson, S.S. Hsiao, Neural mechanisms of tactile form and texture perception. Annu. Rev. Neurosci. **15**, 227–250 (1992)
62. F. Binkofski, E. Kunesch, J. Classen, R.J. Seitz, H.J. Freund, Tactile apraxia—unimodal apractic disorder of tactile object recognition associated with parietal lobe lesions. Brain **124**, 132–144 (2001)
63. A. Bodegård, A. Ledberg, S. Geyer, E. Naito, K. Zilles, P.E. Roland, Object shape differences reflected by somatosensory cortical activation in human. J. Neurosci. **20**(RC51), 1–5 (2000)
64. R.D. Howe, M.R. Cutkosky, Dynamic tactile sensing: perception of fine surface features with stress rate sensing. IEEE Trans. Robot. Autom. **9**(2), 140–151 (1993)
65. L.A. Jones, E. Piateski, Contribution of tactile feedback from the hand to the perception of force. Exp. Brain Res. **168**, 298–302 (2006)
66. S.L. Kilbreath, K. Refshauge, S.C. Gandevia, Differential control of digits in human hand: evidence from digital anaesthesia and weight matching. Exp. Brain Res. **117**, 507–511 (1997)
67. A.S. Augurelle, A.M. Smith, T. Lejeune, J.L. Thonnard, Importance of cutaneous feedback in maintaining a secure grip during manipulation of hand-held objects. J. Neurophysiol. **89**, 665–671 (2003)
68. R.M. Murray, Z. Li, S.S. Sastry, *A Mathematical Introduction to Robotic Manipulation* (CRC Press, Boca Raton, 1994)
69. G. Cadoret, A.M. Smith, Friction not texture, dictates grip forces during object manipulation. J. Neurophysiol. **75**, 1963–1969 (1996)
70. J.R. Flanagan, A.M. Wing, Modulation of grip force with load force during point-to-point arm movements. Exp. Brain Res. **95**, 131–143 (1993)
71. E. Oliver, M. Davare, M. Andres, L. Fadiga, Precision grasping in humans: from motor control to cognition. Curr. Opin. Neurobiol. **17**, 644–648 (2007)
72. R.S. Johannson, J.R. Flanagan, Coding and use of tactile signals from the fingertips in object manipulation tasks. Nat. Rev., Neurosci. **10**, 345–359 (2009)
73. M.S.A. Graziano, M.M. Botvinick, How the brain represents the body: insights from neurophysiology and psychology, in *Common Mechanisms in Perception and Action: Attention and Performance*, ed. by W. Prinz, B. Hommel (Oxford University Press, Oxford, 2002), pp. 136–157
74. M. Gentilucci, I. Toni, E. Daprati, M. Gangitano, Tactile input of the hand and the control of reaching to grasp movements. Exp. Brain Res. **114**, 130–137 (1997)
75. W. Goebl, C. Palmer, Tactile feedback and timing accuracy in piano performance. Exp. Brain Res. **186**, 471–479 (2008)
76. J. Voisin, Y. Lamarre, C.E. Chapman, Haptic discrimination of object shape in humans: contribution of cutaneous and proprioceptive inputs. Exp. Brain Res. **145**, 251–260 (2002)
77. S. Guest, C. Catmur, D. Lloyd, C. Spence, Audiotactile interactions in roughness perception. Exp. Brain Res. **146**, 161–171 (2002)
78. M.O. Ernst, M.S. Banks, Humans integrate visual and haptic information in a statistically optimal fashion. Nature **415**, 429–433 (2002)
79. H.B. Helbig, M.O. Ernst, Optimal integration of shape information from vision and touch. Exp. Brain Res. **179**, 595–606 (2007)

80. R.J. Van Beers, D.M. Wolpert, When feeling is more important than seeing in sensorimotor adaptation. Curr. Biol. **12**, 834–837 (2002)
81. A.M. Gordon, H. Forssberg, R.S. Johansson, G. Westling, Integration of sensory information during the programming of precision grip: comments on the contributions of size cues. Exp. Brain Res. **85**, 226–229 (1991)
82. H.R. Schiffman, *Sensation and Perception—An Integrated Approach* (Wiley, New York, 2001)
83. C. Escoffier, J. de Rigal, A. Rochefort, R. Vasselet, J.-L. Leveque, P.G. Agache, Age-related mechanical properties of human skin—an in vivo study. J. Invest. Dermatol. **93**, 353–357 (1989)
84. G.J. Gerling, G.W. Thomas, Fingerprint lines may not directly affect SA-I mechanoreceptor response. Somatosens. Motor Res. **25**(1), 61–76 (2008)
85. R.S. Johannson, R.H. LaMotte, Tactile detection thresholds for a single asperity on an otherwise smooth surface. Somatosens. Res. **1**(1), 21–31 (1983)
86. T. Maeno, K. Kobayashi, N. Yamazaki, Relationship between the structure of human finger tissue and the location of tactile receptors. JSME Int. J. **41**(1,C), 94–100 (1998)
87. K. Dandekar, B.I. Raju, M.A. Srinivasan, 3-D finite-element-models of human and monkey fingertips to investigate the mechanics of tactile sensing. J. Biomech. Eng. **125**(5), 682–691 (2003)
88. V.B. Mountcastle, *The Sensory Hand: Neural Mechanisms of Somatic Sensation* (Harvard University Press, Cambridge, 2005)
89. M. Pare, C. Behets, O. Cornu, Paucity of presumptive Ruffini corpuscles in the index finger pad of humans. J. Comp. Neurol. **456**, 260–266 (2003)
90. R.D. Howe, Tactile sensing and control of robotics manipulation. Adv. Robot. **8**(3), 245–261 (1993)
91. M.H. Lee, H.R. Nicholls, Tactile sensing for mechatronics—a state of the art survey. Mechatronics **9**, 1–31 (1999)
92. P. Dario, D. de Rossi, Tactile sensors and gripping challenge. IEEE Spectr. **22**(8), 46–52 (1985)
93. J. Dargahi, S. Najarian, Human tactile perception as a standard for artificial tactile sensing—a review. Int. J. Med. Robot. Comput. Assist. Surg. **1**(1), 23–35 (2004)
94. B.V. Jayawant, J.D.M. Watson, Array sensor for tactile sensing in robotic applications, in *IEE Colloquium on Solid State and Smart Sensors* (1988), pp. 8/1–8/4
95. M. Shikida, T. Shimizu, K. Sato, K. Itoigawa, Active tactile sensor for detecting contact force and hardness of an object. Sens. Actuators A, Phys. **103**, 213–218 (2003)
96. F. Castelli, An integrated tactile-thermal robot sensor with capacitive tactile array. IEEE Trans. Ind. Appl. **38**(1), 85–90 (2002)
97. P. Dario, Tactile sensing for robots: present and future, in *Robotics Review 1*, ed. by O. Khatib, J. Craig, T. Lozano-Perez (MIT Press, Cambridge, 1989), pp. 133–146
98. R.S. Fearing, J.M. Hollerbach, Basic solid mechanics for tactile sensing, in *IEEE International Conference on Robotics and Automation*, vol. 1 (1984), pp. 266–275
99. R.S. Dahiya, A. Adami, L. Lorenzelli, Fabrication of single crystal silicon mirco-/nanowires and transferring them to flexible substrates, in *The 37th International Conference on Micro and Nano Engineering (MNE 2011)*, Berlin, Germany (2011), pp. 1–2

Chapter 4
System Issues, Requirements and Expectations

Abstract This chapter presents a discussion on the development of a robotic tactile sensing system, keeping in view the tasks and the system related expectations and requirements. The expectations and requirements generally translate into the constraints (or vice-versa), which can be used to set various limits during the design phase of the tactile sensing system. A number of desired requirements are discussed.

Keywords Tactile sensing system · Artificial skin · Robotic tasks · Mechanical requirements · Electrical requirements · Interface electronics · Wiring complexity · Modular · Conformable · Embedded systems · Communication · Sensor fusion · Representation · Reliability · Sensor placement

4.1 Introduction

"The whole is more than the sum of its parts"—Aristotle. The overall performance of a system is dictated not only by individual components of the system, but also by how these components integrate to achieve a goal. The human sense of touch, discussed in the previous chapter, is a classical example in this context. The receptors (mechanoreceptors, thermoreceptors and nocioceptors) alone are not sufficient to perceive the real world objects via sense of touch. A number of other components of the somatosensory system are also involved in the perceptual task, to derive useful information, and if necessary, an action thereafter. Further, the human body is a complete, multi-level integrated system and hence the 'sense of touch' does not work in isolation. Various sense modalities operate in different ways, each playing a part in the overall perception of the stimuli. Sometimes they compete (for instance, when attention comes into play), and at some other time the whole is an integrated combination of the different inputs. The combination and integration of sensory information from multiple sources is key to robust perception as it maximizes the information derived from the different sensory modalities and improves the reliability of the sensory estimate.

Many questions would come to mind, if the functioning of robotic tactile sensing system is viewed from the perspective of human sense of touch. The most important, and relevant to this chapter, is how to (effectively) include tactile information in

R.S. Dahiya, M. Valle, *Robotic Tactile Sensing*,
DOI 10.1007/978-94-007-0579-1_4,

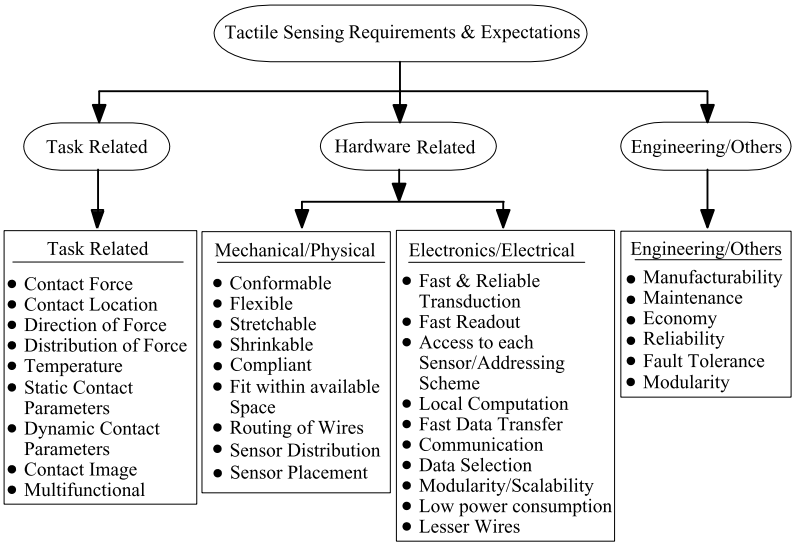

Fig. 4.1 The tactile sensing system requirements and expectations

robotic strategies. This requires not only the development of tactile sensors or sensing system, but also a plan for placing the tactile sensing hardware on the robotic platforms in such a way that robot's normal working is unaffected (or least affected). The development of a tactile sensing system is affected by a large number of constraints, including those related to the task (different sensor types are needed for detecting multiple contact parameters such as forces, pressures, contact, vibrations, temperature etc.), physical problems (placement and robustness of sensors, wiring challenges), hardware development, compatibility with existing hardware (if any), and availability of software etc. Some of these constraints or requirements are given in Fig. 4.1. Some of these issues are also discussed in [1–5]. To incorporate the tactile sense modality in robotics and to effectively utilize the acquired data, the tactile sensing system must therefore be designed keeping in view such constraints. Wherever technologically feasible, the design hints derived from the human sense of touch, and presented in the previous chapter, can also be used for this purpose.

4.2 Task Related Requirements

The task oriented requirements basically define the type of contact parameters that a tactile sensor is supposed to detect and measure when employed in robotic tasks such as (precise or dexterous) manipulation and control, exploration, response [6], and safe interaction [7] etc. Different types of sensors are needed to detect multiple contact parameters during various robotic tasks. Ideally, one would like to equip a robot with various types of tactile sensors and detect all possible contact parameters in a real world environment. However, this may not always be practical due to

technological bottlenecks. Even if it is possible, we may not always need such a solution simply because a robot is not always expected to be like humans. Consider, for instance, the temperature. It may not be the important contact parameter during manipulative task, whereas the same could be important during an exploratory task. Therefore, it is a good strategy to develop a robotic tactile system starting with the consideration of the most desired tactile parameters (and the type of tactile sensors) for the task in hand. A few robotic tasks and corresponding contact parameters of interest are given in the following paragraphs. For the sake of generality, the tasks classification by Cutkosky et al. [6] has been adopted for this discussion.

4.2.1 Response

The simplest use of tactile sensing is to detect if any body part is in contact or not with the environment and allow a robot to respond accordingly. Consider for instance, a mobile robot navigating in an unstructured environment or in a public place. The robot is supposed to find its way by avoiding obstacles or rather unpredictable movements of people. While doing so, some parts of the robot's body may come in contact with the obstacles and therefore the first requirement for these types of tasks is the presence of suitable sensors all over the body i.e. whole body sensing. The next point would be to find the suitable type of sensors needed to avoid collision. Assuming that the robot possesses only the tactile sense modality, the simplest solution is to use switch like sensors. However, the corrective action in this case will take place only after contact has been made—which, at times can be damaging as contact force strength is unknown. Another approach is to anticipate the collision and act accordingly. The range or proximity sensors are ideal for this purpose as corrective action can be taken without even contacting the object. However, in normal practice the requirements lie somewhere between these two extremes i.e. robot may (intentionally or accidentally) come in contact or "soft contact" with the obstacle and corrective action is taken well before the contact force reaches damaging levels. For this purpose, the tactile sensors must be able to measure the strength of the contact force.

4.2.2 Exploration

In exploratory tasks, the tactile sensors are required to compute the following properties of objects: (a) structural properties: size, shape, and weight, (b) surface properties: hardness, elasticity, texture, friction and temperature, and (c) functional properties such as motion of body parts. The exploratory interaction of robots with environment involves both static and dynamic contact forces. Thus, tactile sensors should be able to detect both static and dynamic contact events. This is important for obtaining information like friction, stickiness, texture, hardness and elasticity.

Recognizing the importance of measuring dynamic events, the sensors suitable for detecting dynamic events like stress changes, slip and other temporal contact events have been reported in literature [8, 9].

While exploring objects in an unstructured environment robot's body may bump into an object or an obstacle, causing considerable harm to itself and to the object. If the robot body were to move only under the guidance of tactile sensors (requiring physical contact), bumping into a suddenly discovered obstacle would spell a disaster, since the corrective action can be taken only after the collision. Once the collision has occurred, it would be too late to carry out an avoiding maneuver. The likelihood of occurrence of such an unpleasant situation are higher due to the fact that today's robots bodies are generally made of steel or aluminum, and sometimes of hard plastic. A solution in such situation could be using 'soft-touch' or proximity sensing. Therefore, in addition to conventional tactile sensors, detection of soft-touch should also be explored.

4.2.3 Manipulation

In manipulation and control tasks, the tactile information is used as a control parameter [10–12] and the required information typically includes contact point estimation, surface normal and curvature measurement and slip detection [13] through measurement of normal static forces. A measure of the contact forces allows the grasp force control, which is essential for maintaining stable grasps [14]. In addition to magnitude, the direction of force is also critical in dexterous manipulation to regulate the balance between normal and tangential forces to ensure grasp stability—the so-called friction cone [15]. For full grasp force and torque determination, shear information is also required [16, 17]. Shear information is useful in determining the coefficient of friction and in getting a unique surface stress profile when the sensor is covered with elastomeric layer [18]. Besides, force related contact parameters, the tactile sensor should also measure material properties such as hardness and stiffness [19].

A common sensor requirement for all robotic tasks is that the tactile sensor must be responsive and overall the system must be fast. The sensors must be responsive enough to help carry out the tasks successfully. At the same time they should not provide self-induced signals i.e. the more responsive the sensor, the more likely the robot is to detect its own movements. As sensors become increasingly sensitive, and cover larger portions of the robot body, distinguishing between self-induced activations and other activations becomes a necessity. Quite often, detecting some of the above contact parameters involves complimentary inputs from other sensory modalities (e.g. tactile and proprioception) and also may have to share the hardware support. Therefore, the design of a tactile sensor system should also take into account the constraints from the robotic system.

4.3 Hardware Related Requirements

Once the task related requirements and the type of contact parameters to be detected are known, the implementation of the tactile sensing system can be done in a top–down fashion. In the top–down approach, a robotic system is assumed to be present and a tactile sensing system (or the robotic sub-system) is to be developed keeping in view the required performance related constraints and the compatibility with existing hardware on robot, including sensors belonging to other sensory modalities such as cameras.[1] The assumption makes sense as many existing robotic platforms (e.g. humanoid platforms such as iCub, ASIMO, Robonaut, HRP2 and many more) are already equipped with the sensing hardware belonging to sensory modalities other than tactile sensing. From a robotic system point of view, this is an important step in effectively utilizing the tactile data.

The robotic hardware includes both mechanical and electrical/electronic components—each posing some constraints to the development of the other. For instance, the space constraints in fingertips call for miniaturization of sensors and related hardware. The requirements and features of the tactile sensing system are also strongly affected by such constraints. The mechanical and electrical/electronic constraints or requirements of a tactile sensing system are discussed separately in this section.

4.4 Mechanical/Physical Requirements and Expectations

The mechanical/physical requirements of the tactile sensing system, shown in Fig. 4.1, include features like conformability and stretchability of the sensing structures, spatial distribution and placement of sensors, and skin weight etc. The utility and methods of obtaining these features are discussed in this section.

4.4.1 Flexibility and Conformability

The tactile sensing structure should be flexible and conformable so that it can easily cover the arbitrarily curved body parts of a robot. This is important for better integration of tactile sensing structures on a robotic platform—more so in case of whole body tactile sensing i.e. when tactile sensors are distributed all over the body. The tactile sensing structures woven like fabrics would be an ideal solution as they would be extremely flexible, bendable, conformable and stretchable. However, present day

[1] Developing tactile sensing systems along with the robotic platforms and their sensing hardware will be relatively simpler as many design constraints or boundary conditions can be relaxed. In this sense, the above discussion presents a worst case scenario.

solutions are far from this ideal scenario. Perhaps, with suitable materials and engineering, this could become a reality in near future. The available mechanically flexible tactile sensing solutions typically use standard Printed Circuit Boards (PCB) on rubber like substrates or flexible PCBs as substrate. The off-the-shelf sensing and electronic components are soldered to these PCBs. A few examples of such solutions include tactile skin patches having triangular [20, 21], hexagonal [22] and the tree or comb shaped modules [23, 24]. The degree of flexibility, in these cases, depends on the thickness of the substrate e.g. Kapton. Typically the bending radius of flexible PCBs is large and therefore such solutions are only suitable for body parts like arms of a humanoid. However, extreme flexibility of tactile sensing structures is needed for body parts such as fingertips of a humanoid.

The flexibility of a sensing structure does not always ensure conformability in all directions. Many available tactile sensing structures can bend only along one axis and hence can conform to surfaces such as a cylinder, which approximates the arm of a robot. Whereas, there is a good possibility that one might need to cover a surface that looks like a hemisphere. Consider, for instance, the body parts like shoulders of a humanoid robot. Certainly, many simple flexible PCB based solutions will fail in such cases—except when the PCBs are shaped in particular fashions. For instance, consider the tactile sensing structures that are given triangular or hexagonal (which is a set of six triangles) shapes. Given the fact that triangulation techniques result in a good reconstruction of 3D surfaces, it should be easy to cover the whole body with the tactile sensing modules having triangular shapes. The few examples of tactile sensing structures that can conform to spherical surfaces include, triangular [20, 21], hexagonal [22] and tree or comb [24] shaped structures.

At the beginning of the design stage, one might therefore consider engineering issues such as shaping and placing the tactile sensing modules in such a way that a set of them conform well to the random 3D surfaces. It may be difficult to do the same using hand calculations (as typically done in robotics), especially in case of whole body sensing, and therefore programming tools could be employed for obtaining suitable shapes and the positions for the tactile sensing modules on robot's body. For this purpose, one could start from a CAD (Computer Aided Design) model of the 3D body parts of a robot, unfold the 3D surface and extract the 2D representation, assemble the sensing modules (irrespective of their shapes) in such a way that they cover maximum 2D area, and then fold the assembly of tactile sensing modules to reconstruct the 3D surface of the robot's body. Consider, for instance, the Fuller map[2] or the AirOcean World Map [25] that is obtained by projecting the globe onto the surface of a polyhedron, which can be unfolded and flattened to two dimensions finally resulting in a flat map of the entire surface of the Earth. In case a large 2D surface (with tactile sensors distributed all over) is available, a desired 3D surface

[2]The Fuller Projection is rendered by juxtaposing a grid of triangles on the globe and transferring the data to corresponding triangles on an unfolded icosahedron. The Fuller Projection, or Dymaxion Map, created by Buckminster Fuller, solves the age-old problem of displaying spherical data on a flat surface using a low-distortion transformation. The map also shows the world's land masses without interruption.

can be obtained by simply cutting the 2D surface in a particular fashion and folding it to obtain the final shape. All this can be done by using various algorithms reported in literature and the programming tools based on them [26]. With maximum area coverage as the goal, the process can be useful in deciding the suitable shapes of tactile sensing modules, their suitable placement on the robot's body and also routing of the wires.

4.4.2 Compliance

Compliance or the ability to comply with deformation forces is yet another feature that a tactile sensing structure should possess. For sometime in the past, it was felt that compliance introduces positional uncertainty and should therefore be avoided. However, compliant surfaces facilitate a larger contact area and hence they provide greater amount of contact information. Compliance also helps in safe robotic interaction. For example, consider a robotic device moving in an unstructured environment with no vision sensors. It would not know of an impending collision up until the moment the collision takes place. Since the body has a mass, it is difficult for robotic device to stop instantaneously, regardless of how slowly the robot is moving at the moment of collision. For a tiny fraction of time, robotic device will continue moving in the direction of its prior motion. In such a situation the damage can be prevented if the surface of robot's body (or the robot's body itself) is compliant, as the residual motion will be absorbed by the soft and compliant surface. Sometimes soft coverings are used to introduce small degree of compliance, as discussed in next paragraph. This also enables skin to perform tactile detection in areas not covered directly by a tactile sensor, since the deformation of the flexible substrate propagates the tactile signal to the sensor, allowing for interpolation. Thus the compliant sensors, sensors on compliant substrates, sensors on a rigid substrate but with a compliant cover layer or the sensors embedded in compliant substrates, all have the potential to extract three-dimensional information such as the shape of the object that indents their surface. There is also an increasing awareness that the improved grip and better sensing capabilities of compliant sensors can provide significant advantages for various tasks, including object recognition and dexterous manipulation. Considering these advantages, the tactile sensing structures should have compliant surfaces or compliant surface coverings. However, one also needs to take into account of how much compliance is suitable.

Compliance can be introduced partly by embedding the tactile sensors into (or covered with) elastic materials such as poly(dimethylsiloxane) (PDMS). This is similar to the presence of receptors at different depths in the human skin. For sensors embedded under or within the elastic substrates, the covering additionally affords some level of protection. A drawback of embedding the sensors in an elastic material is the introduction of blurring or spatial filtering effects. Using Finite Element Modeling, Shimojo [27] analyzed the mechanical spatial filtering effect of different types and thicknesses of elastic cover materials and presented the relationship

between the spatial filter gain and the properties of the elastic material. Shimojo concludes that the mechanical spatial filtering effect is a serious factor in utilizing the high spatial resolution (less than 1 mm) sensors. Patterning the soft cover with structures like the fingerprints in human fingers can be used to offset such blurring effects. As discussed in the previous chapter, for long the fingerprints are known to enhance tactile sensitivity in humans. Using a biometric force sensor having a soft cover patterned with parallel ridges, mimicking the fingerprints, Scheibert et al. [28] presented a circumstantial evidence of how fingerprints enhance the tactile sensitivity in artificial tactile sensing solutions.

4.4.3 Stretchability

The tactile sensing structures are also required to have features such as stretchability—especially for body parts such as knees, elbows and cheeks of humanoids. Stretchability also improves conformability of tactile sensing structures. The tactile sensing structures can be made stretchable in at least two ways:

- Using stretchable wires/interconnects to connect tactile sensors in a module or to connect various modules in a skin patch.
- Developing tactile sensors that are intrinsically stretchable.

The wires/interconnects can be made stretchable either using suitable material or with some engineering techniques. Consider, for instance, the wire that connects a telephone receiver to its base. The spiral shape of the wire makes it stretchable (rather expandable) and the telephone receiver can easily be moved away from the base. Similar techniques can be employed for obtaining a stretchable tactile skin. In fact, the method has recently been adopted for realizing large-area tactile skin with expandable spiral electrodes, which are obtained by winding the copper wires around an elastic nylon line [29]. Yet another interesting engineering technique for obtaining stretchable or expandable wires is to give wavelike shape to the conductors. To see how wavelike conductors can expand, one can perform a simple experiment: take a paper and cut a narrow sinusoidal (i.e. wavelike) ribbon or strip. One can observe that the two ends of the ribbon can easily move away from each other. However, the same would not be possible if the ribbon or strip were straight. The stretchable interconnects based on similar approach have recently been reported by Huyghe et al. [30]. Another strategy for stretchable conductors, reported in the recent past, is to fabricate wavy or net-shaped conductive structures by releasing a pre-strained elastic substrate with conductive materials lying on it. Taking advantage of this technique, different stretchable conductors, such as metal-coated net films, wavy one-dimensional metal ribbons or two-dimensional metal membranes have also been demonstrated [31]. These techniques can be quite useful in case of flexible tactile sensing chips for body parts such as fingertips.

A truly stretchable conductor should actually be like rubber—stretching and regaining the original shape after release, and all with minimum or zero variation in

conductivity. A very few examples of this kind of stretchable conductors include the elastic conductors based on Single Walled Carbon Nano Tubes (SWNT)-PDMS composite films embedded in PDMS or coated with dimethylsiloxane-based rubber [32, 33]. The nanotubes carry the electricity, and the rubber provides the flexibility. These conductors allow uniaxially and biaxially stretching of 70–100%—without mechanical or electrical damage. Microfluidics approach is yet another interesting alternative that has been developed in recent years to obtain stretchable conductors. In this approach the wires are replaced with conductive liquid confined in microfluidic channels [34]. Thus far, these approaches have not reached the stage when they can be used for large area sensing in robots. Nonetheless, with more efforts in material engineering they could result in some interesting alternatives.

The other alternative for having the stretchable tactile sensing structure is to build the tactile sensors that are intrinsically stretchable. A few interesting examples include the stretchable skin based on the principle of Electrical Impedance Tomography (EIT)—the noninvasive technique used in medical applications [35, 36]. An interesting feature of EIT based sensors is that electrodes are present on the borders or periphery of the sensing material. This means that the joints where such sensing structures are placed will work without hindrance (e.g. due to lack of stretchability of the wires) during stretching. Having stretchable tactile sensing solutions with no (or minimum) connecting wires in the contact region would simply be great—even if it is difficult to achieve in practice. The stretchable fabrics with knitted tactile sensing materials or the tactile sensitive fabrics are other methods for obtaining stretchable tactile sensors [37, 38].

4.4.4 Sensor Distribution and Placement

The sensor distribution should vary according to the spatio-temporal sensitivity and pressure thresholds requirements of various body sites. There is a general agreement that miniaturized sensors are needed to obtain higher spatial resolution. But, is it always necessary to have sensors that result in higher spatial resolution? The computational means such as *super-resolution algorithms* [39], often used in digital image processing to enhance the resolution of images, can be adopted to obtain higher resolution even if the sensors themselves have low resolution.

Sensors such as Force Sensing Resistors (FSR) or larger sensors often result in low spatial resolution. In such cases techniques such as super-resolution algorithms can be employed to obtain higher spatial resolution. This techniques involves superimposition of multiple images of the contact object (obtained by actively touching the object) in such a way that a single higher-resolution image is obtained [40]. The method, depicted in Fig. 4.2, involves geometrically aligning the images, taken from slightly different orientations at different times by various sensors, into a common reference frame. Simple rotation and translation are used to transform the coordinate system of an image (e.g. I_2) to that of a reference image (e.g. I_1). In case of a robot, the transformations between multiple tactile images can be controlled easily

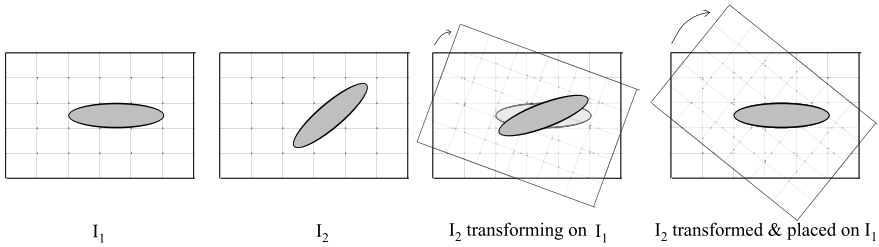

Fig. 4.2 The translation and rotation transforms to obtain a high resolution image using super-resolution techniques [40]

with the awareness of its pose (through modeling or active calibration or through direct measurement etc.). Each taxel in Fig. 4.2 has a unique index associated with it according to its coordinates, e.g. the uppermost left hand taxel is (0,0) and the lowermost right-hand taxel is (3,5). After transformation, the pixels in I_2 get new indices to let the oval correspond with the oval in I_1. The new indices are given by:

$$x_{new} = x\cos\theta + y\sin\theta + tx \tag{4.1}$$

$$y_{new} = -y\sin\theta + y\cos\theta + ty \tag{4.2}$$

The variables tx, ty, and θ must be determined with an optimization technique to get I_2 to be transformed to fit onto I_1. A measure of how well they fit together is obtained by subtracting the two matrices from each other, taking the square of each element and then adding up the remaining element values. If the two matrices are an exact fit, the answer will be zero. Mathematically this can be written as:

$$\chi^2(x, y) = \sum_{i=1}^{N}\left[I_1(x_i) - I_2\left(f\left((x_{new})_i\right)\right)\right]^2 \tag{4.3}$$

This produces a single number indicating how well these two images are aligned. An optimization technique is then used to minimize the number $\chi^2(x, y)$. The variables tx, ty, and θ are adjusted after each iteration of the optimization step. Thus, the minimum value will be the optimum fit. Such technique is usually necessary in image analysis tasks that integrate the information obtained from a combination of data sources, e.g. image fusion, change detection, multichannel image restoration and modal-based object recognition etc.

From the system point of view, the approaches such as the one discussed above are advantageous as a smaller number of sensors means reduced wiring complexity. The smaller amount of data from the low resolution sensors eases up the bandwidth and processing requirements of the tactile system. The approach may therefore result in an overall cost reduction. However, due to the fact that the contact parameters could change by the time a second image is scanned, such techniques are less useful for measuring dynamic contact parameters.

The placement of tactile sensors on the body might affect the quality of measurements. In fact, by suitably placing an appropriate number of sensors over body

parts, one may obtain almost the same quality of measurements as with a large number of sensors. Consider, for instance, the approach adopted by Murakami et al. [41] to effectively place the tactile elements for grasp type recognition. First, a human subject performs different types of grasps, and contact information is obtained from the tactile elements installed uniformly on a glove. The mathematical decision method is then used to select effective placement of the tactile elements using the contact information. The outcome of this study shows that the densities of sensing elements on the thumb and the index finger are higher than those on the other fingers and the palm. Not only does the placement decided by the presented method requires a small number of tactile elements (40 tactile elements), it also achieves a recognition performance as high as placements consisting of many elements (160 tactile elements). Using an appropriate number of sensing elements makes it simpler to handle other issues such as wiring complexity, and data transmission. These observations highlight that it is not always necessary to imitate human cutaneous sensing—especially if the robot is required to perform a specific task. It should also be noted that the placement methods such as the one discussed above, are useful for specific applications or tasks in hand. The same placement of sensors may not work for other applications. The programming tools can be employed for placing the sensors or sensing modules on the skin patches in accordance with some other optimal criteria. For instance, in case programming tools yield multiple sensors placement configurations suitable for a task, the one resulting in minimum wires can be opted.

The above discussion on sensor placement should not be confused with the one presented in the section 'Flexibility and Conformability'. The discussion here is about the location and number of individual sensors on a body part, whereas the previous discussion is about suitably positioning or orienting the sensing modules for maximum body area coverage.

4.4.5 Wiring Complexity

The wiring complexity is one of the major impediments in the effective integration of tactile sensing structures on a robot body. As the number of tactile sensors increases, so does the number of wires needed to address, acquire and transmit the tactile data. With a large number of wires, physical problems such as routing the wires through the articulated joints of a robot also come to the fore. With a number of motors and electronic components already present in the robotic shell, the available space for wires is limited.

The wireless communication could be an ideal solution to the wiring complexity. With wireless communication it is easier to use stretchable and flexible touch sensing arrays, as otherwise flexible and stretchable interconnects are required. Nonetheless, wireless communication presents some very limiting drawbacks in case of the robotic domain and its adoption has still to be adequately addressed (see Section on Transmission). If not using wireless communication, what are the other ways to solve or reduce wiring complexity? Primarily due to the aforementioned reasons of large number of wires and routing, the efforts must be made to:

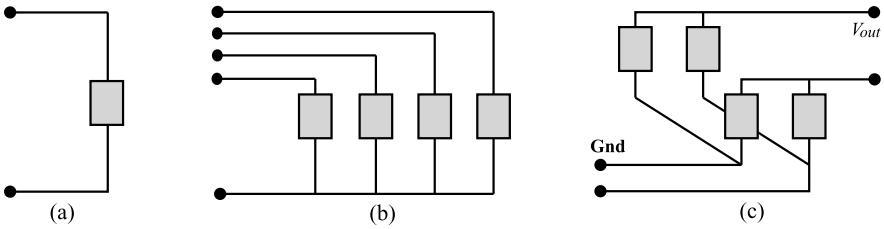

Fig. 4.3 Various schemes to read tactile sensors, (**a**) The scheme with each sensor having two terminals, (**b**) The scheme with all sensors having one common wire, (**c**) The row–column scheme

1. reduce the number of wires to acquire tactile data by using suitable addressing scheme, and
2. find innovative solutions for routing the wires.

The simplest wiring scheme, suitable for most of the two-terminal sensors (e.g. capacitive, piezoelectric, piezoresistive, etc.), requires two data wires for each sensor. This means that $2(n \times m)$ data wires are needed for an array of $(n \times m)$ sensors (Fig. 4.3(a)). Obviously, the scheme results in large number of data wires even for a small sized array. A simple way to reduce the number of data wires in this case is to use a common return wire for all the sensors in the array or module. In this way, $(n + m) + 1$ data wires are needed for an array of $(n \times m)$ sensors (Fig. 4.3(b)). The number of data wires can be further reduced by choosing row–column schemes to read the sensors in an array. For an array of $(n \times m)$ sensors, the row–column scheme requires $(n + m)$ data wires (Fig. 4.3(c)). The above comparison is based on data wires only. For further comparison one must take into account addressing wires too. It may be noted that the scheme for accessing an array of sensors depends also on factors such as the application, the transduction method etc. For instance, the scheme with two data wires for each sensor (differential mode) may be necessary in applications where noise pick-up is a problem.

Innovative solutions are needed to address the critical problem of wiring complexity. Unfortunately very few solutions, reported in the literature, have sought to directly address the issue. For instance, Nilsson [42] proposed an addressing scheme that considers the sensor elements as a series of analog filters, which share the same transmission line and their outputs are delayed temporally much like in a Charge Coupled Device (CCD) array—so that the responses from the sensing elements arrive sequentially at the sampling electronics. Following this technique, 16 tactile sensors require only three connectors—two for the signal carrier and one for the ground. The problem of routing wires and the number of wires are very much linked to each other. The increase in the number of wires certainly increases the problem of routing them suitably. On the other hand, intelligent routing can help in reducing the number of wires. Routing of wires has been a critical aspect in microelectronics and the automated strategies developed for routing in large scale integration can be useful for robotic skin. Not much has been done in this direction. With whole body tactile sensing in robots increasingly getting attention, it is hoped that this problem will get higher priority.

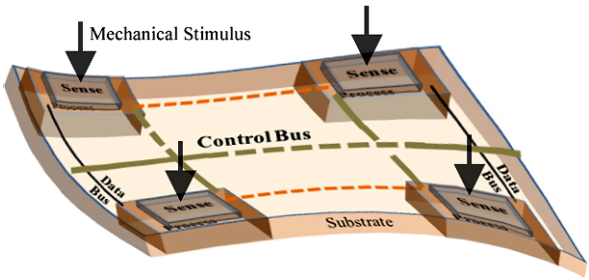

Fig. 4.4 The integration of sensing and electronic components, resulting in 'sensing and processing at the same place'

The wiring problem associated with reading large sensor arrays can also be reduced by incorporating the electronic components with the sensors or by modifying the electronic components to make them work like a sensors. Hybrid implementations, such as flexible PCBs/substrate with interconnections on them, are other alternatives. The shrinking dimensions of microprocessors also make it possible to mount devices for multiplexing, signal conditioning, local computation etc. in the immediate proximity of the sensors. In addition to reducing external wiring to the sensors, the integration of sensor and electronic components, as shown in Fig. 4.4, will result in improved sensor performance. A detailed discussion of such solutions is given in Part II of this book.

4.4.6 Other Mechanical/Physical Requirements

In addition to the above mentioned physical requirements, it is also important to look into issues such as the weight of the tactile sensing structure, the space needed for installation etc. The tactile sensing structures for various body parts are essentially three layered structures: (a) the outer layer to protect the layers underneath (b) the middle layer, where sensors and associated electronics are located, and (c) the inner insulating layer, which insulates the tactile sensing hardware from the electrical and mechanical noise coming from the robot body. Considering that the skin is present all over the body, the tactile sensing structure should be *light-weight* and should not contribute much to the total weight of a robot. Considering the human body as an example, the weight of skin of an adult human, discussed in previous chapter, is about 4.1 kg. This is about 6% of the total weight (around 70 kg) of the adult human. The surface area of the skin in an adult human is about 1.8 m^2 and the skin thickness varies between 0.5–0.9 mm [43]. Assuming these figures as reference, the tactile skin for the new ASIMO (Advanced Step in Innovative Mobility) [44] from Honda should weigh just 3.5 kg (the total weight of new ASIMO would be 57.5 kg, i.e. 54 kg for the humanoid and 3.5 kg for the skin).

The aforementioned mechanical/physical properties have always been on the list of desirable features of robotic tactile sensing systems. However, it is only recently that researchers have started reporting tactile sensing devices and structures possessing some of these features [2, 24, 35, 45].

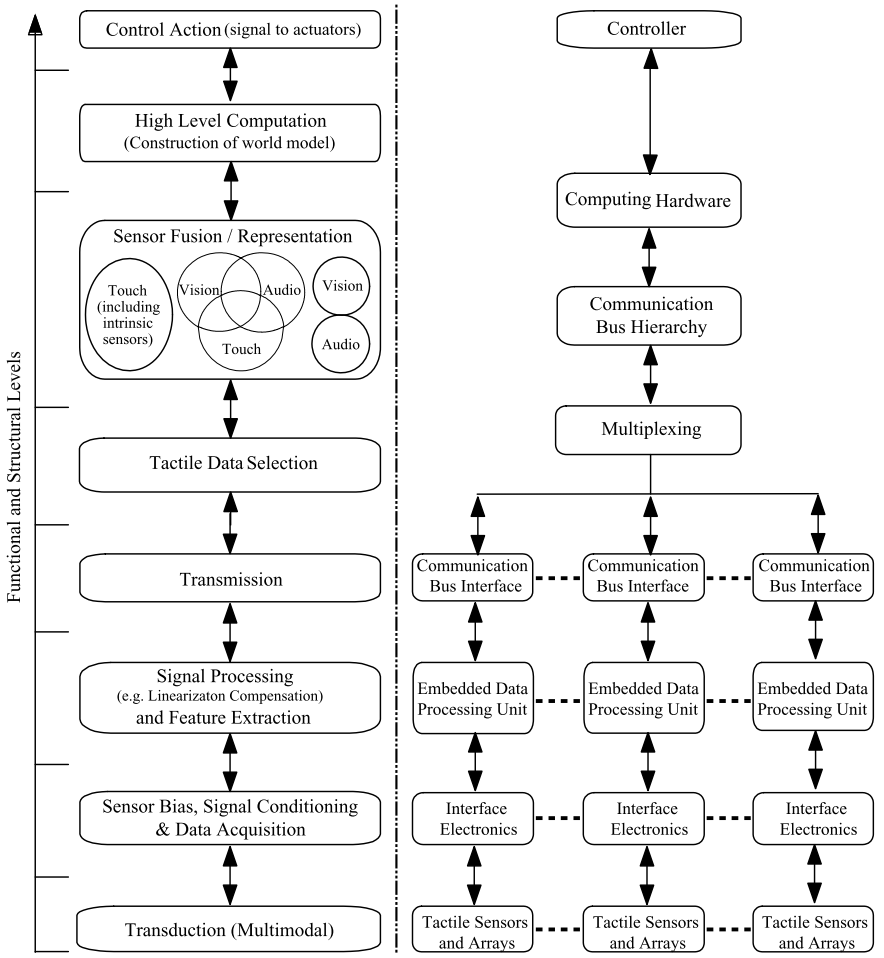

Fig. 4.5 The hierarchical functional (*left*) and structural (*right*) block diagrams of a tactile sensing system. The control loop can be closed at lower levels (e.g. in reflexes). The *arrows* from bottom to top show the direction of tactile data transfer and from top to bottom show the addressing of sensors

4.5 Electronics/Electrical Requirements

After viewing the robotic system in a top–down fashion and understanding the application and mechanical/physical constraints, the tactile sensing system can be developed following a bottom–up approach i.e. starting from the transducer level. A general hierarchical functional and structural block diagram of a tactile sensing system is shown in Fig. 4.5. The tactile sensing system has been divided into sub-components to understand the degree of their involvement in the effective utilization of tactile sensing and hence design various parts to the desired level of complexity.

The levels from bottom to top depict the sensing, acquisition and transferring the tactile data to higher perceptual levels, perception of real world using multiple sensory data and ultimately the action. The degree of complexity vary between the hardware intensive levels at bottom to the computation intensive processes occurring at the top. The challenges in developing an electronic skin system, which can emulate human touch, lie at all the functional and structural levels in Fig. 4.5. Some of the design constraints and choices for various levels of Fig. 4.5 are presented in this section.

4.5.1 Tactile Sensors and Arrays

The tactile sensors and arrays are the basic structural building blocks of the tactile sensing system (see Fig. 4.5). The effective utilization of the tactile information greatly depends on them as they influence the types of contact parameters that can be measured over an area and also the time response with which they can be measured—which, in turn, depends on factors such as the transducer material, number of sensors in the arrays, how the sensors are accessed and read etc. The discussion in this section provides insight into the issues related to the aforementioned factors, especially the transduction method.

The transduction i.e. transforming the contact parameters into electrical signals, constitutes the lowest functional level of the tactile sensing system (see Fig. 4.5). The requirements such as measuring diverse contact parameters for various tasks put a constraint on the choice of transduction method. The diverse contact parameters include magnitude and direction of contact forces, distribution of force in space, stress and rate of change of stress, strain, object proximity, and temperature, etc. Simultaneous use of more than one mode of transduction may be needed to measure these contact parameters. For example, multiple parameters such as the stress, stress rate, or temperature can be measured with a set of sensors that are based on different transduction methods like capacitive (for strain measurement) and piezo-/pyroelectric (for stress or temperature measurement). A tactile sensor based on the combination of capacitive and piezoelectric transduction mechanisms could be an alternative solution. An ideal scenario would however demand a tactile sensor to use the same mode of transduction to measure multiple contact parameters—in other words, a transducer that is "multimodal". The advantages of multimodal transducers include, reduction in the sensing hardware such as interface electronics. Consider for instance, the piezoelectric materials like PVDF that respond to mechanical stimuli (e.g. strain/stress) and temperature. Either the same PVDF based sensor can be used to measure force and temperature at different times or two PVDF based sensors can be used to measure the aforementioned contact parameters at the same time.[3] In both cases, same interface electronics can be used—thus resulting in the

[3]The PVDF polymer possesses both piezoelectric and pyroelectric properties. This means that a PVDF based sensor can be used to measure the mechanical stimulus provided that sensed values are

reduction of interface electronics hardware. On the other hand, using a combination of capacitive and piezoelectric transducers for measuring aforementioned contact parameters would require separate interface electronics.

In practice, however, different transducers are employed to measure various contact parameters. To minimize the interface electronics overhead, in such cases, at least the transduced electrical variables should be of the same type (e.g. charge or current or voltage) and share similar bias and signal conditioning electronics. In doing so, the addressing scheme also gets simplified.

The choice of the transduction method affects the overall response time (as well as the frequency response) of the tactile sensors and arrays. The desired frequency range f_A (or the equivalent expected operating interval, $T_A = 1/f_A$) of a transducer is set by various factors including the task requirements (i.e. the bandwidth of the mechanical signal to be measured), the control bandwidth[4] and compatibility with the existing hardware such as sensors, e.g. joint force/torque sensor, vision sensor, etc. The frequency response characteristics of a transducer should have a flat gain and constant phase curve over the desired frequency range f_A and the maximum frequency in this range should be less than the transducer bandwidth f_{TBW} (i.e. $f_A \leq f_{TBW}$). The transducer bandwidth f_{TBW} determines the maximum speed or frequency at which the transducer is capable of operating. High bandwidth (i.e. $f_{TBW} \gg 0$ Hz) implies fast response, i.e. the speed at which a transducer reacts to the input signal variation. The transducers such as pressure conductive rubber are known to have low bandwidth (i.e. f_{TBW} equal to few Hz) and hence they are slow, with response times of the order of few hundreds of msec. Consider for example the tactile sensing arrays reported in [45, 46]. Despite using innovative silicon and organic FET based approaches, which can result in response times of the order of msec, the overall response time is poor because pressure conductive rubbers are employed as transducers. On the other hand, transducers such as piezoelectric material have a large bandwidth and are therefore pretty faster. In general, it is desirable to have $f_A \ll f_{TBW}$; in this case, the transducer response time can be neglected with respect to the operation period i.e. $T_A = 1/f_A$. Considering the human sense of touch as a reference, the f_A should be about 1 kHz in the case of robotic tactile sensing.

When tactile sensors are arranged in an array, the frequency f_A is related to the array scanning rate f_S (i.e. the frequency at which a single sensor element in an array is accessed and sampled) by the Shannon's Theorem: $f_S \geq 2 \times f_A$. The scanning time t_S, which is the inverse of the scanning rate, is given by the access time (i.e. t_{AC}) of a single sensor element multiplied by the number of sensor elements M in the array, i.e. $t_S = M \times t_{AC}$. The access time is the time between the addressing of the sensor element, the transfer of information at the output of the array and the time sampling for subsequent digitalization. From above, it follows that at Nyquist

compensated for the temperature dependence. The same can either be done mathematically using previously measured temperature dependent response or by measuring the same using another similar but mechanically isolated PVDF based sensor.

[4]The control bandwidth provides the frequency range within which a system can be controlled.

rate (the case of oversampling, i.e. $f_S > 2 \times f_A$, will be dealt in the Section on Data acquisition):

$$f_S = \frac{1}{M \times t_{AC}} = 2 \times f_A \tag{4.4}$$

$$t_{AC} = \frac{1}{2 \times f_A \times M} \tag{4.5}$$

$$M = \frac{1}{2 \times f_A \times t_{AC}} \tag{4.6}$$

From above equations it follows that the required transducer bandwidth and hence the suitable type of transducer material can be determined with the knowledge of the array size and the access time of a sensor element. Alternately, if the transducer material or its bandwidth and the access time of a sensor element are known, then the same can be used to determine the suitable size of the array for acquiring a faithful tactile data. Under the condition that $f_A \ll f_{TBW}$, as typically desired, the (4.4) can be written as:

$$f_S = 2 \times f_A = \frac{1}{M \times t_{AC}} \ll 2 \times f_{TBW} \tag{4.7}$$

In the above condition, the transducer response time is negligible with respect to the array scanning period and there is room for increasing the scanning rate (by decreasing the access time) or increasing the array size or both. However, the margin for such changes is much lower in the case of transducers having large time response or low transducer bandwidth. Consider, for example the 16×16 pressure sensing arrays by Someya et al. [45], where pressure conductive rubber is used as a transducer along with Organic FETs. As mentioned earlier, the pressure sensitive rubbers have a response time of the order of few hundreds of msec (i.e. f_{TBW} equal to few Hz) and OFETs have a response time of around 30 msec—meaning that t_{AC} is approximately 30 msec. Assuming usual row–column scanning of the array, f_A for any task would be just 0.065 Hz. On the other hand, if $f_{TBW} = f_A$ is assumed to be 1 Hz, and $f_S = 2 \times f_A = 2$ Hz, the array size M would be just 16 sensing elements. Nonetheless, it is possible to scan larger arrays with the same frequency, if specific arrangements such as 'active taxels' (analogous of active pixel) are employed.[5] Similar arrangement is used by Someya et al. [45] to scan the 16×16 element pressure array (reading one word per line with 30 msec for each row) in 480 msec (i.e. $f_S \approx 2$ Hz). Such schemes are helpful in collecting tactile data from larger areas. However, the transducer bandwidth f_{TBW} remains the same, the access time decreases, and the scanning rate f_S increases. Nonetheless, f_{TBW} is smaller than the case when $f_A = f_{TBW}$ and therefore one can only acquire slow varying

[5] In the early 1990s, work began on the modern CMOS active pixel sensor (APS), conceived originally in 1968. It was quickly realized that adding an amplifier to each pixel significantly increases the sensor speed and improves its signal-to-noise ratio (SNR), thus overcoming the shortcomings of passive pixel sensors. A local analog pixel memory is also present and a shutter mechanism helps in synchronizing the information captured by the pixel in the array [47].

mechanical signals. Usually, f_A corresponds to the bandwidth of the mechanical input stimuli and therefore even if the active taxel arrangement is adopted f_S can be increased, but f_A is still low. Of course one can oversample a lot the input signal but this does not help in acquiring large bandwidth input signals. Replacing pressure conductive rubbers with the other materials such as piezoelectric polymers can greatly improve the transducer response time (to the order of msec) in the aforementioned example.

From the above discussion, it follows that the value of f_A corresponds to the bandwidth of the mechanical input signal f_{BW} i.e. $f_A = f_{BW}$. On the basis of the value of f_A, a transducer with a proper bandwidth f_{TBW} must be selected in such a way that $f_A \ll f_{TBW}$.

In the previous discussion, we assumed a single output channel (see Eqs. (4.4), (4.5) and (4.6)). In the case of parallel output channels, the scanning rate can be increased accordingly; for instance in the case of two output channels, the scanning rate can be doubled even if at the expenses of an increase of the circuit complexity due to the need of two Analog to Digital circuit converters. With the further requirement of reducing the number of wires, the serial access of data can be pursued. The scanning rate results almost unaffected but the array access strategy results less flexible as the taxels access sequence is fixed and cannot be changed on line.

If the tactile information is to be used in the robot control loop, then another parameter comes into the picture i.e. the control bandwidth f_{CBW} which is the frequency range within which the system can be controlled. The array scanning rate f_S must be sufficiently higher than the control bandwidth f_{CBW} i.e. $f_S \gg f_{CBW}$. If the real time contact profile or image is of interest, the image may be distorted if the Nyquist's criterion is not satisfied i.e. having fixed $f_A = f_{BW}$ if:

$$f_S = \frac{1}{M \times t_{AC}} \leq 2 \times f_A \tag{4.8}$$

To solve this issue, one has to reduce the array size M or to reduce the access time t_{AC} correspondingly. The access time t_{AC} can be optimized by pursuing an Active Taxel arrangement i.e. the output data line is driven by an amplifier whose input is the transducer output. In case the transducer presents a decay time t_D smaller than the scanning period $T_S = 1/f_S$, a circuit arrangement similar to the 'Active Pixels' in CMOS visual imagers can be adopted [48, 49]. In this case, a local analog or digital memory must be implemented. Using a "shutter" like mechanism, the contact "image" is stored onto the local memory for a period which is equal to the array scanning period.

The task requirements such as the accurate reconstruction of contact details, requiring a sufficient number of sensing elements within a fixed space, also place a constraint on the selection of the transduction method. Consider, for instance, the cross-talk problem of the capacitive transduction, which can significantly affect the number as well as spatial resolution of the sensors.

Other factors that one must consider while choosing suitable transduction methods include the dynamic range, sensitivity, linearity and power requirements. The

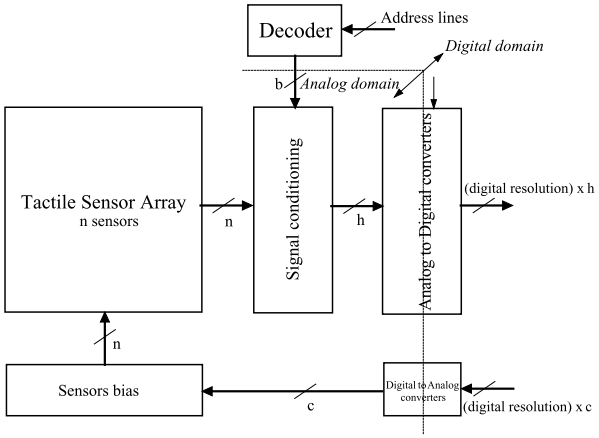

Fig. 4.6 A general functional block diagram of the interface electronics

sensors should be able to detect contacts between light touch and total body-weight. Similarly, the power consumed by the individual tactile elements should be low (an increase of the number of sensors makes it large). Ideally transducers should not consume any power for their operation. Consumption of large amount of power is definitely a cause of concern when the sensors are used in an autonomous robot that relies on battery power.

4.5.2 Interface Electronics

The interface electronics is constituted by structural blocks such as sensor bias, signal conditioning, and data acquisition. These components of the interface electronics are discussed in the following subsections.

A general functional block diagram of the interface electronics is reported in Fig. 4.6. The number of sensors in the Tactile Sensor Array is set to n; each sensor is connected to a signal-conditioning channel (which will be detailed later) which can be partially or fully implemented locally to each sensor. A set of h out of n channels is addressed by the decoder. The h channels outputs are set in input to h Analog to Digital converters.

The sensor bias block generates the voltage/current values to bias the sensor array. The sensor bias block is controlled by c analog signals/lines which are set by c Digital to Analog converters. The bias circuits can be implemented partially or fully locally to each sensor.

4.5.2.1 Sensors Bias

The tactile sensors can be broadly classified into two main categories:[6] (a) sensors that are implemented by passive devices (e.g. capacitors, resistors etc.), and (b) sensors implemented by active devices (e.g. Field Effect Transistors). In the latter case, the biasing is needed to set their operating region and also to get rid of the device switch on time. The operating region and the transfer function of all sensors across the tactile array should be similar i.e. independently of the technology spread. In case of an integrated silicon implementation, the mismatch among the responses of various sensors in the array must be minimized with a proper choice of the operating region and, if necessary, it can be compensated mathematically—at the cost of increased computational burden on the embedded data processing unit.

The bias circuit implementation strongly depends on the array access scheme. A bias circuit can normally be ON or it can be switched ON when accessing the sensor. In the latter case the power consumption of the array is lower at the expense of an increased sensor access time. The sensors access time is given by the bias circuit switch on time plus the sensor device switch on time (See, previous section). A simple solution for reducing the sensor access time is to employ two read out channels and operating them in a time multiplexed way, i.e. when one sensor is accessed, the bias circuit of the next one is switched ON. In this way, switch ON transient time of the bias circuit does not constrain the sensor access time. Of course, such approach can be extended to many signal conditioning channels if an equivalent number of A/D converters are available.

Another cause of concern is the relaxation time of the transducer (which is not always ON), which should be carefully accounted for because it could be unnecessarily long and thus degrade the sensor access time.

The sensors are supplied by voltage values that are different with respect to the ones used for the interface electronics and embedded data processing blocks (usually supplied by a 3.3 V down to 1 V voltage sources). This increases the complexity of the bias circuit implementation. To overcome this, as much as possible, the sensors should be developed to be operated with the voltage supply values similar to that of the interface electronics.

4.5.2.2 Signal Conditioning

A general functional block diagram (where the structure of the signal conditioning channel is shown) of the Signal Conditioning block is detailed in the following Fig. 4.7, where we refer to a voltage mode sensor output.

[6]This classification reflects an electronic viewpoint. There could be other classifications also. For instance classification of tactile sensors based on active and passive transducer materials. The active transducers (e.g. piezoelectric materials) do not require external power for their operation. On the contrary the passive transducers (e.g. resistive, capacitive etc.) require external source of power.

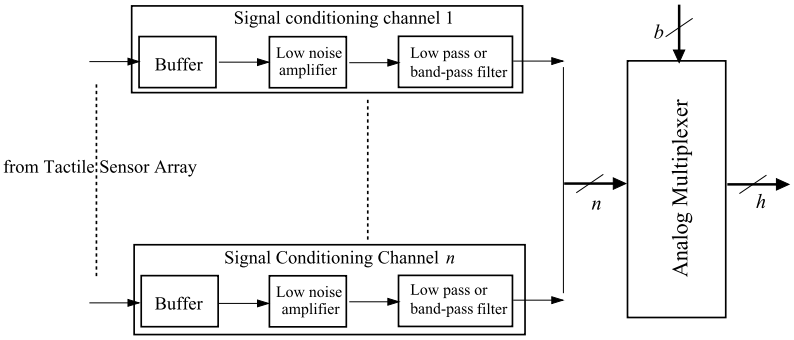

Fig. 4.7 A general functional block diagram of the signal conditioning electronics

The signal conditioning block usually implements a set of circuit level functions such as low noise amplification, input and output impedance values adaptation, setting the reference DC values (e.g. signal ground), low pass or band pass filtering (e.g. anti aliasing low pass filter), etc. The output of the signal conditioning circuit is the input of the analog to digital (A/D) converter. Usually a dedicated signal conditioning channel is needed for each sensor element in the array. To reduce the system complexity, a single A/D converter is normally used and signal conditioning channels (one for each sensor element of the array) are time multiplexed (via an analog multiplexer) at the input of the A/D converter. The sensor elements addressing is implemented by the control signals of the analog multiplexer. The selection of a multiplexer input channel corresponds to sampling of the corresponding signal, which also implies that the low pass or band pass filtering (for avoiding spectra aliasing) must be implemented prior to sampling.

Linearity and low noise are main concerns of signal conditioning circuits. The implementation of the signal conditioning system architecture is strongly related to the sensor array addressing and access scheme. Barring capacitive touch sensors—for which very small analog to digital converter chips are commercially available e.g. AD7147 [50]—the dedicated analog to digital converters chips are missing for various other transduction technologies used in tactile sensing.

4.5.2.3 Data Acquisition

Data acquisition involves addressing the signal conditioning channel and digitalization (i.e. analog to digital conversion) of the analog input value. The tactile sensing system can address the sensor and read tactile data from any selected body part (or all over the body). The provision of selecting tactile sensors from any body part could be helpful in studying the cognitive behavior of the robot, e.g. when 'attention' is paid to a particular part of the body. The issues such as wiring complexity also influence the interface electronics, in particular for large skin area arrays. For instance, if the interconnection wire between the sensor element and the data acquisition circuitry is very long, the signal can be corrupted by noise and interferences

and therefore the signal conditioning block must be implemented close to the sensor element. In case of piezoelectric transducers, the charge readout mode is more robust with respect to the voltage readout mode and should be preferred if the data acquisition block is put far away from the transducer.

Consider a system with a given number of channels (i.e. sensors in the array) and only one Analog to Digital (A/D) converter, as it is generally the case; let us define f_{BW} (see previous sub-section) as the signal source bandwidth (i.e. the bandwidth of the mechanical input stimulus), n as the number of channels, nb as the number of bits of the A/D converter, NR as the Nyquist rate ($NR = 2f_{BW}$). The minimum number of bits needed to reconstruct the input stimulus, which is termed as Effective Bit Rate (EBR), is obtained as: $EBR = n \times NR \times nb$. In principle, this is also the minimum number of bits which must be transmitted if no local signal and data processing is implemented.

The sensor output signal is usually oversampled, i.e. sampled at a rate greater than the Nyquist rate ($fs \gg NR$). Defining k as the oversampling factor, it follows that: $fs = NR \times k$. Similarly, $SR = n \times fs$ is the sample rate in samples/sec and $BR = SR \times nb$ is the bit rate in bits/sec. Oversampling simplifies the signal conditioning circuit implementation at the expenses of an increased complexity of the embedded data processing unit. In this case, the data filtering (e.g. high speed noise filtering) implementation block is followed by a decimation filter. The decimation filter decreases the bit rate *BR* down to *EBR* and the operating data rate from *fs* down to *NR*. As an example, in the case of POSFET based tactile sensing arrays, presented in Chap. 8 of this book, $f_{BW} = 1$ kHz, $n = 16$, $k = 5$ and $nb = 10$ bits [51]. Hence, we have $fs = 10$ kHz, $SR = 160$ ksamples/s, and bit rate $BR = 1.6$ Mbits/s. Moreover, $EBR = 16 \times 2$ kHz $\times\ 10 = 320$ kbits/s. It is evident that the bit rate is quite large. Therefore, it is important to decrease it from the *BR* to *EBR* to cope with available local computing power and communication channel bandwidth. In the given example, the decimation is implemented by the microcontroller by using DSP (digital signal processing techniques) such as *k*-decimation or smooth-moving averages.

An alternative arrangement for signal conditioning and data acquisition could be translating the sensed variable (i.e. the sensor output variable) into the frequency value of a digital signal (something similar to action potentials being converted into train of pulses in humans), which is subsequently digitized and acquired for example through a digital counter. Due to the simplicity of the approach, acquisition can be done in parallel and data addressing can be implemented in the digital domain. The sensor circuit can be an oscillator whose oscillating frequency is modulated by the transducer output and hence by the contact mechanical stimulus signal. The advantage of this approach is the robustness of the sensor output digital signal with respect to noise and disturbances. Wiring is minimized as the sensor output is a single signal/wire. On the other side, the acquisition time can be very long as it depends on the natural oscillating frequency and on the required resolution. Carrier frequency must be much higher with respect to the modulating one e.g. the bandwidth of the sensed mechanical contact stimulus. Many examples are reported in the literature (see for instance to be completed) and commercial components are available.

The embedded data processing unit and interface electronics are needed to digitize and process analog sensors raw data in the tactile sensing system. Design of these components greatly depends on the chosen transduction method. The shrinking dimensions of microprocessors, as a result of advances in electronic technology, makes it possible to mount devices for multiplexing, signal conditioning, etc. in the immediate proximity of the sensors, thereby reducing the amount of raw information that must be relayed back to the robot. The choice of the transduction method and the conditioning circuit are important from the system point of view, as they set the f_{TBW} and t_{AC}.

4.5.3 Embedded Local Data Processing Unit

The requirement of processing large amount of data from a large number of tactile sensors has often been cited as one of the major reasons for slow growth of tactile sensing in robotics vis-a-vis other sense modalities [52].

Some levels of data pre-processing close to the sensory locations, i.e. before transmitting the data to higher levels of the tactile sensing system, can greatly reduce the amount of information sent to the computing hardware and controllers. Distributed computing architecture like this would help in the optimum usage of the limited throughput of robot's processing unit and free up "robot's brain" for more intelligent works. Alternately this will allow scaling up the system to practically any number of sensors.

Similarly, and as discussed in the previous chapter, not all the information collected by mechanoreceptors in the human skin is sent to the brain for processing. Complex local pre–processing is done to fit the limited throughput of the nervous system. This is to say that there is some kind of *local processing* or *sense and process at the same place* scheme, similar to the one shown in Fig. 4.4, in the human skin. In a similar manner, the availability of embedded local data processing unit to perform some low level computations (e.g. simple scaling (amplification), segregation of data from different kinds of touch sensors (e.g. force, temperature etc.), linearization, compensation (e.g. temperature compensation), compressing of information, feature extraction, slip detection, and texture recognition etc.) will be an interesting development for the robotic tactile sensing. Consider for example the well known problem related to the presence of fatigue in various materials. It may result in the changes in the response of transducers over a period of time and repetitive use—thereby leading to sensor calibration issues. Such issues can also be handled computationally (in addition to changing the hardware components) by having suitable firmware at lower levels (let's say, module level). Fatigue tests of the tactile sensors may be conducted, following which the response variation can be expressed mathematically. Once mathematical expression for the variation in response is available, algorithms can be developed to mathematically compensate the variations. In this way, the lifetime of the sensors can also be increased.

The 'sense and process at the same place' paradigm may account for diverse implementation approaches and strategies. As an example, it may account for the

implementation of the bias and signal conditioning circuits, local to each transducer as in the case of the POSFET (see Chaps. 7 and 8). In other cases, it may account for active taxel implementation with, analog or digital, local storage. On the other hand, it may account for the implementation of an embedded system where local data processing is implemented by adopting advanced silicon chip stacking structures [53] whereas the upper chip is the sensor array, the chip below implements electronics interface and the lower chips implements the embedded data processing and communication interface. Such arrangements demand for silicon Integrated Circuit implementations and applications as in robotic manipulators (e.g. fingertips).

A System on Chip (SOC) or System in Package (SIP) approach would be ideal in such cases. In addition to the performance improvement, such approaches can also help in reducing the number of wires, which is a key robotics problem. SOC/SIP approach can provide a tactile analog of CMOS optical arrays/imagers. CMOS imagers have significantly contributed in bringing vision sensing to satisfactory levels and the same can also be true for tactile sensing with SOC/SIP approach. While the approach has benefited closely related application domains like smart fabric [54], MEMS based cantilever force sensors [55] and smart vision [56], it is surprising that tactile sensing for robotics largely remained unaware of its potential benefits.

A completely different approach in addressing interface electronics and local data processing issues, is to adopt a neuromorphic approach as the one proposed for vision chips by Indiveri [57]. Neuromorphic vision sensors are typically analog VLSI devices that implement hardware models of biological visual systems and can be used for machine vision tasks. They can be used for either reducing the computational load on the digital system in which they are embedded or, ideally, for carrying out all of the necessary computations without the need for any additional hardware. In neuromorphic vision chips, photoreceptors, memory elements, and computational nodes share the same physical space on the silicon surface. The specific computational function of a neuromorphic sensor is determined by the structure of its architecture and by the way its pixels are interconnected. Since each pixel processes information based on locally sensed signals and data arriving from its neighbors, the type of computation being performed is fully parallel and distributed. A similar approach could be used for silicon based implementation of tactile sensor arrays thus greatly reducing the wiring complexity and the burden for embedded data processing tasks.

4.5.4 Communication and Transmission

Dedicated strategies are needed to transmit the large amount of data collected by the tactile sensor arrays distributed over the whole body. In this context, the hierarchical architecture of the communication bus and the embedded local data processing (see previous section) can be explored. In the human tactile system, sensed data are progressively processed and salient features are extracted along with the transmission of data from the periphery (i.e. skin) to the central processing unit (i.e. the brain).

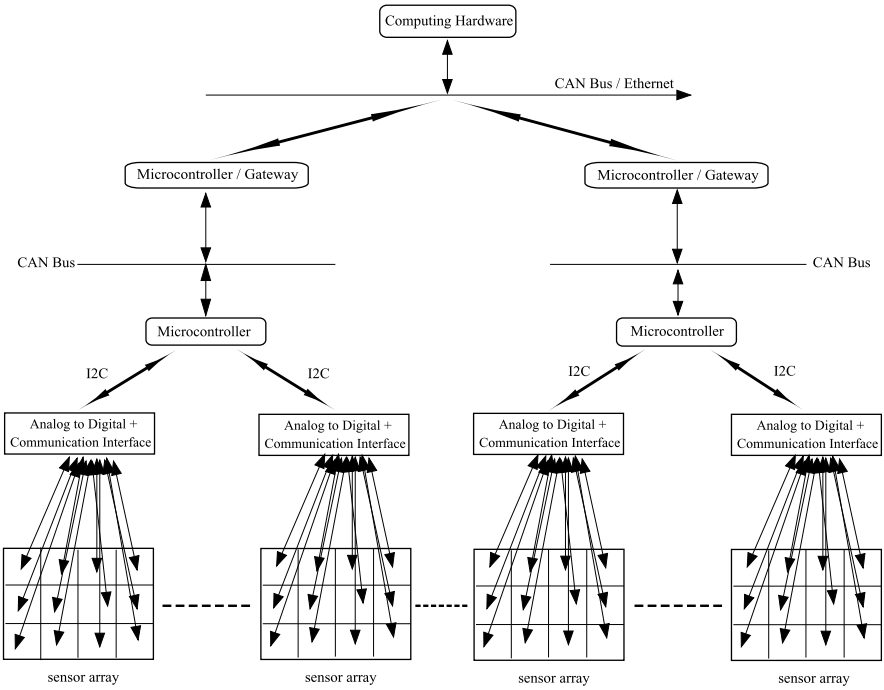

Fig. 4.8 The hierarchical communication architecture in the tactile sensing system

In a similar way, along the path from periphery to the robot controller, local buses are linked at connection points (i.e. gateways) where data from periphery are collected, processed for sensor fusion and feature extracted and forwarded to higher levels. Gateways are themselves arranged in hierarchical network topology up to the central control unit. The communication bus in this topology is star-like with a hierarchal arrangement. The gateway from one layer to the other has local computing resources to implement desired sensor data processing algorithms (see Fig. 4.8). Only salient features are transferred to higher levels.

Going from lower to higher levels (i.e. skin toward controller) protocols are different. Going from periphery upward, bandwidth of the bus increases in order to accommodate an increasing amount of data; protocol complexity increases as well. At lower levels high speed, lower connectivity and short distance wiring buses are preferred (e.g. I2C). Moving up in the hierarchy, more complex protocols and longer wiring buses are preferred (e.g. CAN, Flexray, real-time Ethernet). The desired operation speed, noise and number of wires put a constraint on the type of communication channel used for interaction with higher levels. Serial communication buses are used (e.g. I2C, CAN bus, Flexray, Ethernet, etc.) to decrease wiring. The buses using CAN protocol are generally a preferred choice mostly due to the real-time capabilities, high reliability, and readily availability on most microcontrollers. But, the CAN bus suffers from a moderate transmission bandwidth (up to 1 Mbits/s) which

will either slow down transmission of tactile data from a large number of sensors or put a cap on the number of touch sensors on the body. These issues can be solved either by using buses with higher transmission bandwidth (e.g. up to 10 Mbits/s can be achieved with FlexRay, (see [58] for more details) or using more buses in parallel—which is anyway undesirable. Due to the requirement of real time needed to use the tactile feedback in the control loop, deterministic protocols are mandatory.

In Fig. 4.8 each sensor of the array is connected to a serial bus (i.e. I2C); the serial bus is managed by a microcontroller which acts as a gateway between the I2C and the CAN bus which interconnects similar systems [59]. Sensor arrays cover the body area and are physically arranged in a patchwork way. Contiguous patches/arrays are connected with a single gateway to higher level hierarchy. The gateway (Microcontroller in the Figure) implements also data fusion task and feature extraction algorithms.

Wireless data transmission is another alternative, which is also an ideal solution for reducing the wiring complexity. Very few works using wireless communication for touch sensing have been reported in literature [60, 61]. For example, Shinoda and Oasa [60], embed tiny wireless sensing elements in an elastic skin that uses an inductive base coil to provide power and signal transmission. Each sensing element is a tuned resonator with a distinct resonant frequency, which is stress sensitive. The interference among large number of sensing elements placed close to each other and the power requirements are some of the disadvantages of wireless data transmission. Despite all the technological advances in wireless communication, the safety issues of robots working with humans pose a big hindrance and question its reliability over the wired data communication.

4.5.5 Data Selection and Handling

Following the human tactile sensing system, data transmission is done along with features extraction and data selection by exploiting a communication bus hierarchy. A way of reducing the large amount of tactile sensing data is *data selection* and rejection of redundant data, as the whole set of data collected from the various sensors may not be useful. For example, a grasp may not involve all the fingers and hence data obtained from the fingers other than those involved in the grasp can be rejected. As shown in Fig. 4.5, data selection can be done somewhere between the lower, hardware intensive levels, and the upper computational intensive levels.

Placing large number of tactile sensors over the robot's body is not enough for it to interact and carry out various tasks in real world. Algorithms are also equally important components of tactile sensing system, needed to suitably represent the 3D tactile data, to perform the sensory data fusion, and to *construct the world model*—thereby leading to effective utilization of the tactile data. Computational techniques have often been used to extract the information from large set of tactile data. For instance, the tactile information gained from the contacts between a gripper and the object have been used by Petrovskaya et al. [62] to obtain the pose of the object. Here, particle filter technique is applied on tactile data to determine the pose.

Jiménez et al. [63] have proposed using neural network to determine the surface type (edge, flat, cylindrical, sphere) of the tactile contact. The tactile information extracted from the sensors on a gripper has been used by Chitta et al. [64] to determine deformation properties of objects such as the open/closed and fill or internal state of bottles. Machine learning tools have been used by Sinapov et al. [65] for surface recognition and categorization from the data obtained by letting a robot scratch different surfaces. Self-organizing maps (SOMs) are employed by Johnsson and Balkenius [66] to extract features from sensory data. The objects are distinguished according to shape and size, and properties such as texture and hardness have been extracted from the explored materials. Similarly, Bayes trees have been used by Jamali and Sammut [67] to distinguish different materials based on their surface texture.

In general, the computational intelligence techniques for extracting information from the tactile sensors data have been used to determine the properties of objects or object recognition. More needs to be done in the field to effectively use the tactile data to address more complex problems such as grasp stability, safe grasping and motion planning using tactile data from whole body (not just hands).

4.5.6 Data Representation and Sensor Fusion

Quite often, computational techniques developed to handle visual data are adopted for tactile sensing as well. However, this may not always hold as unlike cameras, the tactile sensors are distributed over three-dimensional robotic body. This means that unlike cameras, the tactile sensors may not provide information from well-defined locations in space. One needs to consider how robots would use tactile data, identify contact conditions, and take appropriate actions. For instance, the information about locations of contacted tactile sensors on the robot body (i.e. in a three-dimensional space) may be needed at the higher computational intensive levels (see Fig. 4.5) of the robotic tactile sensing system. Locating the contacted tactile sensors can be labor intensive and error prone (especially in the case of whole body tactile sensing) because the positions of tactile sensors change with the robot posture. Such information is fundamental to the development of more complex cognitive behaviors, such as quick response to sudden stimuli or compliant human–robot interactions. Therefore, internal models must be developed to *represent the tactile information* from various body parts. This is also an important step for utilizing tactile data in various control strategies. In humans, the presence of somatotopic maps (discussed in the previous chapter) is helpful for these purposes. Similar arrangements can be helpful in utilizing the tactile information in robotics. Inspired from the human somatosensory system, some research works including the models based on the notion of 'somatic alphabet, words and sentences' [68] and artificial brain maps [69], have been reported in this direction. However, a comprehensive scheme is yet to evolve.

A method similar to the somatotopic maps in humans is employed by Stiehl et al. [68] to create the receptive fields from population of sensors and the algorithms based upon the processing methods of the brain are presented to determine

the centroid of an object, as it moves over the population of sensors. The algorithms can be applied to clusters of sensors to determine object properties such as texture, curvature, and orientation. The approach adopted by Stiehl et al. does not take into account the mapping between the taxels located in the three-dimensional space and their representation in two-dimensional artificial somatosensory maps—which is fundamental to use the tactile data in controlled contact tasks as it enables the robot to obtain accurate tactile data no matter what posture it takes. The approach presented by Cannata et al. [69], however considers such mapping by modeling the robot skin as a discrete three-dimensional surface made of a mesh of triangles. The surface parametrization techniques [70, 71] are then used to obtain a piecewise linear mapping between the given 3D surface (skin meshes) and an isomorphic discrete two-dimensional surface (i.e. analogue of somatotopic maps in cortex) while preserving the intrinsic properties (taxels locations, displacements, density and varying resolution etc.) of the three-dimensional surface. While models are required to solve many problems similar to those mentioned above, one should also consider the amount of computational resources needed to implement them and hence the constraints placed on hardware requirements.

To construct the real world model, the robots may require integrating signals from different types of sensors and sensing modalities (e.g. tactile and vision or tactile and kinesthetic) to form a stronger percept. For instance, consider a robot distinguishing two objects using visual information (such as color, shape and location) and the tactile information (such as softness, texture, vibration, temperature, mass etc.). Sensory fusion is not new to robotics. Consider, for instance, the problem of simultaneous localization and mapping (SLAM) for a mobile service robot, where inputs from different sensors (laser scan, ultrasonic, vision) are combined to drive the prediction algorithms. While interacting with the environment, humans combine sensory data from different sensing modalities in statistical optimal fashion [72]. Fusion of the information coming from multiple sensors may help in providing a coherent and reliable description of the world surrounding the robot. This is particularly important when monitoring contacts, e.g., for selecting impedance parameters or for determining the most dangerous control points on the robot to be driven away from a human with higher priority. Suitable algorithms are therefore needed to integrate data from multiple sensory sources. Artificial intelligence (AI) techniques (e.g., fuzzy sets, neural networks) can also be adopted for this purpose. Using multimodal sensory inputs (proprioceptive and load-based tactile information), Platt et al. [73] have proposed an approach to localize the features embedded in flexible materials during robot manipulation. It is shown that during localization, the proprioceptive and tactile data contain complementary information. Interaction with the flexible materials is quite challenging. Similarly, Kroemer et al. [74] proposed a machine learning approach to infer lower dimensional representation of tactile data and classify materials following a weak pairing of tactile and visual information. Combining vision and tactile information to improve the performance of dynamic tactile sensors is an interesting development.

Correct integration of the signals from different sensors is very important for the perception and this calls for compatibility among the sensing hardware. In humanoids, for example, these signals could come from touch sensors (both extrinsic

and intrinsic) or from vision sensors or from audio sensors or a combination of any of them [75, 76]. As said earlier, efficient vision, audio and intrinsic force sensors are commercially available. Thus, assuming their fixed configuration, a compatibility constraint is placed on the tactile sensors. For a reliable control of complex tasks, the tactile sensing parameters like sensor density, resolution, and location are particularly important and thus low levels must be designed keeping these in mind.

4.5.7 Other Electronic/Electrical Requirements

The sensor array and interface electronics are generally powered with different voltage supplies because their implementation technologies are usually different. In robots, the power supply to peripheral circuits, such as the interface electronics for the skin, can be taken from a dedicated cable (with power supply voltage and ground reference). Wherever possible, the power supply can also be taken from the communication bus wires to keep the number of wiring and cables low. For instance, the +5 V supply can be taken from the CAN bus wire, even if it is very noisy, and cannot be used as reference for accurate analog circuit functions. If other supply voltage values (e.g. +3.3 V or +1.8 V) are needed to supply electronic interface and embedded computing hardware (e.g. microcontroller, DSP or Application Specific Integrated Circuit), dedicated voltage regulators have to be used. Besides increasing the physical size, the power consumption of power management circuits also worsen the energy budget of the tactile sensing system.

Generally, the interface electronics and embedded local data processing unit (e.g. A/D converters, microcontrollers, DPSs, etc.) are supplied by positive voltages. On the other hand, sensor arrays in general are not supplied by similar voltage value and, what is more, they are supplied by a negative voltage value. In fact for safety requirements the sensing part of the transducer (i.e. the part which is "in contact"—even through the cover layer—with the object) is set at ground potential. Therefore, one may need to make provisions for generating negative voltage supply. This requirement accounts for a meaningful increase of the complexity of the circuit for power management. The maximum supply current of the communication bus power supply is usually limited (e.g. 350 mA), meaning that the power consumption of the tactile sensing system must be minimized to avoid any increase in number of power supply wires.

The power supply and reference (e.g. ground) potentials maybe taken from long wires, meaning that the reference potential values are not the same (accounting for the wiring cables voltage drops). Even if the cable resistance is constant, current supply during operation causes a voltage drop which is not constant as the wiring cables voltage drops depend on power consumption. This issue can be tackled effectively only with a local power supply source e.g. with fuel cells or energy harvesting circuits. Not much has been done in this direction and this is an important area of future research.

4.6 Other Tactile System Requirements

Besides aforementioned requirements and constraints, the development of tactile sensing systems should also address problems like manufacturing reliable, fault tolerant and economic systems which do not require frequent maintenance. Some of these difficult technological and engineering issues are discussed in this section.

4.6.1 Modular Approach

Modularity is an established technique for organizing and simplifying a complex system. From elementary (flashlight batteries) to complex (the cells of an organism), modularity has a record of success that is hard to challenge. Modularity for tactile sensing system (or any other system) delivers many benefits, including:

- *Scalability*, i.e. ability to scale and grow. System growth, both in size and in new capabilities, can be accomplished simply by adding modules that could interact with existing ones using standard interfaces.
- *Flexibility*, i.e. simpler process of duplication. Duplicating a number of smaller, less complicated modules is easier, faster, and more reliable than duplicating a single complicated system.
- *Simplicity*, i.e. ability to specialize the function of modules. Delegation and specialization of module tasks provide the same effectiveness and efficiencies inherent in teamwork. One kind of module could be for contact parameters such as contact force and its direction, another kind for contact temperature, and so on.
- *Portability*, i.e. rapid adaptation to the requirements. By adding, subtracting, or modifying modules, incremental design changes could be more quickly tried and either adopted or rejected.
- *Reliability*, i.e. fault tolerance. Modularity "packages" a system into smaller pieces, which facilitates redundancy of component parts so that failure of one, or even several, need not adversely affect operation of the system. With redundancy, individual modules could fail without degrading the system, allowing for concurrent module repair without system downtime.
- *Short Development Time*. The modular approach often results in lower development time because design teams can work in parallel on the different modules, once the design is split up into modules.

The robustness of robots depends most essentially on its transducers, the sensors and actuators with which the robot interacts with both the user and the environment. Today's robots are designed with little redundancy in sensing due to the cost not only of the transducers but also the electronics and power supplies. The most effective means of solving this is through miniaturization and modularization. A modular approach [2–4]—with components like transducers, interface electronics and embedded data processing unit in each module—can therefore provide a common, economical and reliable solution for robotic tactile sensing. Due to variability in

functional and spatio-temporal requirements of various body parts, as in humans, location specific modules can be developed. To reduce the overall cost, some of the components of the tactile sensing system (for instance, the logical organization and communication interface) can be similar or common irrespective of where the module is placed. The adoption of a modular concept gives rise to the opportunity to alter and re-configure the tactile sensing hardware when task requirements change. A modular approach can also make it easy to integrate the tactile sensing structures on the robot. The effect that Charge Coupled Device (CCD) camera technology has had on optical sensing needs to be replicated in tactile sensing.

4.6.2 Fault Tolerance

Fault tolerance is the ability of a tactile sensing system to recover from an unexpected faulty behavior or preserve overall functionality. Fault tolerance is needed to operate in real time and safely—even if some components of the tactile system (e.g. sensors, electronics) fail to work properly. Fault tolerance is a fundamental prerequisite in human–robot interaction. Given that a large number of sensors are needed to cover the body of a robot (humanoid, for instance), the probability of faulty devices is significant and therefore provisions must be made for fault tolerance, both, at hardware and software levels.

At hardware level, the fault tolerance can be achieved by employing suitable communication schemes or routing of wires, and component redundancy, etc. One of the simple strategies is not to connect the common electronics components such as microcontrollers to contiguous modules (if a modular approach is adopted) of the tactile system. In this way, the contact parameters from a particular body area can be measured (with poor resolution) even when the electronic component (e.g. microcontrollers) gets damaged. At times, these schemes might also increase the system complexity. Consider, for instance, a communication scheme makes provisions like alternative paths to access tactile sensors and in the process results in an increased wiring complexity. At the software levels, the examples include tasks such as grouping the tactile data from a set of sensors and using the median value of the data to set lower bounds of the overall tactile system operation [4]. Software algorithms and procedures can be implemented (e.g. in the local embedded electronic unit) to identify and isolate a faulty device and/or behavior before it can impair overall system functioning.

4.6.3 Reliability

The tactile sensing system must be reliable, both in terms of performance and usage. The sensors not noticing or measuring a contact event can lead to a very unpleasant situation. Consider, for instance, a robot bumping into humans during human–robot

interaction. The common wisdom says that the chances of malfunctioning components are bigger when the system comprises of many components. The tactile sensing systems for whole body may comprise of thousands of sensors and associated electronic components and it is quite likely that some of the sensors may malfunction or may even die during usage. To overcome such issues and to make the system more reliable, the tactile sensing system must be capable of self-diagnostics, self–healing, and graceful degradation [3].

Self-diagnostics refers to the systems's continuous or regular checking of all its components (sensors and associated electronics) and inform the controller of detected deviations (if any) from the normal behavior. Self-healing implies an automatic repair of the failed hardware as it is available in biological systems. The graceful degradation refers to the tactile sensing system's capacity to direct sensors in the vicinity of a broken sensor to take over its job. In such cases, there is a price to be paid in terms of performance degradation. For instance, in case the job of a broken sensor is taken over by healthy sensor in vicinity, the distance between well-functioning sensors will effectively increase resulting into poor resolution and hence degraded performance. Nonetheless, the system will still function. An economic solution with good reliability would be an ideal solution.

4.6.4 Manufacturability, Maintenance and Cost

The easy manufacturability, maintenance and low cost are other desirable items in the list of requirements for developing an effective tactile sensing system. It makes little or no sense to design products that can not be produced. Any product development requires many inputs ranging from skilled labor to availability of materials etc. Any missing input may render a good design useless. The engineering of development process is therefore a key issue, involving materials and component selection, development of methods and procedures, and possibly ad-hoc processes. One must also consider that the high cost of production and maintenance may lead to non-use of a manufacturable and innovative product. Computer aided design (CAD)/computer-aided engineering (CAE) tools can be used to design multiple alternatives that are cost effective on different accounts.

4.7 Summary

The system as a whole determines in an important way how the parts behave. This chapter, demonstrates that the design of tactile sensors and finally their integration to the robot, is a result of many trade-offs. Taking into account various system constraints like those posed by the presence of other sensors, by robot controller and other system aspects like embedding electronics, distributed computing power, networking, wiring, power consumption, robustness, manufacturability, and maintainability, during the design phase of the tactile sensing devices can be very useful in

their final integration with the robot. This requires understanding of the sensor system architecture at various system levels—right from sensing the external stimulus until the action as a result of the stimulus. It is difficult for a tactile sensor, based on a particular technology, to match all the requirements mentioned in this chapter. Hence, a combination of various technologies and interpretation methods may be needed for an effective utilization of touch information in robotics. However, the basic issues discussed in this chapter apply to tactile sensing in general. Much work needs to be done at the system level before artificial touch can be used in real world environment.

References

1. R.S. Dahiya, G. Metta, M. Valle, G. Sandini, Tactile sensing—from humans to humanoids. IEEE Trans. Robot. **26**(1), 1–20 (2010)
2. Y. Ohmura, Y. Kuniyoshi, A. Nagakubo, Conformable and scalable tactile sensor skin for curved surfaces, in *IEEE International Conference on Robotics and Automation*, Orlando, Florida, USA (2006)
3. V.L. Lumelsky, M.S. Shur, S. Wagner, Sensitive skin. IEEE Sens. J. **1**(1), 41–51 (2001)
4. D. Um, B. Stankovic, K. Giles, T. Hammond, V.L. Lumelsky, A modularized sensitive skin for motion planning in uncertain environments, in *IEEE International Conference on Robotics and Automation*, Leuven, Belgium (1998), pp. 7–112
5. S.C. Jacobsen, I.D. McCammon, K.B. Biggers, R.P. Phillips, Design of tactile sensing systems for dextrous manipulators. IEEE Control Syst. Mag. **8**(1), 3–13 (1988)
6. M.R. Cutkosky, R.D. Howe, W. Provancher, Force and tactile sensors, in *Springer Handbook of Robotics*, ed. by B. Siciliano, O. Khatib (Springer, Berlin, 2008), pp. 455–476
7. B.D. Argall, A.G. Billard, A survey of tactile human–robot interactions. Robot. Auton. Syst. **58**, 1159–1176 (2010)
8. P.A. Schmidt, E. Mael, R.P. Wurtz, A sensor for dynamic tactile information with applications in human–robot interaction & object exploration. Robot. Auton. Syst. **54**, 1005–1014 (2006)
9. R.D. Howe, M.R. Cutkosky, Dynamic tactile sensing: perception of fine surface features with stress rate sensing. IEEE Trans. Robot. Autom. **9**(2), 140–151 (1993)
10. Z. Li, P. Hsu, S. Sastry, Grasping and coordinated manipulation by a multifingered robot hand. Int. J. Robot. Res. **8**(4), 33–50 (1989)
11. R.D. Howe, M.R. Cutkosky, Integrating tactile sensing with control for dextrous manipulation, in *IEEE International Workshop on Intelligent Motion Control*, Istanbul, Turkey (1990), pp. 369–374
12. A.D. Berger, P.K. Khosla, Using tactile data for real-time feedback. Int. J. Robot. Res. **10**(2), 88–102 (1991)
13. R.S. Fearing, Tactile sensing mechanisms. Int. J. Robot. Res. **9**(3), 3–23 (1990)
14. A. Bicchi, J.K. Salisbury, P. Dario, Augmentation of grasp robustness using intrinsic tactile sensing, in *IEEE International Conference on Robotics and Automation*, Cincinnati, USA (1990), pp. 968–973
15. R.M. Murray, Z. Li, S.S. Sastry, *A Mathematical Introduction to Robotic Manipulation* (CRC Press, Boca Raton, 1994)
16. C. Domenici, D. De Rossi, A. Bicchi, S. Bennati, Shear stress detection in an elastic layer by a piezoelectric polymer tactile sensor. IEEE Trans. Dielectr. Electr. Insul. **24**(6), 1077–1081 (1989)
17. D. De Rossi, G. Canepa, G. Magenes, F. Germagnoli, A. Caiti, T. Parisini, Skin-like tactile sensor arrays for contact stress field extraction. Mater. Sci. Eng. **C1**, 23–36 (1993)

18. J.L. Novak, Initial design and analysis of a capacitive sensor for shear and normal force measurement, in *IEEE International Conference on Robotics and Automation*, Scottsdale, AZ, USA (1989), pp. 137–145
19. M. Shikida, T. Shimizu, K. Sato, K. Itoigawa, Active tactile sensor for detecting contact force and hardness of an object. Sens. Actuators A, Phys. **103**, 213–218 (2003)
20. A. Schmitz, P. Maiolino, M. Maggiali, L. Natale, G. Cannata, G. Metta, Methods and technologies for the implementation of large scale robot tactile sensors. IEEE Trans. Robot. **27**(3), 1–12 (2011)
21. G. Cannata, R.S. Dahiya, M. Maggiali, F. Mastrogiovanni, G. Metta, M. Valle, Modular skin for humanoid robot systems, in *The 4th International Conference on Cognitive Systems (CogSys2010)*, Zurich, Switzerland (2010)
22. G. Cheng, P. Mittendorfer, Humanoid multi-modal tactile sensing modules. IEEE Trans. Robot. **27**(3), 13–22 (2011)
23. Y. Ohmura, Y. Kuniyoshi, Humanoid robot which can lift a 30 kg box by whole body contact and tactile feedback, in *(IROS 2007) IEEE/RSJ International Conference on Intelligent Robots and Systems*, San Diego, CA, USA (2007), pp. 1136–1141
24. T. Mukai, M. Onishi, T. Odashima, S. Hirano, Z. Luo, Development of the tactile sensor system of a human-interactive robot "RI-MAN". IEEE Trans. Robot. **24**(2), 505–512 (2008)
25. http://bfi.easystorecreator.com/items/maps/list.htm?1=1
26. E.D. Demaine, J. O'Rourke, *Geometric Folding Algorithms: Linkages, Origami, Polyhedra* (Cambridge University Press, Cambridge, 2007)
27. M. Shimojo, Mechanical filtering effect of elastic cover for tactile sensor. IEEE Trans. Robot. Autom. **13**, 128–132 (1997)
28. J. Scheibert, S. Leurent, A. Prevost, G. Debregeas, The role of fingerprints in the coding of tactile information probed with a biomimetic sensor. Science **323**, 1503–1506 (2008)
29. M.-Y. Cheng, C.-M. Tsao, Y.-J. Yang, An anthropomorphic robotic skin using highly twistable tactile sensing array, in *The 5th IEEE Conference on Industrial Electronics and Applications (ICIEA)*, Taichung (2010), pp. 650–655
30. B. Huyghe, H. Rogier, J. Vanfleteren, F. Axisa, Design and manufacturing of stretchable high-frequency interconnects. IEEE Trans. Adv. Packag. **31**, 802–808 (2009)
31. D.-Y. Khang, H. Jiang, Y. Huang, J.A. Rogers, A stretchable form of single-crystal silicon for high-performance electronics on rubber substrates. Science **311**, 208–211 (2006)
32. T. Sekitani, Y. Noguchi, K. Hata, T. Fukushima, T. Aida, T. Someya, A rubberlike stretchable active matrix using elastic conductors. Science **321**, 1468–1472 (2008)
33. Y. Zhang, C.J. Sheehan, J. Zhai, G. Zou, H. Luo, J. Xiong, Y.T. Zhu, Q.X. Jia, Polymer-embedded carbon nanotube ribbons for stretchable conductors. Adv. Mater. **22**, 3027–3031 (2010)
34. K. Noda, E. Iwase, K. Matsumoto, I. Shimoyama, Stretchable liquid tactile sensor for robot-joints, in *IEEE International Conference on Robotics and Automation (ICRA)*, Anchorage (2010), pp. 4212–4217
35. H. Alirezaei, A. Nagakubo, Y. Kuniyoshi, A highly stretchable tactile distribution sensor for smooth surfaced humanoids, in *The 7th IEEE-RAS International Conference on Humanoid Robots*, Pittsburgh, USA (2007), pp. 167–173
36. S. Tawil, D.C. Rye, M. Velonaki, Improved image reconstruction for an EIT-based sensitive skin with multiple internal electrodes. IEEE Trans. Robot. **27**(3), 425–435 (2011)
37. T. Hoshi, H. Shinoda, Robot skin based on touch-area-sensitive tactile element, in *Proceedings of International Conference on Robotics and Automation* (2006), pp. 3463–3468
38. T. Yoshikai, H. Fukushima, M. Hayashi, M. Inaba, Development of soft stretchable knit sensor for humanoids' whole-body tactile sensibility, in *Humanoids 2009: The 9th IEEE-RAS International Conference on Humanoid Robots*, Paris (2009), pp. 624–631
39. B. Zitová, J. Flusser, Image registration methods—a survey. Image Vis. Comput. **21**(11), 977–1000 (2003)
40. D.J. Van den Heever, K. Schreve, C. Scheffer, Tactile sensing using force sensing resistors and a super-resolution algorithm. IEEE Sens. J. **9**(1), 29–35 (2009)

41. K. Murakami, K. Matsuo, T. Hasegawa, R. Kurazume, A decision method for placement of tactile elements on a sensor glove for the recognition of grasp types. IEEE/ASME Trans. Mechatron. **15**, 157–162 (2010)
42. M. Nilsson, Tactile sensors and other distributed sensors with minimal wiring complexity. IEEE/ASME Trans. Mechatron. **5**, 253–257 (2000)
43. H.R. Schiffman, *Sensation and Perception—An Integrated Approach* (Wiley, New York, 2001)
44. Available online: http://asimo.honda.com/
45. T. Someya, T. Sekitani, S. Iba, Y. Kato, H. Kawaguchi, T. Sakurai, A large-area, flexible pressure sensor matrix with organic field-effect transistors for artificial skin applications. Proc. Natl. Acad. Sci. USA **101**(27), 9966–9970 (2004)
46. M.H. Raibert, An all digital VLSI tactile array sensor, in *IEEE International Conference on Robotics and Automation*, vol. 1 (1984), pp. 314–319
47. A.E. Gamal, H. Eltoukhy, CMOS image sensors. IEEE Circuits Devices Mag. **21**(3), 6–20 (2005)
48. M. Bigas, E. Cabruja, J. Forest, J. Salvi, Review of CMOS image sensors. Microelectron. J. **37**, 433–451 (2006)
49. A. Belenky, A. Fish, A. Spivak, O. Yadid-Pecht, Global shutter CMOS image sensor with wide dynamic range. IEEE Trans. Circuits Syst. II, Express Briefs **54**(12), 1032–1036 (2007)
50. AD7147: CapTouch^{TM}. 2008. Available at: http://www.analog.com
51. L. Barboni, R.S. Dahiya, G. Metta, M. Valle, Interface electronics design for POSFET devices based tactile sensing systems, in *IEEE RO-MAN, 19th IEEE International Symposium in Robot and Human Interactive Communication*, Viareggio, Italy (2010), pp. 686–690
52. M.H. Lee, Tactile sensing: new directions, new challenges. Int. J. Robot. Res. **19**(7), 636–643 (2000)
53. R.-S. Patti, Three-dimensional integrated circuits and the future of system-on-chip designs. Proc. IEEE **94**(6), 1214–1224 (2006)
54. M. Sergio, F. Manaresi, F. Campi, R. Canegallo, M. Tartagni, R. Guerrieri, A dynamically reconfigurable monolithic CMOS pressure sensor for smart fabric. IEEE J. Solid-State Circuits **38**(6), 966–975 (2003)
55. D. Barrettino, S. Hafizovic, T. Volden, J. Sedivy, K.-U. Kirstein, A. Hierlemann, CMOS monolithic mechatronic microsystem for surface imaging and force response studies. IEEE J. Solid-State Circuits **40**(4), 951–959 (2005)
56. W.-C. Fang, A system-on-a-chip design of a low-power smart vision system, in *IEEE Workshop on Signal Process Systems* (1998), pp. 63–72
57. G. Indiveri, Neuromorphic analog VLSI sensor for visual tracking: circuits and application examples. IEEE Trans. Circuits Syst. II, Analog Digit. Signal Process. **46**(11), 1337–1347 (1999)
58. N. Navet, Y. Song, F. Simonot-Lion, C. Wilwert, Trends in automotive communication systems. Proc. IEEE **93**(6), 1204–1223 (2005)
59. G. Cannata, M. Maggiali, G. Metta, G. Sandini, An embedded artificial skin for humanoid robots, in *IEEE International Conference on Multisensor Fusion and Integration for Intelligent Systems* (2008), pp. 434–438
60. H. Shinoda, H. Oasa, Wireless tactile sensing element using stress-sensitive resonator. IEEE/ASME Trans. Mechatron. **5**(3), 258–265 (2000)
61. H. Shinoda, N. Asamura, M. Hakozaki, X. Wang, Two-dimensional signal transmission technology for robotics, in *IEEE International Conference on Robotics and Automation* (2003), pp. 3207–3212
62. A. Petrovskaya, O. Khatib, S. Thrun, A.Y. Ng, Bayesian estimation for autonomous object manipulation based on tactile sensors, in *International Conference on Robotics and Automation* (2006), pp. 707–714
63. A.R. Jiménez, A.S. Soembagijo, D. Reynaerts, H. Van Brussel, R. Ceres, J.L. Pons, Featureless classification of tactile contacts in a gripper using neural networks. Sens. Actuators A, Phys. **62**(1–3), 488–491 (1997)

64. S. Chitta, J. Sturm, M. Piccoli, W. Burgard, Tactile sensing for mobile manipulation. IEEE Trans. Robot. **27**(3), 558–568 (2011)
65. J. Sinapov, V. Sukhoy, R. Sahai, A. Stoytchev, Vibrotactile recognition and categorization of surfaces by a humanoid robot. IEEE Trans. Robot. **27**(3), 488–497 (2011)
66. M. Johnsson, C. Balkenius, Sense of touch in robots with self-organizing maps. IEEE Trans. Robot. **27**(3), 498–507 (2011)
67. N. Jamali, C. Sammut, Majority voting: material classification by tactile sensing using surface texture. IEEE Trans. Robot. **27**(3), 508–521 (2011)
68. W.D. Stiehl, L. Lalla, C. Breazeal, A "somatic alphabet" approach to "sensitive skin" for robots, in *Proceedings ICRA'04, 2004 IEEE International Conference on Robotics and Automation*, vol. 3 (2004), pp. 2865–2870
69. G. Cannata, S. Denei, F. Mastrogiovani, Tactile sensing—steps to artificial somatosensory maps, in *The 19th International Symposium on Robot and Human Interactive Communication*, Viareggio, Italy (2010), pp. 576–581
70. U. Pinkall, K. Polthier, Computing discrete minimal surfaces and their conjugates. Exp. Math. **2**(1), 15–36 (1993)
71. M. Desbrun, M. Meyer, P. Alliez, Intrinsic parametrizations of surface meshes. Comput. Graph. Forum **21**(3), 209–218 (2002)
72. M.O. Ernst, M.S. Banks, Humans integrate visual and haptic information in a statistically optimal fashion. Nature **415**, 429–433 (2002)
73. R. Platt, F. Permenter, J. Pfeiffer, Using Bayesian filtering to localize flexible materials during manipulation. IEEE Trans. Robot. **27**(3), 586–598 (2011)
74. O. Kroemer, C.H. Lampert, J. Peters, Learning dynamic tactile sensing with robust vision-based training. IEEE Trans. Robot. **27**(3), 545–557 (2011)
75. G. Milighetti, T. Emter, H.B. Kuntze, D. Bechler, K. Kroschel, Combined visual–acoustic grasping for humanoid robots, in *IEEE International Conference on Multisensor Fusion and Integration for Intelligent Systems*, Heidelberg, Germany (2006)
76. P.K. Allen, A. Miller, P.Y. Oh, B. Leibowitz, Integration of vision, force and tactile sensing for grasping. Int. J. Intell. Mach. **4**(1), 129–149 (1999)

Chapter 5
Tactile Sensing Technologies

Abstract This chapter presents the state-of the-art of robotic tactile sensing technologies and analyzes the present state of research in the area tactile sensing. Various tactile sensing technologies have been discussed under three categories: (1) transduction methods; (2) structures that generate a signal on touch; and (3) new materials that intrinsically convert mechanical stimulus on touch into usable signals. The tactile sensing technologies are explained along with their merits and demerits. The working principle of various methods have been explained and selected implementations are presented.

Keywords Tactile sensing technologies · Artificial skin · Smart materials · Transducers · Tactile sensor · Tactile sensing array · CMOS · Transistors · MOS · MEMS · Polymer-MEMS · Flexible PCB · PCB · Soft robotics · Smart textile · Intelligent textile · TFT · Organic TFT · Extended gate

5.1 Historical Perspective

Tactile sensing has been a component of robotics for roughly as long as artificial vision and auditory sense modalities. Tactile sensing began to develop in the 1970s—albeit at a slower pace, when compared with the development of other sense modalities. Early surveys on the state of tactile sensing show a wide diversity in the types of sensing device that were developed in the 1980s [1, 2]. Early works on tactile sensing focused on the creation of sensor devices using new transduction techniques and a large number of experimental devices and prototypes were built and reported in the literature. Particular attention was given to the development of tactile sensing arrays for the object recognition [3]. The creation of multifingered robotic hands, in late 1980s, increased the interest in tactile sensing for robotic manipulation and thus started appearing works utilizing tactile sensing in real-time control of manipulation [4–7]. The new applications demanded features such as mechanical flexibility and conformability and accordingly new designs and materials for tactile sensing received attention. While the development of tactile sensors for robotic fingertips and hands continued, the application areas such as motion planning in unstructured environment brought whole body sensing to the fore. As a result, many sensitive

R.S. Dahiya, M. Valle, *Robotic Tactile Sensing*,
DOI 10.1007/978-94-007-0579-1_5,

Table 5.1 The classification of various Tactile Sensing technologies

Transduction Medium/Method	Material	Sensor Structure
Resistive	Composites	Microelectromechanical systems (MEMS)
Capacitive	Carbon Nano Tubes (CNT)	Plastic MEMS
Optical	Conductive Polymers	POSFET
Magnetic	Force Sensing Resistors	Extended Gate Transistors
Ultrasonic	Pressure Sensitive Ink	Organic Field Effect Transistors (OFET)
Piezoelectric	Conductive Gels	Flexible Printed Circuit Boards (PCB)
Electrorheological	Conductive Fibers and Yarns	Mechanical Switches
Magnetorheological	Piezo-/pyroelectric Materials	
Electrochemical	Photoelastic Materials	

skin design projects were undertaken in the late 1980s and 1990s [8–10]. The application domain of robotics has been continuously increasing and the new generation of robots nowadays include social robots, rehabilitation and assistive robots, biorobots, medical robots and humanoids. Compared to the human controlled industrial robots, operating in "No-Humans" working zones, these new generation robots are characterized by close interaction with environment (including humans) and autonomous learning. In addition to the standard manipulation and exploration tasks, the new generation robots are also expected to interact safely. Tactile sensors distribution over the entire body is indispensable to build service robots that can co-exist with humans for support and enhancement of human life. The full-body tactile sensor could generate more tactile information than in the case where only joint force and moment are measured. As a result, nowadays there is an increased interest in developing large area or whole body tactile sensing structures that allow a robot to safely carry out a task while maintaining physical contact [11–13].

Analyzing the present state of research in the area tactile sensing, three strategies emerge for the development of tactile sensing units in robots [14]: (1) developing sensors based on various methods of transduction; (2) development of structures that generate a signal on touch; and (3) the use of new materials that intrinsically convert mechanical stimulus on touch into usable signals. This classification of tactile sensing technologies is given in Table 5.1 and explained in this chapter along with their merits and demerits. The working principle of various methods have been explained and selected implementations are presented. Quite often the tactile sensing schemes belong to one or more aforementioned strategies, which is also reflected by some of the implementation presented in this chapter. The overview presented here also takes into consideration the reviews on the state of research in tactile sensing reported in literature from time to time [2, 4, 7, 13, 15–22].

5.2 Tactile Sensing Based on Various Transduction Methods

The transduction methods described in this section are listed in Table 5.1. These methods can be divided in to two categories: Firstly, the methods with coupled mechanical and electrical transduction—for instance, the capacitive, resistive, and ferroelectric methods, where deformation of the sensor surface due to object contact causes a change in an electrical parameters of the sensor material. Second, the methods with non-coupled electrical and mechanical transduction. Principle among these are the optical, ultrasonic, and magnetic transduction methods. This section describes all these methods in detail.

5.2.1 Resistive Sensors

Resistive tactile sensors utilize the change in resistance of the sensing material for detection and measurement of contact forces. The degree to which resistance of any sensing material changes depends on: (a) the contact location (e.g. potentiometer type); (b) the contact force or contact pressure (e.g. piezoresistance, and elastoresistance). Accordingly, the resistive tactile sensors can be grouped in two categories.

Resistive sensors based on the first type, are either made of two-dimensional grid of sensing elements or composed of two flexible sheets coated with a resistive material (with finite resistivity, typically on the order of 100 Ω/sq.) placed on top of each other and separated by air, microspheres, insulating fabric etc., as shown in Fig. 5.1(a). Accordingly, former arrangement is termed as discrete resistive touch sensing and latter as analog resistive touch sensing. The scheme of analog resistive touch sensing, in typical 4-wire configuration, is shown in Fig. 5.1(a)–(f). During operation, a uniform, unidirectional voltage gradient is applied to the first sheet, as shown in Fig. 5.1(b). When the two sheets are pressed together the second sheet serves like the slider in a linear potentiometer and measures the voltage as distance along the first sheet, thus providing the X coordinate. When this contact coordinate has been acquired, the uniform voltage gradient is applied to the second sheet to ascertain the Y coordinate. The complete method of ascertaining contact location is given in Fig. 5.1(b)–(f). As voltage V_x or V_y is applied over the X or Y plane and the voltage V_{xout} or V_{yout} measured at any of the analog high impedance (Hi-Z) terminals is approximately given by:[1]

[1]The actual expressions of V_{xout} or V_{yout} are:

$$V_{xout} = \frac{R_{x2}R_L}{R_{x1}R_L + R_{x2}R_L + R_{x1}R_{x2}}V_x \qquad V_{yout} = \frac{R_{y2}R_L}{R_{y1}R_L + R_{y2}R_L + R_{y1}R_{y2}}V_y \tag{5.1}$$

where, R_L is the resistance seen from contact point toward the measurement terminal i.e. $R_{touch} + R_{y1}$ (or R_{y2}) + Hi-Z. When impedance at the measuring terminal is high, these expressions in (5.1) reduce to (5.2)–(5.3).

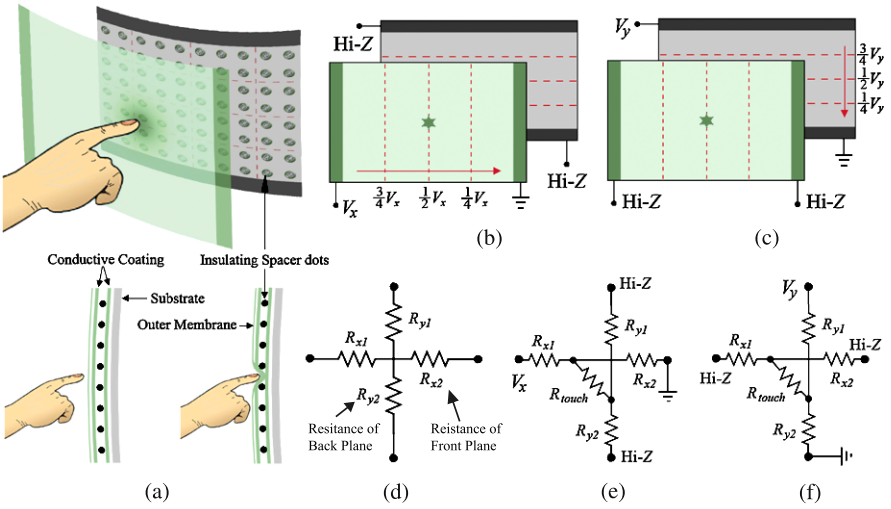

Fig. 5.1 (**a**) The scheme of analog resistive touch sensing; (**b**) X coordinate measurement: Voltage gradient applied across the front sheet and voltage measured at any of the Hi-*Z* terminals of back sheet; (**c**) Y coordinate measurement: Voltage gradient applied across the back sheet and voltage measured at any of the Hi-*Z* terminals of front sheet; (**d**) Circuit configuration under untouched condition; (**e**) Circuit configuration for measuring X coordinate; (**f**) Circuit configuration for measuring Y coordinate

$$V_{xout} = \frac{R_{x2}}{R_{x1} + R_{x2}} V_x \tag{5.2}$$

$$V_{yout} = \frac{R_{y2}}{R_{y1} + R_{y2}} V_y \tag{5.3}$$

proportional to the X or Y coordinate of contact point. Both the sampling of the two voltages and the subsequent calculations are very simple and the operation occurs instantaneously, registering the exact touch location as contact is made. In addition to the contact location, the touch pressure (or Z axis measurement) can also be measured by relating pressure to the resistance [23].

Analog resistive touch sensing technology typically results in high resolution (4096×4096 DPI or higher) and high response speed (10 msec or higher), thus providing fast and accurate touch control. However, the approach results in detection of only one contact location. While suitable for the touch screens of appliances such as personal digital assistants (PDAs), and as generic pointing devices for instruments, the analog resistive sensing technology has limited utility for robotic applications where simultaneous multiple contacts are often observed. With some design modifications the multiple contacts can be measured and hence analog resistive sensing technology can be adapted for robotic applications. Among others, the hybrid resistive tactile sensing [24] is one such technique that allows measurement of multiple contact points. Hybrid resistive sensing is a combination of the analog resistive and the array touch sensing technologies. It also involves two sheets of

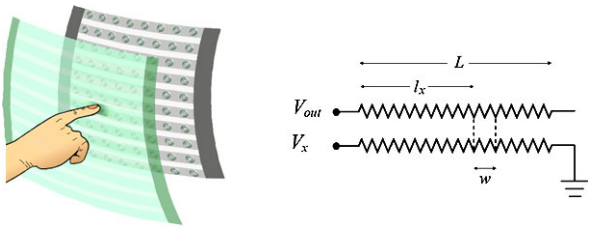

Fig. 5.2 The scheme and equivalent circuit diagram of hybrid analog resistive touch sensing

conductive materials, one on top of the other. However, one or both sheets are divided into multiple strips aligned along their lengths. One such scheme, with both sheets divided into multiple strips, is shown in Fig. 5.2. In this way, the configuration looks like one-dimensional arrays of stripped analog resistive sensors described earlier and the contacts can be sensed along different strips separately. The sensor measurement, along a strip, depends on both the location and the length of contact along each strip. Following a simple circuit analysis, the output of the sensor equivalent shown in Fig. 5.2 can be obtained as:

$$V_{out} = \frac{l_x + w/2}{L - w/2} V_{ref} \tag{5.4}$$

where, V_{ref} is the reference voltage applied across the sheet, w is the contact width, l_x is the contact distance from one of the ends as shown in Fig. 5.2, and L is the length of the strip. Because the sensor is discretized in one direction, each scanning of the sensor produces a set of at least n measurements from which the contact shape is to be reconstructed. In comparison with the n^2 operations needed with a conventional matrix sensor configuration, the number of measurements, and hence the scanning time, is much lower in case of hybrid resistive tactile sensing. The number of measurements in each scanning will, however, become $2n$ if two measurements are made for each contact point—as in analog resistive touch sensing described earlier. Similarly, the scheme discussed above requires a minimum of $n + 2$ connectors/wires (one for the V_{ref}, one for common ground, and n for the sensing the individual strips) against $2n$ (without MUX) needed with a conventional matrix sensor configuration.

Piezoresistive touch sensors are made of materials whose resistance changes with force/pressure. Touch sensing system using this mode of transduction have been used in anthropomorphic hands [25]. Piezoresistive tactile sensing is also popular among the MEMS based and silicon based tactile sensors [26–28]. Some examples of piezoresistive sensors are given in Fig. 5.3. These examples also include the sensors that are based on MEMS approach. The MEMS based tactile sensors are described later in the section on tactile sensing structures.

Recently, the piezoresistive tactile sensors have been realized using materials such as conductive rubber, conductive polymers, conductive gels, conductive fibers and yarns, force sensing resistors (FSR), and pressure sensitive ink etc. Sometimes, the changes in resistance of a conductive elastomer or foam is also termed as elastoresistance or elastoresistivity. However, for simplicity, the term piezoresistance is used in this book. Some of these materials are described later in this chapter.

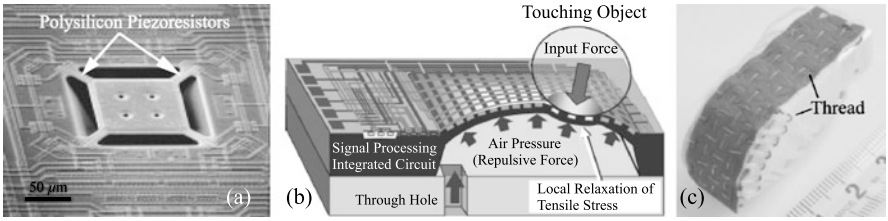

Fig. 5.3 (**a**) An example of piezoresistive based MEMS traction stress sensor consisting of a plate suspended with four bridge structures. (Characteristic dimensions: bridge $= 22 \times 12 \times 2.35$ μm, plate $= 100 \times 100 \times 2.85$ μm, pit depth ≈ 100 μm.) A polysilicon resistor is embedded in each bridge (with permission from [28], ©(2000) IEEE); (**b**) An example of piezoresistive based flexible MEMS sensors array (with permission from [30], ©(2006) IEEE); (**c**) Pressure conductive rubber based touch sensor with wires stitched on it (with permission from [31], ©(2004) IEEE)

The tactile sensors based on a conductive polymer film called FSRs are widely used in pointing and position sensing devices such as joysticks and are commercially manufactured by Interlink [29]. FSRs have rows on one flexible substrate and columns on another. They also feed the output voltage back to the other columns to eliminate a flow of current between the measured column and the others. It takes about 25 μs for the feedback loop to settle. Unlike other conductive polymer, patterned FSRs therefore do not have in-plane conduction between the rows, which reduces sensitivity. The FSR sensors are appealing, because of the low cost, good sensitivity, low noise and simple electronics and, in fact, can be found in many experimental tactile systems. One of their drawbacks is the relatively stiff backing. Although examples of advanced robotic hands equipped with FSRs exist [32, 33], these sensors generally require serial or manual assembly, provide highly non-linear response and suffer from hysteresis.

A number of touch sensors using pressure conductive rubber as transducer have also been reported [31, 34]. They take advantage of change in impedance due to the applied force/pressure. One such sensor by Shimojo et al. [31] is shown in Fig. 5.3. The horizontal and vertical wires (i.e. rows and column wires) are stitched into a layer of conductive rubber and the sensing elements of the array are formed at the intersections of the rows and columns. A total of 16×3 sensor elements are obtained in an area of 44 mm $\times$ 12 mm, with a pitch of 3 mm. The sensor elements show a repeatable but non-linear and hysteric response to applied pressure in the range of 0–200 kPa. The delay between input and output is reported to be 1 ms, which is expected to go up if the time taken by rubber to regain the original shape is also considered. Presence of hysteresis and non-linearity are some of their drawbacks.

In recent years, the stretchable tactile distribution sensors based on conductive sheets (made of one or more layers of conductive materials) have been developed [35–37]. The electrical impedance tomography EIT[2] technique is employed in these

[2]Electrical impedance tomography (EIT) is an imaging technique used to estimate the internal conductivity distribution of an electrically conductive body by using measurements made only at the boundary of the body. The technique is also used in non-invasive medical applications.

sensors to obtain the contact information. In this method, a conductive material with electrodes placed on its boundaries is used as the tactile sensor. The current is injected into the sheet via electrodes and impedance distribution is observed. On application of pressure, the impedance distribution changes resulting in to the change in current distribution, which can be quantified using EIT. The tactile sensing scheme can be used to detect contact events such as stroking, pinching and grabbing. Since most of the sensing area in an EIT based sensitive skin is made of an homogeneous thin material without any wiring, a large, flexible and stretchable skin suitable to cover small and large areas of variable three dimensionally contoured bodies can be realized. The requirement of continuous current injection (and hence loss of energy) is a major area of concern that can hinder effective utility of this approach, especially in the autonomous robots that rely on battery power.

Tactile sensors based on quantum tunneling composites QTC have also come up recently and commercially available from Peratech [38]. QTC's have the unique capability of transformation from a virtually perfect insulator to a metal like conductor when deformed by compressing, twisting or stretching of the material. These materials are described later in this chapter.

The resistive tactile sensing technology is economical and simple to construct and use. Further, the complexity does not increase with the size of the sensor surface and the sensor can be produced with inexpensive materials. Another issue with resistive touch sensing technology is the higher power consumption.

5.2.2 Capacitive Sensors

The capacitive measurement methods have been used for a long time in many applications to measure physical values like distance, pressure, liquid level, acceleration, humidity, and material composition etc. The newer applications, widely using capacitive touch technology, include human–machine interfaces applications such as laptop track pads, computer displays, mobile phones and other portable devices. The capacitive measurement methods are also widely used in many MEMS based touch sensing arrays such as those for high resolution tactile imaging of fingerprints. The techniques has also been employed in robotics to detect contacts over large areas of a robot's body.

At the heart of any capacitive sensing system is a set of conductors that interact with electric fields. Typically, the capacitive sensors are the plate capacitors (Fig. 5.4), consisting of two identical and parallel metal plates or electrodes of area A separated by a distance d with a flexible spacer (usually, silicone or air) of relative dielectric constant ε_r. The basic principle behind working of a capacitive sensor is detection of the change in capacitance when something or someone approaches or touches the sensor. The capacitance of a parallel-plate type capacitor (Fig. 5.4) is given as:

$$C = 4\pi\varepsilon_r\varepsilon_0\frac{A}{d} + C_f \tag{5.5}$$

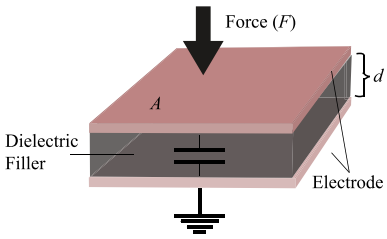

Fig. 5.4 A parallel plate capacitor consisting of tow parallel plates of area A, separated by a flexible insulator of relative dielectric constant ε_r. The thickness of the dielectric film is d

where, ε_0 is the (electric) permittivity of a vacuum, and C_f is the contribution from edges of the electrode (which tend to store more charge than the rest of the electrode). Typically, $A \gg d^2$ in all designs for tactile sensors, therefore, the C_f term is negligible. The distance between the electrodes is usually lower, as the inverse relation between capacitance and gap between electrodes is highly non-linear and the sensitivity drops significantly with larger gaps.

When a force is applied on the capacitive sensors, it changes the distance between the plates or the effective area—resulting in the changed capacitance. The normal force changes the distance between the plates while tangential force changes the effective area between the plates. The capacitive sensor are thus capable of detecting touch by sensing the applied normal or tangential forces; however, they are not efficient enough to distinguish these two types of forces. The change in capacitance is eventually converted into a change in voltage by using an appropriate circuit[3] and a measure of the applied force is obtained. The capacitive sensors therefore convert the physical input signal to the output signal in two steps: firstly, by transducing a physical quantity into a change of electric capacitance; then, by measuring and converting the capacitive signal into an electric output signal.

The capacitive touch sensing systems are of two types: the self- or absolute capacitance type, where the object (such as a finger) loads the sensor or increases the parasitic capacitance to ground; and the mutual capacitance type, where the object alters the mutual coupling between two electrodes.

The self capacitance is defined as the capacitive load, relative to circuit ground, that an electrode presents to the measurement system. A self capacitance type touch sensor, shown in Fig. 5.5(a), has one electrode that represents one plate of the capacitor. The corresponding second plate is represented by the environment of the sensor electrode and another conductive object, like a human finger, to form a parasitic capacitor $C_{Electrode}$. The sensor electrode is the only direct connection to the sensor controller. The capacitance of the sensor pad is measured periodically. When a conductive object, like a human finger approaches or touches the electrode, as shown in Fig. 5.5(b), the measured capacitance will increase by a value C_{Touch}

[3]The measurement circuits used to measure the capacitance change are based on methods like, relaxation oscillator, Charge time versus voltage, Voltage divider, Charge transfer, and Sigma–Delta modulation etc. The capacitance changes are measured using parameters like shift of resonance frequency, frequency modulation, amplitude modulation, charge time measurement, time delay measurement, and duty cycle etc.

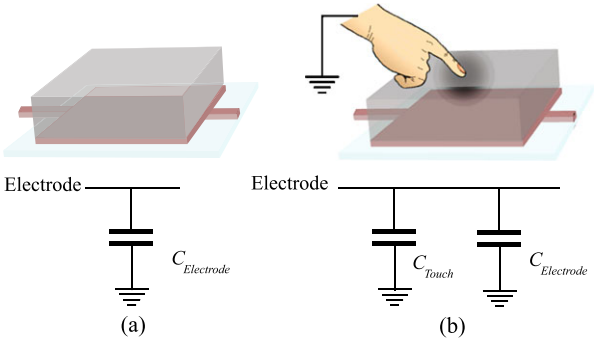

Fig. 5.5 (**a**) The self-capacitance type touch sensor with parasitic capacitance $C_{Electrode}$; (**b**) The additional capacitance C_{Touch} is generated when a conductive object touches the sensor

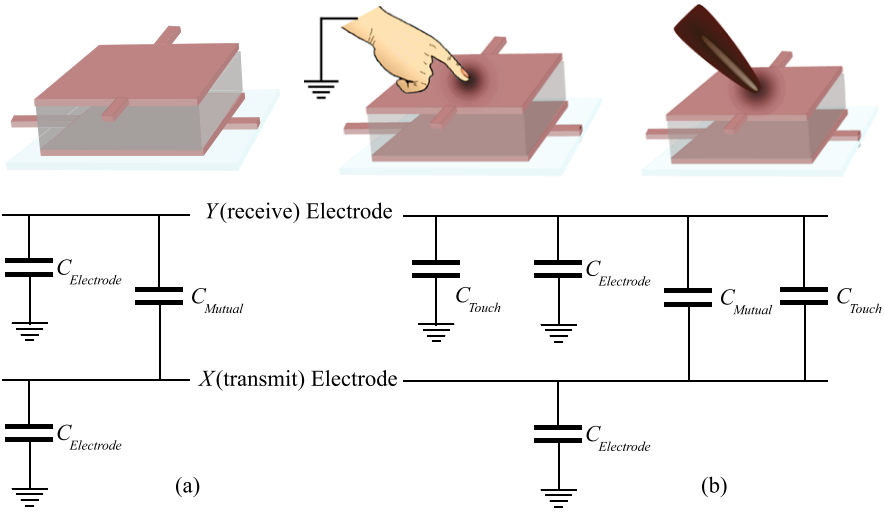

Fig. 5.6 (**a**) The mutual-capacitance type touch sensor. $C_{Electrode}$ is the parasitic capacitance of electrodes and C_{Mutual} is the mutual capacitance between electrodes; (**b**) The additional capacitance C_{Touch} is generated when any object touches the sensor

and the change is detected by the measurement circuit. The capacitance of touch is dependent on sensor design, sensor integration, touch controller design and the touch itself. These sensors tend to emit electric fields in all directions, and as such are quite non-directional. They are prone to false signals from parasitic capacitive coupling. Measuring self capacitance does not easily lend itself to supporting simultaneous multiple contacts, which requires correlation of multiple X and Y touched electrodes into multiple (X, Y) touch coordinates.

The mutual capacitance type touch sensors have two electrodes: an X (transmit) electrode, and a Y (receive) electrode, as shown in Fig. 5.6. The mutual capacitance is the capacitive coupling between the two electrodes. The arrangement is typically

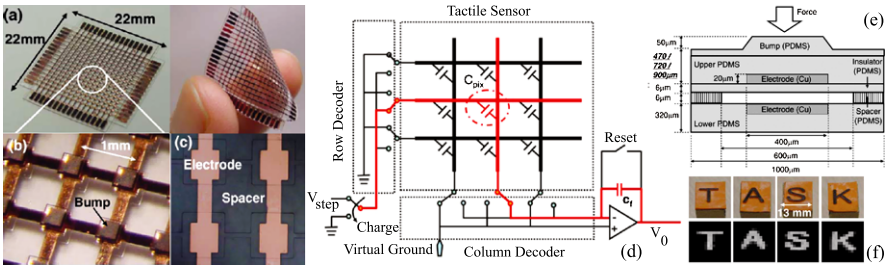

Fig. 5.7 (**a**) The capacitive tactile sensing module; (**b**) The magnified view of the sensing elements; (**c**) The bottom electrodes and the spacers; (**d**) The schematic of the readout circuit; (**e**) The cross-section view of one of the tactile sensors; (**f**) Flipped photographs of rubber stamps and their tactile images captured by the tactile sensing module (with permission from [39], ©(2006) IEEE)

used in array type tactile schemes, with the intersection of each row and each column making a capacitor. A 16×16 array, for example, would have 256 independent capacitors. A voltage is applied to the rows or columns. Bringing an object near the surface of the sensor changes the local electric field which reduces the mutual capacitance. The mutual capacitance from X and Y is measured by the sensor controller. The arrangement of electrodes may differ from the one shown Fig. 5.6. For instance, the two electrodes can also be in same plane as in interdigitated structures. Further, different electrode patterns can be used to create a capacitive sensor. The electrode pattern geometries are an important factor in the overall resolution and touch sensitivity of the sensor. The advantages of mutual capacitance based touch sensors include their ability to detect accurately the multiple contacts at the same time.

The mutual capacitive type touch sensors are more suitable (than the self capacitive type sensors) for robotics applications as the arrangement allows contact detection for human fingers (or conductive objects) and other objects. They can be made by using micromachined silicon technology as well as by the conventional non silicon technology. They can therefore be miniaturized, allowing construction of dense sensor arrays as in many MEMS capacitive sensors, or can be to made larger and suitable to cover various body parts of a robot. Examples of dense tactile sensing arrays include the tactile sensing array by Lee et al. [39], consisting of 16×16 capacitive cells or sensing elements. The key features of this capacitive tactile sensor array, shown in Fig. 5.7(a)–(c), include its mechanical flexibility (owing to its construction using multiple PDMS layers) and scalability. The capacitive tactile elements are formed at the intersection of the orthogonal row and column (or upper and lower) copper electrodes. For maximum sensitivity, air gap (as dielectric) is encapsulated between the electrodes at each intersection. The sensor size and electrode size are $600 \times 600\ \mu m^2$ and $400 \times 400\ \mu m^2$, respectively. The capacitance change at every individual point on the grid is measured to accurately determine the touch location by measuring the voltage in the other axis. The read out scheme employed for this purpose is given in Fig. 5.7(d). The capacitance C_{Mutual} of an element is read in 100 μsec (20 frames per second) by first selecting it with the help

of row and column decoders. The voltage V_{step} is applied to row electrode of this sensor to charge the capacitor. When V_{step} is switched to ground, the stored charge in the capacitor is transferred to the feedback capacitor C_f and changes the output voltage V_0 as:

$$\Delta V_0 = -\Delta V_{step} \frac{C_{Mutual}}{C_f} \tag{5.6}$$

The resolution of tactile sensor response is 1 mN and the full scale range is 40 mN (250 kPa). This capacitive tactile sensing systems is scalable, as multiple modules can be stitched with each other. Realized using MEMS approach, the sensor is composed of five PDMS layers (Fig. 5.7(e)), with the two copper electrodes embedded in the PDMS membrane. Using PDMS elastomer is as a structural material is useful in obtaining a mechanical flexible and compliant tactile sensing array. However, it is challenging to precisely control the thickness of various PDMS layers. For the same applied force, the variation of thickness of various layers results in variation among the responses of various sensing elements in the array.

The examples of capacitive touch sensors obtained using non-silicon technology include, the array of 16 capacitive sensors by Schmidt et al. [40]. The sensor couple to the objects being grasped via small brushes of fibers for dynamic sensing; thus providing two types of dynamical tactile information—speed and vibration—as analogous to the two types detected by human skin. This arrays furthermore is paired with two foil-based piezoresistive force sensors for static sensing. The sensor elements on the array are sensitive (with a threshold of about 5 mN) and robust enough not to be damaged during grasping. Commercially available touch sensors such as 'RoboTouch' and 'DigiTacts' from Pressure Profile Systems [41] are other examples of capacitive touch sensors obtained using non-silicon technology.

Recently, the capacitive (and also resistive) touch sensing technology has made its way to the human–machine interface applications such as mobile phones and other portable devices. The development of 'capacitance to digital converter' Integrated Circuit (IC) chips like 'AD7147 and the AD7143 from Analog Devices [42] has also contributed to wide usage of capacitive technology. These chips provide excitation to the capacitance sensor, sense the changes in capacitance caused by the user's proximity, and provide a digital output. The availability of these chips have made it easier to design paper-thin and reliable contemporary touch controls for the capacitive technology based sensitive touch sensors. Availability of these capacitance to digital converter chips has also been helpful to robotics. The capacitive robotic tactile sensing solutions, utilizing these chips have recently been reported by Maggialli et al. [43]. The tactile skin developed in European Commission funded project 'Roboskin', described later in this chapter, extensively employs these integrated circuits with capacitive tactile sensors to cover various lesser sensitive body parts of robots. Touch sensors based on capacitive mode of transduction are sensitive, easy to fabricate, and immune to temperature variations, but stray capacity and hysteresis are major drawbacks.

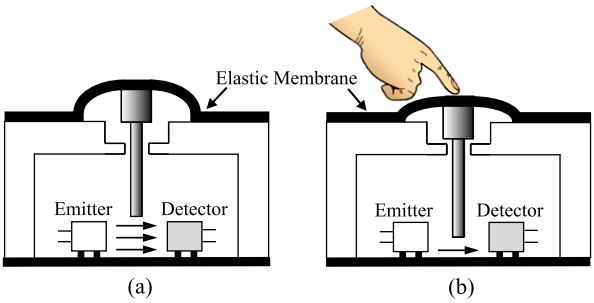

Fig. 5.8 (**a**) The optical transducer before applying the force or before contact; (**b**) The opaque pin moves downward after contact and blocks the block path of light between *emitter* and *detector*, thereby reducing the intensity of light received by *detector*

5.2.3 Optical Sensors

The optical mode of transduction is another alternative for the tactile sensing in robotics. In simple terms, the optical sensing involves "injecting" light into a medium (generally, soft and deformable) and measuring the change in the amount or the pattern of light when force is applied. Depending on how the amount or pattern of light is detected, the tactile sensors based on optical mode of transduction can be grouped into two categories [44]:

1. The *extrinsic* optical sensors, where the physical stimulus interacts with the light external to the primary light path.
2. The *intrinsic* optical sensors, where the optical phase, intensity, or polarization of transmitted light are modulated without interrupting the optical path.

Sometimes, optical fibers are directly used as the transducers in the design of tactile sensors. Therefore, this could also be considered as the third category of optical sensors. The working of optical tactile sensors, along with selected examples are described below.

In case of extrinsic optical sensors, the transducer's surface, generally made of compliant material, has on its underside a grid of elongated pins, as shown in Fig. 5.8. When force is applied to the compliant surface, the pins on the underside move downward and block the light path or modulate the light transmission between emitter and detector. As evident from the names, the function of emitter (a light-emitting diode (LED)) is to emit the light and that of detector (a photodetector) is to detect the same. The amount of downward movement and the degree to which the light is blocked or allowed to pass, gives a measure of the applied force. Correspondingly, the more the applied force, less is the amount of light received by the detector. The major problems with this type of arrangement, especially when the compliant surface is made of rubber, include: creep, hysteresis, and temperature variations. Furthermore, calibration is needed for each emitter–detector pair. Unlike resistive or capacitive sensors, the construction of this type of sensor is quite labor intensive.

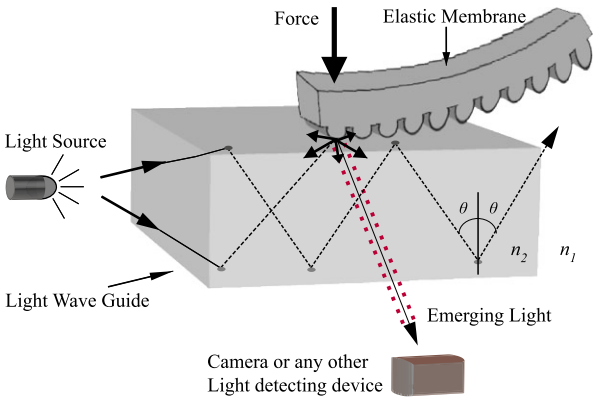

Fig. 5.9 The optical tactile transducer based on the principle of frustrated total internal reflection

The intrinsic optical tactile sensors normally utilize the change in intensity of transmitted light for measuring the tactile parameters such as contact force. Among various possible configurations, the one based on frustrated total internal reflection has been widely reported for the optical based tactile sensing. These tactile sensors use the properties of optical reflection between media of different refractive index, as shown in Fig. 5.9. The transducer structure is composed of a clear plate acting as light guide, a light source, a light detector and a compliant membrane stretched above, but, not in close contact with the plate. The lower surface of the plate acts as the imaging area. Light is directed along an edge of the plate and it goes through total internal reflection (when no force is applied) or diffuse reflection (when force is applied). The total internal reflection occurs when light is propagating in the denser of two media (i.e. refractive index, $n_2 > n_1$) and strikes the interface at an angle larger than a particular critical angle with respect to the normal to the interface (i.e. $n_2 \sin\theta \leq n_1$, where θ is the angle of incidence at the interface of two media). The light coming out of plate due to diffuse reflection can be recorded either by an array of photodiodes, solid state optical sensors, CCD or CMOS cameras placed in the imaging area or transported away from the sensor by optical fibers. The intensity of the light (bright or dark patches on image) is proportional to the magnitude of the pressure between object and plate. A weak point of these tactile sensors is the large consumption of current by various components.

With suitable design, this kind of sensor can also be made sensitive to shear forces. The optical waveguide based three axial tactile sensor by Okha et al. [45] is one such example. The sensing arrangement, shown in Fig. 5.10, designed in a hemispherical dome shape, mimicking the structure of human fingertips, consists of an array of 41 pieces of sensing elements made from silicon rubber, a light source, an optical fiber-scope, and a CCD camera. The silicone rubber element comprises of one columnar feeler and eight conical feelers. When sensor comes in contact with an object, the feelers collapse at the point of contact. At the points where the conical feelers collapse, light is diffusely reflected out of the reverse surface of the optical waveguide. The collapsed feelers are observed as bright spots in the image data

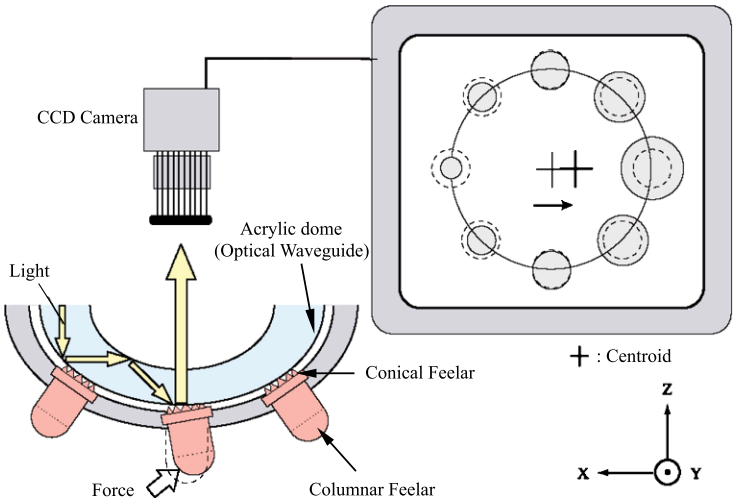

Fig. 5.10 Three-axis optical tactile sensor (with permission from [48]) capable of detecting forces in both normal and shear direction

acquired by the optical fiber-scope, connected to the CCD camera, and transmitted to the computer. In measurement process, the normal force of the F_x, F_y and F_z values are calculated using integrated gray-scale value, while shearing force is based on horizontal center point displacement. The sensor is capable of measuring normal and shear forces in the range 0–2 N, with a resolution of 0.001 N.

The intrinsic optical tactile sensing has also been used to develop the tactile sensing structures that can cover large body parts of a robot. Examples of such structures include the 32 element lightweight, conformable and scalable large area skin by Ohmura et al. [46]. The sensing element consists of photo-reflectors ($3.2 \times 1.1 \times 1.7$ mm) under the urethane foam (thickness 5 mm) and the light scattered by urethane foam upon deformation gives the measure of mechano-electrical transduction. The foam thickness controls the dynamic range and sensitivity of the sensors. This work is also explained later in the section on tactile sensing structures. The KINOTEX tactile sensors that use similar method, are also commercially available [47].

The fiber Bragg grating FBG based sensors also belong to the extrinsic optical sensors category. The basic principle of an FBG based sensor system lies in the monitoring of the wavelength shift of the returned Bragg-signal. The wavelength shift is a function of the parameter to be measured (e.g. strain, temperature and force). The 3×3 tactile sensor by Heo et al. [49] is an example of the FBG based optical tactile sensors. The sensor capable of measuring normal forces as low as 0.001 N with the spatial resolution of 5 mm.

Highly sensitive electrooptical tactile sensors based on CdS nanoparticles (capable of emitting visible light or the electroluminescence light on application of load) have been reported recently by Maheshwari and Saraf [50]. This tactile sensing is

described the next section, where many other new materials for tactile sensing are also described.

Many times fibers have also been used as transducers in the design of tactile sensor. As an example, the light coupling between adjacent fibers can be used to detect the contact events. Usually, the light propagates along an optical fiber with very little loss. However, the light can leave and enter the fiber from a point if its surface at that point is roughened. Therefore, light coupling can take place between two optical fibers passing close to each other, and both having a roughened surfaces. Measuring the increase in light attenuating due to microbending (which otherwise is considered as a disadvantage of the optical sensors) is another way of using the optical fiber as transducers. This effect has been put to use in microbend touch sensors by Winger and Lee [51]. The experimental 2×2 robot sensor is capable of detecting a 5 gm variation in the applied load within its linear region, which ranges between 125 gm and 225 gm per sensor element. The plastic optical fibers have also been used for the tactile sensor working on the principle of microbending [52]. With plastic optical fibers the limitations like rigidity and fragility can be overcome.

Some potential benefits of optical tactile sensors include, immunity to external electromagnetic interference, flexible, intrinsic safety, high resolution, low cost, and design simplicity. Some of the optical sensors suffer from the loss of light, for example by micro bending and chirping, causing the distortion in the signal. Owing to the paraphernalia needed to emit (source) and receive (detector) the light, at times they are bulky and it is difficult to reduce their dimensions. With the advent of smaller surface mounted silicon components it is possible to mount the small light emitter and detector pair inside the sensing element itself—raising hopes for small size optical tactile sensing systems.

5.2.4 Magnetism Based Sensors

The touch or tactile sensors based on magnetic transduction are developed using two approaches. Firstly, the sensors measuring the applied force led change in the magnetic flux using either the Hall effect or magnetoresistance.[4] Second, the sensors measuring the change in the magnetic coupling or change in the inductance of a coil as a result of applied force or pressure. A few tactile sensors using these approaches have been reported in literature [53–55].

[4]The charge carriers flowing through a conductive material, in presence of a magnetic field, experience a force orthogonal to their flow directions and the magnetic field direction. As a result the charge carriers are deflected, leading to the appearance of Hall potential in direction of the deflection. This is termed as Hall Effect. Due to this deflection, the charge carriers take a longer path to travel the length of the conductive material, meaning that the deflected particles have a lower mobility and hence an increased electrical resistance. This effect is known as magnetoresistance. Both the Hall effect and magnetoresistance can be used to measure magnetic field intensity.

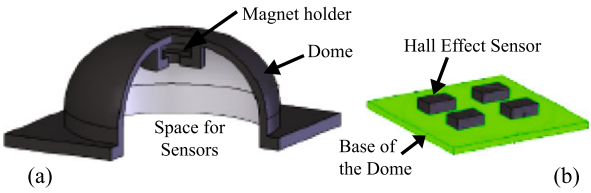

Fig. 5.11 Compliant magnetic tactile sensor (with permission, from [55]). (**a**) Silicone rubber dome as compliant cover. (**b**) Circuit board using hall effect sensors to detect deformation

If a very small permanent magnet is held above the Hall effect type detection device by a compliant medium, the change in flux caused by the magnet's movement due to an applied force can be detected and measured. The field intensity follows an inverse relationship, leading to a nonlinear response, which can be easily linearized by processing. In case of the Hall effect type detection devices, the change in magnetic flux is reflected into the change in Hall voltage, which can be easily measured. In a similar way, the magnetoresistance type detection devices are also used. It may be noted that a Hall effect sensor is only sensitive to magnetic fields in one direction while the magnetoresistive effect can be used to detect magnetic field having any orientation within a plane normal to the current flow. An example of Hall effect type tactile sensing arrangement is given in Fig. 5.11 [55]. This tactile sensing arrangement by Eduardo et al. has a small magnet embedded in the top of the dome. The base of the dome is glued to a printed circuit board (PCB), which also contains four Hall effect sensors. The difference in the signals from these four sensors is used to detect roughly the lateral displacement and the average of signals is used to obtain the vertical displacement. Four domes, similar to the one shown in Fig. 5.11(a), have been used at each phalange of robot's finger. The sensitivity of the sensor can be controlled by changing the shape of the domes. The optical version of this sensing arrangement has also been presented by Eduardo et al. [56]. All these sensing arrangements can detect normal, lateral and shear forces. Further, they can deal with the saturation when applied forces are out of range. The arrays of sensors by Eduardo et al. [55, 56] have also been tested in robots like Obrero and GoBot while doing actual tasks.

In the case of sensors measuring the change in the magnetic coupling or change in the inductance of a coil as a result of the applied force or pressure, the core of the inductor is generally made of magnetoelastic materials. The magnetoelastic materials deform under pressure and cause the magnetic coupling between transformer windings, or a coil's inductance to change. These materials change their magnetic permeability when they are deformed. A sensor array of 16×16 magnetoelastic sensor elements with 2.5 mm spacing has been reported by Luo et al. [57].

The tactile sensors based on magnetic principle have a number of advantages that include high sensitivity and dynamic range, no measurable mechanical hysteresis, a linear response, and physical robustness. They are capable of measuring three dimensional force vectors. Major drawback of magnetic based tactile sensor is that they cannot be used in magnetic medium.

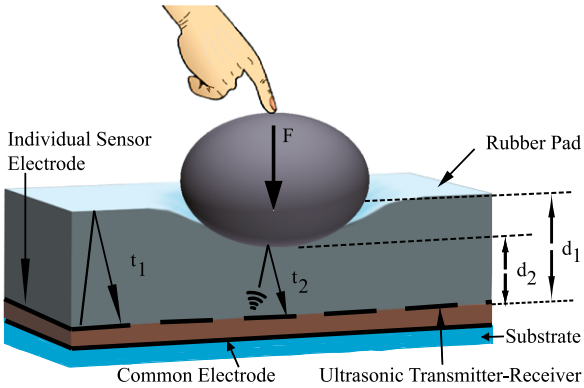

Fig. 5.12 Working of an ultrasonic tactile sensor

5.2.5 Ultrasonics Based Sensors

The ultrasonic transduction for tactile sensing is one of the methods where mechanical transduction is decoupled from electrical transduction. A typical ultrasonic sensing arrangement, shown in Fig. 5.12, involves a thin rubber covering that is deformed when an object presses into it. The amount of this deformation depends upon the magnitude of the force applied to the object and the stiffness of the rubber. Underneath this rubber covering are ultrasonic transmitters and receivers. The ultrasonic transmitters launch a small ultrasonic pulse of a few megahertz into the rubber pad. This pulse then propagates through the pad and is reflected from the exposed surface of the rubber. The reflected or echo pulse is received by the receiver, which is usually the same element that launched it. The round-trip travel or transit time is proportional to the thickness of the rubber pad overlying a particular tactile element. Therefore, by measuring the change in the round-trip travel or transit time (i.e. $t_1 - t_2$) of the pulse, it is possible to measure parameters like change in the thickness of the rubber pad (i.e. $d_1 - d_2$) and hence the applied force. The operation of the sensor can be expressed as:

$$d_1 - d_2 = \frac{1}{2}(t_1 - t_2) \tag{5.7}$$

$$F = k(d_1 - d_2) = \frac{1}{2}k(t_1 - t_2) \tag{5.8}$$

where, F is the compressing force, c is the speed of propagation of the ultrasonic wave in the rubber covering, and k is the rubber stiffness. Typically, the ultrasonic pulse transit times through the pad and back are on the order of few microseconds and changes in pad thickness of a few microns can therefore be detected. The strength of the echo pulse depends upon the acoustic properties of the rubber pad and the material contacting the pad.

The microphones based on ultrasonics have been used to detect surface noise occurring at the onset of motion and during slip. A 2×2 tactile array of polyvinylidene fluoride (PVDF), by Ando and Shinoda [58], senses contact events from their ultrasonic emission at the contact point. Here, PVDF polymer is used as receiver

to localize the contact point on a silicone rubber-sensing dome. The sensor is reportedly very effective in detecting slip and surface roughness during movement. The piezoelectric materials such as PVDF polymer and PZT are typically used as transmitters and receivers in the ultrasonic sensing applications.

The six-axis deformation sensing scheme by Ando et al. [59] is another example. The deformation sensing scheme is based on precise encoding and decoding of deformation components into ultrasound wavefronts. The arrangement consists of a 2×2 ultrasonic transmitter matrix and a 2×2 ultrasonic receiver matrix, placed face to face at a distance of a few tens of wavelengths. The prototype tactile sensor is embedded in a flexible hemispherical fingertip-like body. All of the transmitter elements are driven sinusoidally and simultaneously, but they are switched into the same, reversed, or quadrature phases to generate a particular shape of wavefront on the receiver matrix. The sensing scheme is able to detect three translational components and three rotational components of displacement around a transmitter position nearly simultaneously.

The resonant frequency of the piezoelectric materials changes when they come in contact with the objects having different acoustic impedances [60, 61]. The change in resonance frequency of the sensor, in accordance with the contact object's acoustic impedance, is also sometimes used to detect contact parameters. The change in resonance frequency has been used for detecting hardness and/or softness of objects [62] and to detect force/pressure [63]. Simple and elastic tactile sensors utilizing acoustic resonance frequency to detect contact parameters like principal stress, friction, and slip are also described in [64, 65]. The ultrasonic-based tactile sensors have fast dynamic response and good force resolution. However, many such sensors use materials like lead zirconate titanate (PZT), which are difficult to process in miniaturized circuits.

5.2.6 Piezoelectric Sensors

The piezoelectric transducers generating charge/voltage proportional to the applied force/pressure. They are also able to generate force due to applied electrical input. They can therefore be used both as sensors and actuators—the property that makes them 'Smart Materials'. The mechanical and electrical transduction are coupled in case of piezoelectric sensors. A simplified explanation of the piezoelectric phenomenon and the main concepts and working of piezoelectric sensors and transducers are given in Appendix A of this book.

A typical piezoelectric tactile sensor element has the same construction as the capacitance-based sensors (Fig. 5.4), where the dielectric material is piezoelectric with thickness t and area A. The piezoelectric material deforms by Δt on touching with contact force F to generate charges $+Q$ and $-Q$ at the two electrodes. As the element is also a capacitor, the induced charge leads to a potential V across the tactile element, as given by:

$$V = \frac{Q}{C} \approx \frac{dF}{C} = \frac{dt}{4\pi\varepsilon\varepsilon_r A} F \tag{5.9}$$

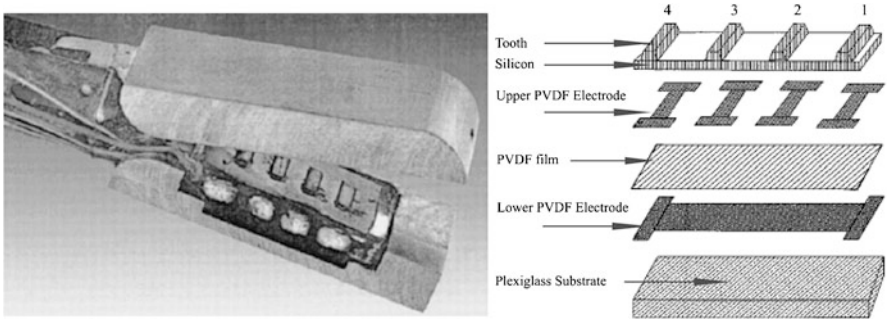

Fig. 5.13 An endoscopic grasper prototype integrated with the piezoelectric tactile sensor. The photograph (*left*) of the endoscopic grasper prototype and (*right*) the expanded view of the piezoelectric polymer PVDF based tactile sensor unit (with permission, from [66], ©(2000) IEEE)

where d is the piezoelectric constant of the material and C is the static capacitance. As given in Appendix A, d is a tensor with values depending on the orientation of the crystal in the film. For a simple uniaxial case (most often used) the tensor notation of d would be d_{33}. Similar to the capacitance-based device, the sensitivity of response to the applied contact force F is proportional to the signal V. However, in contrast to the capacitance device, the value of t should be large and that of ε_r should be low. In other words, to achieve high sensitivity, the d/ε_r ratio of the piezoelectric material must be as large as possible.

The piezoelectric sensors are highly sensitive with high voltage outputs even to small dynamic contact deformations. If a load is maintained, then the sensor output decays to zero. Therefore, these sensors are most suited for sensing dynamic forces. The sensing elements do not require power supply for its operation, and hence the sensor using piezoelectric transduction are reliable and efficient in terms of power consumption. Depending on the design of the sensor, different modes (longitudinal, transversal and shear) can be used to load the piezoelectric element. The tactile sensors based on piezoelectric transduction exhibit high sensitivity, a large dynamic range, a wide bandwidth with good linearity, and a high signal-to-noise ratio (SNR). The piezoelectric materials often used in tactile sensing schemes are described later in the section on tactile sensing materials.

A large number of tactile sensors, using either silicon micromachining technique or simply the polymer foils, have been reported in literature. A tactile sensor developed using PVDF piezoelectric polymer film and micromachining techniques is given in Fig. 5.13. This tactile sensor unit, by Dargahi et al. [66], is integrated with an endoscopic grasper suitable for minimally invasive surgery. The micromachined silicon part is patterned like a rigid tooth-like structure to transfer force to the PVDF film. As may be noted from Fig. 5.13, the sensor structure consist of three layers: the top layer, made of micromachined silicon to have a rigid tooth-like structure; the bottom layer, a flat plexiglass substrate; and, a 25 μm thick PVDF film sandwiched between the plexiglass and silicon. The top side of PVDF film consists of four strips of aluminum electrodes and the bottom side has a single common electrode. Four

output signals are therefore derived from the sensing device. When force is applied to any point on the surface of the silicon part, the stress in the PVDF results in a polarization charge at each surface. The difference between the response signals at four electrodes is used to indicate the localized position of the applied force.

A stress-component-selective tactile sensing array, based on piezoelectric polymers is presented in [67]. This multi-component touch sensing array consists of an assembly of seven elemental sub-arrays—each consisting of six miniaturized sensors, supported by a polyimide sheet and sandwiched between two elastic layers. Dario and Buttazzo [68] have developed a anthropomorphic robotic finger that uses piezoelectric polymer (PVDF) film as tactile sensor. This sensor contains two force-sensing layers and has the additional capability of sensing thermal properties. PVDF film sensors are also used in another implementation of robotic fingertip by Hosoda et al. [69]. In this arrangement, the PVDF films and strain gauges sensors are randomly embedded into a silicone layer.

Some other piezoelectric transduction based tactile sensors, including novel POSFET tactile sensing devices and the high resolution tactile sensing arrays, are discussed in Part II of this book.

In general, the piezoelectric transducers also exhibit pyroelectric properties, i.e. they generate charge/voltage when contact or ambient temperature changes. This is useful property as same sensor can be used to measure multiple contact parameters such as force and temperature. However, it is difficult to decouple or separate the responses when both piezoelectric and pyroelectric effects occur simultaneously. In such cases, the contribution from one of the effects could become significant source of noise in the overall response. For instance, if contact force is the parameter of interest, then ambient temperature variation may introduce noise in the overall response. Thus, protection from thermal variations may be necessary if force or pressure variations are important. Such errors can also be mathematically compensated, as explained later in Chap. 8, by recording the temperature variations with a temperature sensors and finding out corresponding pyroelectric response from pre-recorded database. The latter can then be subtracted from overall response to obtain the response due to force or pressure only.

5.2.7 Electrorheological Sensors

Some gels or electrorheological (ER) fluids have the ability to transform from a liquid to a plastic state, in milliseconds, on application of a strong electric field across them. This is known as the electrorheologic effect. The fluid viscosity of the ER fluid is proportional to the applied field strength. The ER fluids are a suspension of a dielectric solid or polymeric particles (the dispersed phase) in an insulating base oil (the continuous phase), which under normal conditions behaves as a Newtonian fluid. Examples of ER fluids include, silicone oil with $Na_{12}Al_{12}Si_{12}O_{48}$, and a nematic liquid crystalline (LC) E7 mixed with lithium polymethacrylate (LiPMA) [70]. A widely accepted description of the electrorheologic effect states that the dielectric solid particles in the fluid become polarized and form microstructures

(chains or clusters) under the presence of an electric field. Whereas a majority of applications use the ER fluids in shear mode, they are subjected to both shear and squeeze in case of tactile arrays.

A tactile actuator and a matching sensor, based on the aforementioned principle, is reported by Voyles et al. [71]. The actuator–sensor pair has male–female symmetry for the purpose of remote monitoring of touch sensing. The fingertip-shaped sensor detects contact events on its external surface using a gel layer as a dielectric in capacitive sensing, while the similarly shaped actuator recreates the remotely sensed tactile events on its internal surface by changing the solidity of areas of the gel in contact with the human operator. The ER fluid based robotic fingers have also been reported in literature [72].

The ER fluids are attractive because they are controlled electrically, which is convenient as there are no moving parts. They require little power (although voltages can be very high) and they can be made very compact. In fact, the smaller the dimensions, the higher the field strengths and the stronger the ER effect. These characteristics make ER fluids attractive for the haptic interfaces.

5.2.8 Magnetorheological Sensors

Similar to the ER effect, discussed above, there exists magnetorheological (MR) effect whereby the MR fluids exhibit rapid, reversible and significant changes in their rheological (mechanical) properties while subjected to an external magnetic field [70]. The MR fluids are suspensions of micron sized ferromagnetic particles dispersed in different proportions of a variety of nonferromagnetic fluids. As with ER fluids, the MR fluids are also in liquid state without external stimuli. While MR fluids are subject to a magnetic field, they behave as solid gels, typically becoming similar in consistency with dried-up toothpaste. In recent years, MR fluid based haptic displays and haptic interfaces have been investigated by some researchers. Carlson and Koester have developed a prototype of portable hand and wrist rehabilitation device based on MR fluid [73]. MR fluid have also been used to construct tactile and haptic displays to replicate perceived biological tissue compliance [74, 75]. The challenges of producing strong magnetic fields over large surface areas, however, limits the application of MR fluid sensors.

From above discussion it may be noticed that tactile sensors based on nearly all possible modes of transduction exist. Some of the least explored transduction methods not explained above include, electrochemical and acoustics methods. The advantages and disadvantages of some of the frequently used tactile sensing methods are summarized in Table 5.2. Some of these methods combine mechanical and electrical transduction (e.g. capacitive, resistive, and ferroelectric) and some other do not have such coupling (e.g. optical, ultrasonic, and magnetic). The main problem with coupled mechanical–electrical transduction schemes is the difficulty in optimizing one form of transduction without compromising the other. This is simply because there is no material with just the right combination of mechanical and electrical attributes. By separating the mechanical and electrical transduction in the sensor, both

Table 5.2 Merits and demerits of various tactile sensors types and implementations

Sensor Type	Merits	Demerits
Resistive	1. High Sensitivity	1. High Power Consumption
	2. Low Cost	2. Generally detect single contact point
		3. Lack of contact force measurement
Piezoresistive	1. High sensitivity	1. Stiff and Frail
	2. Low Cost	2. Non-linear response
	3. Low noise	3. Hysteresis
	4. Simple electronics	4. Temperature sensitive*
		5. Signal drift
Capacitive	1. Sensitive	1. Cross-talk
	2. Low Cost	2. Hysteresis
	3. Availability of commercial A/D chips	3. Complex electronic
Optical	1. Sensitive	1. Bulky
	2. Immune to electromagnetic interference	2. Loss of light by micro bending
	3. Physically flexible	3. Chirping
	4. Fast response	4. Power consumption
	5. No interconnections	5. Complex computations
Ultrasonic	1. Fast dynamic response	1. Limited utility at low frequency
	2. Good force resolution	2. Complex electronics
		3. Temperature sensitive
Magnetic	1. High sensitivity	1. Restricted to non-magnetic medium
	2. Good dynamic range	2. Complex computations
	3. No mechanical hysteresis	3. Somewhat bulky
	4. Robust	4. High Power consumption
Piezoelectric	1. High Sensitivity	1. Temperature sensitive
	2. Dynamic Response	2. Lacks robust electrical connections
	3. High bandwidth	3. Unsuitable for static contact events
Conductive rubbers/composites	1. Mechanically flexible	1. Hysteresis
	2. Easy fabrication	2. Non-linear response
	3. Low cost	3. Slow time response

forms of transduction can be optimized without compromising the other. Consider for instance, the elastic material typically used in the sensor covering can be chosen for the most appropriate combination of stiffness, resistance to abrasion, tearing, oxidation, chemicals and other environmental factors. Since the rubber covering simply overlies the sensor, it can be replaced when it is worn or damaged or when different rubber characteristics are required; such as less stiffness to provide higher force sensitivity.

5.3 Materials for Tactile Sensing

In the past, most devices have relied on fairly rigid, solid materials for their construction. Perhaps this was the natural choice to start as rigid systems are simpler and there are fewer variables to control or design. Nowadays, however, there is a demand for flexible large-area sensors that can be embedded, for example, into the flexible skin material of robotic fingers and used for sensing multiple locations. Taking cues from human tactile studies and the physical nature of the tissues and skin, it seems that softer materials may have much to offer. Elastic overlays and compliant contact surfaces are often advocated for their frictional and other properties, even if their low pass filtering behavior can be a disadvantage. Softer materials such as rubber, fluids and powders are therefore being examined. Some commercial touch sensors like those from Tekscan [76] using pressure sensitive ink or rubber are already available. Conductive gels have been considered for their remarkable softness showing a 20% change in impedance for pressure 0–400 kgf/cm^2 [77]. A range of materials with different consistencies have been examined in [78] for impact and strain energy dissipation conformability to surfaces and hysteresis effects. It is found that soft surfaces have more desirable characteristics for contact surfaces than hard materials. Among soft materials, gels are better than plastic, rubber, sponge, or paste, with powders being the second best. A range of materials used in various tactile sensing schemes are discussed in this section.

5.3.1 Piezoelectric Materials

Piezoelectric materials are insulators that generate charge when they are mechanically deformed or strained. As explained in Appendix A, the charge generation can occur in two ways: Firstly, due to specific crystal structure of the material—the deformation causes the cations and anions to move asymmetrically, thus leading to a high polarization; and, second by aligning the permanent dipole moment of the molecules forming the crystal. The piezoelectric effect arising from the crystal structure usually occurs in inorganic materials, such as $BaTiO_3$, the lead zirconate titanate class of ceramics ($Pb(Zr_xTi_{1-x})O_3$, PZT), ZnO, and CdS. The molecular effect is observed for macromolecules that have intrinsic permanent dipole moments, such as PVDF, and nylon [79].

A wide variety of materials, including PZT, ZnO, and $PVDF$ have been used to make tactile devices. As the material is not perfectly oriented, they are normally "poled[5]" in the direction orthogonal to the film plane to achieve maximum polarization. In this way the value of piezoelectric constant (d) is increased to the maximum that is practically feasible. The PZT and $PVDF$ are the materials of choice for

[5]Poling is the method of aligning or orienting the dipoles in a particular direction. Generally, poling is done by applying a strong electric field (sometimes in combination with mechanical processes such as stretching), whose direction also sets the direction of polarization.

tactile sensing because of the requirements for high sensitivity, ease of fabrication, and mechanical properties. In particular, PZT has a higher piezoelectric constant ($d_{33} = 117$ pC/N) than single-crystalline materials such as quartz ($d_{11} = 2.3$ pC/N) and zinc oxide ($d_{33} = 12$ pC/N), and additives can be used to alter its electrical and mechanical properties. PVDF has a lower piezoelectric constant ($d_{33} = 30$ pC/N), but its much lower ε_r value (100-fold lower than PZT) makes it an ideal material to make tactile devices [80]. Furthermore, the polymers such as PVDF have some excellent features, such as, mechanical flexibility, workability and chemical stability [81]. The low cost and ease of processing the polymer (compared to ceramics) has also led to its wide use as a piezoelectric material. A marked phenomenological analogy exists among epidermis sample of human skin and PVDF [82]. The PVDF or its copolymers have been used in a large number of tactile sensing schemes, including one based on piezoelectric effect and also the ultrasonics [66, 83–86].

5.3.2 Conductive Polymer Composites

The conductive polymer composites (CPC) are becoming popular and offering attractive alternatives for developing new generation of mechanically flexible tactile sensing devices that can be wrapped around curved surfaces and spanned over large areas (tens of cm^2). The CPCs are obtained by adding micro/nano sized conductive filler particles or structures to an insulating polymer matrix. Incorporation of conductive fillers into a host polymer/elastomer matrix constitutes an excellent approach for the development of special materials, which combine electronic conductivity with elasticity and other important mechanical properties imparted by the insulating rubber (polymer/elastomer) matrix. Investigators have used conductive filler materials such as carbon based fillers (e.g. carbon black, graphite powder, carbon fibers) and metal particles or metal flakes (e.g. Ni, Cu, Ag, Al and Fe). On compression the polymer matrix deforms and the filler particles are brought closer, thereby causing an increase in conductivity. Therefore, the sensor based on these materials are essentially piezoresistive in nature. The transition of the composite from insulator to conduction, commonly explained using statistical models and percolation theory [87–89], takes place when the volume fraction (V_c) of the conductive filler particles is above a certain value, which is called percolation threshold.[6] The conductivity rises at the percolation threshold as the conductive particles begin to aggregate to produce chains of particles in intimate contact, providing conductive paths spanning the sample. The conductivity increases rapidly as more percolation paths form until saturation is approached, when the conductivity rises slowly to its

[6]The percolation theory model fails below the percolation threshold, where it predicts that the composite is an insulator. Effective medium theories have been developed that provide a good description of the evolution of the conductivity across the full range of filler concentrations. Discussion on such theories is beyond the scope of this book and reader may refer to relevant literature [87].

maximum value or resistance (or piezoresistance) falls to minimum value. Theoretically, the percolation threshold for uniformly dispersed (random distributed) particles is about 16% by volume [90]. In practice, however, the value may vary between 1–30% as it depends on the shape and size of the filler particles, which affect their spatial distribution [19]. If relationship between compressive strain, conductivity, and the mechanical properties of the composite film are known, the local strain (and stress) can be obtained by measuring the local conductivity through the film.

Several conductive polymer composites have been explored for tactile sensing. Depending on the type of filler particles, they can be categorized as composites with: (a) metal nanoparticle fillers; (b) conductive polymer nanoparticle fillers; (c) carbon microcoil fillers; (d) graphite nanosheet fillers; (e) carbon black nanoparticle fillers; and (f) carbon nanotube (CNT) fillers. These conductive polymer composites are explained below, with suitable examples.

5.3.2.1 Conductive Polymer Composites with Metal Nanoparticle Fillers

The conductive polymer composites with metal nanoparticle fillers include QTC (Quantum Tunneling Composites) by Peratech [38], which consists of nickel particle (with sharp projections) in silicone matrix. Typically silicone rubber matrix is used in various composites because it has excellent elastic, thermal, and mechanical properties and a very good environmental stability. The QTC sheets are mechanically flexible and the flexibility depends on the grade of elastomer used as matrix, the filler loading and the sheet thickness. Thin sheets with low filler loading are the most flexible. The principal conduction mechanism depends on the tunneling between filler particles, which is evident from the exponential dependence of sample response on deformation. In QTCs the metal particles never come into contact. Rather they get so close that quantum tunneling (of electrons) takes place between the metal particles. The transition from insulator to conductor follows a smooth and repeatable curve, with the resistance dropping exponentially. Under modest compression the resistance of QTC can fall from about 10^{12}–10^{13} Ω to less than 1 Ω, an exceptionally large dynamic range for a property of a solid material at room temperature [91]. When compressed into the low resistance state these composites can carry large currents without observable damage. Robot hands with QTC based tactile sensors have also been reported in literature [92, 93].

5.3.2.2 Conductive Polymer Composites with Conductive Polymer Fillers

There has been a growing interest in the intrinsic conductive polymers (ICP) due to their good electrical properties. Examples of these polymers include polypyrrole (PPy), polythiophene (PTh) and polyaniline (PANI) [94]. These polymers are either used as fillers in composites or coated on textiles. The modification of fibers and yarn using conductive polymers is an interesting approach for obtaining "intelligent textiles". Conductive fibers and yarn are discussed is a separate section later in this

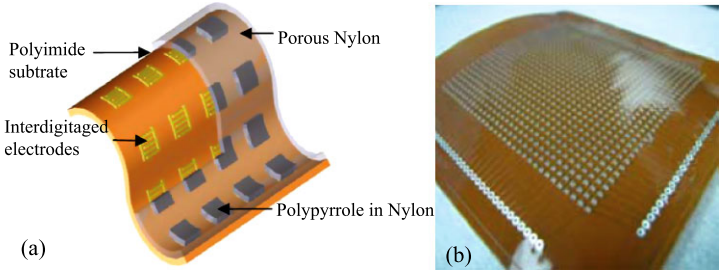

Fig. 5.14 (**a**) The schematic of porous nylon–polypyrrole composites based flexible tactile sensing array; (**b**) The 32 × 32 array realized on polyimide substrate (with permission from [95], ©(2008) IEEE)

chapter. The examples of tactile sensors based on composites with ICP fillers include the 32 × 32 flexible tactile sensing arrays developed by Yu et al. [95]. The array consists of 32 × 32 sensing elements, each of which consists of interdigitated copper electrodes on a flexible polyimide (PI) film. The overall size of the array is 89.9 × 89.9 mm^2, the sensing element size is 1 mm × 1 mm size and the center–center distance between two sensing elements is 1.9 mm. The PI film is covered with porous nylon, to which polypyrrole fillers are electrochemically added. The fillers are added only on the pre-defined positions of interdigitated electrodes. The scheme and the fabricated tactile sensing arrays are shown in Fig. 5.14. The polypyrrole polymers (electrical conductivity in the range 500–7500 S/cm) form electrically conductive paths in the porous nylon. These conductive paths are shortened when external pressure is applied and as a result the resistance decreases. An interesting aspect of this sensor is that more conductive paths are formed in the absence of conductive materials such as water. This property allows using the same sensor to measure contact pressure/force and also the moisture sensation. The flexible tactile sensor has stable sensitivity ($\Delta R/R_0$) of 0.1%/kPa for pressure up to 30 kPa. Another example of composites with conductive polymer fillers is the strain sensor by Flandlin et al. [94]. The strain sensing material is obtained by mixing an insulating latex of styrene-butyl acrylate copolymer with a colloidal suspension of polypyrrole. Since elastomer molecules as a matrix can be more thoroughly mixed with the conductive polymer, the composites made from them offer an attractive alternative for sensing applications.

5.3.2.3 Conductive Polymer Composites with Carbon Microcoils Fillers

Tactile sensors using composites with uniformly distributed carbon microcoils (CMCs) fillers in the silicone matrix have been proposed by Chen et al. [96]. The carbon microcoils have a three dimensional spiral structure with 10–15 μm diameter. Obtained by the Ni catalyzed pyrolysis of acetylene, these microcoils can be stretched up to 5–10 times their original lengths. The changing *LCR* (inductance, capacitance and resistance) parameters of the CMCs (increase with extension and

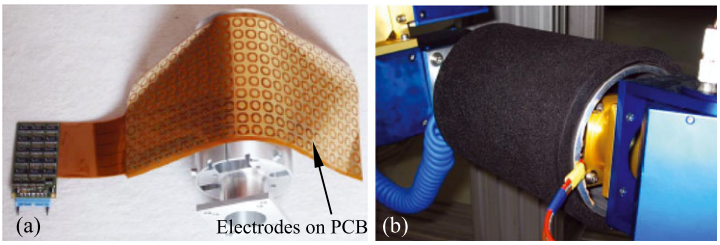

Fig. 5.15 The tactile sensor system based on graphite–elastomer composites; (**a**) The base of flexible sensor array on PCB; (**b**) The electrodes on the sensor array covered with graphite–elastomer composite. The tactile sensing arrangement is integrated on the forearm of a robotic hand (with permission from [98], ©(2003) IEEE)

decrease with contraction) is used to detect the applied force. The micro tactile elements, $80 \times 80 \times 80\ \mu m^3$ in size, have high sensitivity of 0.3 mgf (1 Pa) and response time of the order of milliseconds.

5.3.2.4 Conductive Polymer Composites with Graphite Nanosheet Fillers

Conductive graphite filler based composites present another alternative for tactile sensors. Composites with graphite nanosheet fillers (diameters ranging from 5–20 μm and thickness from 30–80 nm) incorporated in to poly(methyl methacrylate) (PMMA), polystyrene (PS), nylon 6, and silicone rubber have been reported in literature [97]. In each case only a slight amount of graphite nanosheet (about 1.0 vol %) is sufficient to satisfy the critical percolation transition. The advantage of lesser amount of graphite fillers is that the satisfactory electrical properties are achieved without compromising the mechanical properties of the composite. The graphite nanosheet–silicone rubber composite with 1.36 vol % of graphite nanosheet exhibits a much stronger and reversible positive piezoresistive effect. The change of electrical resistance is many orders of magnitude of pressing and a high sensitivity of the finger-pressure range. An implementation of graphite–elastomer composites for robotic tactile sensing system is reported by Kerpa et al. [98]. The sensor, shown in Fig. 5.15 consists of a 10×23 array of electrodes on a printed circuit board (PCB) which is covered with a few millimeters thick foam made of cellular rubber–graphite fillers composite. The overall size of tactile array is 175 mm × 376 mm and the spatial resolution of the sensors is 15 mm. The wiring is done on the PCB. Under pressure the resistance between the foam and the electrodes changes and this change is measured via the electrodes. The electrodes are selected via multiplexers and the corresponding signal is forwarded to a microcontroller, where signal is digitized, locally pre-processed, and converted in to a serial data stream. The serial data stream is transferred via CAN bus to the main control PC. The tactile sensor by Kerpa et al. [98] requires loading for at least 20 seconds before precise pressure can be measured. A common issue with conductive composites is that the creep of polymer matrix results in the time dependence of the composite resistance. The graphite

filler based composites are thus not completely free from such issues, even if their performance in this regard is better than other composites [97].

5.3.2.5 Conductive Polymer Composites with Carbon Black Fillers

Carbon black, an amorphous form of carbon, is another material which is widely used as a conductive filler. Carbon black with only small diameter and large surface area are suitable as the filler to improve electric conductivity. An example of carbon black based sensors includes the low cost solution for thin (0.125 mm) and flexible pressure sensor array by Wang et al. [99]. The sensing element uses conductive carbon black powder and vulcanized liquid silicone rubber as conductive filler and insulating matrix, respectively in the mass ratio of 0.08:1. The sensing array consists of nine sensing elements, formed at the intersections of rows and columns electrodes. The rows and column electrodes have been realized on opposite surfaces of the composite. On application of force, the gap between carbon black particles is reduced and they touch or come close to each other—leading to the formation of local conductive path due to contact effect or tunneling effect. The change is resistance is thus gives a measure of applied pressure. Another similar tactile sensing scheme, based on carbon black filler based composites, is used in the prototype of DLR touch sensor by Strohmayr et al. [100]. However, in this case the conductive composites have been obtained by blending the ultra-soft Poly[styrene-b-(ethylene-cobutylene)-b-styrene] (SEBS) polymers with carbon black filler material. Using carbon black as an additive to achieve electrical conductivity usually requires a concentration so high that it will increase the melt viscosity and decrease the mechanical properties of the polymers. One of the recent trends to overcome this drawback is to use multiphase polymer blends and hence reduce the overall carbon black concentration [101].

5.3.2.6 Conductive Polymer Composites with Carbon Nanotube Fillers

Carbon nanotubes (CNT) are interesting materials for designing highly sensitive tactile devices, owing to their electrical and electromechanical properties. They are highly conductive as well as super compressive, both of which make them highly pressure sensitive material [102]. Like graphite fillers, the nanocomposites with aligned CNTs have significantly small percolation threshold (three order of magnitude lower than conventional particulate carbon-black fillers [103]), implying that the conductivity of composite will rise monotonically over a long range of strain. This also means that satisfactory electrical properties can be achieved without compromising the mechanical properties of the composite. The performance (sensitivity, resolution, dynamic range etc.) of tactile sensors using pressure sensitive elastomers can therefore be significantly improved by replacing conventional carbon-black filler with CNTs.

A comparison of composites with carbon black filling and multi-walled carbon nanotube (MWNT) by Engel et al. [104] shows an 8-fold improvement in sensitivity

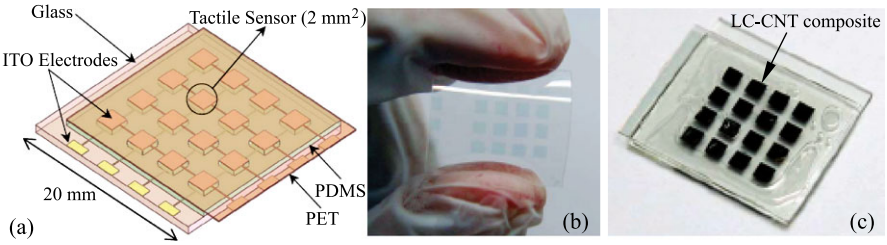

Fig. 5.16 A carbon nanotube–liquid crystals composite based tactile sensor array. (**a**) The schematic of the sensing array; (**b**) The ITO (Indium tin oxide) electrodes of the array on PET; (**c**) The fabricated 4 × 4 tactile sensing array (with permission from [107], ©(2011) IEEE)

through the use of MWNT. Furthermore, a comparison between MWNT blended polydimethylsiloxane (PDMS) and polyurethane (PU) elastomers shows that the former exhibits a lower percolation threshold (approximately 2% versus 10% in PU). Using PDMS–MWNT composite in a capacitive tactile sensor in place of the non-conductive PDMS capacitors can result in an improved performance. For example, the PDMS–MWNT composite based capacitive tactile sensor by Engel et al. [104] has linear output i.e. change in capacitance above 19 kPa load (below this load the response is not linear) and the sensitivity 1.67%/kPa. The sensitivity is more than twice the sensitivity of a non-conductive PDMS (0.7%/kPa [105]) capacitor. Simple CNT based flexible tactile sensing structures for measuring normal and shear forces have been developed by Hua et al. [106]. Depending on the sensor structure, the reported range of sensitivities (i.e. change in resistance per unit force) for normal (from 0 to 6 N) and shear forces (from 0 to 0.10 N) are 0.49%/N to 22.76%/N and 18%/N to 95%/N respectively.

A 4 × 4 tactile sensing array based on liquid crystal (LC)–CNT composites by Lai et al. [107] is shown in Fig. 5.16. The sensing material of each tactile sensor consists of the LC–CNT composite (MWCNT:LC concentration 0.01:1), a deformable PDMS elastomeric structure, an ITO glass substrate and an ITO PET film. An interesting aspect of this tactile sensing arrangement is that the sensing ranges can be tuned by varying the magnitude of the applied external field (supplied by the array scanning circuitry).

Various CPC materials, and tactile sensing solutions based on them, discussed above present a low cost alternative for robotic tactile sensing with interesting properties like mechanical flexibility. As such the field of CPC based sensors is still nascent and therefore, faces a set of challenges. Some of the major concerns include temperature and chemical stability, long term stability, performance shift over time, creep, relaxation, hysteresis, and tolerance to high electric field [108]. For example, the resistance of nanocomposite elastomers may incur changes in the presence of changes in stress/strain, temperature, humidity, and chemical environment. The cross talk is a primary issue for sensor applications. Due to the degradation and the non-linearities, elastomers/composites are not suited for accurate absolute force measurements, but they are good enough for force distribution measurements, which

is not affected by the non-linearities. The advancements in the processing technologies and improvements in material properties of CPCs will help solve many of above challenges—eventually allowing integration of CPCs semiconductors, and the underlying electronics collectively to be used as hybrid sensors and almost complete tactile system.

5.3.3 Conductive Fibers, Yarns and Intelligent Textiles

For years the textile industry has been weaving metallic yarns into fabrics for decorative purposes. However, recently it is the new generation of fibers, fabrics and the intelligent textiles produced from them, that has been attracting considerable attention. Conductive materials such as conductive fibers, yarns, coatings and ink, etc. have been used in intelligent textiles for a range of applications including sensing, electrostatic discharge, welding of plastics, electromagnetic interference shielding, data transfer in clothing, as well as military applications like camouflage and stealth technology. Smart or intelligent textiles using fabric-based sensors to monitor gesture, posture or respiration have been exploited in many applications. The idea for the most intelligent or smart textile is to used conductive fibers as transmission lines to connect the sensors and other technological components attached to the textile like embroidery. The textile transmission line consists of conductive yarns integrated into a flexible textile base. Conductive yarns are either pure metal yarns or composites of metals and non-conductive textile materials that help improve mechanical properties. Conductive fibers coated with sensitive material (e.g. piezoresistive material) are also used as sensors. Depending upon different applications, several sensing segments can be embedded into textiles such that distributed strains can be measured with the sensors. The conductive and semiconductive yarns can also be used to further improve the intelligent textile based sensors systems by building reliable transistors with well-defined electrical properties using them. Examples of conductive and semiconductive yarns topology, proposed by Bonfiglio et al., to build transistors are given in Fig. 5.17 [109]. When inserted in a fabric, this can be seen as an elementary network where purely metallic “drain” (D) and “source” (S) wires cross the yarn-like transistor indicated with “gate” (G). Current advances in new materials, textile technologies, and miniaturized electronics make wearable systems more feasible.

5.3.4 Polymer Gels and Fluids

A gel consist of an elastic cross linked network and a fluid filling the interstitial spaces of the network. The network of long polymer molecules holds the liquid in place and so gives the gel what solidity it has. Gels are wet and soft and look like a solid material but are capable of undergoing large deformation. The polymer gels

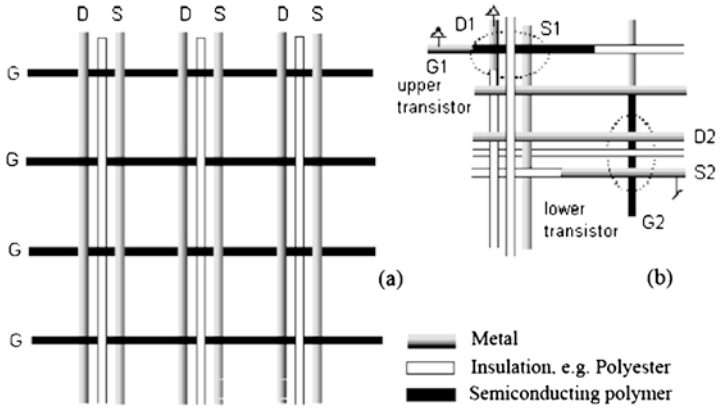

Fig. 5.17 The electronic devices in yarn textile topology. (**a**) The transistor array structure. GS represents textile ribbons with the gate contact and the organic semiconductor; (**b**) The ring oscillator structure to implement different conductivity properties (insulating, metal, semiconductor) on the same yarn (with permission from [109], ©(2005) IEEE)

induce a spontaneous ionization on mechanical compression. The potential in gels is produced by the chemical free energy of the polymer network[7] [110]. Soft touch sensors can be obtained using polyelectrolyte gels. The polyelectrolyte gels induce a spontaneous ionization on mechanical compression and thus electrical potential as large as a few millivolts is produced. They also exhibit reverse piezoelectric effect, i.e. an applied potential causes the gel to swell visibly. Using this phenomenon, Sawahata et al. [111] constructed a simple touch sensor capable of lighting a photo diode array according to the amplitude of mechanical deformation. The fact that human tissue is also composed of electrolytic materials with very similar mechanical properties suggests intriguing possibilities for new designs of sensing fingers.

A weakly conductive fluid based tactile sensing arrangement that mimics the mechanical properties and distributed touch receptors of the human fingertip is presented by Wettels et al. [112]. The sensing structure consists of a rigid core surrounded by a weakly conductive fluid contained within an outer elastomeric skin. Multiple electrodes are mounted on the surface of the rigid core and connected to impedance-measuring circuitry, embedded within the core itself. On contact, the outer elastomeric layer is deformed, leading to deformation of the fluid path around the electrodes, which eventually results in a distributed pattern of impedance changes. The resulting impedance pattern given an indication about the forces (e.g. magnitude and direction) and the objects (e.g. shape, hardness/softness) that ap-

[7] When a piece of weak polyelectrolyte gel is pressed, the pH of the gel changes reversibly. The pH change is associated with an enhanced ionization of the carboxyl groups under deformation. The compression in one direction expands the gel laterally and induces a one-dimensional dilatation of the polymer network in this direction. This brings about an increased chemical free energy (a decrease in entropy) of the polymer chain, which should be compensated for by a simultaneous increase in its degree of ionization.

plied them. The sensor system is able to detect forces ranging from 0.1–30 N that produce impedances ranging from 5–1000 kΩ. The factors affecting the sensitivity of this tactile sensor include, conductivity of the fluid, the viscoelastic properties of the combined system of skin and pressurized fluid, volume and pressure of fluid, and the material and geometry of the electrode contacts. It is generally desirable for the fluid to have a low viscosity to minimize damping and hysteresis, and a high resistivity so that the measured impedance of the series circuit (electrodes plus fluid) is dominated by the fluid resistance rather than the capacitive reactance of the metal–electrolyte interfaces. For these reasons, water with a low concentration of NaCl (1/12th the concentration of physiological saline) has been used by Wettels et al. [112].

The tactile sensors made of polymer gels and fluids have similarities with tactile perception in living organisms in a sense that the macroscopic deformation in both of them induces the ionic rearrangement that gives rise to a certain amount of transmembrane potential. Many of the features of gels, such as softness, wetness, and elasticity etc. are also similar to that of natural tissues. Because of these similarities, the gel based soft system may open new possibilities in the investigation of artificial tissue-like tactile perception for prosthetics and robotics.

5.3.5 Electro-Optic Materials and Sensors

In recent years, electro-optic[8] polymers (e.g. chromophores) and semiconductor nano-crystals (e.g. CdS, CdSe) have been used to make various optical and sensing devices due to several advantages, such as large and fast electro-optic (EO) response. The EO response of semiconductor nano-crystals is higher than that of response electro-optic polymers because of surface and quantum size effects. The semiconductors with their band gap in visible region of light spectrum are of interest as they emit visible light; hence their photoluminescence (and electroluminescence) is visible to human eye and can be imaged using a CCD. Group II–VI semiconductors such as cadmium sulfide (CdS), cadmium selinide (CdSe) and zinc sulfide (ZnS) are widely used materials in this regard.

A highly sensitive sensor using semiconductor nanoparticles, presented by Maheshwari and Saraf [50], is shown in Fig. 5.18. The sensor comprises of five nanoparticle monolayer structure separated by dielectric layers and it is constructed on transparent ITO electrodes by using layer-by-layer self-assembly technique (Fig. 5.18(a)). The organic dielectric layers, which as approximately 5–6 nm thick, are made of four alternating monolayers of poly(allylamine hydrochloride) (PAH) and poly(styrene sulfonate) (PSS). The sensor (2.5 cm^2 in size) works on the principle of electron tunneling. On application of bias voltage V across the film, the electric current flows through it and the CdS nanoparticles emit visible light at

[8]The electro-optic effect is the change in refractive index of materials with external field.

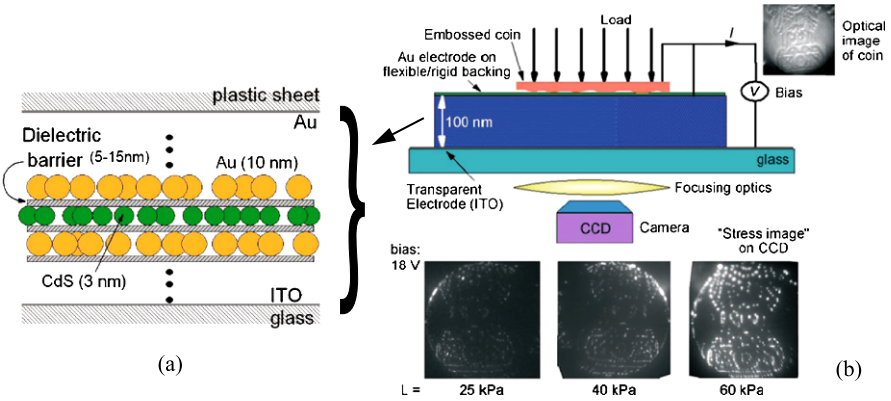

Fig. 5.18 A tactile sensor based on electro-optical device. (**a**) Schematic representation of the tactile sensor showing the nanoparticle monolayers spaced by organic dielectric layers; (**b**) The working of tactile sensor. Pressing a coin on the surface of the device generates its electroluminescence image on the CCD. The intensity of image increases with the load (Reproduced with permission from [19], Copyright Wiley-VCH Verlag GmbH & Co. KGaA)

a wavelength of 580 nm. When a load is applied to the top Au/plastic electrode (Fig. 5.18(b)), the dielectric layer is compressed and the particles are brought closer, facilitating the electron tunneling and thus causing an increase in both the local current density and the electroluminescent light. Thus, the device directly converts stress into electroluminescent light and modulation in local current density, both of which are linearly proportional to local stress. The change is electroluminescent light can be recorded on a digital camera, as in Fig. 5.18(b) and hence a high resolution image of the load can be obtained. The spatial resolution better than that of the human fingertip ($\sim$40 μm) can be obtained with the above approach.

A major concern with measuring the electroluminescent light is related to the increase in overall size of the sensing arrangement, as the CCD camera adds to the sensor size. This issue can be overcome by recording the stress distribution in terms of change in the local current density distribution. The current through a nanoparticle based tunneling device is exponentially sensitive to the magnitude of energy barrier between the nanoparticles and the physical distance between them. This means that the current can be modulated by increasing the electric field (voltage bias) across the nanoparticles (which increases the energy of the electrons and hence lowers the energy barrier) or by decreasing the barrier width by reducing the separation between the nanoparticles. Therefore, instead of measuring the electroluminescent light, the stress distribution can be obtained by measuring the local current density distribution (in a configuration similar to liquid-crystal display) [19]. Thus, above sensing device can also achieve high resolution without any optical components.

5.4 Tactile Sensor Structures

Various transduction methods and materials discussed in previous sections have been utilized in various tactile sensing structures. Some of these structures, such as microelectromechanical systems (MEMS), silicon transistors, printed circuit boards, and fabric etc. are discussed in this section.

5.4.1 MEMS Based Sensors

The MEMS based tactile sensors are obtained either by micromachining the silicon or by using the polymers. In general, they employ capacitive [113–118] or piezoresistive [28, 30, 119] mode of transduction. The early works on piezoresistive and capacitive micromachined sensors have produced arrays of force sensing elements using diaphragms or cantilevers as the sensing principle [120, 121]. The silicon-diaphragm based tactile sensors are dominated by piezoresistive sensing methods, even if the capacitive devices are an order of magnitude more sensitive. One of the reasons for this dominance could be that the capacitive sensing method, though very effective for measuring normal loads, is difficult to use when measuring shear loads—meaning that the method cannot be used practically for 3-D load detections. The piezoresistive devices also offer higher linearity. A few examples of the MEMS tactile sensing structures obtained using both the micromachined silicon and polymers are given below.

5.4.1.1 Si-MEMS Approach

The MEMS based tactile devices realized by silicon micromachining, are quite sensitive and result in higher spatial resolution. With a piezoresistive bridge arrangement on the sensing element, the MEMS based sensing devices can detect both the shear and normal components of applied stress. For example, the 64×64 element high resolution (≈ 300 μm) traction sensors array by Kane et al. [28] shown in Fig. 5.3(a) is composed of a central shuttle plate suspended by four bridges, with each of the four bridges containing a polysilicon piezoresistor. The strains in each of the bridges due to pure applied shear (σ_s) and normal (σ_n) stresses are given as [28]:

$$\varepsilon_s = \frac{b^2}{2\sqrt{2}(EA)}\sigma_s \tag{5.10}$$

$$\varepsilon_n = \frac{b^2 L}{2(EA)\delta}\sigma_n \tag{5.11}$$

where ε_s and ε_n are the shear and normal strains respectively; b is the shuttle plate width; (EA) is the overall axial stiffness of the bridge; L is the length of the bridge;

and δ is the normal deflection of the shuttle plate. This overall axial stiffness parameter (EA) is the sum of the products of the Young's moduli, E, and the cross-sectional area A, for each of the materials in the bridge. The equation (5.10) is obtained by assuming that the structural deformation is primarily the axial strain of the bridges. Further, the deflections are assumed to be small in calculating both normal and shear strains. Using each of the piezoresistors as the variable leg of a resistive half-bridge and by monitoring the intermediate node voltage of the half-bridge (by differentially comparing to the output of an off-chip voltage divider circuit that served as the second leg of a full Wheatstone bridge circuit), a measure of the strain (and hence applied stress) can be obtained as [28]:

$$V_i = \frac{kG(\varepsilon_{ni} + \varepsilon_{sxi} + \varepsilon_{syi})}{4} V_d \tag{5.12}$$

where V_i is the unamplified measurement node voltage for bridge i; ε_{ni} is the strain induced in bridge due to applied normal stress; ε_{sxi} is the strain due to the shear stress applied in the x-axis direction; ε_{syi} is the strain due to the shear stress applied in the y-axis direction; G is the piezoresistive gauge factor; V_d is the bridge drive voltage; and k is the amplification factor. Through differential addition of the four voltage signals (V_1, V_2, V_3, V_4), the independent voltage measures of the three components of an applied traction stress can be obtained as [28]:

$$T_n = [V_1 + V_2 + V_3 + V_4] = \frac{kV_d b^2 LG}{2(EA)\delta} \sigma_n \tag{5.13}$$

$$T_{sx} = [-V_1 - V_2 + V_3 + V_4] = \frac{kV_d b^2 G}{2\sqrt{2}(EA)} \sigma_{sx} \tag{5.14}$$

$$T_{sy} = [-V_1 + V_2 + V_3 - V_4] = \frac{kV_d b^2 G}{2\sqrt{2}(EA)} \sigma_{sy} \tag{5.15}$$

The above equation indicate that the measure of normal stress T_n and the shear stress components T_{sx} and T_{sy} are linear functions of the applied stresses and independent of the orthogonal stresses applied to the sensor. Following above equations the normal and shear stress sensitivities of the sensor by Kane et al. [28] are 1.59 mV/kPa (normal stress range 0–35 kPa) and 0.32 mV/kPa (shear stress range 0–60 kPa) respectively. The method similar as above has been adopted in many MEMS based tactile sensing schemes to obtain the normal and shear component of the applied force. One such example of polymer-MEMS based tactile sensor by Hwang et al. [122] is discussed below in this section.

The utility of MEMS based tactile sensing structures, realized by silicon micromachining, to practical robotic systems has been limited until now because of reasons like brittle nature of silicon. The MEMS based tactile sensors are unable to withstand large forces/pressure due to inherent fragile nature of the structure—even if the sensor is normally embedded or covered with an elastic covering. The packaging of MEMS based tactile sensors has also been a challenging issue. A few examples of silicon based piezoresistive force sensor that address the problems of robust packaging, small size and overload tolerance include the sensor by Beebe

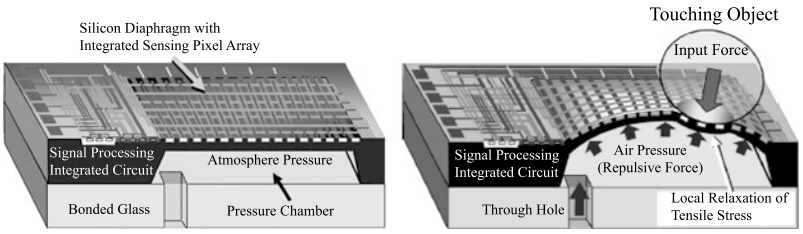

Fig. 5.19 (**a**) MEMS based tactile Image Sensor with piezoresistive pixels integrated on single-silicon diaphragm. (**b**) Pneumatically controlled flexible surface of diaphragm (with permission from [30], ©(2006) IEEE)

et al. [26]. The sensor measures the force (rather than pressure) applied to a 4 mm raised dome on the device surface. The device exhibits a linear response, good repeatability and low hysteresis, and has a flexible and durable packaging. In general, devices that incorporate brittle sensing elements such as silicon based diaphragms, including those embedded in protective polymers, have not proven to be reliable interfaces between a robotic manipulator and the manipulated object [49].

It is difficult to realize flexible tactile sensors through micromachining of brittle materials such as silicon. A novel method of obtaining MEMS based flexible tactile sensing structure has been reported by Takao et al. [30]. The sensing structure consists of a silicon diaphragm, with an array of 6×6 piezoresistive sensing elements on it and a pressure chamber beneath, as shown in Fig. 5.19. The diaphragm is swollen like a balloon by the pressurized air, provided to the chamber through the hole and hence the stiffness of the diaphragm is controlled by the air pressure. In this way, a force in the range of 2.1–17.6 gmf can be controlled by applying pressure in the range of 5–64 KPa. The extra provisions needed to supply and monitor the air are quite cumbersome and as such the arrangement is bulky. The alternative solutions explored to obtain flexible MEMS tactile sensors include using polyimide (PI) layers as a connecting material between silicon-diaphragm sensors, mounting silicon-diaphragm sensors on flexible printed circuit board substrates with a conductive epoxy etc. [123].

5.4.1.2 Polymer-MEMS Approach

Recently, a considerable effort is focused on the use of polymers in microelectronics systems and MEMS due to their potential for conformability. Polymers have been extensively used as both structural and functional materials for micro-devices. A number of examples given in previous section are related to the use of polymers (mainly, fibers and elastomers) as functional materials for tactile sensing. The discussion here primarily focuses on using polymers as structures and tactile sensing

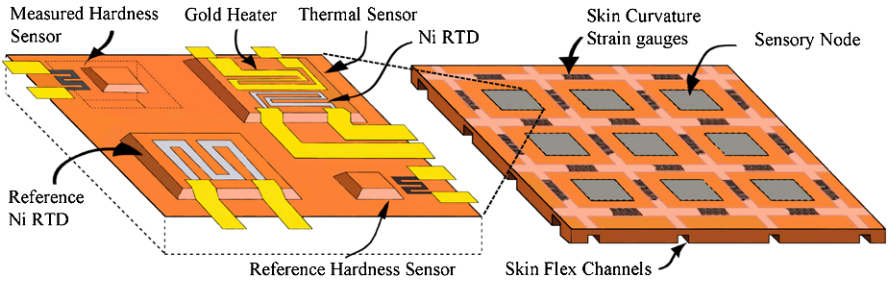

Fig. 5.20 (*left*) The scheme of a multimodal sensory node on polyimide substrate. (*right*) Distribution of sensing nodes on the flexible skin, (Reprinted from [124], ©(2005) with permission from Elsevier)

systems developed from them using MEMS approach. The polymer-MEMS[9] approach for developing tactile sensing structures has gained interest, partly because of the difficulty in obtaining a practical mechanically flexible system from silicon. The development of silicon-diaphragm-based tactile sensors requires both complex and expensive processes. A polymer-MEMS based process, on other hand, is a simple and low cost solution. Furthermore, unlike silicon micromachining the dimensions of the tactile sensing skin are not limited by the finite sizes of silicon wafers.

Multimodal polymer-MEMS based tactile sensor developed by Egnel et al. [124] is shown in Fig. 5.20. Realized on flexible polyimide (PI) substrate the sensor skin is capable of sensing the hardness, roughness, temperature and thermal conductivity of the object in contact. The skin is made on flexible polyimide sheet and consists of multiple sensor nodes arranged in an array format. Each node consists of four elements: a thermal conductivity measurement unit, a temperature measurement unit, and two membranes with metal strain gauges for measuring surface roughness and contact force. The two membranes also work in tandem to provide measurement of the hardness without knowledge of the contact force. The thermal conductivity measurement unit consists of a micro patterned metallic resistive heater and a thermal resistor. Electric current supplied to the resistive heater causes ohmic heat generation, which is transferred to a nearby temperature sensor (made of Ni) by thermal conduction via the substrate. The heat is sensed by the thermal resistor located 10–50 μm away. The steady-state read out of the thermal resistor is a function of the thermal conductivity of the object in contact, as it provides a parallel thermal conductive path. The two membranes with metal strain gauges use metallic strain gauge elements to detect strain developed in the polyimide substrate when the sensor is in contact with an object. The above sensing arrangement by Egnel et al. is a good attempt toward measuring multiple contact parameters other than force/pressure.

[9]Polymer-MEMS does not mean that the device is entirely made of polymers. In fact, heterogeneous integration of organic and inorganic materials is often necessary and desired. For example, it is often necessary to integrate signal conditioning and signal processing electronics directly with sensors. For large area sensor skin, the ability to integrate electronics and sensors is indispensable to reduce lead routing complexity.

However, utility of the sensor is limited by wiring complexity and the scalability of the wiring interconnects. Furthermore, the finished sensing arrangement does not contain signal processing electronics.

Another polymer-MEMS based tactile sensing arrangement, capable of detecting both normal and shear load, is presented by Hwang et al. [122]. The sensor is realized on PI and PDMS substrates and uses thin-film metal strain gauges for measuring 3-D forces. Unlike the tactile sensors obtained with micromachining of silicon, the sensor by Hwang et al. has no diaphragm like structures. When an external force is applied to the device, the thin metal film structure and the polymer incur a deformation that causes changes in the electric resistance. The sensor is capable of measuring normal loads up to 4 N. However, the sensitivity to shear loads is much lower. Furthermore, the sensor fails to discriminate between shear and normal loads when they are applied at same time. The changes in resistance corresponding to the magnitude and direction of applied force can be measured by connecting the strain-gauge in bridge arrangement similar to one described earlier in this section. The sensitivity of this type of tactile sensor is expected to be lower than that of the silicon-diaphragm based tactile sensors because: (a) the polymer substrates allow relatively small strain, and (b) the gauge factor of thin metal film used to make strain gauge is lower than that of polysilicon resistors.

5.4.2 Transistor Based Sensors

An interesting development in the field of sensing has been the use of electronic devices as sensors. For long, the electronic devices such as diodes and transistors have been used for measuring parameters like temperature and pH of solutions. In recent years, tactile sensing too has benefited from this development. Initially limited to the silicon transistor based arrangements (e.g. extended gates [125–127], and POSFET [128] etc.), the tactile sensing skin using organic transistors [34, 129] are being developed nowadays. The approach is particularly interesting, as it allows integrating the sensor and measurement circuit on same substrate and therefore opens up possibilities of performing the signal processing very close to the sensors. Besides improving the signal to noise ratio, the marriage of transducer and electronics will improve the force resolution, spatial resolution, signal to noise ratio, and has potential of reducing the number of wires, which is a key robotics issue. Some of these silicon and organic transistor based tactile sensing structures are presented below. A detailed discussion on silicon based extended gate tactile sensing arrays and high resolution POSFET tactile sensing arrays is presented in Part II of the book.

5.4.2.1 Silicon Transistor Based Tactile Sensors

The tactile sensors and sensing arrays have been developed using hybrid organic–inorganic structures such as coupling the piezoelectric polymers with the transistor.

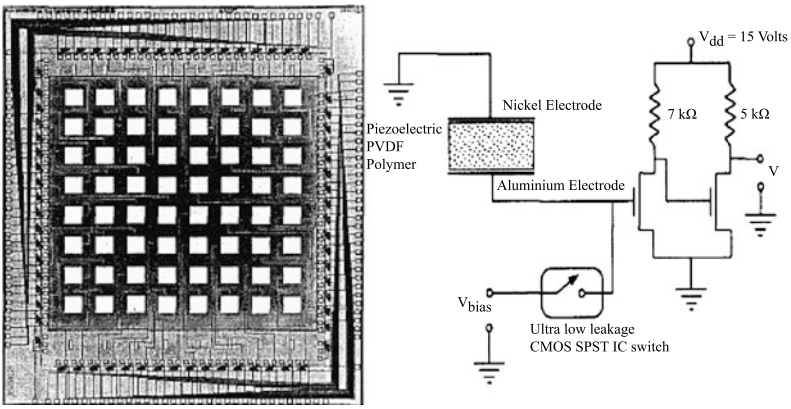

Fig. 5.21 (*left*) The tactile sensing array based on the extended gate approach. An 8 × 8, array of electrodes in the center, is surrounded by MOSFET devices on the periphery of the chip. (*right*) Schematic of a discrete in situ MOSFET amplifier (with permission from [83], ©(1996) IEEE)

The location, size and shape of the piezoelectric polymers in such cases may vary and accordingly the size and location of transistors too may differ. The two alternatives that have come to notice are: the tactile sensors using transistors having extended gates, and the conventional transistor with metal over the gate area only.

In the case of extended gate devices, the MOSFET is confined to a small portion of the cell area and gate metal is extended to occupy most of the cell. The extended gate electrode, which acts as a charge collector for the relatively small transistor, may be of arbitrary shape and size. The transducer material such as piezoelectric polymer (e.g. PVDF) is deposited over the extended gate electrode, which acts the lower electrode of the transducer. The electric charge resulting from piezoelectric action in the transducer will thus appear directly on the gate of the MOS transistor. The working principle is further described in Chaps. 6 and 7. As the MOSFET is an uncommitted circuit element, it may be used to provide amplification of this electrical signal or as a multiplexer to select for further processing one signal from many such transducer elements [130].

The tactile sensing array (overall size—9200 × 7900 μm) by Kolesar et al. [83, 125] is based on aforementioned extended gate approach. The 8 × 8 extended electrodes, shown in Fig. 5.21, act as the lower electrodes for the PVDF piezoelectric film. The PVDF film (40 μm thick) is epoxy adhered to the lower electrodes (dimension—400 × 400 μm). The lower/extended electrodes are thus capacitively coupled to the PVDF, via the insulating glue bond. An oxide layer on the surface of the silicon electrically isolates these electrode from the silicon. The extended gates are connected to the MOSFET devices located on the periphery of the chip. The spatial resolution of the array is less than 1 mm and response of tactile sensor is linear for loads spanning 0.8–135 gmf (0.008–1.35 N). A response bandwidth of 25 Hz has been achieved. The tactile sensing array also possesses simple amplifier circuitry (Fig. 5.21). The problem of response stability and reproducibility, associated with piezoelectric based tactile sensors, is taken care by a pre-charge bias technique.

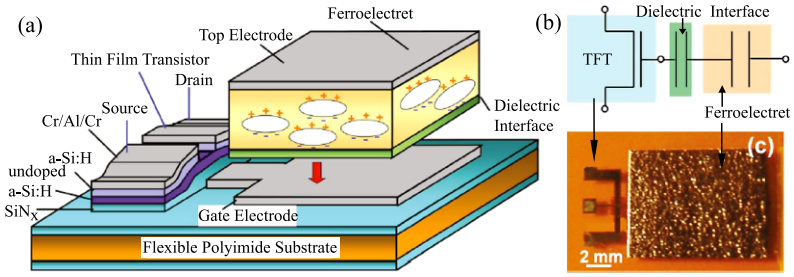

Fig. 5.22 (**a**) Sketch of the ferroelectret field effect transducer. The ferroelectret film is mechanically and electrically interfaced with the amorphous Si field-effect transistor via a thin dielectric coupling layer; (**b**) Equivalent circuit diagram; and (**c**) Photograph of one transducer element (Reprinted with permission from [126] ©[2006] American Institute of Physics)

The pre-charge bias feature incorporated in the sensor design (and operated by external circuitry), impresses a short-duration (0.1 seconds), low-level, direct current voltage ($V_{bias} = 2.5$ V) to the upper and lower electrodes of the PVDF film. The sensor is thus initialized before each cycle and eventually the voltage fluctuations is minimized.

Following a similar approach, a 32 element tactile sensing array, epoxy-adhered with 25, 50 and 100 μm piezoelectric polymer film (PVDF-TrFE) [127, 131], is presented in the next chapter. The touch sensing elements have been tested over a much wider range of dynamic forces (up to 5 N in the frequency range of 2 Hz–5 kHz) and a spatial resolution of 1 mm has been reported. With charge and voltage amplifiers, designed specifically for testing and discussed in Appendix C, the response of discrete sensing elements is found to be linear in above said test range. The use of the tactile sensing array for detecting objects based on their hardness has also been demonstrated.

Another example of extended gate approach is the sensor by Graz et al. [126] where ferroelectret material has been used as transducer. The ferroelectret material (made from 70 μm thick cellular polypropylene films) is epoxy adhered to the extended electrode of an amorphous silicon (a-Si:H) thin film transistor (TFT). As depicted in Fig. 5.22, the sensor has been realized on the a 50 μm thick polyimide film. The ferroelectrets can be used in capacitive and piezoelectric modes and accordingly the ferroelectret TFT sensor can be used to detect static and dynamic contacts. Other advantages of ferroelectrets are the large longitudinal piezoelectric signals and the corresponding negligible pyroelectric and transverse piezoelectric responses. This makes ferroelectrets insensitive to temperature drifts and device bending. However, due to lower charge carrier mobility the a-Si:H based transistor are much slower than the standard silicon transistors. Another example of extended gate transistor based tactile sensor, using zinc oxide (ZnO) as transducer is presented by Polla et al. in [132].

The extended gate approach brings the sensor and analog sensors frontend closer and hence overall response is better than that of conventional approach, where the sensor and analog sensors frontend are separated by some distance. One problem

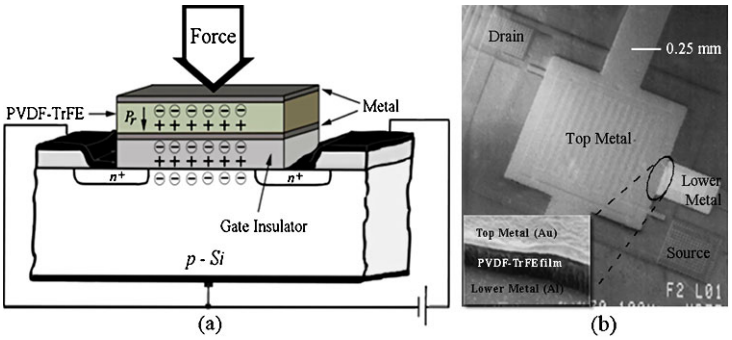

Fig. 5.23 (**a**) The structure and working of a POSFET touch sensing device; (**b**) SEM image of a POSFET device. The cross section of piezoelectric polymer film is shown in *inset*

with the extended gate structures (realized on silicon) is the capacitance between the extended gate electrode and the conductive silicon wafer, with the insulating oxide layer acting as a dielectric. Because of the limitations of IC technology, the oxide layer is usually much thinner (≈1.5 μm) than the piezoelectric film. With a dielectric constant comparable to that of the PVDF, the oxide capacitance will be much larger than that of the PVDF. This means the oxide layer may result in a significant reduction of overall sensitivity and increases the propagation delay [60]. Thus, benefits of closely located sensor and electronics are not fully exploited with extended gate approach. Such effects can be reduced by depositing the piezoelectric polymer film on the gate area of the transistor itself, as explained in following para and later in Chaps. 7 and 8.

The issues such as negative effect of the large oxide capacitance introduced by the extended gates, can be overcome by depositing the piezoelectric material on the gate ares of the transistor. This is precisely what is done in case of POSFET touch sensing devices that are described in detail in Chaps. 7 and 8. However, for completing the discussion, POSFET tactile sensing devices are briefly described here. The structure of a POSFET touch sensing devices is shown in Fig. 5.23 [128]. It can be noticed that the piezoelectric polymer film is present over the gate area of the MOS device. Thus, transducer material is an integral part of a POSFET device. The structure of POSFET device is similar to that of metal-ferroelectric-metal-insulator-semiconductor type FeRAM (Ferroelectric Random Access Memory) devices [133], which are used for memory applications. However, working of POSFET devices is fundamentally different from that of FeRAM—as former responds to changes in mechanical stimulus and the output in latter results from electric field switching. The remanent polarization (P_r) of the polarized polymer and the principle of charge neutrality lead to the appearance of fixed charges $\pm Q$, as shown in Fig. 5.23. For piezoelectric polymers in thickness mode, as in this work, the mechanical stress T_3, electric field E_3 and electric displacement D_3 are related as [61]:

$$D_3 = d_{33} \times T_3 + \varepsilon_{33} \times E_3 \tag{5.16}$$

where, d_{33} and ε_{33} are the piezoelectric and dielectric constants of piezoelectric polymer respectively. Following (5.16), the electric displacement can be controlled either by varying the electric field E_3 and/or by the mechanical stress T_3 (or the contact force). While former is used in FeRAM to switch the polarization state, latter is used in the POSFETs (and also in extended gate devices) to modulate the charge in the induced channel of underlying MOS device. Thus, the (contact) force variation is directly reflected as variation in the channel current of POSFET devices—which can be further processed by an electronic circuitry that may also be integrated on the same chip. It should be noted that silicon based devices are also known to exhibit piezoresistive effect i.e. their resistivity changes due to applied stressed. This raises an important question about the source of the change in channel current—piezoelectric action of P(VDF-TrFE) polymer film present on the gate area or the piezoresistive behavior of silicon? The same argument holds for previous discussed extended gate devices. In practice, both piezoelectric and piezoresistive effects contribute. As demonstrated by Dahiya et al. in [128], the contribution of piezoresistive effect is about 1% of the total output and therefore the change in the channel current of a POSFET (and hence its output) is primarily because of the piezoelectric action of the P(VDF-TrFE) polymer film. However, the same may not be true in case of flexible transistors which experience large piezoresistive effect due to large bending.

The POSFET tactile sensing devices are very sensitive with recorded sensitivity of more than 100 mV/N [134, 135]), have spatial resolution of about 1 mm and linear response to normal dynamic forces ranging from 0.01 N to 5 N [128, 135] with frequencies up to 2 kHz. Unlike extended gate approach, the POSFETs occupy lesser area on the chip. The silicon real estate thus saved can be used to accommodate on-chip electronics and signal processing circuitry. The local processing of the tactile signal will also help reduce the amount of tactile data transferred to higher perceptual levels of a robot. A detail discussion on POSFET tactile sensing devices and the tactile sensing chips made from them later is given in Chaps. 7 and 8.

5.4.2.2 Organic Transistor Technology Based Sensors

A few notable tactile sensing structures reported in literature are based on organic field effect transistors (OFETs) [34, 129]. The OFET based tactile sensing solutions have the advantage of being mechanically flexible, low cost solution, relative ease of fabrication and easy implementation over large areas. As presented earlier in this chapter, the OFETs can also be implemented in yarn textile topology, making wearable electronics more real [109]. The examples of OFETs based tactile skin include the 32×32 pressure sensing array by Someya et al. [34]. Realized on ultra-high heat-resistant and mechanically flexible poly(ethylene naphthalate) (PEN) substrate (thickness 100 μm), the sensing structure and its equivalent circuit are shown in Fig. 5.24. The OFET is based on pentacene and pressure conductive rubber is employed as the transducer. Unlike previously discussed transistor based tactile sensors (where transducer is connected to gate terminal), in this case the pressure sensitive

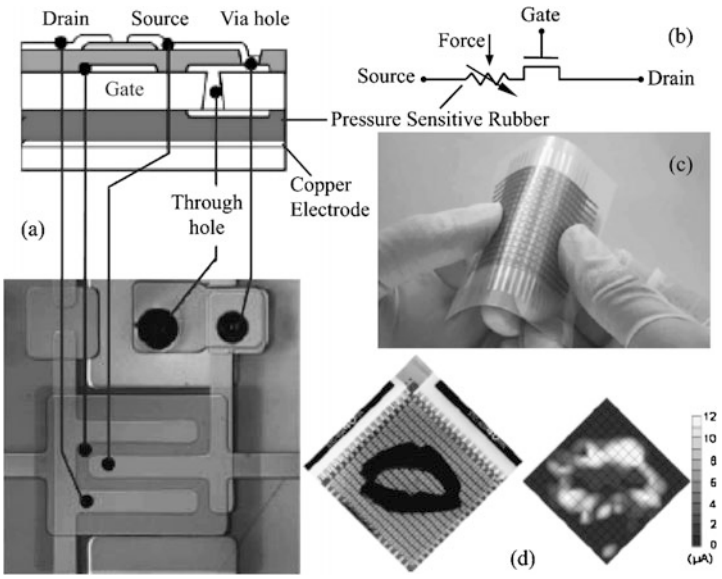

Fig. 5.24 (**a**) The section and top view of the organic FET sensing element with pressure sensitive rubber; (**b**) Equivalent circuit of the sensing element; (**c**) The 16 × 16 OFET array; (**d**) A pressure image of a kiss mark taken with the presented sensors (with permission from [34], ©(2004) National Academy of Sciences, USA)

rubber is placed in the source–drain path. The applied pressure results in a resistance change of the pressure conductive rubber, which in turn results in a change in the current I_{ds} flowing between the source and drain. The applied pressure is thus modulates I_{ds}, which can be easily measured using external circuitry. In a sense the OFET technology has been used as the readout element for the pressure conductive rubber. The applied pressure in the range 0 to 30 kPa ($\approx$ 300 gmf/cm^2) results in the resistance variation from 10 MΩ to 1 kΩ. The sensing elements have a pitch of 2.54 mm. In this study, the cycle time of each transistor is around 30 milliseconds, from which the total time to access 16 × 16 transistors is estimated to be 480 milliseconds if one word line is read at the same time. These figures are quite high with respect to the tactile sensing structures based on silicon technology and as such the sensors are suitable for slow varying (quasi static) mechanical stimuli.

Another OFET based tactile sensing structure is presented by Mannsfeld et al. [129]. In this arrangement, a pyramid structured highly pressure sensitive PDMS thin film is employed as the dielectric over the gate area of a rubrene based OFET (on PET substrates).[10] On application of pressure, the PDMS is compressed and the

[10]There is an analogy between this structure and the human skin. The pyramid like microstructure can be viewed similar to the intermediate ridges present at the dermis–epidermis junction of human skin (Chap. 3). The ridge microstructures in skin are also known to improve the tactile sensitivity in humans [136–138].

dielectric capacitance changes (due to reduction in thickness), eventually resulting in a change of the source–drain current (I_{ds}) of the transistor. Since the transducer is placed on the gate area, the structural arrangement is similar to the previously discussed POSFET touch sensing devices. However, in this case the channel current is modulated by change in dielectric capacitance. In case of POSFET, the channel current is primarily modulated by the change in polarization level of the piezoelectric polymer film. The response of this tactile sensing arrangement to the application of pressure is non-linear, which is expected due to the fact that in OFETs the source-drain current (I_{ds}) linearly depends on the dielectric capacitance but the PDMS film capacitance has non non-linear dependence on the pressure. By using 6×6 μm^2 pyramid-structured PDMS film, Mannsfeld et al. demonstrated the improvements in sensitivity of the dielectric material. The maximum slope of the relative capacitance change of the pyramidal PDMS film in the 0.2 kPa range is 0.55 kPa^{-1}. This is about 30 times higher than the sensitivity of unstructured film in the same range. The loads as low as 3 Pa have been detected. The microstructured PDMS also results in an improved relaxation time of the transducer. The structured films relaxed on the millisecond timescale, and unstructured films relaxed over times as long as 10 s, which is about 10^4 times slower. This means the transducer will again be ready for use in few milliseconds after the load is removed. However, the overall response time depends on both the transducer and the transistor and in this context the slow response of OFET remains a concern.

A major drawback of the OFET based tactile sensing arrangements is that their overall speed of response is slow. For instance, the response time of above described pentacene based OFET by Someya et al. [34] is 30 milliseconds. With further lower charge carrier mobility (1.0 cm^2/V.s as compared to 1.4 cm^2/V.s in [34]) the rubrene based OFET by Mannsfeld et al. [129] is expected to be more slower. From the point of view tactile sensing, the overall response depends on both transducer and the OFET. As far as transducer is concerned, the response speed can be improved by using a material that responds faster. Consider for instance, the pressure sensitive rubber used by Someya et al. [34] typically has the response time of the order of hundreds of milliseconds. Replacing pressure sensitive rubber with polymers like PVDF can significantly improve the response speed. Sometimes, shaping the transducer suitably can also result in improved response speed. For instance, a structured PDMS film can respond faster that an unstructured film. The above discussed tactile sensing arrangement by Mannsfeld et al. [129] is one such example. Comparing the response of an unstructured PDMS film with a structured PDMS film (having two dimensional arrays of square pyramid microstructures), Mannsfeld et al. noted that although the response to an external load (15 kPa) was immediate in both films, the relaxation times were quite disparate. The structured films relax on the millisecond timescale, and unstructured films relaxing over times as long as 10 seconds, which is about 10^4 times slower. The lengthy response time of unstructured PDMS films severely limits their usefulness as pressure sensors. Unfortunately, not many alternatives are available for improving the response speed of the organic transistors. It is well known that the mobility of organic semiconductors is about three orders of magnitude lower than that of silicon, which makes them much slower than the standard silicon based devices [139] and hence issue of overall slow response remains.

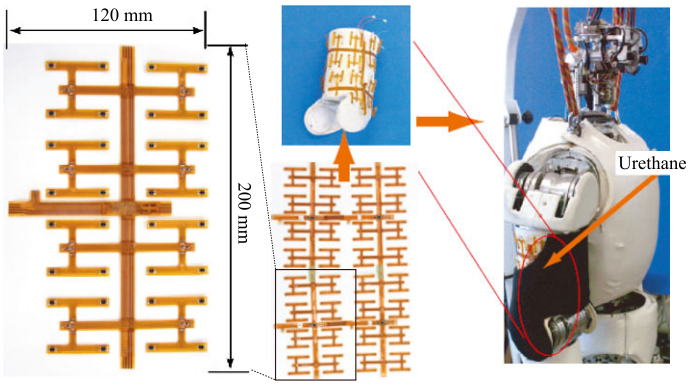

Fig. 5.25 A lightweight, conformable and scalable large area skin on flexible printed circuit board (with permission from [46], ©(2006) IEEE)

Other issues with organic devices are that they typically have short life and their operational stability is influenced by various factors, including dependence on stress voltage and duty cycle, gate dielectric, environmental conditions, light exposure, and contact resistance [140].

The tactile sensing arrays based on organic semiconductor technology cannot attain (at least in the present state of the technology) the high-speed performance exhibited by their silicon counterparts, but, features like physical flexibility and the low cost of fabrication make them good candidates for large-area skin. As presented in Chap. 3, the spatio-temporal requirements are not same for all body parts. For body parts such as belly and back (that make a large portion of the body) the spatio-temporal requirements are not high. Same argument when applied to robotics (e.g. humanoids), the organic transistor based solutions can be useful in future for less sensitive parts.

5.4.3 Sensors on Flexible Substrates

This concluding section presents the flexible tactile sensing structures realized on flexible substrates (sensor is not necessarily flexible), which is normally the flexible printed circuit board (PCB). As argued in previous chapter, for better integration and effective utilization of tactile data, the tactile sensing schemes are required to be conformable. In this context, many tactile sensing structures have been realized on flexible PCBs. Generally, these structures employ off-the-shelf sensing and electronics components. It is difficult to discuss all such solution and therefore only a selected few (having sensing component based on different transduction methods) with an aim to cover large area of a robot's surface are discussed below.

A conformable and scalable large area tactile sensing skin, having pressure sensing elements based on optical mode of transduction, is shown in Fig. 5.25. As discussed earlier in this chapter, each touch element on this tactile skin by Ohmura et

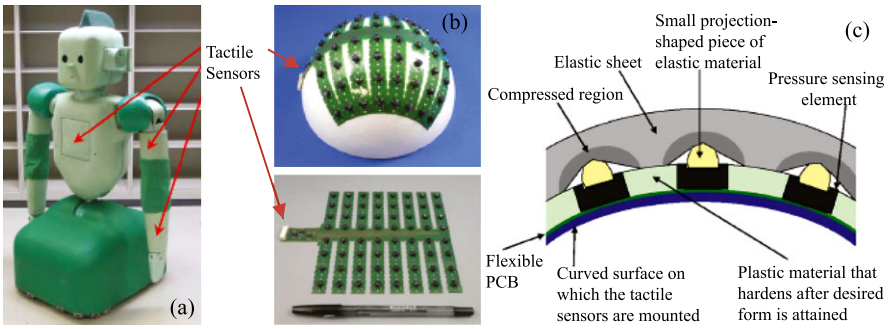

Fig. 5.26 The tactile skin structure with piezoresistive pressure sensors distributed on a flexible printed circuit board. (**a**) The location of tactile sensor on the humanoid robot RI-MAN; (**b**) The comb-shaped sensor patch; (**c**) Sensor embedded in elastic sheet (with permission from [11], ©(2008) IEEE)

al. [46] consists of photo-reflectors (3.2 mm × 1.1 mm × 1.7 mm) under the urethane foam (thickness 5 mm) and the light scattered by urethane foam upon deformation gives the measure of mechano-electrical transduction. The foam thickness controls the dynamic range and sensitivity of the sensors. The sensor sheet (120 mm × 120 mm) is lightweight (1.7 gram) and consists of 32 tactile sensing elements, one micro-controller and four serial bus terminators mounted on a flexible substrate. This modular skin can be folded and cut and the sensor coverage is adjustable via the addition/deletion of the modules. A couple of tactile sensor sheets are integrated to obtain a larger tactile sensor sheet (of 120 tactile sensor elements) and the final sheet is mounted on the arm of a humanoid robot is shown in Fig. 5.25. Time to scan one sensor element is 0.2 milliseconds (the interval between the instant when host computer sends the address packet until receiving the sensor data) and spatial resolution is approximately 3 cm. The sensing elements communicate via serial bus. To overcome the difficulties associated with serial bus for real-time communication at high speed, a ring-type network is proposed. The serial busses are connected with slave nodes of a custom designed ring-type network, with each node having a small-sized microcontroller as a serial-bus master. One major disadvantage of this scheme is the large current consumption by LEDs (∼50 mA per sensing element). To overcome this problem Ohmura et al. have proposed scanning control scheme, whereby the number of powered-on LEDs are restricted through time-sharing control. As the control is time-shared, the analog to digital converters and the analog signal wires can also be shared. The current in each LED can also be controlled through pulse width modulation. In fact, the same can also be employed to tune the sensitivity of the tactile sensing elements. Other concern related to this approach stems from the fact that urethane foam used in sensing element inevitably causes strong hysteresis and creep.

Another tactile sensing scheme on flexible printed circuit board, presented by Mukai et al. [11], is shown in Fig. 5.26. The piezoresistive semiconductor pressure sensors have been distributed on comb-shaped printed circuit board and embedded

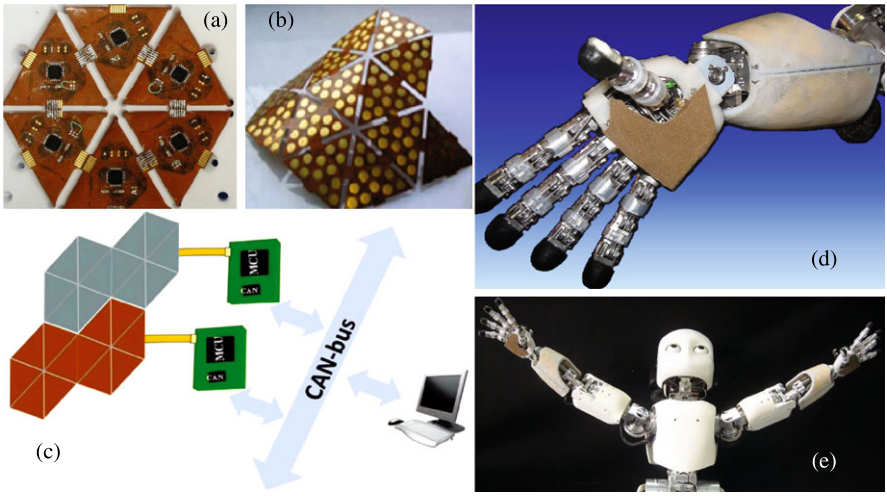

Fig. 5.27 The conformable triangular modules on flexible PCB. (**a**) The back side of the sensor patch based on capacitive technology (sensors on other side); (**b**) The flexibility of structure, owing to triangular shape of modules and the flexible PCB; (**c**) The scheme for making large networked structure; (**d**) Implementation of sensors patch on hand of humanoid robot iCub; (**e**) Humanoid robot iCub with equipped with the sensor patches (with permission from [141], ©(2011) IEEE)

in an elastic sheet (5 mm thick). Each sensor sheet (comb-shaped PCB) has an array of 8×8 pressure-sensing elements with an 18 mm pitch. The piezoresistive semiconductor pressure sensors can detect the absolute pressure between 0.434–4.46 kgf/cm^2. These sensors have been employed because they have little hysteresis or creep and accuracy is better (though soft cover introduces some hysteresis and creep). The skin specifications target the sensing capabilities of a human when carrying another human in his/her arms (0–20 mm spatial resolution and 0.434–4.46 kgf/cm^2 pressure range, similar respectively to the human palm and 20×20 cm^2 of arm contact while holding a 60 kg human). All the wiring is concentrated into a comb-shaped region. The complete sampling of one tactile sensor patch with 8×8 elements requires about 15 ms, which is not always sufficient for the tactile feedback control. The sensor sheets cover the arms and chest of the 158 cm tall humanoid "RI-MAN" with a total of 320 pressure-sensing elements.

The capacitive technology based conformable sensor patches have been presented by Maggiali et al. [43]. The implementation of these patches is shown in Fig. 5.27(a), (b). Each triangular shaped modules, realized on flexible printed circuit board, contains 12 round pads on which capacitive pressure sensors are present and a capacitance-to-digital converter (AD7147 from Analog Devices [42]). A thick elastic sheet (silicone foam, 3–5 mm thick) covers the skin patch, allowing limited degree of compliance. However, it also adds to the challenges related to sensor calibration and drift in the response. The communication port on all three sides of triangle facilitates communication with adjacent modules—enabling creation of a large networked structure, as shown in Fig. 5.27(c). The signals from touch sen-

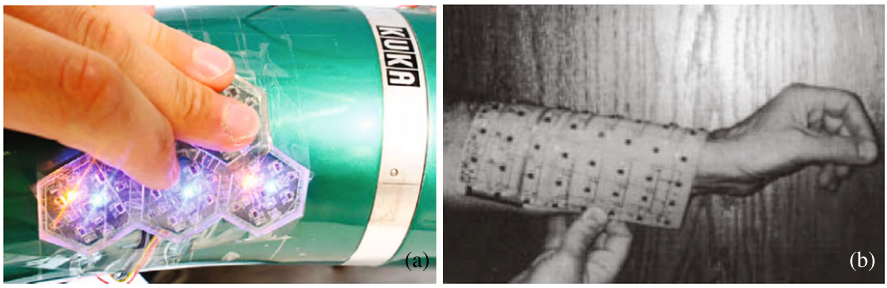

Fig. 5.28 Skin modules with proximity sensors. (**a**) The multimodal HEX-O-SKIN modules mounted on a KUKA lightweight arm (with permission from [142], ©(2011) IEEE); (**b**) The sensitive skin module on Kaptan substrate. The module uses 8×8 infrared sensors pairs (LEDs and detectors) as proximity sensors (with permission from [143], ©(2001) IEEE)

sors are sent to a microcontroller using I^2C serial bus communication interface. The sensor patch has low power consumption ($\sim$5 watts/m^2). This technology has been employed to cover large body parts of robots like iCub (Fig. 5.27(d), (e)), KASPAR and NAO [141]. The transducers and signal conditioning electronics wrap the robot surface, with components like microcontroller units installed in the inner body.

A vast majority of sensing structures are capable of detecting and measuring either contact force or pressure. The contact parameters are however not just limited to the contact force or pressure. There is a need to have sensing modules with multiple types of sensor to detect multiple contact parameters. The multimodal hexagonal shaped tactile sensing modules (HEX-O-SKIN), presented by Mittendorfer and Cheng [142] and shown in Fig. 5.28(a), are interesting in this context. The modules, implemented on printed circuit board, are equipped with multiple discrete sensors for temperature, acceleration, and proximity to emulate the human sense of temperature, vibration and soft or light touch respectively. Each module comprises of seven temperature sensors, three acceleration sensors and four proximity sensors. The modules, each weighing less than 2 grams, are embedded into elastomeric material to introduce limited degree of conformability.

Proximity or light touch sensing can be important for safe interaction. Covering of a manipulator with proximity sensing elements distributed all over it and their effective use in motion planning was first demonstrated in [8] and later followed in [9, 10, 143]. As shown in Fig. 5.28(b), distributed proximity sensing elements based on optical transduction were used as touch sensors in these works. Five sensor modules—each with 16 sensor pairs, consisting of a photo transistor and an IRLED were used. The distance between neighboring pairs is 25 mm. Scanning time of each module was 20 ms (serial access within a module), which was also the scanning time of all five modules (parallel access among modules). Thus a speed higher than that of PUMA robot velocity commands update rate (36 ms) was obtained and hence the data from sensing arrays could easily fit into the real-time operations performed by manipulator. The IRLEDs used in this work, were primarily used as proximity sensors and real contact with the sensor was avoided. But, a realistic situation would require safe interaction of robot while touching the objects. Nonetheless, for

Table 5.3 Tactile sensing arrays for parts like fingertips with high density receptors [28, 30, 40, 45, 83, 113–115, 127, 132, 144–154]

Year	Author	Transduction Method	Miniaturization Technique	No.of Sensing Element	Spatial Res. (mm)	Signal Condition Circuit	Sensor BW (kHz)	Range of Force^{+} (N)/Pressure* (kPa)	Force/ Pressure Sensitivity
1984	Raibert et al.	Resistive	Si-micromachining	6 × 8	∼0.6	Yes[a]	–	–	–
1985	Polla et al.	Piezoelectric	Si-micromachining	8 × 8	0.07	Yes[a]	–	2^{+}	5.2 mV/gm
1988	Suzuki et al.	Capacitive	Si-micromachining	32 × 32	0.5	No	–	0.01^{+}	0.45 pF/g
1990	Sugiyama et al.	Piezoresistive	Si-micromachining	32 × 32	0.25	Yes[a]	60	–	0.02 mV/kPa
1993	Liu et al.	Piezoresistive	Si-micromachining	4 × 4	1	Yes[a]	–	200*	0.032 mV/kPa
1994	Audet et al.	Magnetic	Si-micromachining	–	–	Yes	–	–	–
1996	Chu et al.	Capacitive	Si-micromachining	3 × 3	2.2	No	–	0.01^{+}	0.13 pF/g (nf) 0.32 pF/g (shf)
1996	Gray et al.	Capacitive	Si-micromachining	8 × 8	0.1	No	–	$1.0 \times 10^{-4+}$	20 µN
1996	Kolesar et al.	Piezoelectric	Si-micromachining	8 × 8	0.7	Yes[a]	0.025	$0.008–1.35^{+}$	–
1997	Desouza et al.	Capacitive	Si-micromachining	16 × 16	500 dpi	No	–	–	100 µN
2000	Kane et al.	Piezoresistive	MEMS on Si	64 × 64	0.3	Yes[a]	–	35*	1.59 mV/kPa
2000	Leineweber et al.	Capacitive	Si-micromachining	8 × 1	0.24	Yes[a]	–	100–300*	13.5 mV/kPa
2002	Castelli	Capacitive	–	8 × 8	>2	No	–	120*	–
2002	Hellard et al.	Optical	–	4 × 4	>1	No	–	–	–
2003	Wen et al.	Field Emission	MEMS on Si	8 × 8	1	Yes[a]	–	150*	30.1 mV/kPa
2005	Choi et al.	Resistive & Piezoresistive	–	24	∼1	No	–	2^{+}	–
2006	Okha et al.	Optical	–	–	2	No	–	2^{+}	1 mN
2006	Schmidt et al.	FSR & Capacitive	–	1_{static} $16_{dyn.}$	–	No	∼0.003 35	$0.05–10^{+}$ $<0.01^{+}$	5 mN
2006	Takao et al.	Piezoresistive	MEMS on Si	6×6	0.42	Yes[a]	–	$0.021–0.176^{+}$	0.5–1 V/N
2009	Dahiya et al.	Piezoelectric	Si-micromachining	32	1	Yes	5	5*	0.5 V/N
2010	Dahiya et al.	Piezoelectric	Si-micromachining	5×5	1	Yes	2.13	5*	0.5 V/N

[a]Electronics circuitry (partly) on the sensing array; nf—Normal force; shf—Shear force

Table 5.4 Tactile sensing arrays for parts like large area skin with low density of receptors [8, 10, 11, 25, 34, 43, 46, 49, 67, 124, 155, 156]

Year	Author	Transduction Method	Miniaturization Technique	No.of Sensing Element	Spatial Res. (mm)	Signal Condition Circuit[a]	Sensor BW (kHz)	Range of Force$^+$ (N)/Pressure* (kPa)	Force/ Pressure Sensitivity
1989	Cheung et al.	Optical	–	16	–	Yes	–	–	–
1992	Domenici et al.	Piezoelectric	On Polyimide	6 × 7	2.5	No	–	–	–
1992	Lumelsky et al.	Optical	–	500		Yes			
1998	Um et al.	Optical	–	1000	25	Yes	–	–	–
2004	Someya et al.	FSR	Organic FET	32 × 32	2.54	No	0.003	30*	–
2004	Weiss et al.	Resistive	–	3 × 8	4	No	–	–	–
2005	Engel et al.	Resistive	MEMS on Polymer	25	∼5	No	–	–	–
2005	Shan et al.	Piezoresistive	MEMS on Si	4 × 4	10	No	–	2$^+$	228 mV/N (nf) 34 mV/N (shf)
2006	Heo et al.	Optical	–	3 × 3	5	No	–	5 N	1 mN
2006	Kim et al.	Strain Gauge	MEMS on Polymer	4 × 4	2.5	No	–	0.6$^+$	0.52 V/N (nf) 0.25 V/N (shf)
2006	Ohmura et al.	Optical	–	8 × 4	∼30	No	–	–	–
2008	Maggiali et al.	Capacitive	Flexible PCB	12	10	Yes	–	–	–
2008	Mukai et al.	Piezoresistive	Flexible PCB	8 × 8	18	Yes	0.1	128*	–

[a]Electronics circuitry (partly) on the sensing array; nf—Normal force; shf—Shear force

first time it was demonstrated that motion planning can be done with no a priori knowledge about the environment (or dynamic environment).

5.5 Summary

A wide spectrum of tactile sensing technologies ranging from single tactile sensor elements to arrangements suitable for large areas have been discussed in this chapter. Some of the sensing arrangements reported in literature are grouped in Tables 5.3 and 5.4—mainly on the basis of their reported spatial resolution. The touch sensing arrays in Table 5.3 are suitable for high sensor density body locations like the fingertips and those in Table 5.4 are suitable for low density sensory body locations like palm, belly, etc. Current trend is to develop tactile sensing structures with mechanical/physical features like flexibility, stretchability etc. to cover various body parts of a robot. Sensor coverage that is continuous, and spanning the entire robot body, is desired for many robotic applications including the safe and effective robot operation. A growing interest can be found for tactile sensing schemes able to detect multiple contact parameters and the fusion of different tactile sensors data to detect multiple contact parameters. It is noted that packaging and integration of tactile sensing solutions with the robot has received a considerable attention. Encapsulation of sensor elements, wires and the integration of processing and communication hardware directly on to flexible PCBs are steps in this direction. Recent developments in materials chemistry, nano-structures, nano-devices, and single-molecule devices have great potential in improving the current technology. Current methods using a pressure sensitive elastomer can be significantly improved by replacing conventional fillers such as carbon-black with fillers like carbon nano tubes. An interesting aspect of some nano-materials based devices is their relatively low cost of fabrication, processing under ambient conditions and the ability to directly make large-area devices on curved surfaces. It is noted that the tactile sensor technology has reached quite a level of maturity and now it is also the time to consider important issues like interface electronics, the techniques to handle the tactile data and take out useful information from it, as otherwise potential technological benefits will make little sense for robotics.

References

1. L.D. Harmon, Automated tactile sensing. Int. J. Robot. Res. **1**(2), 3–31 (1982)
2. H.R. Nicholls, M.H. Lee, A survey of robot tactile sensing technology. Int. J. Robot. Res. **8**(3), 3–30 (1989)
3. W.D. Hillis, Active touch sensing. Int. J. Robot. Res. **1**(2), 33–44 (1982)
4. P. Dario, D. de Rossi, Tactile sensors and gripping challenge. IEEE Spectr. **22**(8), 46–52 (1985)
5. S.C. Jacobsen, I.D. McCammon, K.B. Biggers, R.P. Phillips, Design of tactile sensing systems for dextrous manipulators. IEEE Control Syst. Mag. **8**, 3–13 (1988)

6. R.D. Howe, M.R. Cutkosky, Dynamic tactile sensing: perception of fine surface features with stress rate sensing. IEEE Trans. Robot. Autom. **9**, 140–151 (1993)
7. R.D. Howe, Tactile sensing and control of robotics manipulation. Adv. Robot. **8**, 245–261 (1994)
8. E. Cheung, V.L. Lumelsky, Proximity sensing in robot manipulation motion planning: system and implementation issues. IEEE Trans. Robot. Autom. **5**(6), 740–751 (1989)
9. E. Cheung, V.L. Lumelsky, A sensitive skin system for motion control of robot arm manipulators. Robot. Auton. Syst. **10**, 9–32 (1992)
10. D. Um, B. Stankovic, K. Giles, T. Hammond, V.L. Lumelsky, A modularized sensitive skin for motion planning in uncertain environments, in *IEEE International Conference on Robotics and Automation*, Leuven, Belgium (1998), pp. 7–112
11. T. Mukai, M. Onishi, T. Odashima, S. Hirano, Z. Luo, Development of the tactile sensor system of a human-interactive robot "RI-MAN". IEEE Trans. Robot. **24**(2), 505–512 (2008)
12. Roboskin Project (2010). Available at: http://www.roboskin.eu/
13. R.S. Dahiya, G. Metta, M. Valle, G. Sandini, Tactile sensing—from humans to humanoids. IEEE Trans. Robot. **26**, 1–20 (2010)
14. R.S. Dahiya, G. Metta, G. Cannata, M. Valle, Guest editorial special issue on robotic sense of touch. IEEE Trans. Robot. **27**, 385–388 (2011)
15. B.V. Jayawant, Tactile sensing in robotics. J. Phys. E, Sci. Instrum. **22**, 684–692 (1989)
16. M.H. Lee, H.R. Nicholls, Tactile sensing for mechatronics—a state of the art survey. Mechatronics **9**, 1–31 (1999)
17. M.E.H. Eltaib, J.R. Hewit, Tactile sensing technology for minimal access surgery—a review. Mechatronics **13**, 1163–1177 (2003)
18. J. Dargahi, S. Najarian, Advances in tactile sensors design/manufacturing and its impact on robotics applications—a review. Ind. Robot **32**, 268–281 (2005)
19. V. Maheshwari, R. Saraf, Tactile devices to sense touch on a par with a human finger. Angew. Chem., Int. Ed. Engl. **47**, 7808–7826 (2008)
20. P. Puangmali, K. Althoefer, L.D. Seneviratne, D. Murphy, P. Dasgupta, State-of-the-art in force and tactile sensing for minimally invasive surgery. IEEE Sens. J. **8**, 371–381 (2008)
21. M.R. Cutkosky, R.D. Howe, W. Provancher, Force and tactile sensors, in *Springer Handbook of Robotics*, ed. by B. Siciliano, O. Khatib (Springer, Berlin, 2008), pp. 455–476
22. D. De Rossi, E.P. Scilingo, Skin-like sensor arrays, in *Encyclopedia of Sensors*, vol. X, ed. by C.A. Grimes, E.C. Dickey, M.V. Pishko (American Scientific Publishers, Valencia, 2006), pp. 1–22
23. P. Svyatoslav, Touch screen control and calibration—four-wire, resistive. Application Note AN2173, Cypress Microsystems (2004)
24. H. Zhang, E. So, Hybrid resistive tactile sensing. IEEE Trans. Syst. Man Cybern., Part B, Cybern. **32**(1), 57–65 (2002)
25. K. Weiss, H. Worn, Tactile sensor system for an anthropomorphic robotic hand, in *IEEE International Conference on Manipulation and Grasping*, Genoa, Italy (2004)
26. D.J. Beebe, A.S. Hsieh, D.D. Denton, R.G. Radwin, A silicon force sensor for robotics and medicine. Sens. Actuators A, Phys. **50**, 55–65 (1995)
27. M.R. Wolffenbuttel, P.P.L. Regtien, Polysilicon bridges for the realization of tactile sensors. Sens. Actuators A, Phys. **A2**(1–3), 257–264 (1991)
28. B.J. Kane, M.R. Cutkosky, G.T.A. Kovacs, A traction stress sensor array for use in high-resolution robotic tactile imaging. J. Microelectromech. Syst. **9**(4), 425–434 (2000)
29. FSR Sensors, Interlink Electronics Inc. (2008). Available at: http://www.interlinkelectronics.com
30. H. Takao, K. Sawada, M. Ishida, Monolithic silicon smart tactile image sensor with integrated strain sensor array on pneumatically swollen single-diaphragm structure. IEEE Trans. Electron Devices **53**(5), 1250–1259 (2006)
31. M. Shimojo, A. Namiki, M. Ishikawa, R. Makino, K. Mabuchi, A tactile sensor sheet using pressure conductive rubber with electrical-wires stitched method. IEEE Sens. J. **4**(5), 589–596 (2004)

32. H. Liu, P. Meusel, G. Hirzinger, A tactile sensing system for the DLR three-finger robot hand, in *International Symposium on Measurement and Control in Robotics* (1995), pp. 91–96
33. M.A. Diftler, R. Platt Jr., C.J. Culbert, R.O. Ambrose, W.J. Bluethmann, Evolution of the NASA/DARPA robonaut control system, in *IEEE International Conference on Robotics and Automation* (2003), pp. 2543–2548
34. T. Someya, T. Sekitani, S. Iba, Y. Kato, H. Kawaguchi, T. Sakurai, A large-area, flexible pressure sensor matrix with organic field-effect transistors for artificial skin applications. Proc. Natl. Acad. Sci. USA **101**(27), 9966–9970 (2004)
35. H. Alirezaei, A. Nagakubo, Y. Kuniyoshi, A highly stretchable tactile distribution sensor for smooth surfaced humanoids, in *7th IEEE-RAS International Conference on Humanoid Robots*, Pittsburgh, USA (2007)
36. Y. Kato, T. Mukai, T. Hayakawa, T. Shibata, Tactile sensor without wire and sensing element in the tactile region based on EIT method, in *IEEE Sensors Conference* (2007), pp. 792–795
37. D.S. Tawil, D. Rye, M. Velonaki, Improved image reconstruction for an EIT-based sensitive skin with multiple internal electrodes. IEEE Trans. Robot. **27**(3), 425–435 (2011)
38. Peratech Ltd., UK Patent PCT/GB98/00206 (WO 98/33193) Available at: http://www.peratech.co.uk
39. H.-K. Lee, S.-I. Change, E. Yoon, A flexible polymer tactile sensor: fabrication and modular expandability for large area deployment. J. Microelectromech. Syst. **15**(6), 1681–1686 (2006)
40. P.A. Schmidt, E. Mael, R.P. Wurtz, A sensor for dynamic tactile information with applications in human–robot interaction & object exploration. Robot. Auton. Syst. **54**, 1005–1014 (2006)
41. RoboTouch (2007). Available at: http://www.pressureprofile.com
42. AD7147: CapTouch™ (2008). Available at: http://www.analog.com
43. M. Maggiali, G. Cannata, P. Maiolino, G. Metta, M. Randazzao, G. Sandini, Embedded tactile sensor modules, in *11th Mechatronics Forum Biennial International Conference*, Limerick, Ireland (2008)
44. Available at: http://www.soton.ac.uk/~rmc1/robotics/artactile.htm
45. M. Ohka, H. Kobayashi, J. Takata, Y. Mitsuya, Sensing precision of an optical three-axis tactile sensor for a robotic finger, in *15th International Symposium on Robot and Human Interactive Communication "RO-MAN"* (2006), pp. 214–219
46. Y. Ohmura, Y. Kuniyoshi, A. Nagakubo, Conformable and scalable tactile sensor skin for curved surfaces, in *IEEE International Conference on Robotics and Automation*, Orlando, Florida, USA (2006)
47. E.M. Reimer, L. Danisch, Pressure sensor based on illumination of a deformable integrating cavity. U.S. Patent 5,917,180 (1999)
48. H. Yussof, J. Takata, M. Ohka, Measurement principles of optical three-axis tactile sensor and its application to robotic fingers system, in *Sensors: Focus on Tactile, Force and Stress Sensors*, ed. by J.G. Rocha, S. Lanceros-Mendez (I-Tech Publishers, Vienna, 2008), pp. 123–142
49. J.-S. Heo, J.-H. Chung, J.-J. Lee, Tactile sensor arrays using fiber Bragg grating sensors. Sens. Actuators A, Phys. **126**, 312–327 (2006)
50. V. Maheshwari, R. Saraf, High-resolution thin-film device to sense texture by touch. Science **312**, 1501–1504 (2006)
51. J. Winger, K.-M. Lee, Experimental investigation of a tactile sensor based on bending losses in fiber optics, in *Proceedings of the IEEE International Conference on Robotics and Automation*, Raleigh, North Carolina, USA (1988), pp. 754–759
52. J.-S. Heo, J.-Y. Kim, J.-J. Lee, Tactile sensors using the distributed optical fiber sensors, in *Proceedings of the 3rd International Conference on Sensing Technology* (2008), pp. 486–490
53. T.J. Nelson, R.B. Van Dover, S. Jin, S. Hackwood, G. Beni, Shear-sensitive magnetoresistive robotic tactile sensor. IEEE Trans. Magn. **Mag-22**(5), 394–396 (1986)
54. W.C. Nowlin, Experimental results on Bayesian algorithms for interpreting compliant tactile sensing data, in *IEEE International Conference on Robotics and Automation*, Sacramento,

California, USA (1991)
55. E. Torres-Jara, I. Vasilescu, R. Coral, A soft touch: compliant tactile sensors for sensitive manipulation. Technical report, CSAIL, Massachusetts Institute of Technology (2006)
56. E. Torres-Jara, Sensitive manipulation. Ph.D. thesis, Massachusetts Institute of Technology (2007). http://hdl.handle.net/1721.1/36371
57. R.-C. Luo, F. Wang, Y. Liu, An imaging tactile sensor with magnetorestrictive transduction, in *Robot Sensors*, vol. 2, ed. by A. Pugh (Springer, Berlin 1985), pp. 113–122
58. S. Ando, H. Shinoda, Ultrasonic emission tactile sensing. IEEE Control Syst. Mag. **15**(1), 61–69 (1995)
59. S. Ando, H. Shinoda, A. Yonenaga, J. Terao, Ultrasonic six-axis deformation sensing. IEEE Trans. Ultrason. Ferroelectr. Freq. Control **48**(4), 1031–1045 (2001)
60. R.S. Dahiya, M. Valle, G. Metta, L. Lorenzelli, POSFET based tactile sensor arrays, in *IEEE ICECS'07: The 14th International Conference on Electronics, Circuits and Systems*, Marrakech, Morocco (2007), pp. 1075–1078
61. R.S. Dahiya, M. Valle, L. Lorenzelli, Spice model of lossy piezoelectric polymers. IEEE Trans. Ultrason. Ferroelectr. Freq. Control **56**(2), 387–396 (2009)
62. S. Omata, Y. Murayama, C.E. Constantinou, Real time robotic tactile sensor system for the development of the physical properties of biomaterials. Sens. Actuators A, Phys. **112**(2–3), 278–285 (2004)
63. G.M. Krishna, K. Rajanna, Tactile sensor based on piezoelectric resonance. IEEE Sens. J. **4**(5), 691–697 (2004)
64. H. Shinoda, K. Matsumoto, S. Ando, Tactile sensing based on acoustic resonance tensor cell, in *Proceedings of TRANSDUCERS 1997, International Conference Solid-State Sensors and Actuators* (1997), pp. 129–132
65. K. Nakamura, H. Shinoda, A tactile sensor instantaneously evaluating friction coefficients, in *Proceedings of TRANSDUCERS 1997, International Conference Solid-State Sensors and Actuators* (1997), pp. 1430–1433
66. J. Dargahi, M. Parameswaran, S. Payandeh, A micromachined piezoelectric tactile sensor for an endoscopic grasper—theory, fabrication and experiments. J. Microelectromech. Syst. **9**(3), 329–335 (2000)
67. C. Domenici, D. De Rossi, A stress-component-selective tactile sensor array. Sens. Actuators A, Phys. **13**, 97–100 (1992)
68. P. Dario, G. Buttazzo, An anthropomorphic robot finger for investigating artificial tactile perception. Int. J. Robot. Res. **6**(3), 25–48 (1987)
69. K. Hosoda, Y. Tada, M. Asada, Anthropomorphic robotic soft fingertip with randomly distributed receptors. Robot. Auton. Syst. **54**, 104–109 (2006)
70. A.M. Taylor, D.M. Pollet, A. Hosseini-Sianaki, C.J. Varley, Advances in an electrorheological fluid based tactile array. Displays **18**, 135–141 (1998)
71. R.M. Voyles, G. Fedder, P.K. Khosla, Design of a modular tactile sensor and actuator based on an electrorheological gel, in *IEEE International Conference on Robotics and Automation*, USA, vol. 1 (1996), pp. 13–17
72. G.L. Kenaley, M.R. Cutkosky, Electrorheological fluid-based robotic fingers with tactile sensing, in *IEEE International Conference on Robotics and Automation*, USA, vol. 1 (1989), pp. 132–136
73. J.D. Carlson, S.P. Koester, Magnetically-controllable active haptic interface system and apparatus. U.S. Patent 6,283,859 B1
74. E.P. Scilingo, N. Sgambelluri, D. De Rossi, A. Bicchi, Haptic displays based on magnetorheological fluids: design, realization and psychophysical validation, in *The 11th Symposium on Haptic Interfaces for Virtual Environment and Teleoperator Systems (HAPTICS'03)* (2003), p. 10
75. Y. Liu, R.I. Davidson, P.M. Taylor, J.D. Ngu, J.M.C. Zarraga, Single cell magnetorheological fluid based tactile displays. Displays **26**, 29–35 (2005)
76. Pressure sensitive ink (2008). Available at: http://www.tekscan.com/

77. R. Kageyama, S. Kagami, M. Inaba, H. Inoue, Development of soft and distributed tactile sensors and the application to a humanoid robot, in *IEEE International Conference on Systems, Man, & Cybernetics*, vol. 2 (1999), pp. 981–986
78. K.B. Shimoga, A.A. Goldenberg, Soft materials for robot fingers, in *IEEE International Conference on Robotics and Automation*, Nice, France (1992), pp. 1300–1305
79. H.S. Nalwa, *Ferroelectric Polymers: Chemistry, Physics, and Applications* (Marcel Dekker, Inc., New York, 1995)
80. A.J. Lovinger, Ferroelectric polymers. Science **220**(4602), 1115–1121 (1983)
81. J.R. Flanagan, A.M. Wing, Modulation of grip force with load force during point-to-point arm movements. Exp. Brain Res. **95**, 131–143 (1993)
82. D. De Rossi, C. Domenici, Piezoelectric properties of dry human skin. IEEE Trans. Electr. Insul. **EI-21**(3), 511–517 (1986)
83. E.S. Kolesar, C.S. Dyson, R.R. Reston, R.C. Fitch, D.G. Ford, S.D. Nelms, Tactile integrated circuit sensor realized with a piezoelectric polymer, in *8th IEEE International Conference on Innovative Systems in Silicon*, Austin, Texas, USA (1996), pp. 372–381
84. B. Choi, H.R. Choi, S. Kang, Development of tactile sensor for detecting contact force and slip, in *IEEE/RSJ International Conference on Intelligent Robots and Systems* (2005), pp. 2638–2643
85. E.S. Kolesar, R.R. Reston, D.G. Ford, R.C. Fitch, Multiplexed piezoelectric polymer tactile sensor. J. Robot. Syst. **9**(1), 37–63 (1992)
86. Y. Yamada, T. Maeno, I. Fujimoto, T. Morizono, Y. Umetani, Identification of incipient slip phenomena based on the circuit output signals of PVDF film strips embedded in artificial finger ridges, in *SICE Annual Conference* (2002), pp. 3272–3277
87. R. Strümpler, J. Glatz-Reichenbach, Conducting polymer composites. J. Electroceram. **3**(4), 329–346 (1999)
88. D. Staufer, A. Aharony, *Introduction to Percolation Theory* (Taylor & Francis, London, 1992)
89. V.I. Roldughin, V.V. Vysotskii, Percolation properties of metal-filled polymer films, structure and mechanics of conductivity. Prog. Org. Coat. **39**, 81–100 (2000)
90. J.K.W. Sandler, J.E. Kirk, I.A. Kinloch, M.S.P. Shaffer, A.H. Windle, Ultra-low electrical percolation threshold in carbon-nanotube-epoxy composites. Polymer **44**(19), 5893–5899 (2003)
91. D. Bloor, K. Donnelly, P.J. Hands, P. Laughlin, D. Lussey, A metal-polymer composite with unusual properties. J. Phys. D, Appl. Phys. **38**, 2851–2860 (2005)
92. R. Walker, Developments in dextrous hands for advanced robotic applications, in *10th International Symposium on Robotics and Applications* (2004)
93. Shadow hand. Available at: http://www.shadowrobot.com
94. L. Flandin, G. Bidan, Y. Brechet, J.Y. Cavaille, New nanocomposite materials made of an insulating matrix and conductive fillers: processing and properties. Polym. Compos. **21**(2), 165–173 (2000)
95. S.-L. Yu, D.-R. Chang, L.-C. Tsao, W.-P. Shih, P.-Z. Chang, Porous nylon with electro-active dopants as flexible sensors and actuators, in *MEMS 2008. IEEE 21st International Conference on Micro Electro Mechanical Systems* (2008), pp. 908–911
96. X. Chen, S. Yang, M. Hasegawa, K. Kawabe, S. Motojima, Tactile microsensor elements prepared from arrayed superelastic carbon microcoils. Appl. Phys. Lett. **87** 054101, (2005)
97. L. Chen, G. Chen, L. Lu, Piezoresistive behaviour study on finger-sensing silicone rubber/graphite nanosheet nanocomposites. Adv. Funct. Mater. **17**, 898–904 (2007)
98. O. Kerpa, K. Weiss, H. Wörn, Development of a flexible tactile sensor system for a humanoid robot, in *IEEE/RSJ International Conference on Intelligent Robots and Systems*, Las Vegas, Nevada, USA (2003), pp. 1–6
99. L. Wang, T. Ding, P. Wang, Thin flexible pressure sensor array based on carbon black/silicone rubber nanocomposite. IEEE Sens. J. **9**(9), 1130–1135 (2009)
100. M.W. Strohmayr, H.P. Saal, A.H. Potdar, P. van der Smagt, The DLR touch sensor I: a flexible tactile sensor for robotic hands based on a crossed-wire approach, in *The 2010 IEEE/RSJ*

International Conference on Intelligent Robotics and Systems, Taipei, Taiwan (2010), pp. 897–903
101. J.-C. Huang, Carbon black filled conducting polymers and polymer blends. Adv. Polym. Technol. **21**(4), 299–313 (2002)
102. A.Y. Cao, P.L. Dickrell, W.G. Sawyer, M.N. Ghasemi-Nejhad, P.M. Ajayan, Super-compressible foam-like carbon nanotube films. Science **310**, 1307–1310 (2005)
103. J.K.W. Sandler, J.E. Kirk, I.A. Kinloch, M.S.P. Shaffer, A.H. Windle, Ultra-low electrical percolation threshold in carbon-nanotube-epoxy composites. Polymer **44**(19), 5893–5899 (2003)
104. J. Engel, J. Chen, N. Chen, S. Pandya, C. Liu, Multi-walled carbon nanotube filled conductive elastomers: materials and application to micro transducers, in *MEMS 2006: The 19th IEEE International Conference on Micro Electro Mechanical Systems*, Taipei, Taiwan (2006), pp. 246–249
105. B.S. Chiou, A.R. Lankford, P.E. Schoen, Modifying tubule distribution in tubule-filled composites by using polyurethane–polydimethylsiloxane interpenetrating polymer networks. J. Appl. Polym. Sci. **89**, 1032–1038 (2003)
106. H. Chia Hua, S. Wang-Shen, H. Chih-Fan, L. Chia-Min, F. Weileun, Y. Fu-Liang, A flexible, highly-sensitive, and easily-fabricated carbonnanotubes tactile sensor on polymer substrate, in *10th IEEE International Conference on Solid-State and Integrated Circuit Technology (ICSICT)*, Shanghai, China (2010), pp. 1388–1391
107. Y.-T. Lai, W.-C. Kuo, Y.-J. Yang, A tactile sensing array with tunable sensing ranges using liquid crystal and carbon nanotubes composites, in *The 24th IEEE International Conference on Micro Electro Mechanical Systems (MEMS)*, Cancun, Mexico (2011), pp. 553–556
108. C. Liu, Recent developments in polymer MEMS. Adv. Mater. **19**, 3783–3790 (2007)
109. A. Bonfiglio, D. De Rossi, T. Kirstein, I.R. Locher, F. Mameli, R. Paradiso, G. Vozzi, Organic field effect transistors for textile applications. IEEE Trans. Inf. Technol. Biomed. **9**(3), 319–324 (2005)
110. Y. Osada, J.-P. Gong, Soft and wet materials: polymer gels. Adv. Mater. **10**(11), 827–837 (1998)
111. K. Sawahata, J.P. Gong, Y. Osada, Soft and wet touch-sensing system made of hydrogel. Macromol. Rapid Commun. **16**, 713–716 (1995)
112. N. Wettels, V.J. Santos, R.S. Johansson, G.E. Loeb, Biomimetic tactile sensor array. Adv. Robot. **22**, 829–849 (2008)
113. B.L. Gray, R.S. Fearing, A surface micromachined microtactile sensor array, in *International Conference on Robotics and Automation*, Minneapolis, Minnesota, USA (1996)
114. Z. Chu, P.M. Sarro, S. Middelhoek, Silicon three-axial tactile sensor. Sens. Actuators A, Phys. **54**, 505–510 (1996)
115. M. Leineweber, G. Pelz, M. Schmidt, H. Kappert, G. Zimmer, New tactile sensor chip with silicone rubber cover. Sens. Actuators A, Phys. **84**, 236–245 (2000)
116. K. Suzuki, K. Najafi, K.D. Wise, A 1024-element high-performance silicon tactile imager. IEEE Trans. Electron Devices **37**(8), 1852–1860 (1990)
117. H.-K. Lee, S.-I. Chang, E. Yoon, A flexible polymer tactile sensor: fabrication and modular expandability for large area deployment. J. Microelectromech. Syst. **15**(6), 1681–1686 (2006)
118. U. Paschen, M. Leineweber, J. Amelung, M. Schmidt, G. Zimmer, A novel tactile sensor system for heavy load applications based on an integrated capacitive pressure sensor. Sens. Actuators A, Phys. **68**, 294–298 (1998)
119. M. Adam, E. Vazsonyi, I. Barsony, C.S. Ducso, Three dimensional single crystalline force sensor by porous Si micromachining, in *IEEE Sensors* (2004), pp. 501–504
120. M.R. Wolffenbuttel, P.P.L. Regtien, Design considerations for a silicon capacitive tactile cell. Sens. Actuators A, Phys. **A24**(3), 187–190 (1990)
121. M.R. Wolffenbuttel, P.P.L. Regtien, Polysilicon bridges for the realization of tactile sensors. Sens. Actuators A, Phys. **26**, 257–264 (1991)

122. E.-S. Hwang, J.-h. Seo, Y.-J. Kim, A polymer-based flexible tactile sensor for both normal and shear load detections and its application for robotics. J. Microelectromech. Syst. **16**(3), 556–563 (2007)
123. F. Jiang, G.-B. Lee, Y.-C. Tai, C.-M. Ho, A flexible micromachined based shear-stress sensor array and its applications to separation-point detection. Sens. Actuators A, Phys. **79**(3), 194–203 (2000)
124. J. Egnel, J. Chen, Z. Fan, C. Liu, Polymer micromachined multimodal tactile sensors. Sens. Actuators A, Phys. **117**, 50–61 (2005)
125. E.S. Kolesar, C.S. Dyson, Object imaging with a piezoelectric robotic tactile sensor. J. Microelectromech. Syst. **4**(2), 87–96 (1995)
126. I. Graz, M. Kaltenbrunner, C. Keplinger, R. Schwodiauer, S. Bauer, S.P. Lacour, S. Wagner, Flexible ferroelectret field-effect transistor for large-area sensor skins and microphones. Appl. Phys. Lett. **89**, 073501 (2006)
127. R.S. Dahiya, M. Valle, G. Metta, Development of fingertip tactile sensing chips for humanoid robots, in *5th IEEE International Conference on Mechatronics*, Malaga, Spain (2009), pp. 1–6
128. R.S. Dahiya, G. Metta, M. Valle, L. Lorenzelli, A. Adami, Piezoelectric oxide semiconductor field effect transistor touch sensing devices. Appl. Phys. Lett. **95**(3), 034105 (2009)
129. S.C.B. Mannsfeld, B.C.K. Tee, R.M. Stoltenberg, C.V.H.H. Chen, S. Barman, B.V.O. Muir, A.N. Sokolov, C. Reese, Z. Bao, Highly sensitive flexible pressure sensors with microstructured rubber dielectric layers. Nat. Mater. **9**, 859–864 (2010)
130. R.G. Swartz, J.D. Plummer, Integrated silicon-PVF2 acoustic transducer arrays. IEEE Trans. Electron Devices **26**(12), 1920–1932 (1979)
131. R.S. Dahiya, M. Valle, G. Metta, L. Lorenzelli, C. Collini, Tactile sensor arrays for humanoid robot, in *IEEE PRIME'07: The 3rd International Conference on Ph.D. Research in Microelectronics and Electronics*, Bordeaux, France (2007), pp. 201–204
132. D.L. Polla, W.T. Chang, R.S. Muller, R.M. White, Integrated zinc oxide-on-silicon tactile-sensor array, in *International Electron Devices Meeting* (1985), pp. 133–136
133. H. Ishiwara, Current status of ferroelectric-gate Si transistors and challenge to ferroelectric-gate CNT transistors. Curr. Appl. Phys. **9**, S2–S6 (2009)
134. A. Adami, R.S. Dahiya, C. Collini, D. Cattin, L. Lorenzelli, POSFET touch sensor with on-chip electronic module for signal conditioning, in *TRANSDUCERS 2011: The 16th IEEE International Conference on Solid-State Sensors, Actuators and Microsystem*, Beijing, China (2011), pp. 1982–1985
135. A. Adami, R.S. Dahiya, C. Collini, D. Cattin, L. Lorenzelli, POSFET touch sensor with CMOS integrated signal conditioning electronics. Sens. Actuators A, Phys. (2012). doi:10.1016/j.sna.2012.02.046
136. N. Cauna, Nature and functions of the papillary ridges of the digital skin. Anat. Rec. **119**, 449–468 (1954)
137. J. Scheibert, S. Leurent, A. Prevost, G. Debregeas, The role of fingerprints in the coding of tactile information probed with a biomimetic sensor. Science **323**, 1503–1506 (2009)
138. R.S. Dahiya, M. Gori, Probing with and into fingerprints. J. Neurophysiol. **104**, 1–3 (2010)
139. S.R. Forrest, The path to ubiquitous and low-cost organic electronic appliances on plastic. Nature **428**, 911–918 (2004)
140. S. Henning, Reliability of organic field-effect transistors. Adv. Mater. **21**, 3859–3873 (2009)
141. A. Schmitz, P. Maiolino, M. Maggiali, L. Natale, G. Cannata, G. Metta, Methods and technologies for the implementation of large-scale robot tactile sensors. IEEE Trans. Robot. **27**(3), 389–400 (2011)
142. P. Mittendorfer, G. Cheng, Humanoid multimodal tactile-sensing modules. IEEE Trans. Robot. **27**(3), 401–410 (2011)
143. V.L. Lumelsky, M.S. Shur, S. Wagner, Sensitive skin. IEEE Sens. J. **1**(1), 41–51 (2001)
144. R.J. De Souza, K.D. Wise, A very high density bulk micromachined capacitive tactile imager, in *IEEE International Conference on Solid-State Sensors and Actuators (TRANSDUCERS)*, Chicago, USA (1997), pp. 1473–1476

145. M.H. Raibert, An all digital VLSI tactile array sensor, in *IEEE International Conference on Robotics and Automation*, vol. 1 (1984), pp. 314–319
146. K. Suzuki, K. Najafi, K.D. Wise, A 1024-element high-performance silicon tactile imager, in *International Electron Devices Meeting* (1988), pp. 674–677
147. S. Sugiyama, K. Kawahata, M. Yoneda, I. Igarashi, Tactile image detection using a 1 K-element silicon pressure array. Sens. Actuators A, Phys. **A21–A23**, 397–400 (1990)
148. L. Liu, X. Zheng, L. Zhijian, An array tactile sensor with piezoresistive single-crystal silicon diaphragm. Sens. Actuators A, Phys. **32**, 193–196 (1993)
149. Y. Audet, G.H. Chapman, Design of a large area magnetic field sensor array, in *IEEE International Conference on Wafer Scale Integration*, San Francisco, USA (1994), pp. 272–281
150. F. Castelli, An integrated tactile-thermal robot sensor with capacitive tactile array. IEEE Trans. Ind. Appl. **38**(1), 85–90 (2002)
151. G. Hellard, A.R. Russell, A robust, sensitive and economical tactile sensor for robotic manipulator, in *Australian Conference on Robotics and Automation*, Auckland (2002), pp. 100–104
152. Z. Wen, Y. Wu, Z. Zhang, S. Xu, S. Huang, Y. Li, Development of an integrated vacuum microelectronic tactile sensor array. Sens. Actuators A, Phys. **103**, 301–306 (2003)
153. B. Choi, S. Kang, H. Choi, Development of fingertip tactile sensor for detecting normal force and slip, in *International Conference on Control, Automation and Systems*, Gyeong Gi, Korea (2005)
154. R.S. Dahiya, L. Lorenzelli, G. Metta, M. Valle, Development of fingertip tactile sensing chips for humanoid robots, in *IEEE-ISCAS 2010: The IEEE International Symposium on Circuits and Systems*, Paris, France (2010), pp. 1–4
155. J.H. Shan, T. Mei, L. Sun, D.Y. Kong, Z.Y. Zhang, L. Ni, M. Meng, J.R. Chu, The design and fabrication of a flexible three-dimensional force sensor skin, in *IEEE/RSJ International Conference on Intelligent Robots and Systems* (2005), pp. 1818–1823
156. J.-H. Kim, W.-C. Choi, H.-J. Kwon, Development of tactile sensor with functions of contact force and thermal sensing for attachment to intelligent robot finger tip, in *IEEE Sensors*, Daegu, Korea (2006), pp. 1468–1472

Part II
Integrated Tactile Sensing

This part of the book comprises of three chapters i.e. Chaps. 6–8 and Appendices A–C, which all together present a detailed discussion on the work toward integration of tactile sensing systems on chip. In particular, various stages of development of POSFET devices based tactile sensing chips are presented in Chaps. 6–8. Part II begins with a discussion on using microelectrode arrays, with piezoelectric polymers, as the extended gate tactile sensors. This is followed by the detailed discussion on the novel POSFET (Piezoelectric Oxide Semiconductor Field Effect Transistor) tactile sensing devices. The POSFET approach does away with the extended gates by having piezoelectric polymers on the gate area itself. The technological advances, challenges and the fabrication of POSFETs have been discussed in detail. Chapter 8 of the book, presents the extension of POSFETs devices toward tactile sensing arrays and chips with on-chip electronics. The further advances in the area, including current research, are also described briefly. The three appendices at the end of this part present detailed discussion on the theory of piezoelectric polymers as sensors, electrical model of piezoelectric polymers and the electronics needed to acquire the response of piezoelectric materials based sensors.

Chapter 6
Integrated Tactile Sensing on Silicon

Abstract Using semiconductor devices as sensor enables true system integration as the integration of sensor and electronics begins right from the transducer level. This concept is presented in this chapter and also followed in next two chapters. The work presented in this chapter, focuses on the development of high resolution tactile sensing arrays for the fingertips of a robot. Considering constraints like limited space on the robot fingers ($\sim$1 cm $\times$ 1 cm), miniaturization is a plausible way of accommodating a large number of sensors and the same has been adopted in the work described in this chapter. Development of high resolution tactile sensing chips and the experimental results from their first phase of development are presented in this chapter. In the first phase, 32 elements microelectrode (MEA) array, epoxy-adhered with thin piezoelectric polymer films, is used as the tactile sensing array. The "smart materials" like PVDF and P(VDF-TrFE) are used as transducer on the MEA. Each microelectrode can act as extended gate, when connected to the gate terminal of the FET devices (external to the chip).

Keywords High resolution tactile sensing · Tactile sensing array · Artificial skin · Sensor integration · Multifunctional · Wiring complexity · Integrated systems · FET · Extended gate · Microelectrode array · PVDF · PVDF-TrFE · Piezoelectric polymers · Microfabrication

6.1 Introduction and Historical Perspective

In general, the sensor integration means the physical presence of sensors or sensor arrays and the signal processing elements on the same substrate. The sensor arrays in an integrated system may consist of: (a) sensors with same or similar function; (b) multiple sensors with each sensor having a different function; and (c) multifunctional sensors with each sensor capable of measuring multiple parameters. To this end, an interesting development has been the use of semiconductor devices or their variants as the sensors. As an example, Field Effect Transistors (FET) has been used as stress sensors. The FETs can be made to possess inherent sensing capability by modifying their structures and integrating the transducer materials. The sensitive or transducer layers may be made of insulating, semiconducting, or conductive materials. A general principle behind working of FET devices based sensors is that

R.S. Dahiya, M. Valle, *Robotic Tactile Sensing*,
DOI 10.1007/978-94-007-0579-1_6,

the semiconductor surface potential is modulated by the electric charge or potential variations elsewhere in the structure (usually at gate, where sensitive layer is present). The sensing effect of the semiconductor device based sensors changes their most important characteristic and/or parameter, for example, altering the threshold voltage of the MOSFET, and the channel current etc. The basic idea to measure the controlling parameter to be sensed (by the characteristic shifts of a device) can also be realized by using other types of semiconductor devices, e.g., diodes. For instance, a pn-junction can be applied to a temperature or photo-semiconductor devices as sensors. A similar effect can be used in chemical sensors. For instance, metal semiconductor diodes, the so-called Schottky barrier devices, built from n-GaAs and discontinuous platinum films, can be used as detectors of different gases over a wide range of temperatures [1].

Using semiconductor devices as sensor enables true system integration as the integration of sensor and electronics begins right from the transducer level. This concept is adopted in the work presented in following three chapters. Incorporating semiconductor devices as sensors within an integrated sensing systems is also advantageous due to easier fabrication and improved performance.

From historical perspective, the development of semiconductor devices with inherent sensing capability goes back to late 1960's i.e. immediately after the introduction of standard silicon planar technology for developing integrated circuits. Around that time, Gieles [2] first presented the miniature pressure sensor, Bergveld [3] first showed that an ISFET could measure pH in ionic solutions, Van Putten and Middelhoek [4] demonstrated that silicon could be used for an anemometer and Lundström et al. [5] showed that a MOSFET with a Pd gate could detect hydrogen. Inspired by the novel ideas, initial successes and the promise of low cost, small size and a short development time, many laboratories around the world started researching semiconductor device sensing and a deluge of novel semiconductor device sensors followed. The field of tactile or touch sensing too benefited from this approach and early touch sensors based on semiconducting devices were reported by Raibert and Tanner [6] and Polla et al. [7]. Initially started with silicon based semiconductor devices, the approach nowadays also includes both organic and inorganic semiconducting materials based devices. Few such sensing devices are described in Chap. 5 and more can be found in large number of research papers and books available on silicon sensors or semiconductor sensors.

For a variety of reasons it is desirable to have tactile sensing arrays, or a group of tactile sensors distributed across robot's body. The density and spatial distribution of tactile sensing elements or 'taxels' may vary across robot's body, as in humans (see Chap. 3). In this context, the tactile sensors are roughly divided in two classes (see Chap. 2): First, the sensors at body sites like fingertips, where high density (large number of taxels in a small space), fast response and good spatial resolution ($\sim$1 mm) are needed; and second, at body sites like palm, belly etc., where the requirements of high density and spatial resolution can be relaxed. The work presented in this and following chapters, focuses on the development of high resolution tactile sensing arrays for the fingertips of a robot. Considering constraints like limited space on the robot fingers ($\sim$1 cm $\times$ 1 cm), miniaturization is a plausible way

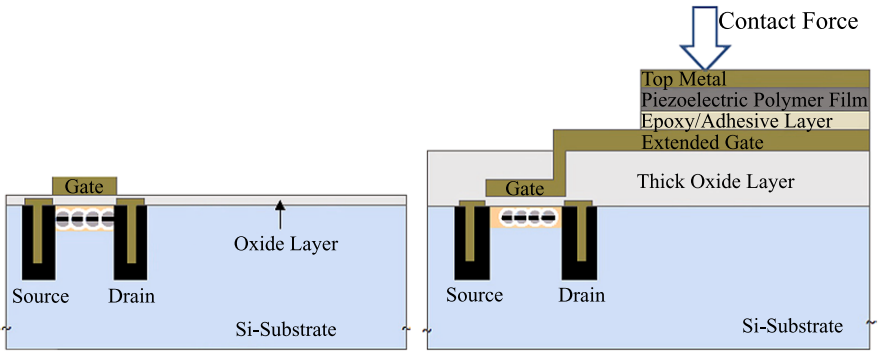

Fig. 6.1 Comparison of an extended gate tactile sensing device (*right*) with conventional field effect transistor (*left*). In the case when piezoelectric polymer is spin coated, the epoxy/adhesive layer on extended gate (*right*) will not be present

of accommodating a large number of sensors and the same has been adopted in the work described in this chapter. Following sections describe the development of high resolution tactile sensing chips and the experimental results from their first phase of development [8, 9]. In the first phase, 32 elements microelectrode (MEA) array, epoxy-adhered with thin piezoelectric polymer films, is used as the tactile sensing array. The "smart materials" like PVDF and P(VDF-TrFE) are used as transducer on the MEA. Each microelectrode can act as extended gate, when connected to the gate terminal of the FET devices (external to the chip). As discussed in Chap. 5, the extended gate approach brings the sensor and conditioning electronics closer and hence the overall response is better than that of conventional approach, where the sensor and conditioning electronics are placed at apart.

6.2 Extended Gate Based Tactile Sensing Arrays

6.2.1 The Concept and Working

Figure 6.1 shows the cross section of a conventional metal-oxide-semiconductor FET (MOSFET) device, as well as the structure of an extended gate FET based touch sensor. The thin insulating layer (oxide layer) and the covering (metalization and/or sensing) layer comprise the gate or extended gate, which mainly controls the action of the transistor. In the conventional transistors, a controlling gate voltage is applied to the gate and, depending on the type of transistor (n-type of p-type), a negative/positive charge is first induced at the silicon surface, and electrons are attracted toward or repelled away from this region. At the point, called the turn-on (or threshold) voltage the charge carrier electrons or holes are induced at the surface and the transistor channel starts to conduct between the source and drain. In the most simple version, (i.e. n-channel MOSFET), a p-type silicon substrate (bulk) contains

two n-type diffusion regions (source and drain). The structure is covered with a silicon dioxide insulating layer on top of which a metal gate electrode is deposited. When a positive voltage (with respect to the silicon) is applied to the gate electrode, electrons (which are the minority carriers in the substrate) are attracted to the surface of the semiconductor. Consequently, a conducting channel is created between the source and the drain, near the silicon dioxide interface. The conductivity of the channel can be modulated by adjusting the strength of electrical field between the gate electrode and the silicon, perpendicular to the substrate surface. At the same time a voltage can be applied between the drain and the source (V_{ds}), which results in a drain current (I_d) between the n-regions. In the extended gate FET devices, the sensitive layer (e.g. piezoelectric polymer) produces the controlling potential that is a function of the quantity to be measured and can be detected as variation in the channel current.

A piezoelectric film working in the sensing mode generates a charge/voltage when mechanical force/stress is applied. This charge/voltage is proportional to the applied force/stress [10, 11] and they are related as:

$$D_3 = d_{33} \times T_3 + \varepsilon_{33} \times E_3 \tag{6.1}$$

where, Q_t is the charge developed on a taxel due to applied force, F and d_{33} is the piezoelectric constant. Details on the working of piezoelectric materials as sensors are given in Appendix A of this book. By connecting the piezoelectric polymer to the gate terminal of FET devices (Fig. 6.1) or by depositing the piezoelectric polymer directly on the gate area of FET devices (Chap. 7), such a charge/voltage of the piezoelectric polymer can be used to modulate the charge in the induced channel of FET, which is then amplified by the FET and further processed by an electronic circuitry. A somewhat similar approach was used by Swartz et al. [12] for the development of ultrasonic sensors and by Kolesar et al. [13] for the tactile sensors. In both cases, the extended gate FET devices epoxy-adhered with PVDF film were used. In present work, the P(VDF-TrFE) polymer films are used, for the reasons better explained in the next chapter. In brief, PVDF-TrFE is preferred over PVDF as it is easy to manufacture these polymer, they are less lossy and have comparable piezoelectric constant—thus, generate more or less the same charge/voltage output for a same force input.

Based on Fig. 6.1, the equivalent model of the extended gate sensing device, assuming that transistor is used in a common source configuration, is given in Fig. 6.2. It can be noticed that both epoxy, used as adhesive to deposit the polymer film on extended gate [12, 13], and oxide under the extended gate introduces additional capacitances in the equivalent circuit. Keeping in view the presence of these additional capacitances, the ratio of voltage available at gate terminal and the stimulus generated voltage at polymer, can be written as:

$$\frac{V_g}{V_{polymer}} = \frac{C_{polymer}}{C_{polymer} + (C_{polymer}/C_{adhesive} + 1)[C_{gs} + C_{sub} + C_{gd}(1 + A_v)]} \tag{6.2}$$

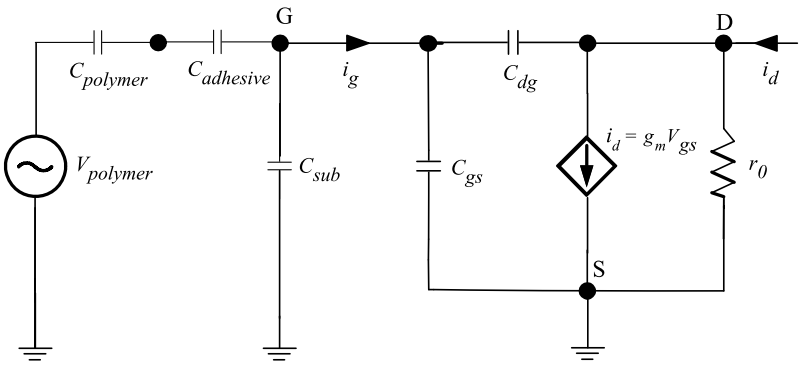

Fig. 6.2 Small Signal equivalent circuit of extended gate device shown in Fig. 6.1. Here, piezoelectric polymer is represented by its approximate equivalent model

where, A_v is the voltage amplification (i.e. intrinsic gain) of the transistor and other terms are clear from Fig. 6.2. It is evident from Eq. (6.2) that a large substrate capacitance, C_{sub}, together with the capacitance of epoxy, $C_{adhesive}$, attenuates the voltage at the gate terminal. The effect is significant, if the substrate capacitance is much larger than that of polymer capacitance, $C_{polymer}$.

6.2.2 MEA Based Tactile Sensing Arrays

As a first step toward realizing the tactile sensing system, two dimensional, 32 taxel, MEAs based test arrays were designed and fabricated. The MEAs are implemented on a fuse silica quartz substrate with a Al:Si 1%/Ti/TiN (410/30/140 nm thick respectively) low resistance multilayer for both microelectrodes and electrical connections. The TiN top-layer guarantees a low contact resistance to the final Au/Cr (5/150 nm) seed-layer. The metal wires passivation has been guaranteed by a SiO_2/Si_3N_4 (20/210 nm) layer deposited by PECVD. The chosen thicknesses restrict the substrate capacitance to low values, which enables the maximum availability of the voltage produced by polymer at the gate terminal. Here, quartz wafer is used instead of silicon to minimize the cross talk. The fabrication steps for MEA based tactile sensing arrays are described in Fig. 6.3 and the fabrication steps related to the deposition of piezoelectric polymer films are given in Table 6.1 The overall size of MEA chip is 1 cm $\times$ 1 cm and each taxel on the chip has a diameter of 500 μm. To get a spatial resolution comparable to that of human tactile sensing ($\sim$1 mm), the center to center distance between the taxels was kept as 1 mm. The fabricated MEA test chip and enlarged view of one of the taxels are shown in Fig. 6.4. As mentioned earlier, each sensing element on the MEA test chip can be used as an extended gate of FET devices, which are external to the chip.

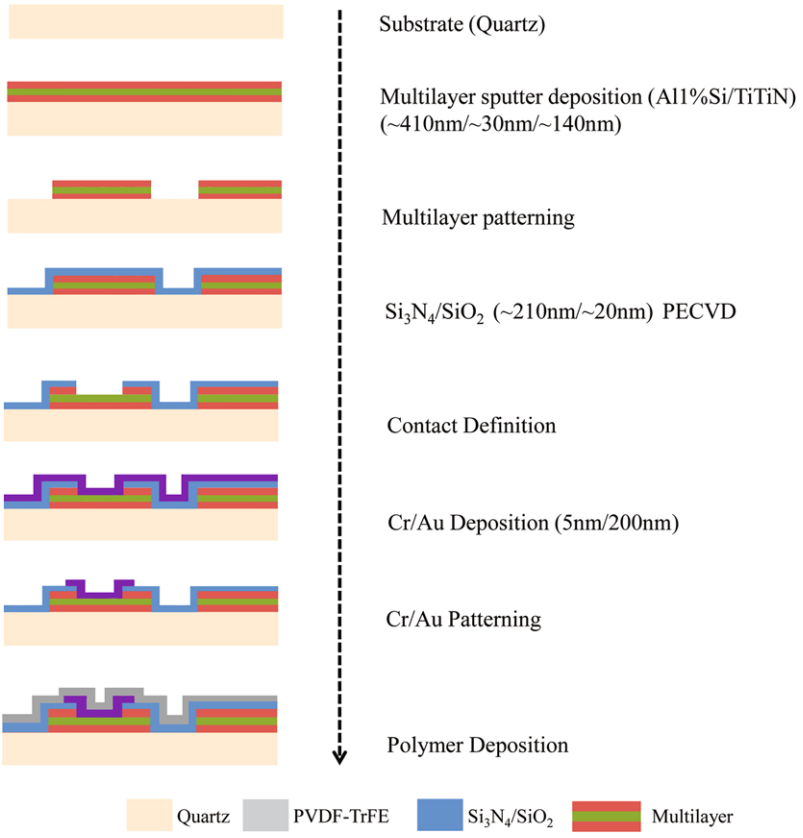

Fig. 6.3 Fabrication process of MEA based tactile sensing arrays

Table 6.1 Preparation and deposition of P(VDF-TrFE) film on MEA [8]

a	PVDF-TrFE films of 7×7 mm^2 area and 25, 50 and 100 μm thicknesses, metalized from both sides (supplied by Piezotech) were deposited on a glass slide using epoxy adhesive. Another glass slide was kept on top of the polymer and this arrangement was kept in vacuum for one hour. Then the arrangement was heated at 65 degree for 30 minutes. Then the polymer film was peeled off from the glass slide to remove the metal layer from one side of the polymer.
b	The unmetalized side of the film, obtained in step (a), was deposited on MEA using epoxy adhesive, covering all 32 taxels. The film was covered with glass slide and the arrangement was again kept under vacuum to remove air between polymer and MEA and to ensure uniform thickness of the adhesive. For better adhesion the arrangement was kept at 65 degrees for thirty minutes.

The MEA test chips were epoxy-adhered with one side metalized piezoelectric polymer (70:30, P(VDF-TrFE)) thin films of 25 μm, 50 μm and 100 μm (different thickness for testing purpose only). The front and backsides of a MEA test chip

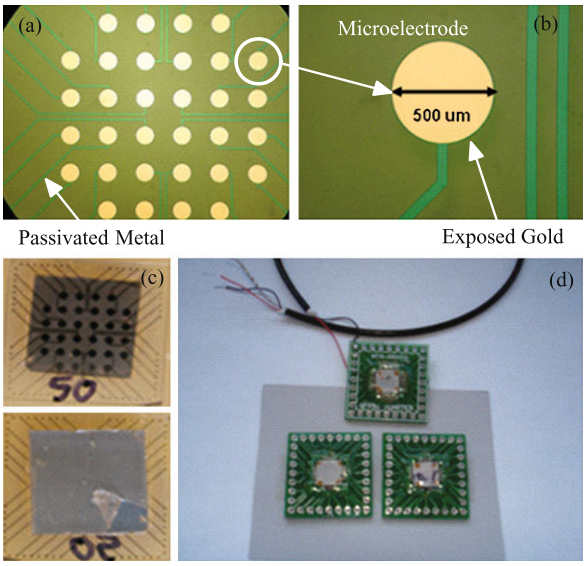

Fig. 6.4 (**a**) MEA after fabrication; (**b**) Enlarged view of a microelectrode; (**c**) Front and backsides of the MEA based tactile sensing array; (**d**) Packaged MEA based tactile sensing arrays

with a 50 μm polymer film and the chip on package are shown in Fig. 6.4(b). On the package, only 28 terminals (out of 32) are gold bonded to the pads of MEA as all corners are gold bonded to the upper metal layer of the piezoelectric polymer film. Thus, corners of the package serve as one of the terminals for reading the charge/voltage developed due to applied force.

6.3 Experiment Set up

6.3.1 Mechanical Arrangement

The experimental set up developed for testing the tactile sensing chips is shown in Fig. 6.5. This set up can be used to test the tactile sensing chip for the applied forces and to study the response of polymer to ambient temperature variations. The TIRA shaker (Model-TV50018) on the set up can apply random dynamic forces up to 18 N with frequency in the range 2 Hz–18 kHz. The shaker can be fixed at any angle θ ($0 < \theta < 90°$) by adjusting turnbuckles and hence the direction of applied forces can also be changed. The force generated by the shaker is measured by piezoelectric load cell (Model-208C01, from PCB Piezotronics) which is fixed on a platform that can move along the z-axis. The load cell has a sensitivity of 112.41 mV/kN and the measurement range of 0.04448 kN (both in compression and tension). Special probes are needed to apply force on a single taxel at a time or on many taxels simultaneously. To ensure that the whole taxel is pressed during testing, the diameter of the probes should be slightly more than that of the taxel.

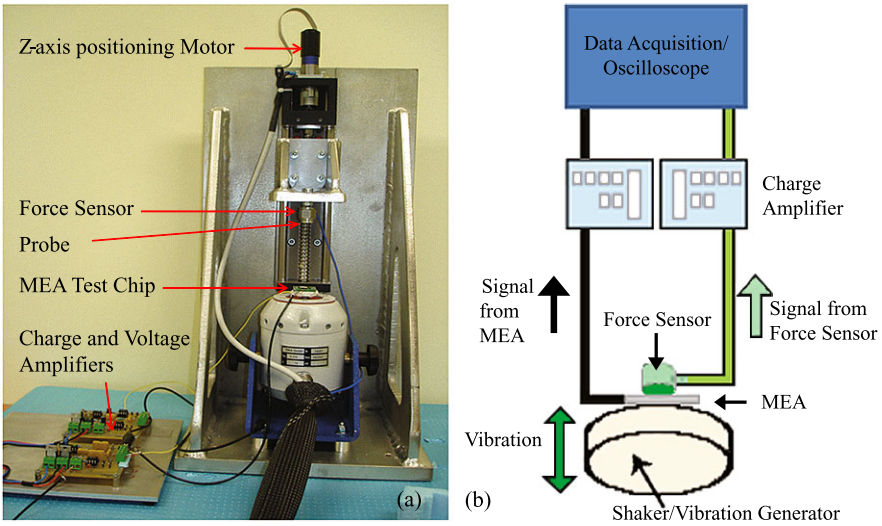

Fig. 6.5 The experiment set up developed for characterizing the tactile sensing arrays

The probes are attached to the load cell with a screw. With a manual x-y positioning system the probe is aligned with the taxel under observation. The MEA test chip can be placed on the shaker, as shown in Fig. 6.5 and then the load cell is brought in contact with it using the z-axis positioning motor. The vibration generator/shaker, piezoelectric load cell and the z-axis positioning motor and the output of taxel are all measured and controlled with LABVIEW through NI-DAQ device (PCI-6221) which can acquire and control the data from 16 analog outputs, 24 digital I/O and 2 analog inputs.

6.3.2 Electrical Arrangement

To measure the output of the taxels on the MEA test chip, both, charge and voltage amplifiers were designed on two separate PCBs. Both charge and voltage amplifiers were designed for a frequency range of 2 Hz–18 kHz. Voltage amplifier is designed to have a gain of 46 db and the gain of charge amplifier depends on the capacitance of polymer sample under test. The advantages of the charge amplifier arrangement are independence of its output from the cable capacitances and the minimization of the charge leakage through the stray capacitance around the sensor. The arrangement of the charge amplifier and an approximate equivalent model of a taxel are shown in Fig. 6.6. The complete electrical equivalent model of piezoelectric polymers is given in Appendix B and the design of charge amplifier and voltage amplifiers is described in Appendix C of this book.

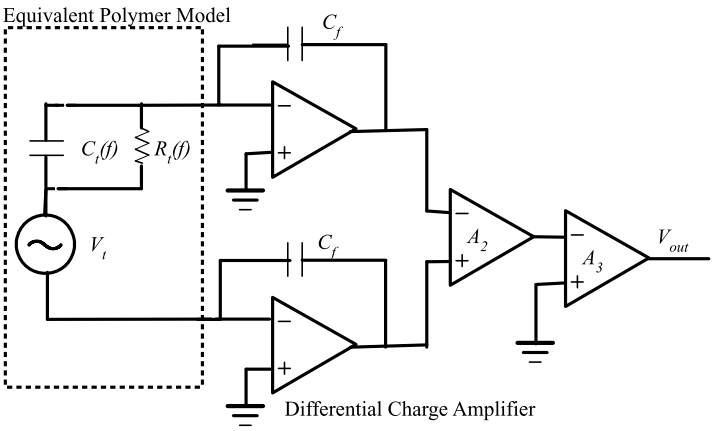

Fig. 6.6 Approximate equivalent model of a touch element (inside the *dotted box*) with charge amplifier

6.4 Experimental Results

After packaging the MEA based tactile sensing chips (with 25 μm, 50 μm polymer films), their performance was evaluated for both variable force-constant frequency and constant force-variable frequency configurations—under ambient conditions. In the variable force-constant frequency mode, a normal force in the range of 0.02–4 N (∼2–400 gmf) and at a frequency of 15 Hz was applied on the taxels. To prevent the chip from getting damaged, the upper limit of force was kept as 4 N, during testing. In these experiments the taxels were preloaded to avoid any loss of contact with the force sensor. Since piezoelectric polymers do not respond to static stimuli, the prestressed force does not contribute to the output of a taxel. The approximate expression of output voltage at the terminals of each taxel, V_t and at the output terminals of charge amplifier, V_{out} are respectively given by:

$$V_t \approx \frac{d_{33} \times F \times A_t}{C_t(f) \times A_p} \tag{6.3}$$

$$V_{out} \approx \frac{2 \times C_t(f) \times A_2 \times A_3 \times V_t}{C_f} \tag{6.4}$$

$$\frac{V_{out}}{F} \approx \frac{2 \times d_{33} \times A_2 \times A_3 \times A_t}{C_f \times A_p} \tag{6.5}$$

where, A_t is the area of each taxel; A_p is the area of probe (or the area on which force is applied); $C_t(f)$ is the capacitance of polymer on each taxel; C_f is the capacitance in the feedback path of first stage of amplifier and A_2, A_3 are the gains of second and third stage of the amplifier respectively. From (6.5), it can be noticed that at a particular frequency, the voltage output of a taxel is linearly dependent on

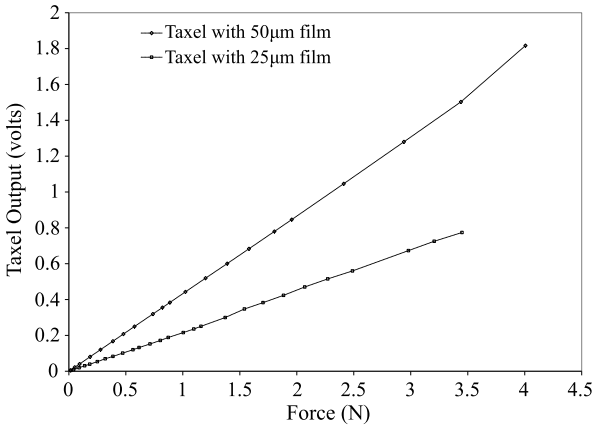

Fig. 6.7 Average maximum of sinusoidal taxel output versus maximum value of 15 Hz sinusoidal input force

the input force. The plots between taxel output and the force input in Fig. 6.7 also follow this trend over the tested range of forces. These plots relate average of the maximum values of sinusoidal outputs from three taxels, with corresponding maximum values of the applied sinusoidal forces. The response of each of the three taxels tested in this case was within $\approx 6\%$ of the average output shown in Fig. 6.7. The variation among outputs of different taxel could be due to the non-uniform thickness of polymer or due to slight misalignment of probe and taxel. Among others, the uniform deposition of a thin polymer film is a challenging task for the tactile sensing arrays presented here. The relatively low melting point ($T_m \approx 150°C$) of P(VDF-TrFE), places a tight constraint on chip packaging, post-processing and assembly conditions.

The response of taxels on both chips with 50 μm and 25 μm thick polymer films was further investigated for "cross-talk", as the spatial resolution also depends on it. Higher the cross talk, poorer is the spatial resolution. To investigate cross talk, the force was applied on a particular taxel and the voltage output from the adjacent taxels was observed. Figure 6.8 shows the normalized output of various taxels, with respect to the output of the particular taxel (say, taxel no. 1) at the center of chip, on which force is applied. With the taxel outputs noted in this way, the crosstalk in both the chips was observed to be approximately 20%. Although the taxels are independent entities under the polymer film (MEA side of the film); they are all connected by a uniform thin metal film on the top. In other words, taxels are still mechanically connected, which could be the reason higher cross talk. The parasitic capacitance between adjacent elements also contributes to cross-talk. The problem of cross-talk can be reduced by patterning the metal layer on the top side of polymer film and thus reducing the taxels dependence on each other.

In the constant force-variable frequency mode, the chip was evaluated in the frequency range of 2 Hz–5 kHz for three different forces, viz: 0.2 N, 0.5 N and 1 N. The gain ($= V_{out}/F$) and phase plots are shown in Fig. 6.9. Using the actual values of $A_2 = 5$, $A_3 = 4$, $d_{33} = 24 \times 10^{-12}$ (at 1 kHz), $A_t = 0.196 \times 10^{-6}$ m^2, and $A_p = 0.78 \times 10^{-6}$ m^2, and $C_f = 820$ pF in (6.5), the gain in db (at 1 kHz)

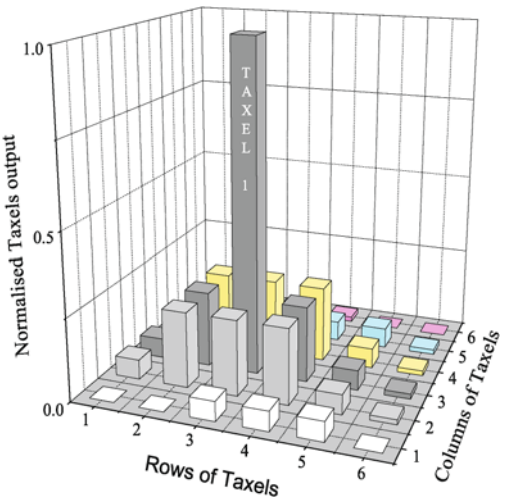

Fig. 6.8 Normalized output of various taxels on the array with respect to the output of taxel (marked as '*Taxel 1*') on which force is applied. Normalized valued were obtained by dividing output of various taxels with that marked as '*Taxel 1*'

is −16.5, which closely matches with the experimental values shown in Fig. 6.9. It can be noticed that the gain has a drooping characteristic over the entire range of frequency for which the chip was evaluated. It is a general practice to use a constant value of the piezoelectric polymer capacitance (at 1 kHz). But, in case of piezoelectric polymers this is not true, as can be seen from Fig. 6.10, where the capacitance, $C_t(f)$ and resistance, $R_t(f)$ of a taxel are plotted against the frequency. These values of $C_t(f)$ and $R_t(f)$ are measured with an impedance analyzer. In addition, the value of piezoelectric constant also depends on the frequency. Thus, the drooping gain characteristic can be attributed to the frequency dependent constants. The phase plot shows more or less a constant value of phase over the above said frequency range. The lower cut off frequency is not seen in these plots, because the charge amplifier was designed to have a lower cut-off frequency less than 2 Hz. In Fig. 6.9, the values of gain and phase deviate significantly from the general trend at

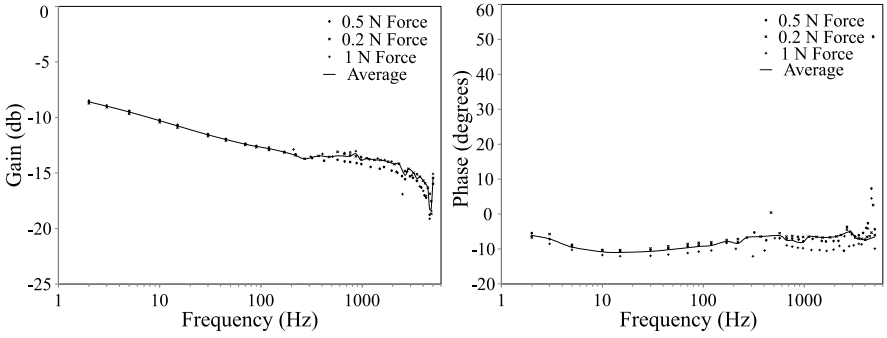

Fig. 6.9 Gain (*left*) and phase (*right*) plots of MEA with 50 μm polymer film at three different applied forces, viz: 0.2 N, 0.5 N and 1 N. *Solid line* corresponds to the average values of the three forces

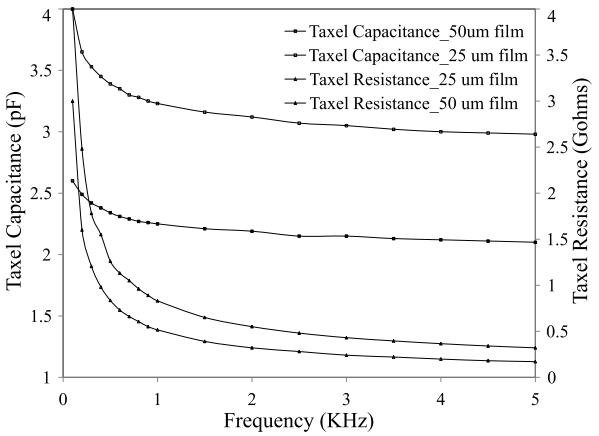

Fig. 6.10 Variation of the capacitance, C_t and resistance, R_t of taxels with frequency

around 500 Hz, 2600 Hz and 4800 Hz. This is due to mechanical resonance of the shaker at these points. These points are neglected in the average values calculations.

The performance of the chips was further evaluated for their ability to differentiate objects on the basis of hardness. For this purpose probes with 1 mm diameter were made from brass (density ~8500 kg/m^3), polycarbonate plastic (density ~1200 kg/m^3) and wood (density ~500 kg/m^3) and the outputs of a taxels were noted by applying the same force in the three conditions. The observed outputs from taxels with both 50 μm and 25 μm thick polymer films are shown in Fig. 6.11. The outputs of taxels from both chips were noted by applying forces of 0.2 N and 0.4 N at frequencies between 5–70 Hz. Higher forces were avoided to prevent the damage of the probe, especially the one made of wood. With the exception at 5 Hz in the case of taxel with 50 μm film, the output with brass probe is higher than that from polycarbonate plastic and wooden probe. In the case of taxel with 25 μm film, the difference between outputs from brass probe and polycarbonate plastic/wooden probe is higher than that of taxel with 50 μm film. The difference between outputs obtained from wooden probe and polycarbonate plastic probe is not high due to

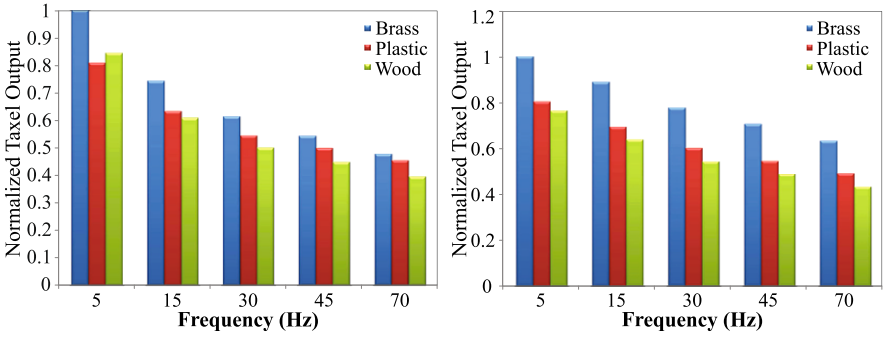

Fig. 6.11 Output voltage of the taxel from MEA with 50 μm film (*left*) and 25 μm film (*right*) when it is pressed by probes made of brass, plastic and wood

small difference between their densities. The object identification based on hardness is more distinct at frequencies (approx 24 MHz and 48 MHz for 50 μm and 25 μm polymer films) close to the resonant frequency of the polymer film [14]. The data from this study has also been used to investigate the utility of computational intelligent tools in tactile data classification of contact materials [15].

6.5 Summary

The tactile sensing arrays using microelectrodes arrays have good spatio-temporal resolution and the taxel have a linear response over a wide range of dynamic forces. The presence of piezoelectric polymer film as a transducer helps in improving the speed of response and the marriage of transducer and electronics, as suggested in this and following chapter, can improve the overall performance. Besides these, the approach can potentially reduce the wiring complexity—which is a key robotics problem. The capability of segregating the objects on the basis of their hardness has also been demonstrated. Such features are important for robotic applications, especially when exploring the objects. From sensor point of view the capability to detect multiple parameters is always an added advantage. The MEA based tactile sensor arrays, as a precursor to the POSFET based tactile sensing array presented in the following chapter, provide a positive feasibility study for manufacturing POSFET devices and the promising results strengthen the case for POSFET based tactile sensing arrays.

References

1. L.M. Lechuga, A. Calle, D. Golmayo, F. Briones, J. De Abajo, J.G. De La Campa, Ammonia sensitivity of Pt/GaAs Schottky barrier diodes—improvement of the sensor with an organic layer. Sens. Actuators B, Chem. **8**(3), 249–252 (1992)
2. A. Gieles, Subminiature silicon pressure transducer, in *IEEE International Solid-State Circuits Conference*, vol. XII (1969), pp. 108–109
3. P. Bergveld, Development of an ion sensitive solid-state device for neurophysiological measurements. IEEE Trans. Biomed. Eng. **17**, 70–71 (1970)
4. A.F.P. van Putten, S. Middelhoek, Integrated silicon anemometer. Electron. Lett. **10**, 425–426 (1974)
5. I. Lundström, S. Shivaraman, C. Svensson, L. Lundkvist, Hydrogen sensitive MOS field-effect transistor. Appl. Phys. Lett. **26**, 55–57 (1975)
6. M.H. Raibert, J.E. Tanner, Design and implementation of a VLSI tactile sensing computer. Int. J. Robot. Res. **1**, 3–18 (1982)
7. D.L. Polla, W.T. Chang, R.S. Muller, R.M. White, Integrated zinc oxide-on-silicon tactile-sensor array, in *International Electron Devices Meeting* (1985), pp. 133–136
8. R.S. Dahiya, M. Valle, G. Metta, L. Lorenzelli, C. Collini, Tactile sensor arrays for humanoid robot, in *IEEE PRIME'07: The 3rd International Conference on Ph.D. Research in Microelectronics and Electronics*, Bordeaux, France (2007), pp. 201–204
9. R.S. Dahiya, M. Valle, G. Metta, Development of fingertip tactile sensing chips for humanoid robots, in *5th IEEE International Conference on Mechatronics*, Malaga, Spain (2009), pp. 1–6

10. H.S. Nalwa, *Ferroelectric Polymers: Chemistry, Physics, and Applications* (Marcel Dekker, Inc., New York, 1995)
11. R.S. Dahiya, M. Valle, L. Lorenzelli, SPICE model of lossy piezoelectric polymers. IEEE Trans. Ultrason. Ferroelectr. Freq. Control **56**(2), 387–396 (2009)
12. R.G. Swartz, J.D. Plummer, Integrated silicon-PVF2 acoustic transducer arrays. IEEE Trans. Electron Devices **26**(12), 1920–1932 (1979)
13. E.S. Kolesar, C.S. Dyson, Object imaging with a piezoelectric robotic tactile sensor. J. Microelectromech. Syst. **4**(2), 87–96 (1995)
14. R.S. Dahiya, M. Valle, G. Metta, L. Lorenzelli, POSFET based tactile sensor arrays, in *IEEE ICECS'07: The 14th International Conference on Electronics, Circuits and Systems*, Marrakech, Morocco (2007), pp. 1075–1078
15. S. Decherchi, P. Gastaldo, R.S. Dahiya, M. Valle, R. Zunino, Tactile-data classification of contact materials using computational intelligence. IEEE Trans. Robot. **27**, 635–639 (2011)

Chapter 7
POSFET I—The Touch Sensing Device

Abstract This chapter presents POSFET devices that can detect contact parameters such as dynamic contact forces and/or temperature variations. Unlike the conventional arrangements where transducer and electronics are separate entities, a POSFET is an "integral sensing unit" comprising of transducer, i.e. P(VDF-TrFE) piezoelectric polymer film, and the electronic unit, i.e. MOS transistor. These novel and integral sensing units are obtained by depositing a P(VDF-TrFE) piezoelectric polymer film on the gate area of MOSFET devices. Accordingly they are termed as POSFET (Piezoelectric-Oxide-Semiconductor-Field-Effect-Transistors) touch sensing devices or simply POSFETs. These devices differ from the extended gates based sensors, discussed in the previous chapter, in terms of the location of piezoelectric material vis-a-vis MOS device. Such difference are described later in this chapter. The structure, working principle, fabrication process, and the experimental evaluation of the POSFETs are presented in following sections.

Keywords POSFET · Tactile sensing device · Artificial skin · Sensor integration · Multifunctional · Wiring complexity · Integrated systems · FET · Extended gate · MOS · PVDF · PVDF-TrFE · Piezoelectric polymers · Microfabrication · Miniaturization · Modeling and simulation

7.1 The Structure and Working of POSFETs

The structure of a POSFET device is shown in Fig. 7.1. The two n-type regions diffused into the p-type silicon wafer (or in the p-well of a n-type wafer) form the source and drain diffusions of the MOS transistor. The P(VDF-TrFE) piezoelectric polymer film is present over the gate area of the MOS device. The transduction material, i.e. P(VDF-TrFE), is thus an integral part of the device and therefore the resulting structure is called Piezoelectric-Oxide-Semiconductor-Field-Effect-Transistor or "POSFET". The lower electrode of the P(VDF-TrFE) layer, over the insulating SiO_2 layer, constitutes the gate of the MOSFET. When a POSFET is employed to detect contact events, this lower metal or the gate can be used for biasing the MOSFET or it may be left unconnected in case of a floating gate operation. Another metal electrode is present over the P(VDF-TrFE) layer, as can be seen from Fig. 7.1. During poling this top metal layer can serve as one of the electrodes for applying

R.S. Dahiya, M. Valle, *Robotic Tactile Sensing*,
DOI 10.1007/978-94-007-0579-1_7,

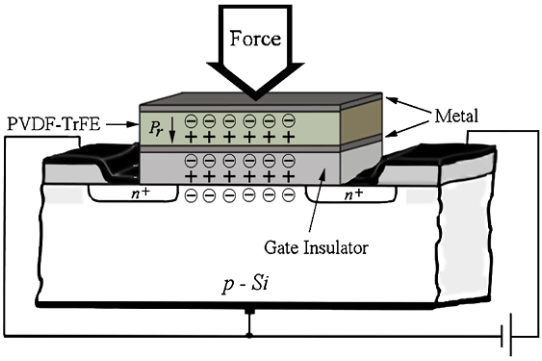

Fig. 7.1 The structure of a POSFET touch sensing device

the polarizing voltage. Poling, described later, is an important step needed to orient dipoles in the piezoelectric polymer along a particular direction—along thickness in case of POSFETs. When POSFET is employed as a touch sensor, this top metal can be connected to electrical ground or to a fixed voltage to minimize the stray noise.

The structure of a POSFET is similar to that of Metal-Ferroelectric-Metal-Insulator-Semiconductor (MFMIS) type FeRAM (Ferroelectric Random Access Memory) devices [1] that are used for memory applications. However, working of POSFETs is fundamentally different from that of FeRAMs—as former respond to changes in mechanical stimulus and the output in latter results from electric field switching. Further, the typical thickness (100–200 nm) of ferroelectric material (PZT, PVDF polymer etc.) layer in FeRAM devices is an order of magnitude lower than that used in POSFETs [1]. Using thicker polymer films in POSFETs, however, brings up new challenges that are discussed in subsequent sections of this chapter.

For piezoelectric polymers working in the thickness mode (i.e. when both stress and electric field are along the 3-direction or along thickness, as in Fig. 7.1) the electric displacement or polarization D_3 is related to the mechanical stress T_3 and the electric field E_3 as [2, 3]:

$$D_3 = d_{33} T_3 + \varepsilon_{33} E_3 \tag{7.1}$$

where, d_{33} and ε_{33} are the piezoelectric and dielectric constants respectively. Depending on the choice of independent variables, the electromechanical response of Eq. (7.1) can also be expressed in three other forms. For such details, as well as for a quick insight in to the working piezoelectric materials for sensing and actuating applications, reader may refer to Appendix A. Following Eq. (7.1), the electric displacement or polarization can be controlled either by varying the electric field E_3 and/or by the mechanical stress T_3 (or the contact force). While former is used in FeRAM to switch the polarization state, latter is used in the POSFETs to modulate the charge in the induced channel of underlying MOS device [4].

The working of a POSFET device can be explained by how the charges appear on the surface of P(VDF-TrFE) and how they are subsequently reflected in the induced channel of the MOS device. The remanent polarization (P_r) of the polarized polymer and the principle of charge neutrality lead to the appearance of fixed

charges $\pm Q$ on the surface of piezoelectric polymer, as shown in Fig. 7.1. The additional variation in contact force or the variation in temperature experienced by the POSFET, when it comes in contact with an object, further changes the polarization level as per Eq. (7.1). This results in generation of more charges that are subsequently reflected in the induced channel and modulate the channel current. Thus, the (contact) force or the temperature variation is directly reflected as variation in the channel current of POSFET devices—which can be further processed by an electronic circuitry that may also be integrated on the same chip.

Unlike MOSFETs, where the gate voltage controls the current in the induced channel, the piezoelectric or pyroelectric property of P(VDF-TrFE) modulates the channel current. In this sense, a POSFET can also be referred as POSPET or Piezoelectric-Oxide-Semiconductor-Piezoelectric-Effect-Transistor. It should be noted that silicon based devices are also known to exhibit piezoresistive effect, i.e. change in resistivity when stressed. This raises an important question about the source of the change in channel current—piezoelectric action of P(VDF-TrFE) polymer layer present on the gate area or the piezoresistive behavior of silicon? In practice, both piezoelectric and piezoresistive effects contribute. However, as discussed later in the experimental section, in case of POSFETs the change in the channel current, and hence the output, is primarily because of the piezoelectric action of the P(VDF-TrFE) polymer layer.

7.2 Choice of Piezoelectric Material

The material selection is an important part of a "smart material" integrated system such as POSFET. In previous section it is mentioned that the piezoelectric layer in POSFETs comprises of P(VDF-TrFE) polymer. This section explains why P(VDF-TrFE) polymer is particularly suitable for POSFET like sensing device.

Selecting a suitable material involves considerations of such factors as the frequency bandwidth, temperature sensitivity, stiffness, spatial resolution and maximum achievable strain. Traditionally, piezoelectric ceramics such as lead zirconate titanate (PZT) and barium titanate ($BaTiO_3$) have been preferred for many applications due to their dielectric strength and stable electromechanical properties at high temperatures up to 400°C. However, the potentials of piezoelectric ceramics are limited because these materials are brittle, somewhat heavy, and are difficult to scale to larger applications. In this regard piezoelectric polymers offer definite advantages because they are light, flexible, easy to shape, and can be bonded to almost any surface. Piezoelectric polymers can be easily integrated in structural design as active elements that can sense and respond intelligently to external stimuli. However, the effectiveness of piezoelectric polymers is limited to a temperature range not exceeding 100°C.

The diverse group of piezoelectric polymers includes a variety of synthetic polymers such as polypropylene, polystyrene, and poly(methyl methacrylate); semicrystalline polyamide such as nylon-11; and amorphous polymers such as vinyl acetate [2]. However, piezoelectric effects in these materials are weak, often unstable,

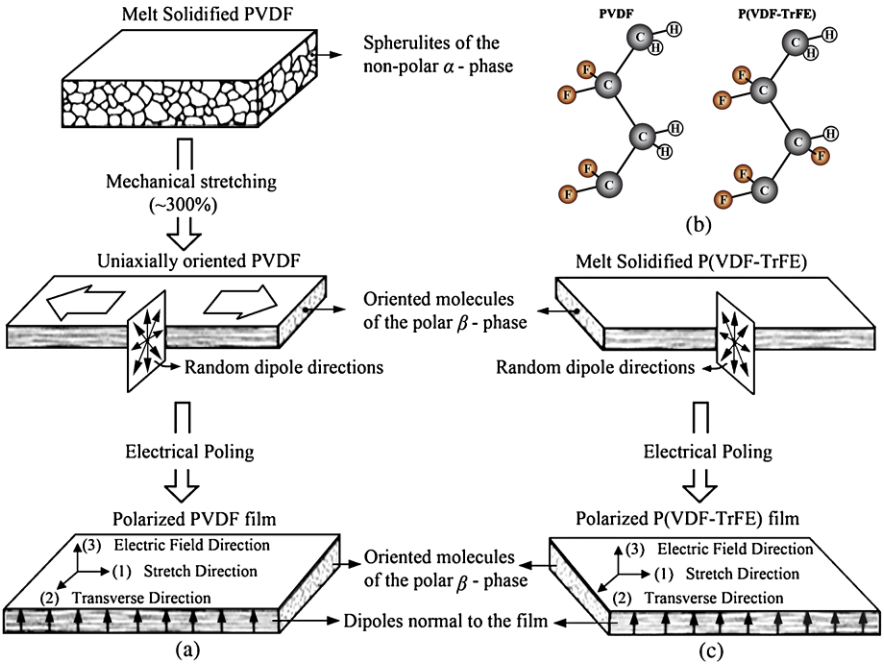

Fig. 7.2 (**a**) The procedure for making PVDF piezoelectric polymer films [*adapted from* [5]]; (**b**) The $[-CH_2-CF_2-]_n$ and $[-CHF-CF_2-]_n$ monomer units of PVDF and P(VDF-TrFE) respectively; (**c**) The procedure for making P(VDF-TrFE) piezoelectric polymer films. The mechanical stretching is not needed in P(VDF-TrFE)

and hence they are considered of limited practical significance. Strong piezoelectricity has been observed only in the synthetic polymer poly(vinylidene fluoride) (PVDF or PVF_2) and its copolymers such as P(VDF-TrFE). The monomer units of these polymers are given in Fig. 7.2(b). The attractive features of PVDF and copolymers include stable response characteristics in a wide frequency range up to 10^9 Hz, low acoustic impedance, and a high degree of resistance to: impact, moisture absorption, intense ultraviolet, and nuclear radiation [6]. In addition to these, the close matching of the mechanical impedance of these polymers with that of human tissues make them ideal for medical applications. Given these excellent features and the fact that piezoelectric polymer films of various thicknesses can be easily deposited on different substrates, the choice of piezoelectric material in POSFETs narrows down to PVDF and its copolymer P(VDF-TrFE).

Between PVDF and copolymer P(VDF-TrFE), the latter suits POSFETs because of its the tendency to crystallize directly in the polar β-phase [2]—as shown in Fig. 7.2(c). The implications of direct crystallization in polar β-phase is that, unlike PVDF, no mechanical stretching is required to yield β-phase. This particularly makes P(VDF-TrFE) attractive for POSFETs as mechanical stretching is difficult once the polymer is spin-coated on the wafer. On the other hand, PVDF requires mechanical stretching to transform from the non-polar α-phase to the polar β-phase,

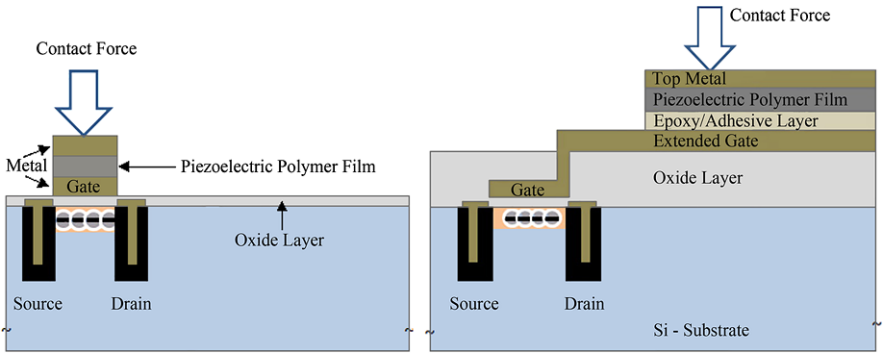

Fig. 7.3 The simplified structures of the POSFET and the extended gate devices [7–10]. Thicknesses of various layers are *not to scale*

as shown in Fig. 7.2(a). In other words, mechanical stretching is needed to induce piezoelectric properties into PVDF and this becomes a critical issue if such a film is to be integrated. However, PVDF films can be bonded to a surface using adhesive or epoxy. This is generally done in case of the extended gate based sensors [7–9], discussed in previous chapter. In addition to crystallizing directly in the polar β-phase, P(VDF-TrFE) crystallizes to a much greater extent than PVDF (up to 90% crystalline) and yields higher remanent polarization, a lower coercive field, and much sharper hysteresis loop. The crystalline structure, and consequently the piezoelectric and pyroelectric properties of the P(VDF-TrFE) depend on the molecular proportion x $(0.5 < x < 0.9)$ of vinylidene fluoride (VDF) in P(VDF_x-TrFE_{1-x}). Among various compositions of P(VDF-TrFE), the one with 70/30 weight ratio exhibits good ferroelectric response [2]. However, the piezoelectric constant resulting from this composition is not as large as that of PVDF. Nonetheless, the advantages of P(VDF-TrFE) in terms of processibility, enhanced crystallinity, and higher use temperature make it favorable for integrated sensing structures such as the POSFETs. Therefore, the piezoelectric layer in POSFETs comprises of P(VDF-TrFE) having 70 mol% of VDF content.

7.3 POSFETs Versus Extended Gate Approach

The extended gate approach presented in the previous chapter results in touch sensors that work in a manner similar to that of POSFETs. Yet POSFETs are different from them in many ways. Among others the structure, design, and fabrication of sensing devices are some of the primary differences. For a quick comparison, the structures of a POSFET and the extended gate based sensing device are shown in Fig. 7.3. It can be seen from the figure that in case of extended gate sensing devices the piezoelectric layer and the MOS transistor can be on the same substrate and yet placed apart and connected with the extended gates. Unlike conventional approaches, where transducer and electronics are separate entities, both POSFETs

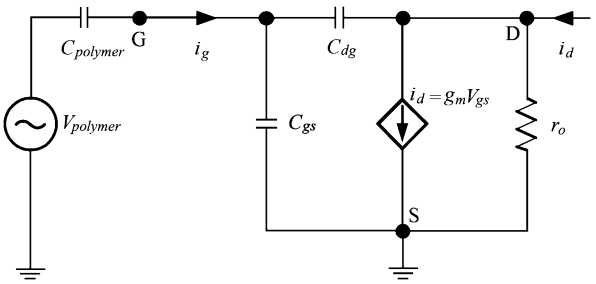

Fig. 7.4 The small signal equivalent of a POSFET tactile sensing device

and the extended gates based touch sensors integrate the transducer and electronics and facilitate a close coupling between them. However, the piezoelectric layer in extended gate based sensors is still not an integral part of the MOS device. In this sense, sensors based on extended gate approach fall somewhere in between the conventional approaches and the POSFET approach. With piezoelectric polymers on the gate area of MOS devices, POSFETs occupy much less space—thus saving the silicon real-estate or providing room for on-chip electronics. The same argument holds even if a substrate different from silicon is used.

Assuming a common-source configuration of MOS transistor (which allows worst case study) the small signal equivalent of a POSFET is shown in Fig. 7.4. In this figure, the piezoelectric layer is represented by its approximate electrical equivalent i.e. the voltage source $V_{polymer}$ in series with $C_{polymer}$—the capacitance of piezoelectric layer. For a simple analysis, the source and body in this figure are assumed to be connected to an electrical ground. Following the small signal equivalent of a POSFET, the amount of generated voltage in the piezoelectric polymer layer ($V_{polymer}$) that is transferred to gate terminal of MOS transistor (V_g) can be expressed as:

$$\frac{V_g}{V_{polymer}} = \frac{C_{polymer}}{C_{polymer} + C_{gs} + C_{gd}(1 + A_v)} \tag{7.2}$$

where, A_v is the voltage amplification of the transistor, and C_{gs} and C_{gd} are the gate–source and gate–drain capacitances of MOS device respectively. A similar expression for the extended gate devices, obtained using their small signal model of Fig. 6.2, has been presented in previous chapter. For a quick comparison, the expression for the extended gate based touch sensors is repeated below:

$$\frac{V_g}{V_{polymer}} = \frac{C_{polymer}}{C_{polymer} + (C_{polymer}/C_{adhesive} + 1)[C_{gs} + C_{sub} + C_{gd}(1 + A_v)]} \tag{7.3}$$

where, C_{sub} is the substrate capacitance mainly due to the oxide layer under the extended gate and $C_{adhesive}$ is the capacitance due to the epoxy or any other adhesive employed to adhere a separately prepared piezoelectric polymer film on to extended gates. It can be noted that both C_{sub} and $C_{adhesive}$ make denominator of Eq. (7.3) higher than that of Eq. (7.2) and hence for the same $V_{polymer}$, the V_g is higher in POSFETs. In other words, the substrate capacitance C_{sub} (which has larger value in

case of extended gate devices) and the capacitance due to epoxy $C_{adhesive}$ result in lesser voltage at the gate terminal of MOS device. The epoxy layer in Fig. 7.3, and hence the capacitance due to epoxy $C_{adhesive}$ in Eq. (7.3), can be avoided by depositing the piezoelectric polymer layer directly on the extended gates. In this way, a higher part of the voltage generated in piezoelectric layer can be made available at the gate terminal of MOS device. However, V_g will still be lower than that in POSFETs. Therefore, the overall sensitivity of POSFETs is better than the extended gate based touch sensors. In addition to the higher value of capacitances C_{sub} and $C_{adhesive}$, the longer interconnects needed to connect the lower metal of piezoelectric layer with the gate terminal of MOS devices, in the extended gate approach, also result in higher resistance. Combined together, they result in a higher RC time constant and hence contribute to make extended gate devices slower. On other hand, POSFETs are relatively free from such parameters and thus respond faster in comparison with the extended gate based touch sensing devices [11].

From above discussion, it is clear that the POSFETs perform better than the sensors based on extended gate approach. Nonetheless, depending on the application and sensing arrangement, the extended gate approach can offer advantages in terms of ease of fabrication, cost, and reliability etc. As an example, if piezoelectric polymer layer and the MOS devices are present on the separate chips, then fabrication can be simpler and fabrication cost will be lower—as in such cases, the MOS devices and the electronic circuity for subsequent signal processing can be developed using standard technology and the piezoelectric layer can be realized on a separate chip with a reduced number of fabrication steps. Further, the arrangement would be robust as only piezoelectric layer will come in contact with the objects and electronic circuitry remains isolated. In case of damage, replacing only the chip with piezoelectric layer can bring back whole system in order. This improves the reliability of the touch sensing system and makes the replacement economical too. However, a suitable package may be needed for such an arrangement to be effective. Such separation of piezoelectric layer and MOS devices in not possible in POSFETs. Thus, both extended gate approach and the POSFET approaches have their relative advantages and based on application requirements any of these solutions can be adopted. In fact, there are situations where both approaches complement each other.

7.4 Design Issues in POSFET Devices

The design of POSFETs, and the arrays discussed in the following chapter, is influenced by the sense of touch in human fingertips—where, the tactile acuity and spatial resolution is about 1 mm, as discussed in Chap. 3. The POSFETs, shown in Fig. 7.5, are therefore designed to have a dimension of 1 mm $\times$ 1 mm. However, the transistor size can also be scaled up/down to obtain a different spatial response. From device point of view, the n-MOS devices are designed to have a higher aspect ratio and hence large transconductance. It should be noted that the final design of POSFETs involves many trade-offs. As an example, the higher aspect ratio is generally desired for a larger voltage gain. However, higher channel width also results in

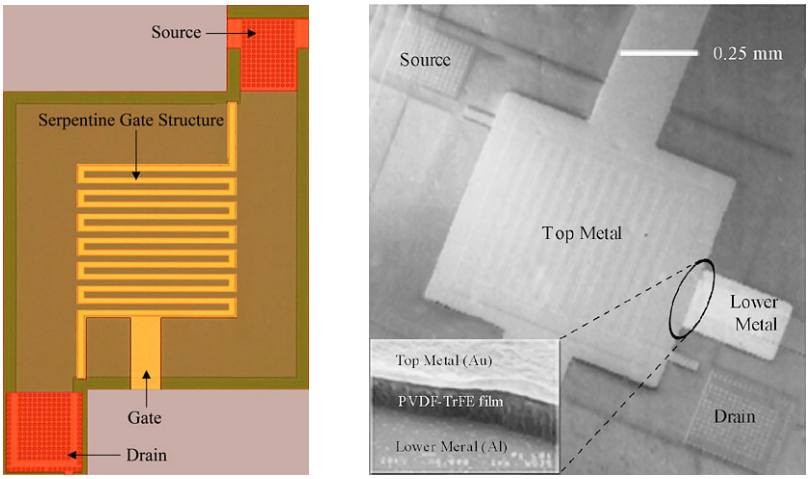

Fig. 7.5 (**a**) The POSFET device without piezoelectric polymer layer. The gate is shaped as serpentine for higher aspect ratio; (**b**) The SEM image of a 1 mm × 1 mm sized POSFET device after fabrication. The SEM image of piezoelectric polymer layer on POSFET device is shown in *inset*

higher C_{gs} and C_{gd} [12]. According to Eq. (7.2), for a higher voltage transfer from piezoelectric polymer to the gate terminal these capacitances should be low with respect to the piezoelectric polymer layer capacitance i.e. $C_{polymer}$. Thus, design of POSFETs involve a trade-off between a high aspect ratio and the low value of device capacitances with respect to that of piezoelectric polymer layer. The effect of transistor capacitances on the voltage transfer from piezoelectric polymer layer to the gate terminal can also be reduced by employing a source-follower arrangement—even if the arrangement is known to increase the noise and non linearity [12]. The POSFETs have been designed to have a channel width (W) of 7500 μm and a channel length (L) of 12 μm—resulting in an aspect ratio (W/L) of more than 600. The large W is obtained with a serpentine like gate structure, shown in Fig. 7.5(a).

The discussion in the previous paragraph assumes a fixed capacitance $C_{polymer}$ of the piezoelectric polymer layer. However, one may counter the effect of increased MOS device capacitances by relaxing that assumption. In other words, if C_{gs} and C_{gd} are increased due to higher aspect ratio, their effect on the voltage transfer to gate terminals, as per Eq. (7.2), can be countered by increasing $C_{polymer}$. Alternately, if C_{gs} and C_{gd} are assumed to be fixed, a pre-determined voltage ratio can be obtained by changing the $C_{polymer}$ only. Thus, assuming fixed area ($A = WL$), a pre-determined value of $V_g/V_{polymer}$ can be obtained by changing the thickness of piezoelectric polymer layer—thereby changing the capacitance of piezoelectric polymer layer. From design point of view, this argument can be followed to fix the thickness of piezoelectric polymer layer. Substituting $C_{polymer} = \varepsilon_{33}A/t$ in Eq. (7.2), the thickness of piezoelectric polymer needed to transfer more than eighty

percent of the asymptotic ($t = \infty$) value of $V_{polymer}$ to the gate terminal, is given by [11]:

$$t \geq \frac{\varepsilon_{33} A}{4(C_{gs} + C_{gd}(1 + A_v))} \tag{7.4}$$

where, ε_{33} is the permittivity of piezoelectric polymer. Using $W = 7500$ μm, $L = 12$ μm, $C_{gs} + C_{gd}(1 + A_v) = 2$ pF, and $\varepsilon_{33} = 61 \times 10^{-12}$, in Eq. (7.4), at least 0.75 μm thick polymer is needed for transferring eighty percent of the voltage generated in piezoelectric polymer to the gate terminal of MOS device. Given these facts, the POSFETs have been designed to have 2.5 μm thick piezoelectric polymer layer. This thickness value is also commensurate with the requirements of in situ poling of the piezoelectric polymer.

In terms of temporal response too, the POSFETs have been designed to match the capabilities of human fingertips. Various mechanoreceptors present in the skin allow detecting mechanical vibrations up to 1 kHz. Thanks to the faster response of piezoelectric polymers as well as of MOS devices, the POSFETs easily meet such requirements—as can be noticed from the experimental results discussed later in this chapter. In fact, this is one of the reasons behind choosing piezoelectric material for transduction in POSFETs. The response of a POSFET device depends on a number of parameters related to piezoelectric polymer layer as well as MOS device. For a further discussion on the effect of various parameters of piezoelectric polymer layer such as the elastic constant, piezoelectric constant, dielectric constant, the thickness of polymer, area, and the materials on the two sides of the polymer etc. reader may refer to Appendix B.

7.5 Fabrication of POSFETs

The fabrication steps for realizing the POSFET devices can be divided in to two parts: the steps for fabricating the MOS device, and the steps for depositing and in situ processing of piezoelectric polymer layer. The complete sequence of the fabrication steps is shown in Fig. 7.6. The fabrication steps related to the MOS part are quite standard. The steps related to fabrication of piezoelectric polymer layer are, however, non-standard in nature. For details on the MOS device fabrication, reader may refer to the literature on standard MOS device technology [14, 15]. The fabrication step for the MOS and piezoelectric layer are separately described below.

7.5.1 Fabrication Steps Related to MOS

The steps 1 through 6 in Fig. 7.6 refer to the fabrication of the MOS part of a POSFET device. The MOS part of POSFETs is basically an n-MOS transistor on p-well, realized starting from a 4 μm aluminum gate CMOS technology [16]. The n-channel

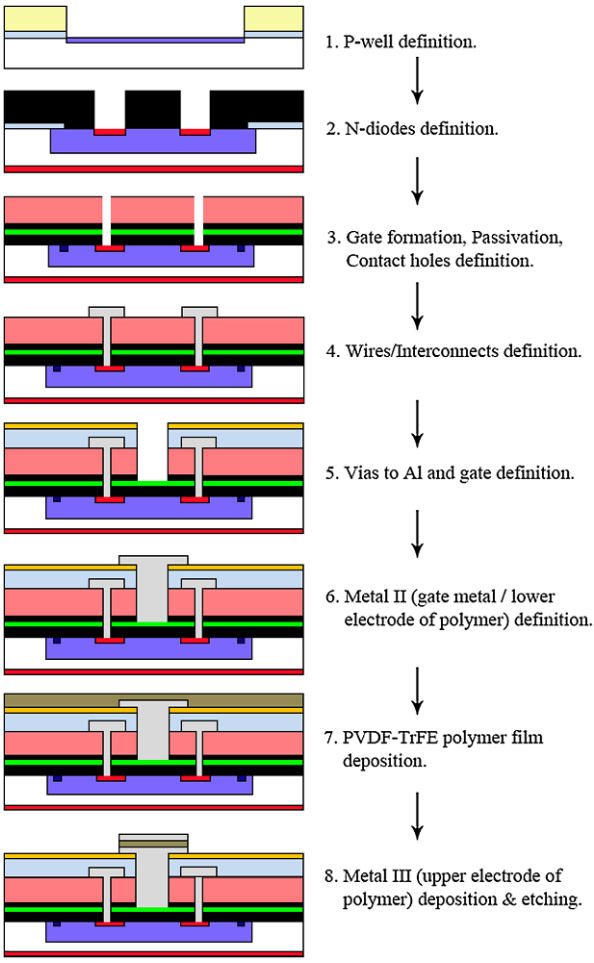

Fig. 7.6 Fabrication steps of POSFET touch sensing devices [13]

transistor is used in POSFETs because of higher charge carrier mobility. The channel width (W) and the channel length (L) of these transistors are 7500 μm and 12 μm respectively. For current version of POSFETs, complementary technology is not needed and hence the fabrication process for implementing n-channel devices only is sufficient. Accordingly, seven lithography masks are required up to step 6 of Fig. 7.6.

Starting from n-type 4 inch silicon wafers, the semiconductor structure of POSFETs is realized as n-channel transistors on a p-well (boron implant and diffusion, final junction depth 4.7 μm). The p-well insulates the devices from the n-type substrate. The source and drain n+ regions and the substrate contacts are realized by diffusion from phosphorus pre-deposition with a final junction depth of 750 nm. With this technology, the gate dielectric is implemented as a double layer of thermal oxide and stoichiometric Low Pressure Chemical Vapor Deposition (LPCVD) silicon nitride with two different thicknesses. The two process splitting have an equiva-

Table 7.1 The fabrication steps for piezoelectric polymer layer

Number	Fabrication Step	Method
1	Thin film deposition	Spin-Coating
2	Annealing	–
3	Etching	Plasma etching
4	Poling	Thermal poling

lent gate oxide thickness of 45 and 60 nm. The ohmic contacts to p-well are realized with BF2 implant and the electrical insulation is provided by a Low Temperature Oxide (LTO) layer. Two level of aluminium multilayer wiring respectively provided electrical connections and gate contact, while the further electrical insulation has been implemented with a Plasma-Enhanced Chemical Vapor Deposition (PECVD) Si_3N_4 layer. All process steps were performed at the fabrication facility at the Fondazione Bruno Kessler, Trento, Italy.

7.5.2 Fabrication Steps Related to Piezoelectric Layer

The last two steps i.e. step 7 and 8 in Fig. 7.6 are related to the deposition and processing of piezoelectric polymer layer. A 2.5 μm thick piezoelectric layer of P(VDF-TrFE) is deposited on the gate of the n-MOS. The polymer film is then processed in situ to obtain working POSFET touch sensing devices. The major steps related to deposition and processing of piezoelectric polymer layer are summarized in Table 7.1. The deposition of piezoelectric polymer film is followed by annealing, dry etching and finally the poling. However, it is not necessary to follow the same sequence for fabricating piezoelectric polymer layer. As an example, the poling step may precede the etching of polymer—as done in the past for depositing and processing the piezoelectric polymer film [9]. However, it is observed that the etching, especially the wet etching, after polarizing the polymer results in the depolarization or reduction in the remanent polarization—which ultimately makes POSFETs less sensitive. Various steps related to deposition and processing of piezoelectric polymer layer are described below in detail. As mentioned earlier, the fabrication steps related to piezoelectric polymer layer are non-standard in nature and hence the procedures described below were first performed on Si test wafers having 0.5 μm Al metal layer, i.e. without any n-MOS device. After stabilizing the polymer related fabrication steps, POSFETs were realized by depositing P(VDF-TrFE) on the gate of the n-MOS devices.

7.5.2.1 Polymer Film Deposition

The deposition of thin film piezoelectric layer is an important step in the development of POSFETs. Thin P(VDF-TrFE) films can be deposited from solution in

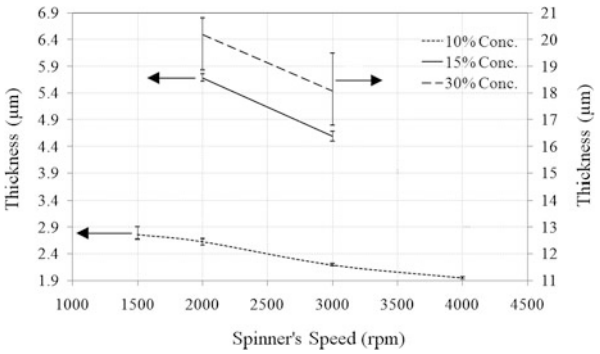

Fig. 7.7 P(VDF-TrFE) layer thickness as a function of spin rate and solution concentration [17]

a number of ways such as spin-coating, electrospinning and electrophoresis. Spin-coating is particularly interesting for depositing P(VDF-TrFE) layer at wafer scale and therefore the same is used while fabricating POSFETs. The thickness of polymer layer is an important parameter having a direct bearing on the performance of POSFETs. The thickness of polymer layer depends on the concentration of solution, speed of spin coating and the time of spin coating [18, 19]. Therefore, 10%, 15% and 30% concentrated P(VDF-TrFE) solutions were prepared by stirring the P(VDF-TrFE) pallets in RER500 solvent at 80°C for about 30 minutes. Organic solvents such as methyl ethyl ketone (MEK) or butanone can also be used for preparing the P(VDF-TrFE) solution. It should be noted that the molar ratios of VDF in P(VDF-TrFE) that display the most striking piezoelectric properties range from about 50 to over 90 mol%. For this reason, the solution of P(VDF-TrFE) is obtained from the pellets that have 70 mol% of VDF. Then spin-coating is performed in three steps—each with different sets of spin rate and spin time. The spin rate and spin time are kept low (500 rpm for 2 sec followed by 600 rpm for 8 sec) in first two spinning step as this allows the uniform spreading of the solution on the wafer. In the third spinning step, the spin rate and spin time are higher for obtaining the desired polymer thickness. The thickness of the piezoelectric polymer films at various spin rates, measured with optical profilometer, are given in Fig. 7.7. The spinning time during for all entries in Fig. 7.7 was 30 seconds—even if it is known to affect the thickness of polymer film [18]. It can be noticed from Fig. 7.7 that for a particular solution concentration the polymer thickness decreases with increase in the spin rate and that the plot is more or less linear. Further, the films with 10% and 15% solutions are more uniform than those obtained with 30% solution. This pattern of thickness variation with spin rate in consistent with the previous results presented in literature [18]. Finally, the POSFETs have a 2.5 µm thick piezoelectric polymer layer—obtained by spin-coating a 10% P(VDF-TrFE) solution at 2500 rpm, for 30 seconds.

7.5.2.2 Annealing of the Polymer Layer

Before evaporating the top metal electrode, the step 8 of fabrication process given in Fig. 7.6, the piezoelectric polymer layer is annealed at 120°C for two to three hours.

The annealing process typically improves the crystallinity of P(VDF-TrFE)—which is believed to provide higher piezoelectric properties. The level of crystallinity has been one of the most important parameters affecting the piezoelectric properties of semi-crystalline or amorphous polymers like P(VDF-TrFE). Besides improving crystallinity, annealing also helps evaporate any left out particles of the solvent, and enables release of the local stresses that are generated during deposition. Therefore, POSFETs with P(VDF-TrFE) piezoelectric polymer layer were placed in thermal chamber at temperature of 120°C over a period of three hours. This temperature was reached in more than an hour at a slow rate of 1.5°C/min. After maintaining the temperature of 120°C for three hours, the temperature of thermal chamber is brought down to room temperature at a slow rate of 1.5°C/min so as to release the stresses slowly. After annealing, the wafers with polymer films are treated with HDMS, and then a 0.2 μm top metal layer is vacuum deposited. HDMS treatment improves the adhesion of polymer and metal electrodes. POSFETs with top metal layers of Al/Cr and Au/Cr were fabricated. However, the adhesion of Au/Cr and polymer was found to be better. Subsequently, the top metal was then patterned using standard photolithography and wet etching steps.

7.5.2.3 Etching of Polymer Layer

To clearly define the sensing area in POSFETs, the piezoelectric polymer layer should be etched from the areas other than the gate of the n-MOS. The same is needed to gain access to the various contact pads on the chip. The P(VDF-TrFE) can be etched using either wet or dry etch methods—as evident from a number of wet [9, 18] and dry [20] etch schemes reported in past. The wet etching does not define the edges of the piezoelectric layer very well, especially when the thickness of the polymer film is of the order of few μm. It is observed that poor definition of edges makes the poling of polymer layer difficult, as sparking occurs close to poorly defined edges. The poor definition of edges may also result in the variation of effective piezoelectric area of POSFETs, thereby leading to the variations in their outputs. Precise definition of piezoelectric layer is essential to ensure the uniformity among the responses of many POSFETs. In this context, dry etch method is preferred as it results in well defined edges of piezoelectric layer. In case of POSFETs, the dry etch method is employed to remove the piezoelectric material from areas other than the gate of n-MOS devices. It is observed that the dry etch with oxygen (20 sccm) at 20 mBar pressure and He (40 sssm) is sufficient to remove P(VDF-TrFE) with a etching rate of 1 μm/min. The top metal electrodes, deposited and defined in previous step, act as the mask during dry etching of polymer. The SEM image of POSFETs in Fig. 7.5(a) shows a well defined piezoelectric layer.

7.5.2.4 In Situ Poling of Piezoelectric Polymer Layer

To maximize the use of the piezoelectric effect, a high value of the piezoelectric constant is desirable. However, the spontaneous polarization in piezoelectric film

is usually not uniformly aligned in same direction throughout the film—resulting into reduced or no piezoelectric effect. The piezoelectric materials are therefore "poled" to align the dipoles along a direction and thus net spontaneous polarization is obtained. The poling of piezoelectric materials is performed by subjecting them to high electric field, under high temperature conditions, in a chosen direction. The polarization direction is determined by the direction of electrical field employed for poling. However, applying a high electric field opposite to the poling direction may cause the material to be depoled or become accidentally poled in the opposite direction. At even higher voltages, electric breakdown occurs and the material can lose all its piezoelectric properties. The same is true for high temperatures. If the operating temperature is above a certain temperature called the Curie temperature then the piezoelectric properties are destroyed.

A number of methods, such as thermal poling (electrode poling) [21], corona poling [9, 22], electron-beam poling [23] etc. exist for polarizing piezoelectric polymers. The earliest and most widely available method applied to pole PVDF and its copolymer P(VDF-TrFE) films is the room temperature "corona poling". The corona poling, however, does not result in uniform poling and may thus be suitable for applications that do not require a very high electrical quality of the samples. The corona poling is useful for large volume production where quality and reproducibility of data is not necessary. Like corona poling, the polarization profiles obtained with electron-beam poling are less uniform [24]. For applications and materials studies requiring high quality and reproducibility, individual samples must be produced with well-defined electrical properties in a process, which controls the amplitude, duration, and the history of the electric field. By controlling the electrical field applied to individual samples, the electric displacement, displacement current, remanent polarization, and homogeneity of polarization can be also controlled. In this context, thermal or electrode poling method is useful as it results in uniform polarization and allows monitoring of various parameters. The methods thus suits well for integrated sensing devices such as POSFETs.

The poling procedure, in general, consists of applying an electric field E, at a temperature T for a certain time t. The polarization achieved depends on the applied field, poling temperature and poling time. For long enough poling times, the polarization is only a function of the poling field while the poling temperature affects merely the rate at which the polarization builds up. As stated above, poling at a stronger field, at higher temperature, and for longer periods does not necessarily yield better results. Hence, these parameters should be chosen properly according to the mechanism by which the material is poled. The electric field strength up to 100 V/μm for around ten minutes is generally sufficient to polarize the polymer films. In case of integrated smart sensors such as POSFETs and extended gates, the high poling voltage may damage the active devices that are present on same chip. Hence, in all such cases poling must be performed carefully and measures must be taken to ensure that applied high voltage appears only across the piezoelectric layer.

The instruments and the scheme for in situ poling the piezoelectric polymer layer on POSFETs is given in Fig. 7.8(a). To prevent the device damage source, drain, gate and the substrate are electrically grounded, as shown in Fig. 7.8(a), and poling

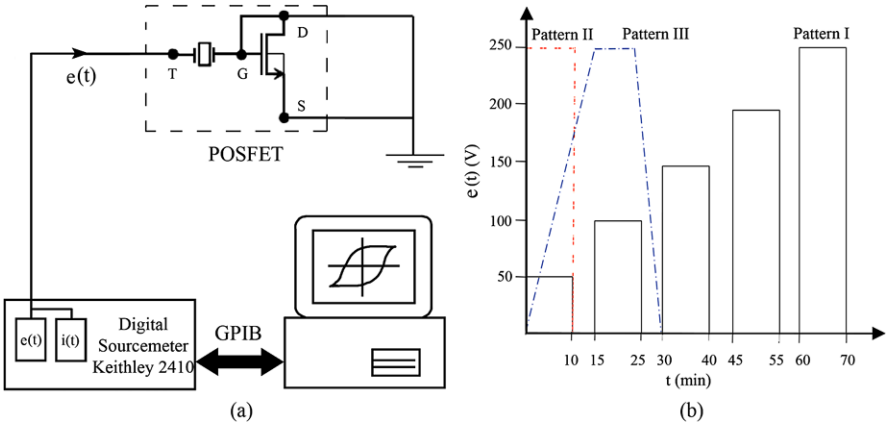

Fig. 7.8 (**a**) The arrangement for polarizing or orienting dipoles along the thickness of piezoelectric layer in POSFETs; (**b**) The timing patterns of the polarizing voltage

voltage is applied at the top metal at a rate of 100 V/μm. The Keithley 2410 source meter is used applying poling voltage. The 2.5 μm thick piezoelectric polymer layer requires up to 250 V during poling. The effect of poling voltage is investigated using three patterns of the electric field shown in Fig. 7.8(b). The pattern I in Fig. 7.8(b) involves application of the electric fields up to 250 V—in five incremental steps of 50 V. The poling time of 10 minutes is followed by a short circuit period of 5 minutes. Short circuiting the two metal sides of polymer helps neutralize any access charge. In pattern II, which is similar to standard electrode poling method, the electric field is applied across piezoelectric layer in single step of 250 V for about 10 minutes. In pattern III, the electric field is slowly reaches the maximum of 250 V in 15 minutes, maintains this maximum value for 10 minutes, and thereafter returns back to zero in 5 minutes. The above poling voltages were applied at 60°C poling temperature. The polarization with pattern II poling voltage takes less time, but results is more sparking. On the contrary, the multi-step poling process with pattern I takes more time but results in a polarized piezoelectric layer that is relatively clean i.e. free from sparks. Therefore, poling voltage with pattern I is finally employed to polarize the polymer on POSFETs. A comparison of the input and output characteristics of the MOS transistors in POSFETs, before and after in situ poling, is given in Fig. 7.9. No appreciable change in the characteristic plots before and after poling point toward sufficiency of measures taken to ensure application of voltage across piezoelectric layer only and hence to ensure proper working of POSFETs.

7.5.2.5 Measuring the Level of Polarization in Piezoelectric Layer

The standard scheme, called Sawyer Tower circuit [25], typically used to obtain the piezoelectric hysteresis (P–E plot) is given in Fig. 7.10(a). In this scheme, a known capacitor C_L (having capacitance much higher than that of piezoelectric layer) is

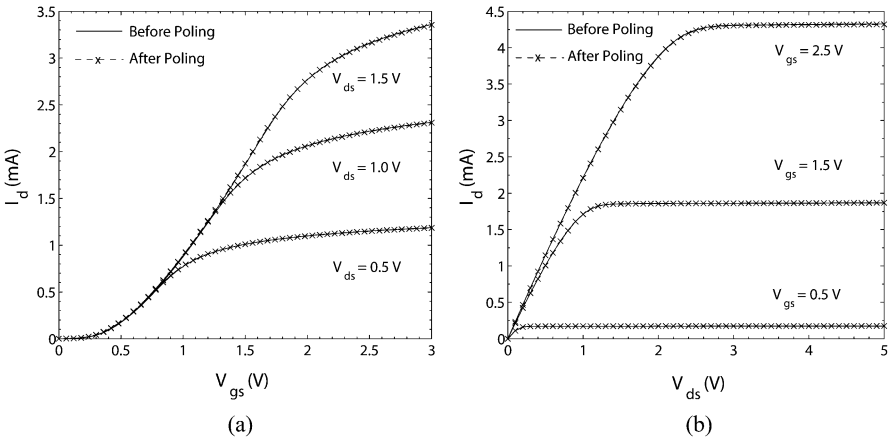

Fig. 7.9 (**a**) Comparison of the input characteristics of a POSFET device before and after poling; (**b**) Comparison of the output characteristics of the POSFET device before and after poling [4]

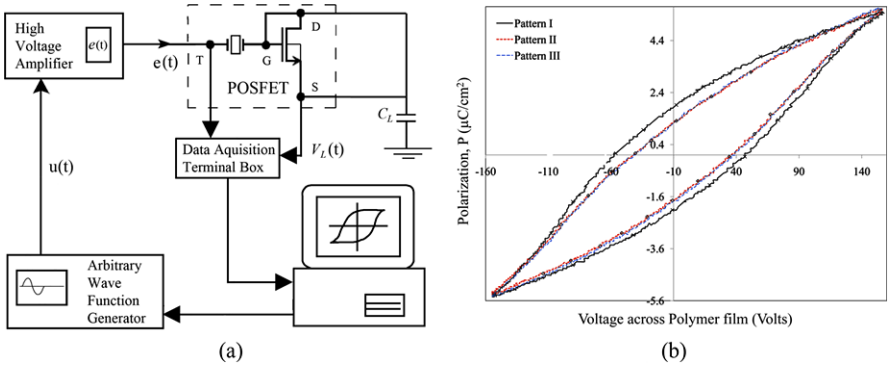

Fig. 7.10 (**a**) The scheme of Sawyer Tower circuit for obtaining polarization hysteresis; (**b**) Polarization versus applied field (P–E) hysteresis loop (at 10 Hz). The remnant polarization (P_r) for the samples polarized with pattern-I is 1.98 μC/cm^2 and that for other samples it is 1.31 μC/cm^2

employed, as in Fig. 7.10, to obtain the polarization. A sinusoidal voltage E (generated by the function generator and amplified by power amplifier 609C from Trek Inc.) is applied to the top metal of piezoelectric layer in POSFETs. The voltage applied on top of piezoelectric layer and the voltage V_L across the known capacitor are acquired and sent to computer for obtaining P–E plots. The mathematical relations used to obtain the polarization are discussed below.

Since $C_L \gg C_{polymer}$, almost all the charges generated in piezoelectric layer pass through the known external capacitor and hence $Q_{polymer} \approx Q_L$. This can be expressed as:

$$Q_{polymer} \approx Q_L \approx C_L V_L \tag{7.5}$$

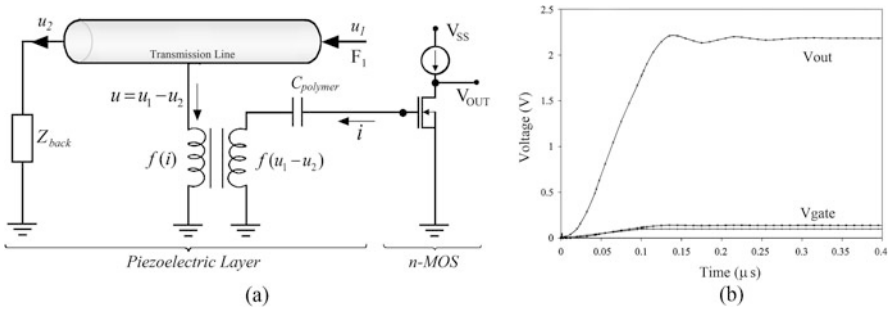

Fig. 7.11 (**a**) The transmission line approximate electrical equivalent model of POSFETs; (**b**) The simulated output of a POSFET touch sensing device

If C_L is known, the charge $Q_{polymer}$ and hence the polarization $P_{polymer}$ can be obtained from voltage V_L as:

$$C_L V_L = (\varepsilon_0 \varepsilon_{polymer} E_{polymer} + P_{polymer}) A_{polymer} \tag{7.6}$$

where $\varepsilon_{polymer}$, $E_{polymer}$, $P_{polymer}$ and $A_{polymer}$ are the dielectric constant, electric field, polarization and area of the piezoelectric layer respectively. Generally, the first term on right hand side of (7.6) is negligible and hence can be ignored. Thus, using (7.6), the polarization can be approximately expressed as:

$$C_L V_L \approx P_{polymer} A_{polymer} \tag{7.7}$$

The P–E plots for the piezoelectric layer on POSFETs are shown in Fig. 7.10(b). The plots compare the polarization levels of various samples that were polarized with different patterns of poling voltage given in Fig. 7.8(b). The plots were obtained by using a known capacitor of 0.1 μF, which is five orders of magnitude higher than the capacitance of piezoelectric layer ($C_{polymer} \approx 50$ pF). The maximum polarization P_{sat} for a 10 Hz sine waveform is ≈ 5.5 μC/cm^2 and the remanent polarization P_r is ≈ 2 μC/cm^2.

7.6 Modeling and Simulation

The work presented in this section is a first attempt toward modeling the behavior of POSFET devices. The model of POSFET is obtained simply by combining the models of piezoelectric polymers and n-MOS devices. In present form, the model does not consider additional issues that quite likely occur at the interface of two materials—in this case that of piezoelectric polymer and the n-MOS device. Since this is the first attempt to model POSFETs, surely there is lot more than that can be explained with the model presented here. Nonetheless, the model presented here sets the direction for modeling of POSFET device.

The approximate electrical equivalent model of POSFETs, shown in Fig. 7.11(a), consists of two components: (a) the transmission line equivalent model for the piezo-

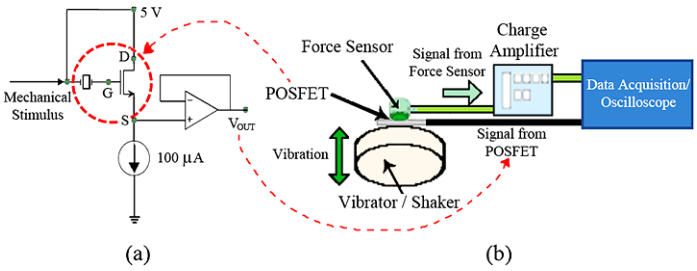

Fig. 7.12 (**a**) The POSFET connected in a source-follower configuration with floating gate; (**b**) The scheme of the experiment set up employed for testing POSFET's electromechanical response

electric layer, and (b) the model of n-MOS device. The output terminal of the piezoelectric layer is connected to the gate of the n-MOS device. Among a number of attempts made to model the electromechanical response of piezoelectric materials, the transmission line model has been used quite often. In this model, the mechanical stimulus i.e. force F_1, is the input to one side of the acoustic transmission line and other side of the line is terminated into an impedance that is equivalent of the mechanical impedance of the substrate. When force F_1 is applied, the particles inside the transmission line move at a velocity u_i. The electrical current equivalent coming out of the transmission line is the difference of particle velocities at two ends of the line. The length of this transmission line is equal to thickness of piezoelectric layer. The mechanical to electrical conversion is represented by the transformer, as shown in Fig. 7.11(a). A detailed discussion on the transmission line model for piezoelectric polymers such as PVDF and P(VDF-TrFE) along with its PSPICE implementation are given in Appendix B. The PSPICE implementation of the POSFET's model is also given in Appendix B. For a detailed discussion of modeling of n-MOS device, reader may refer to standard literature on device modeling [26]. The output of the POSFETs, simulated using PSPICE is given in Fig. 7.11(b). A level 2 model of n-MOS device is used in this simulation. For a 0.1 N force applied at the free side of transmission line, the output of POSFETs at drain terminal is about 2.25 V. These results indicate toward the high sensitivity of the POSFETs.

7.7 Experimental Results

Before putting to use, it is important to test and quantify the response of POSFETs. The experimental arrangement used to test the POSFETs is essentially same as the one presented in previous chapter. However, for better understanding the scheme of the experiment setup is presented again in Fig. 7.12(b). As can be seen in the figure, the POSFET device is sandwiched between the shaker/vibration generator and the force sensor. To ensure the contact between POSFETs and the force sensor, the POSFETs are prestressed. Since piezoelectric materials do not respond to static

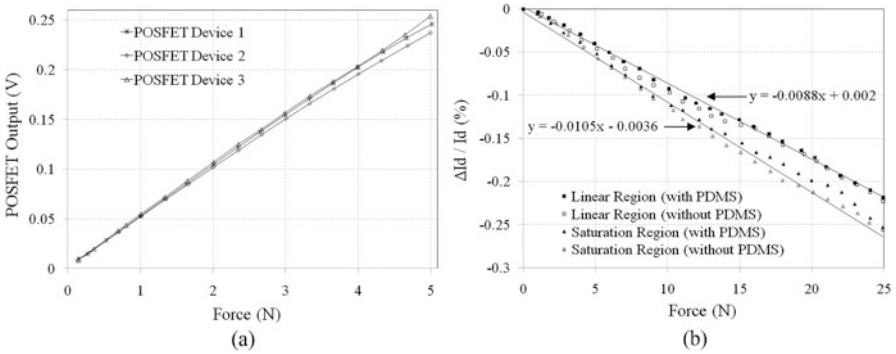

Fig. 7.13 (**a**) The output of the POSFETs at different (20 Hz sinusoidal) forces; (**b**) The change in drain current due to piezoresistive behavior of MOS device [4]

stimuli, the pre-stressing does not affect the output of POSFETs. The shaker applies the dynamic forces in normal direction and the force sensor measures the amount of force applied by shaker on the POSFET. The force sensor, in this arrangement, is equipped with a probe of dimensions 1.1×1.1 mm^2 so as to apply force on entire piezoelectric layer. Force sensor is affixed to a 3-axis micro-positioning system to control its the position vis-a-vis POSFET. When applying the force, the sensor is covered with a thin 200 μm protective PDMS rubber. The POSFET touch sensing devices are used in a source-follower floating gate configuration, as shown in Fig. 7.12(a). The choice of source-follower configuration is influenced by the fact that transistors in this configuration have a voltage gain less than unity and this allows evaluating POSFETs over a large range of dynamic forces. The output of POSFET and that of force sensor are acquired and sent to computer or visualized on oscilloscope.

The performance of POSFETs is evaluated under ambient conditions both for the variable force–constant frequency and constant force–variable frequency configurations. The response of three POSFET devices to a range of dynamic normal forces is shown in Fig. 7.13(a). These results are obtained by applying 20 Hz sinusoidal force on the POSFETs in a normal direction. The plots in Fig. 7.13(a) relate the maximum values of sinusoidal outputs from three taxels to corresponding maximum values of the applied sinusoidal forces. It can be seen from figure that the response is linear over entire test range of 0.15–5 N and the slope is $\approx$ 50 mV/N. The force resolution can be improved either by using POSFETs in common-source configuration or by using an external amplifier. Considering various parameters, related to piezoelectric polymer and the n-MOS device, the expected response of POSFETs should be $\approx$ 78 mV/N—a value little higher than the observed response. The gain of MOS devices is less than unity in a source-follower configuration and hence the POSFET devices could be tested over a range of forces that is wider that the range of contact forces experienced by humans in normal manipulative tasks. In a normal manipulative task, humans experience forces in the range from 0.15 N to 0.9 N.

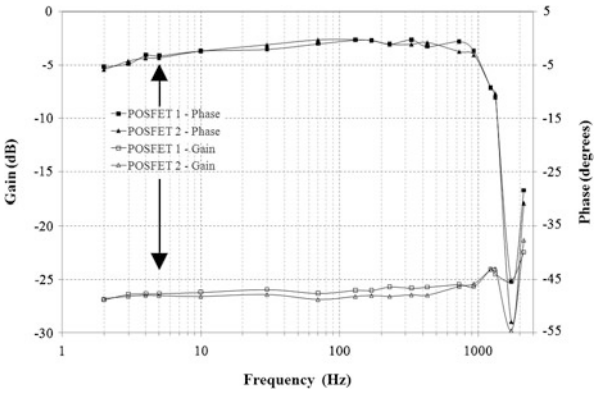

Fig. 7.14 Gain and Phase plots of two POSFET tactile sensing devices obtained by applying a sinusoidal 1 N force in the frequency range from 2 Hz to 2.13 kHz [28]. The peaks at around 2 kHz reflect the mechanical resonance of the experiment set up

In the constant force–variable frequency mode, a force of 1 N is applied on POSFET and the frequency of applied force is varied between 2 Hz–2.13 kHz. The response of POSFETs under these conditions is shown, as gain ($= V_{out}/F_{in}$) and phase plots, in Fig. 7.14. The gain is constant (~ -26 dB) over the entire range of frequency and the phase plot is flat with approximately zero phase. The values of gain and phase deviate significantly from the general trend at around 2 kHz because of the mechanical resonance in the experiment set up.

An interesting feature of MOS device is that their drain current (I_d) changes with stress—mainly as a result of mobility variations [27]. In other words, there is some piezoresistive effect as well. In fact this piezoresistive property has been exploited to obtain MOS based pressure sensors as well. The extent to which this effect can contribute to the POSFET response can be estimated by removing the P(VDF-TrFE) layer, applying force on the MOS device and measuring the output. Such an experiment was performed on POSFETs and forces up to 25 N were applied with and without a thin PDMS film on the gate. For better comparison, the device was connected as in Fig. 7.12(a) and the gate voltage varied to obtain the response in linear and saturation regions. The response due to piezoresistive effect varies with biasing condition, as evident from plots in Fig. 7.13(b). It is observed that the $\Delta I_d/I_d$ of 0.01 is needed to obtain 50 mV/N output with POSFET connected as in Fig. 7.12(a). On other hand, the $\Delta I_d/I_d$ due to piezoresistive effect is about 0.0001 for 1 N—which is 1% of $\Delta I_d/I_d$ needed to obtain 50 mV/N POSFET output. This therefore means that the response of POSFETs is mainly due to the piezoelectric behavior of P(VDF-TrFE) layer and the piezoresistive contribution can be neglected.

7.8 Summary

The concept, design, fabrication and experimental evaluation of novel POSFET touch sensing devices is presented in this chapter. The fabrication challenges such as in situ processing of the piezoelectric layer have been successfully overcome. The POSFETs have been tested for a wide range of dynamic normal force (0.15–5 N)

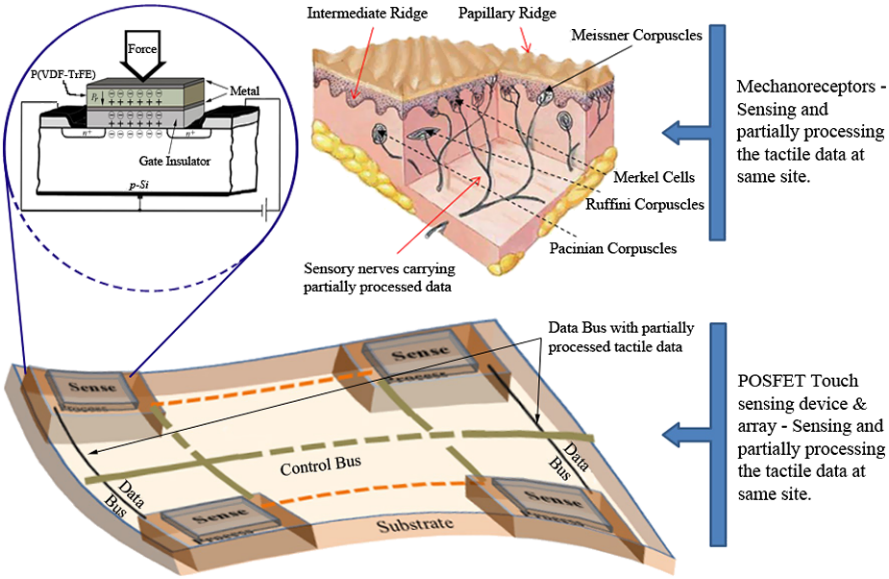

Fig. 7.15 The concept of POSFET based conformable and distributed touch sensing structures, and the analogy between POSFETs and the mechanoreceptors in human skin [29, 30]

and frequency (2 Hz–2.13 kHz) and average response is found to be approximately 50 mV/N. The average response can be higher if instead of source-follower configuration the POSFET device are connected in common-source configuration. In that case, a human fingertip like force resolution of 0.01 N (1 gmf) can be easily obtained. As the transduction is performed by piezoelectric polymers, the POSFETs can be employed for detecting the variable contact conditions such as incipient slip. It may also be noted that piezoelectric polymers exhibit anisotropic behavior. From the application point of view this property is interesting as, in principle, it allows measuring not only the contact force but also its direction. In other words, the piezoelectric material based sensors can be employed to detect both normal and the tangential component of contact force. However, in practice it is difficult to separate the two components. It is therefore difficult for a POSFET to detect normal as well as tangential component by itself. Instead, the gradient of responses from multiple POSFETs in an array could be employed to obtain information related to the tangential force. The small size of POSFETs will also be helpful in such an event. The pyroelectric property of P(VDF-TrFE) can also be exploited to use the same device for detecting temperature variations. In this sense the POSFETs can be said to be multifunctional. The small size of 1 mm $\times$ 1 mm, linear response over wide range of dynamic forces, and multifunctional behavior make the POSFET devices suitable for body sites such as fingertips of a robot.

The integration of smart materials and electronic devices results in devices that have better signal to noise ratio, faster response, wider bandwidth, and better force sensitivity etc. From robotic application point of view, such an integration is use-

ful because of resulting reduction or complete absence of wires that are typically needed to connect transducer and electronic devices. The marriage of transducing materials with the electronic devices like transistor impart in POSFETs the capability to 'sense and partially process' the contact parameters at the contact site itself. In this context, POSFETs can be loosely compared with the mechanoreceptors in human skin that not only sense the contact parameters, but also partially process the tactile data at same site [31]. This analogy is given in Fig. 7.15. This analogy can be further strengthened by having a network of POSFET like device distributed over an area and using the ensemble of these devices to derive the tactile information from that areas. An idea for such a network is given in Fig. 7.15. The figure shows a conformal electronic surface with mechanically distinct sub-circuit islands of POSFET like devices. Many such islands can be embedded in a soft and compliant polymer like PDMS (Polydimethylsiloxane) and connected with flexible and stretchable interconnects. However, many challenges, especially related to the packaging and reliable interconnects, await before we arrive at such a solution.

References

1. H. Ishiwara, Current status of ferroelectric-gate Si transistors and challenge to ferroelectric-gate CNT transistors. Curr. Appl. Phys. **9**, S2–S6 (2009)
2. H.S. Nalwa, *Ferroelectric Polymers: Chemistry, Physics, and Applications* (Marcel Dekker, Inc., New York, 1995)
3. R.S. Dahiya, M. Valle, L. Lorenzelli, SPICE model of lossy piezoelectric polymers. IEEE Trans. Ultrason. Ferroelectr. Freq. Control **56**(2), 387–396 (2009)
4. R.S. Dahiya, G. Metta, M. Valle, L. Lorenzelli, A. Adami, Piezoelectric oxide semiconductor field effect transistor touch sensing devices. Appl. Phys. Lett. **95**(3), 034105 (2009)
5. A.J. Lovinger, Ferroelectric polymers. Science **220**(4602), 1115–1121 (1983)
6. A. Vinogradov, Piezoelectricity in polymers, in *Encyclopedia of Smart Materials*, vols. 1–2, ed. by M. Schwartz (Wiley, New York, 2002), pp. 780–792
7. R.G. Swartz, J.D. Plummer, Integrated silicon-PVF2 acoustic transducer arrays. IEEE Trans. Electron Devices **26**(12), 1920–1932 (1979)
8. E.S. Kolesar, R.R. Reston, D.G. Ford, R.C. Fitch, Multiplexed piezoelectric polymer tactile sensor. J. Robot. Syst. **9**(1), 37–63 (1992)
9. J.V. der Spiegel, A. Fiorillo, Method of manufacturing ferroelectric MOSFET sensors. U.S. Patent 5,254,504 (1993)
10. E.S. Kolesar, C.S. Dyson, Object imaging with a piezoelectric robotic tactile sensor. J. Microelectromech. Syst. **4**(2), 87–96 (1995)
11. R.S. Dahiya, M. Valle, G. Metta, L. Lorenzelli, POSFET based tactile sensor arrays, in *IEEE ICECS'07: The 14th International Conference on Electronics, Circuits and Systems*, Marrakech, Morocco (2007), pp. 1075–1078
12. B. Razavi, *Design of Analog CMOS Integrated Circuits* (McGraw-Hill, New York, 2000)
13. R.S. Dahiya, M. Valle, G. Metta, L. Lorenzelli, A. Adami, Design and fabrication of POSFET devices for tactile sensing, in *Proceedings of TRANSDUCERS 2009—The 15th IEEE International Conference on Solid-State Sensors, Actuators and Microsystems* (2009), pp. 1881–1884
14. G.S. May, S.M. Sze, *Fundamentals of Semiconductor Fabrication* (Wiley, New York, 2003)
15. R.C. Jaeger, *Introduction to Microelectronic Fabrication*. Modular Series on Solid State Devices, vol. 5 (Prentice Hall, New York, 2001)

16. S. Martinoia, N. Rosso, M. Grattarola, L. Lorenzelli, B. Margesin, M. Zen, Development of ISFET array-based microsystems for bioelectrochemical measurements of cell populations. Biosens. Bioelectron. **16**(9), 1043–1050 (2001)
17. R.S. Dahiya, M. Valle, L. Lorenzelli, G. Metta, S. Pedrotti, Deposition processing and characterization of PVDF-TrFE thin films for sensing applications, in *Proceedings of IEEE Sensors 2008* (2008), pp. 490–493
18. D. Setiadi, P.P.L. Regtien, P.M. Sarro, Application of VDF/TrFE copolymer for pyroelectric image sensors. Sens. Actuators A, Phys. **41–42**, 585–592 (1994)
19. M. Akcan, C. Topacli, Pyroelectric and dielectric properties of spin-coated thin films of vinylidene fluoride-trifluoroethylene copolymers. Polym. Int. **50**, 835–840 (2001)
20. E. Edqvist, N. Snis, S. Johansson, Gentle dry etching of P(VDF-TrFE) multilayer micro actuator structures by use of an inductive coupled plasma. J. Micromech. Microeng. **18**, 1–7 (2008)
21. M.Z. Sleca, R.D. Briggs, W.D. Hunt, A micromachined poly(vinylidene fluoride-trifluoroethylene) transducer for pulse-echo ultrasound applications. IEEE Trans. Ultrason. Ferroelectr. Freq. Control **43**, 257–262 (1996)
22. A.S. Fiorillo, J. Van Der Spiegel, P.E. Bloomfield, D. Esmail-Zandi, A PVDF-TrFE based integrated ultrasonic transducer. Sens. Actuators A, Phys. **A21–A23**, 719–725 (1989)
23. B. Gross, M. Gerhard, A. Berraissoul, G.M. Sessler, Electron-beam poling of piezoelectric polymer electrets. J. Appl. Phys. **62**, 1429–1432 (1987)
24. D. Setiadi, T.D. Binnie, P.P.L. Regtien, M. Wubbenhorst, Poling of VDF/TrFE copolymers using a step-wise method, in *9th International Symposium on Electrets*, Shanghai, China (1996)
25. C.B. Sawyer, C.H. Tower, Rochelle salt as a dielectric. Phys. Rev. **35**(3), 269–273 (1930)
26. P. Antognetti, G. Massobrio, *Semiconductor Device Modeling with Spice* (McGraw-Hill, New York, 1993)
27. A.T. Bradley, R.C. Jaeger, J.C. Suhling, K.J. O'Connor, Piezoresistive characteristics of short-channel MOSFETs on (100) silicon. IEEE Trans. Electron Devices **48**(9), 2009–2015 (2001)
28. R.S. Dahiya, L. Lorenzelli, G. Metta, M. Valle, POSFET devices based tactile sensing arrays, in *Proceedings of 2010 IEEE International Symposium on Circuits and Systems (ISCAS)* (2010), pp. 893–896
29. R.S. Dahiya, Human-inspired tactile sensing, in *Learning from Nature: Biologically-Inspired Sensors*, ed. by D.H.B. Wicaksono, P. French (Springer, Berlin, 2010), pp. 455–476
30. R.S. Dahiya, G. Metta, M. Valle, G. Sandini, Tactile sensing—from humans to humanoids. IEEE Trans. Robot. **26**(1), 1–20 (2010)
31. R.S. Johannson, I. Birznieks, First spikes in ensembles of human tactile afferents code complex spatial fingertip events. Nat. Neurosci. **7**(2), 170–177 (2004)

Chapter 8
POSFET II—The Tactile Sensing Chip

Abstract This chapter extends the research on POSFET devices, presented in previous chapter, toward the tactile sensing system on chip. The tactile sensing chip presented in this chapter comprises of 5×5 array of POSFET devices and two integrated temperature sensors. The size of each POSFET device on the chip is 1 mm^2 and the center–center between two adjacent POSFETs is 1.5 mm. With these features, the tactile sensing chips have human fingertip like spatial resolution and spatial acuity. With a 2-D array of POSFETs and the integrated temperature sensors, the tactile sensing chips are capable of measuring dynamic contact forces and the contact temperature. The chips have been extensively tested over wide range of dynamic contact forces and temperatures and the test results are presented. The experiments presented in this chapter have been performed with the aim to examine the collective performance of a set of POSFETs. The reader interested in the electromechanical evaluation of an individual POSFET device may refer to the results presented in the previous chapter. In fact, this chapter is fundamentally linked to previous chapter hence the reader may first go through previous chapter. Since the time the POSFET tactile sensing chips were reported first, they have been redesigned and the new version have POSFETs with integrated readout electronics on the chip. A discussion is also presented in context with the redesigned tactile sensing chip and the future trend in this area. Finally, new application areas of POSFET like devices are discussed.

Keywords High resolution tactile sensing · POSFET · Tactile sensing chip · System on chip · Artificial skin · Sensor integration · Multifunctional · Wiring complexity · Integrated systems · FET · CMOS · PVDF · PVDF-TrFE · Piezoelectric polymers · Microfabrication · Flexible electronics

8.1 POSFET Tactile Sensing Chip—Design and Fabrication

The design of a distributed tactile sensing structure is greatly influenced by the target application. Referring to a humanoid robot as an example, the distribution of sensors in an area depends on the part of robot's body where sensing structure is to be placed [1, 2]. For fingers, involved in precise manipulative tasks, the sensors must be close enough to yield a good spatial resolution. This is also important for getting a better tactile image of the contacted object and for the medical applications. However, if

R.S. Dahiya, M. Valle, *Robotic Tactile Sensing*,
DOI 10.1007/978-94-007-0579-1_8,

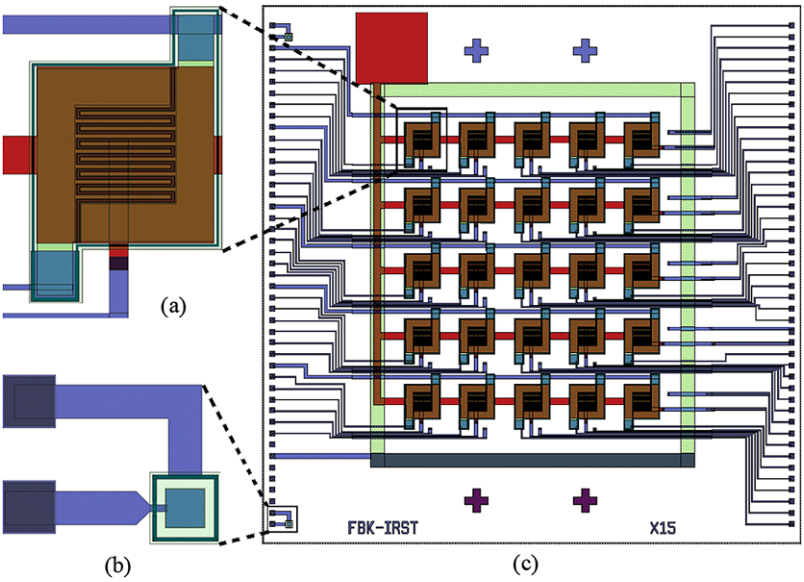

Fig. 8.1 (**a**) The layout of a POSFET device on the chip; (**b**) The layout of temperature diodes on the chip; (**c**) The layout of tactile sensing chip with 5 × 5 POSFET devices array and two temperature diodes

the sensors are to be distributed over body area such as belly or back of a humanoid then one can probably settle with lesser number of sparsely distributed sensors. If cues are taken from the human body then the sensitivity and pressure thresholds should also vary across the body.

The layout of the tactile sensing chip is shown in Fig. 8.1(c). The tactile sensing chip consists of an array of 5 × 5 POSFET touch sensing devices and two integrated temperature sensors. The layouts of a POSFET device in the tactile sensing arrays is given in Fig. 8.1. The overall dimension of the tactile sensing chip is 1.5 cm × 1.5 cm. The size of each POSFET device on the array is 1 mm × 1 mm and the center–center distance between two adjacent POSFETs is 1.5 mm. The size and spacing between POSFETs ensure human like spatial acuity and spatial resolution. With integrated sensing structures such as POSFETs it is easy to scale up/down the size and spacing between sensing elements and hence the spatial resolution. The tactile sensing chips presented here are designed for human fingertip like spatio-temporal characteristics.

The tactile sensing chip shown in Fig. 8.1(c) have integrated temperature sensors for measuring the contact temperatures. These integrated temperature sensors are basically the diodes whose output is known to vary with temperature. The lay out of a temperature diode on chip is given in Fig. 8.1(b). These integrated temperature diodes have been designed to work at 100 μA forward bias current and they have linear response up to temperature value of 70°C. A human like tactile sensing system should be able to measure multiple contact parameters such as force, temperature,

hardness etc. The integration of temperature sensors on the chip, therefore, extend the capability of tactile sensing chips toward measurement of multiple dynamic contact events—the contact temperature and dynamic contact forces in present case.

The fabrication steps for the tactile sensing chips are essentially same as those followed to realize the single POSFET devices [3, 4]—presented in previous chapter. The fabrication of tactile sensing chip, however, involves some additional challenges related to—(a) deposition of the piezoelectric polymer layer with uniform thickness over all POSFETs in the array; (b) fabrication of the chip with minimum spread in the characteristics of n-MOS devices; and (c) simultaneous and uniform polarization of the piezoelectric polymer layer over all POSFETs in the array.

A number of experiments, performed on dummy silicon wafers (i.e. without any n-MOS device), to investigate the steps for obtaining uniform and controlled thickness of polymer films over large areas are reported in [5]. The concentration of solution, spinner's speed and spinning time are used as variables in these experiments. The outcome of these experiments is also described in previous chapter. The particular outcome from these experiments is spin coating a 10% P(VDF-TrFE) solution, at spin rate of 3000 rpm over for a time period of 30 sec. This combination of solution concentration, spinner's speed and spinning time results in a uniform 2.5 μm thick piezoelectric polymer layer having $<1\%$ variation across a 4 inch Si wafer. The same recipe is used in the POSFETs of the tactile sensing chips presented here. On measuring the thickness of the polymer film on various POSFETs with a profilometer (Zygo NewView 6000), the above mentioned recipe is found to yield uniform polymer film thickness.

The spread among the devices on a wafer is a common problem and a large number of factors are responsible for it. The reader interested in investigating these reasons may refer to standard literature on the device fabrication [6, 7]. The 'spread' among devices means that no two devices on a wafer have the same characteristics—they only have similar characteristics. The degree of dissimilarity is often represented as 'spread'. By carefully following the fabrication steps the spread among devices can be brought down to the permissible limits. The spread among the n-MOS devices on the tactile sensing chip can be obtained from their input characteristics. The threshold voltages (V_{TH}) and transconductance (g_m) values, obtained from the input characteristics of various n-MOS devices, are shown in Fig. 8.2. It can be noticed from figure that V_{TH} and g_m of various POSFETs are fairly uniform. The spread among POSFETs is quite low, if not negligible, and there is need to bring it down further.

The in situ polarizing of the piezoelectric polymer film is another challenge due to the fact that a voltage of 200–250 V is needed to polarize the 2.5 μm thick polymer film. Such high voltages can alter the MOS device characteristics. In addition to this, the uniform polarization of polymer, over all POSFETs, is also desired. These challenges related to polarization were met by adopting the measures highlighted in previous chapter. These measure include: (a) electrical grounding of the substrate and the metal layers under the piezoelectric polymer film of all the POSFETs on the chip; (b) putting the top metal of polymer in all POSFETs at same higher potential; and (c) increasing the potential across piezoelectric polymer in four cumulative steps

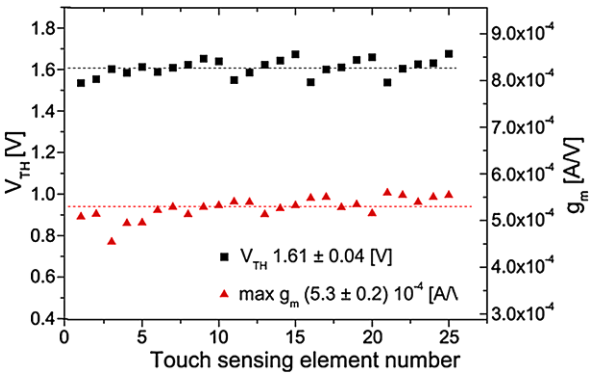

Fig. 8.2 The threshold voltages (V_{TH}) and transconductance (g_m) (at $V_{DS} = 0.5$ V and $V_{GS} = 2.5$ V) of all POSFET elements on the chip

of 50 V each. In this way, uniform polarization can be obtained in all POSFETs—without altering their characteristics. The SEM images of resulting POSFETs array before and after processing the piezoelectric layer are shown in Fig. 8.3.

8.2 Experimental Evaluation

The quantitative and qualitative evaluation of the tactile sensing chips has been carried out by applying dynamic normal forces on single or a group of POSFETs. The experimental arrangement and the source-follower (floating gate) connection scheme of POSFETs in these experiments are same as those used in previous chapter. However, they are again shown here in Fig. 8.4(a)–(b). The POSFET tactile

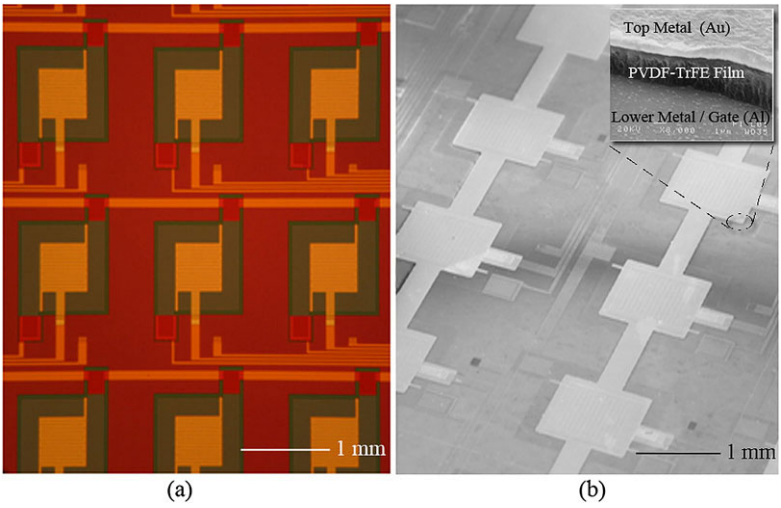

Fig. 8.3 (**a**) A part of the 5 × 5 POSFET tactile sensing array before polymer deposition; (**b**) The SEM image of the POSFET tactile sensing array after polymer film deposition [8]

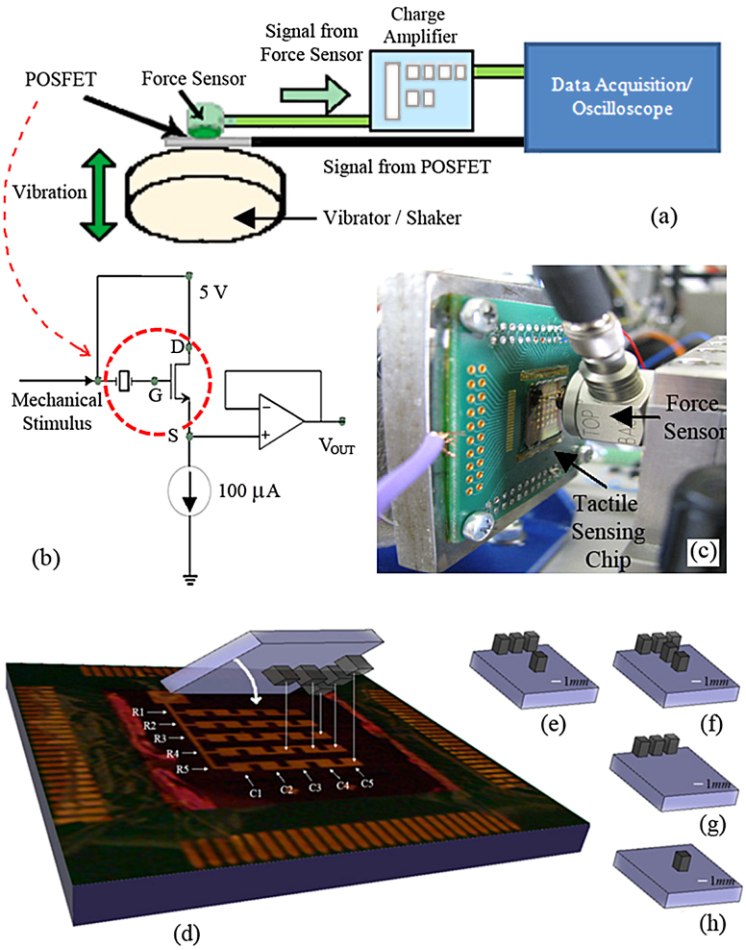

Fig. 8.4 The experimental arrangement. (**a**) The scheme of the experiment set up; (**b**) The connection scheme of POSFETs; (**c**) The image of the experiment set up; (**d**) The placing of the probes on the chip; (**e**)–(**h**) The probes employed for applying the force on single/multiple POSFETs

sensing chip is firmly placed on the TIRA shaker/vibrator, as shown in Fig. 8.4(c). The shaker is driven by a waveform generator. The dynamic force applied to the sensor is measured by an uniaxial PCB—Piezotronics force sensor. The force sensor is anchored to a manual 3D micrometer positioning device, which facilitates placing the probe right on the desired POSFETs. The 1 mm^2 sized probes are attached to the force sensor and they are employed to apply the dynamic forces on single/multiple POSFETs—as shown in Fig. 8.4(d). Various probes used for evaluating the performance of tactile sensing chips are given in Fig. 8.4(e)–(h). These probes are obtained with Eden250 3D printing system that provides high quality rapid prototyping with typical tolerance of 100 µm. During the experiments, the

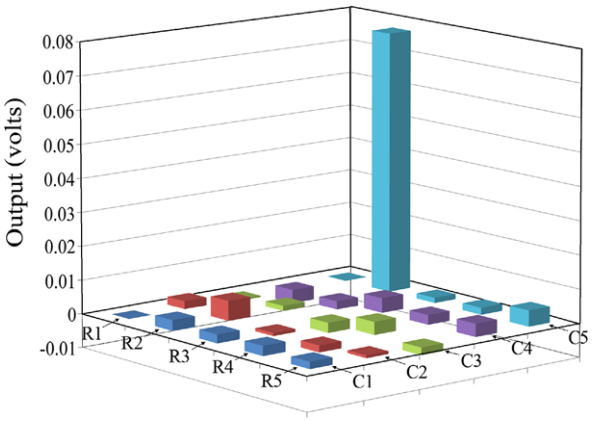

Fig. 8.5 The snap-shot of the outputs of all the POSFETs on the array at the moment when output of POSFET (2,5) is maximum. A 20 Hz sinusoidal force is applied only on the POSFET (2,5)

chip is covered with a 200 μm PDMS protective film. A pre-load is also used in some of the experiments to avoid loss of contact between the POSFETs and the probe. The outputs of the POSFETs and the force sensor are acquired with NI Data Acquisition board NI6259 that can synchronously acquire up to 32 analog inputs and 4 analog outputs with 16 bits of resolution and single-channel sampling rate of 1.25 MS/s.

8.2.1 Experiments with Single POSFET Device

Before putting the tactile sensing chips to use, it is useful to quantify the response of tactile sensing elements in terms of gain/sensitivity and range of stimuli etc. For this purpose, individual POSFETs (one at a time) on the chip were evaluated. The experimental conditions for these experiments were similar to that reported in previous chapter. Likewise, the experimental results too were found to be agreement with those reported in previous chapter. For this reason, the results related to single POSFETs are not presented here and reader may refer to previous chapter for more details.

An additional experiment related to single POSFET is to investigate the cross-talk among the sensing devices on the array. For this purpose, a dynamic force can be applied on a particular POSFET and the outputs of all the POSFETs on the array is recorded at the same time. Applying a 20 Hz sinusoidal force on the POSFET labeled (2,5), using a probe similar to the one shown in Fig. 8.4(h), results in the array of outputs shown in Fig. 8.5. The outputs shown in this figure, refer to the moment when response of POSFET (2,5) is maximum. The X and Y, in a label (X, Y), refer to the row and the column of the array respectively. From Fig. 8.5 it is clear that the outputs of POSFETs other than the one labeled (2,5) are negligible and so is the cross-talk. In a sense this also means that the tactile sensing chip can provide accurate location of the contact and good spatial resolution. The negligible cross-talk and good spatial resolution are desired for better shape/object recognition.

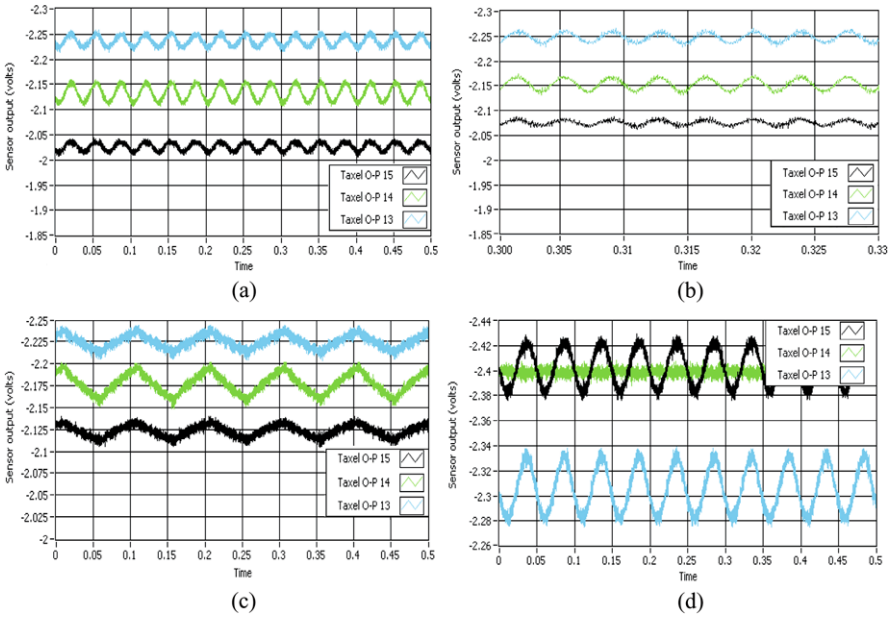

Fig. 8.6 (**a**) The outputs of POSFETs (1,3), (1,4) and (1,5) for a 30 Hz sinusoidal applied force; (**b**) The outputs of the same POSFETs for a 270 Hz sinusoidal applied force; (**c**) The outputs of the same POSFETs for a 10 Hz triangular force; (**d**) The outputs of the same POSFETs for a 20 Hz sinusoidal applied force. In this case force is applied only on POSFETs (1,3) and (1,5)

8.2.2 Experiments Involving Multiple POSFETs

The previous section presents a snap-shot of the outputs of the POSFETs on the chip when force is applied only on one of them. That experiment is repeated here, but with force applied simultaneously on multiple POSFETs. Measuring the response of all POSFETs while force is applied on the selected few, one may investigate the degree of cross-talk and the variation among outputs of POSFETs. Some of the measurements made by applying dynamic normal force on multiple POSFETs are shown in Fig. 8.6.

The plots shown in Fig. 8.6(a)–(b) have been obtained by applying sinusoidal forces in normal direction on the top of POSFETs (1,3), (1,4) and (1,5)—which form a small line. The frequency of applied force in these experiment varied between 10 and 270 Hz. Using a snap-shot of these outputs, at a particular moment, one may conveniently say that response is because of a line contact. This observation is true even at higher frequencies of applied force—as evident from Fig. 8.6(b). The observations also hold if the applied force is triangular instead of sinusoidal—as evident from Fig. 8.6(c), which shows the output of POSFETs when applied force varies in triangular form. The outputs of POSFETs (1,3), (1,4) and (1,5), when a 20 Hz sinusoidal force is applied only on POSFETs (1,3) and (1,5), are shown in Fig. 8.6(d). As the spacing between two adjacent POSFETs is just 0.5 mm, one might

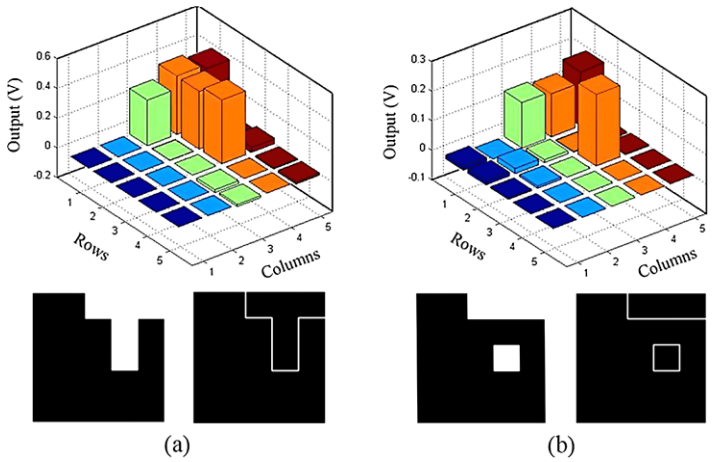

Fig. 8.7 The response of POSFETs when force is applied using (**a**) 'T' probe of Fig. 8.4(e); (**b**) partial 'T' probe of Fig. 8.4(f)

expect some output from POSFET (1,4) due to undesired feature such as cross-talk etc. However, such spurious output is absent in the plots shown in Fig. 8.6(d). These results indicate that the tactile sensing chips have low or negligible cross-talk and the high spatial resolution (< 1 mm).

The response of various POSFETs to a 670 Hz sinusoidal force, applied on the POSFETs (1,3), (1,4), (1,5), (2,4), and (3,4), is shown in Fig. 8.7(a). The POSFETs (1,3), (1,4), (1,5), (2,4), and (3,4) all-together make a 'T' shape. The 'T' shaped probe of Fig. 8.4(e) is employed in this case for applying the force. In Fig. 8.7(a), the POSFETs pressed by the probe can clearly be differentiated from others. The variation among the responses of the POSFETs that were pressed is low (maximum of 18.1 mV is recorded for POSFET (3,4) and minimum 16.4 mV from POSFET (1,3)) and as expected they are in phase. A snap-shot of the bar and binary images, obtained from the normalized response of various POSFETs is also shown in Fig. 8.7(a). Similar outputs is observed with 20, 120, 370 Hz sinusoidal forces. The same experiment when repeated with the probe of Fig. 8.4(f) results in the response given in Fig. 8.7(b). The negligible output of POSFET (2,4), in Fig. 8.7(b), is in tune with the results presented in Fig. 8.6(d). These result validate the high spatial resolution (< 1 mm)—for which, the chip is designed. The data obtained from these experiments is also used to detect the edges of the contact. The edge detection results, carried out using gradient operators, are also shown in Fig. 8.7.

The experimental results presented above extensively evaluate the performance of tactile sensing chips. These experimental studies involve the application of dynamic normal force on selected POSFETs or the selected points in space, whereas a real world stimulus generally varies both in time and space. Therefore, it is also important to see if and how much effective are the tactile sensing chip when they are subjected to such a stimuli. As an example, would it be possible to detect or reproduce the motion of an object if it rolls over the chip—as in Fig. 8.8. In case

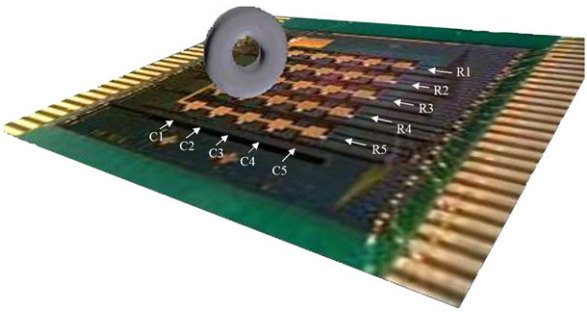

Fig. 8.8 A *ring* bearing rolling over the diagonal POSFET devices on the chip

of rolling the contact point moves over one POSFET to next and therefore involves both spatial and temporal variations. With this in mind, the performance of the chip is evaluated by rolling a probe manually over the diagonal POSFETs on the array. The probe used in this experiment is a ring bearing that is 3 mm wide and has outer diameter of 1.5 cm. The width of probe is good enough to fully cover and press the diagonal POSFETs and partially the adjacent ones (immediately next to diagonal POSFETs). The representative arrangement of the experiment is shown in Fig. 8.8. Since the probe is rolled manually, the force applied in this experiment is not controlled as it is hard keep it constant. In this context, the results from this experiment are qualitative in nature. The response of various POSFETs is shown in Fig. 8.9(a)–(b). The response of diagonal POSFETs is higher than that of the off-diagonal elements as they were fully covered by the probe. The maximum response of the diagonal POSFETs is around 0.15 V. The response of adjacent POSFETs is less than half of this value. The minor variations among the outputs of diagonal POSFETs is mainly because the controlled force is not applied. The contact sequence reproduced from the POSFETs' responses is shown in Fig. 8.9(c)–(j). It clearly demonstrates the capability of tactile sensing chip to detect dynamic contact events that are distributed, both, in space and time. The time period (from t1 to t17; from t2 to t18 etc.) of 0.41 sec for one rolling cycle (i.e. back and forth rolling of diagonal elements) obtained from Fig. 8.9 is found to be in good agreement with the actual travel time of 0.416 sec. A total of six rolling cycles are completed in period of 2.5 seconds shown in Fig. 8.9(a). Thus, the tactile sensing chips presented here are also capable of detecting the complex dynamic contact events like rolling of an object.

8.2.3 Temperature Measurement

In addition to the array of POSFET devices, each tactile sensing chips contains two temperature diodes that can be used to measure the ambient as well as contact temperatures. The performance of temperature diodes can be evaluated from the diode characteristics at various temperatures. The characteristic plots of the temperature diodes at various temperatures, in the range 25°C–75°C, are given in Fig. 8.10(a).

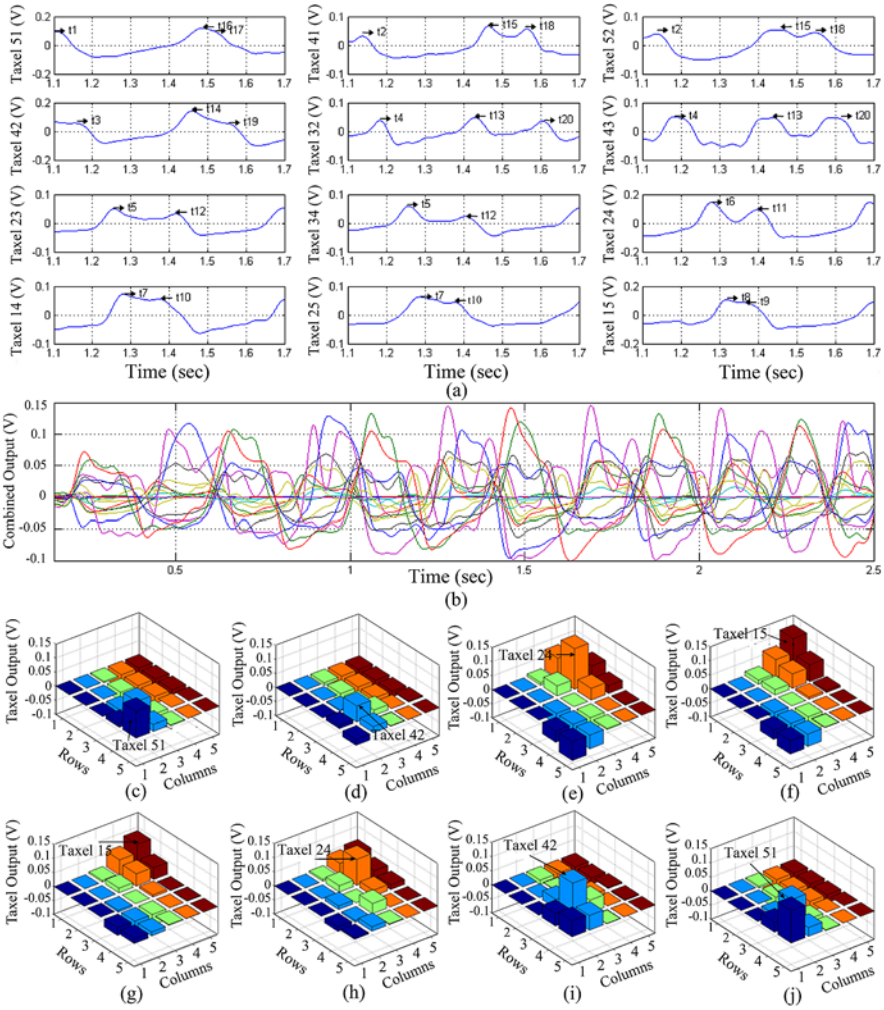

Fig. 8.9 (**a**) The outputs of all POSFETs (or taxels) on the chip when probe is rolled over the diagonal elements. The time t1–t8 refer to the instants of maximum outputs when probe rolls over the POSFETs from (5,1) toward (1,5). Similarly, t9–t17 refer to instants when probe rolls in the opposite direction; (**b**) The outputs of diagonal and adjacent POSFETs during the period between t1=1.1 sec and t21=1.7 sec; (**c**)–(**j**) The snap-shots of the outputs at instants: t1 → t3 → t6 → t8 and t9 → t11 → t14 → t16. The POSFET (3,3) on the chip is not working

Using these plots one can obtain the diode potentials at a fixed diode current, but at different temperatures. In this manner, the diode potential is related to the contact temperature and changes in diode potentials is used to obtain the changes in temperature. In case of tactile sensing chip presented here, the temperature diodes are designed for forward bias current of 100 μA and hence the same is used to obtain the relation between diode potential and temperature. The variation of diode output

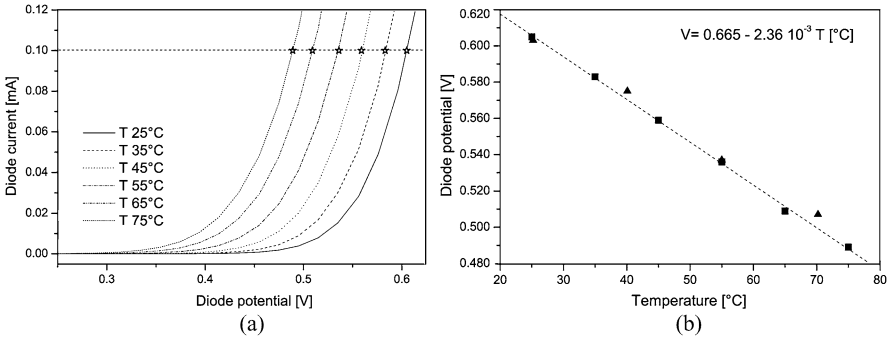

Fig. 8.10 (**a**) The characteristics plots of a temperature diode at various temperatures; (**b**) The output of the diode at various temperatures. The diode current value is 100 μA

(i.e. diode potential) with the temperature is shown in Fig. 8.10(b). It is clear from the figure that the temperature diode output is linear with sensitivity of 2.36 mV/°C.

It should be noted that even if the temperature diodes have primarily been integrated on the chip to measure the contact temperatures, they can also be used to detect variations in the ambient temperature. The latter gains significance in the light of the fact that P(VDF-TrFE) polymer also exhibits pyroelectric behavior i.e. the variations in the ambient temperature also results in the generation of charge [9, 10]. This means that while measuring contact forces any variation in the contact or ambient temperature could introduce error in the POSFET's output. Such errors can be mathematically compensated by using the value of temperature variation recorded by the diode and relating the same with the database carrying the response of P(VDF-TrFE) at various temperatures. In this regard, the presence of temperature diodes is especially useful when the chip is put to use in a real world environment.

8.3 Future Dimensions

The experimental result presented in this chapter, as well as in previous chapter, tell a great deal about the utility of POSFETs based tactile sensing chips. However, it is worthwhile to note that the chips are yet to employed in a real world environment. There are many challenges to be overcome before that happens. As an example, it is desirable to have digital and reduced amount of data coming out of the chip. Digitizing the signal on the chip certainly helps in reducing the number of wires needed to transfer the data to other levels of processing. Reduced number of wires are highly desirable in applications like robotic hands where large number of wires can counter the dexterity of the hand. Similarly, it is desirable to reduce the data coming out of the chip—not only to efficiently utilize the communication channel but also for optimum usage of the limit computational throughput. The data coming out of the chip can either be reduced by rejecting any redundant data on the chip itself or by locally processing the raw data on the chip. Similarly, it is also desired

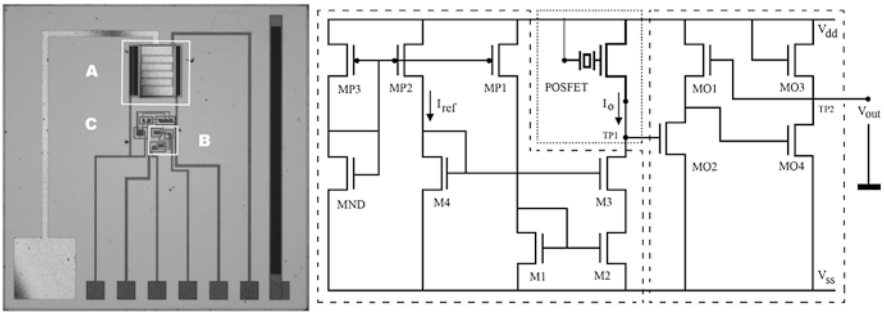

Fig. 8.11 (*left*) The image of the chip with a POSFET tactile sensing chip (*A*) and the integrated electronics (*B*) and the high compliance current sink (*C*). (*right*) The circuitry scheme of the chip. POSFET is used in source-follower (floating gate) configuration, connected to a current sink (on the *left side*) and an output buffer (on the *right side*), highlighted with *dashed contours*

to have touch or tactile sensing structure that can bend, stretch and conform to any surface. All these desired requirements become important especially when touch sensors or tactile sensing arrays are to be spread over large areas. The reader may refer to Chap. 4 *(on system issues)*, where some related issues are discussed. The work in this section is related to some of the recent advances on POSFETs and related research.

8.3.1 Toward Tactile Sensing System On-Chip

8.3.1.1 POSFET Device with On-Chip Signal Conditioning Module

One of the recent additions to the advances on POSFET research, is the design of new POSFET tactile sensing devices with on-chip electronics and its implementation using CMOS technology [11]. The chip shown in Fig. 8.11 consists of POSFET device and the integrated bias and signal conditioning circuitry to obtain a compact miniaturized system, keeping in view the system level extension planned for the future. In particular, a high compliance current sink and an output buffer have been integrated. The high compliance current sink provides the current I_{DS} ($= 90$ μA) for the POSFET device and the output buffer help in impedance matching and decoupling the sensing device from the chip output. Furthermore, for large transconductance the n-MOS device in POSFET has also been redesigned with an aspect ratio (W/L) of 273. The POSFET device has been designed to have an active area of 0.9 mm $\times$ 0.6 mm so as to obtain spatial acuity comparable to that of human fingertips ($\sim$1 mm). The large value of channel width (W) is obtained by designing a serpentine like or interdigitated gate structure, similar to the one shown in the layout in Fig. 8.1(a). The length of source and drain diffusions has been reduced in the new design to reduce the source and drain parasitic resistance by a factor 5, which reflects a significant improvement of the actual transconductance over

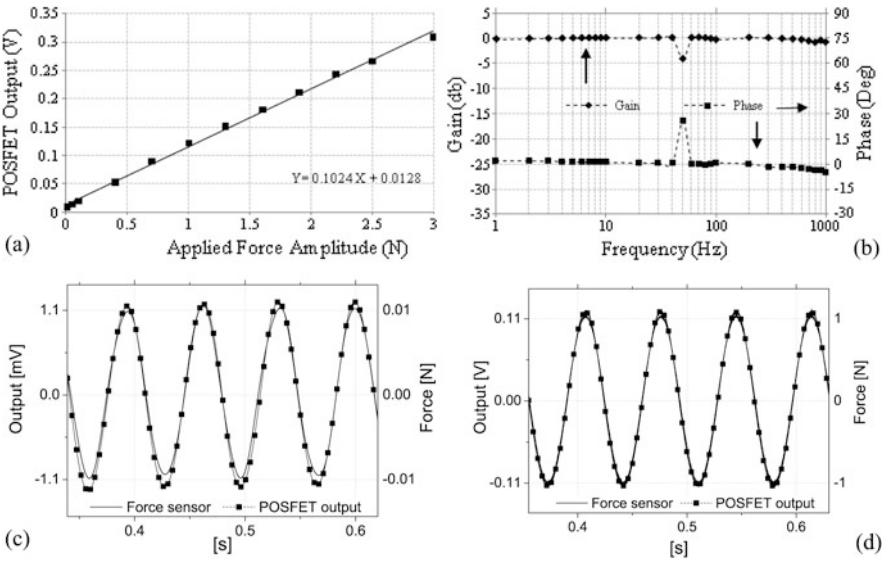

Fig. 8.12 (**a**) The response of POSFET tactile sensing device to normal dynamic forces in the range 0.01–3 N; (**b**) The gain-phase plots. The peaks at 50 Hz are due to the 50 Hz electrical noise; (**c**) The output of POSFET when 0.01 N, 15 Hz sinusoidal force is applied; (**d**) The output of POSFET when 1 N, 15 Hz sinusoidal force is applied

the previous version of POSFET. In the chosen circuitry implementation, shown in Fig. 8.11, the POSFET is connected in source follower configuration. In operative conditions the FET gate i.e. the lower electrode of the P(VDF-TrFE) piezoelectric film is floating and the top contact is short-circuited to drain. The chosen source-follower configuration does not provide amplification like a common source configuration. Nonetheless, this configuration provides higher output robustness to gain mismatches between different devices, which is useful when an arrays of sensors is used.

The response of POSFET devices to normal dynamic forces in the range 0.01–3 N is given in Fig. 8.12. The new POSFET devices are capable of detecting contact forces as low as 0.01 N (∼1 gmf), with negligible delay between input force and output of POSFET. It should be noted that the POSFET outputs in the results presented here are unamplified. The response plot is linear in the tested range and the sensitivity of POSFET devices is 102.4 mV/N—which is more than twice the value for previous version of POSFET device. Therefore, the on chip electronic module and redesigned POSFET have resulted in an improved sensitivity. The gain-phase plots are flat in the tested frequency range of 1–1000 Hz.

8.3.1.2 POSFET Array with On-Chip Electronics

Another extension of the POSFET research is toward the tactile sensing chips consisting of tactile sensing arrays and on-chip electronics. The scheme of the new

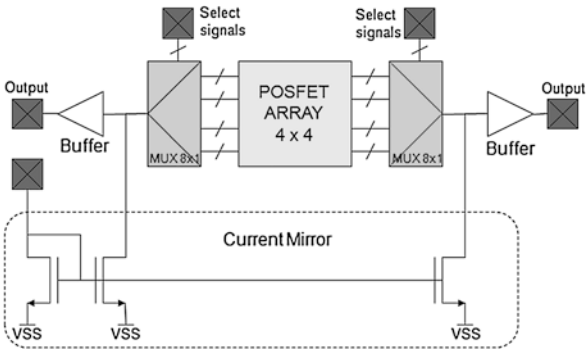

Fig. 8.13 The scheme of the POSFET tactile sensing chip with biasing and array interface circuits

POSFET tactile sensing chip is given in Fig. 8.13. In addition to the POSFETs array, the new scheme also includes the biasing and interface circuitry. The new scheme has a reduced number of sensing elements (4×4) in the POSFETs array. The choice of 4×4 array is better than 5×5 as it results in an optimum usage of the read out circuitry. The scheme of new tactile sensing chip, given in Fig. 8.13, has a POSFET array, two multiplexors, two current mirrors and output buffers. Going by the earlier POSFET connection scheme, shown in Fig. 8.4(b), sixteen current sources would be required on the chip. If followed, this would mean a large area on the chip would be consumed by the current sources. Therefore, to save the silicon area, only two current mirrors are used in the new scheme. These current mirrors bias a given POSFET only when it is addressed for reading, i.e. when a POSFET is addressed it is biased as well (through the output of current mirror) [12]. The new scheme has two independent reading channels, for reading even and odd POSFET devices. The independent reading channels are employed to speed up the array scanning. When a particular POSFET is addressed and being read (e.g. an even numbered POSFET) the next (odd numbered POSFET) is biased at the same time. In this way, the transients related to biasing of the next (i.e. odd numbered) POSFET device does not increase the acquisition time. The output buffers in the new scheme provided impedance adaptation.

The layout of new tactile sensing chip, following the scheme presented in Fig. 8.13, is given in Fig. 8.14 [13]. As mentioned earlier, the chip consists of a 4×4 POSFET array, two multiplexors, two current mirrors and output buffers. The size of POSFET array has been reduced to 4×4—which has made available more space for on chip read out circuitry. The POSFET devices have been designed to be compatible with the CMOS (Complementary Metal Oxide Semiconductor) technology. The overall dimension of this tactile sensing chip is 0.8 cm $\times$ 1.0 cm, size of each POSFET is 0.9 mm $\times$ 0.9 mm, and the aspect ratio is high (Channel width, $W = 3096$ μm; Channel length, $L = 18$ μm). With center to center distance of 1 mm between adjacent POSFETs, the tactile arrays will have human fingertip like spatial resolution. The biasing and interface circuits are integrated with the array on the chip. To save the silicon area, only two current mirrors have been implemented. The output buffers too have been implemented on the chip for impedance adaptation. Many other test structures and chip architectures, not shown in Fig. 8.14, have also

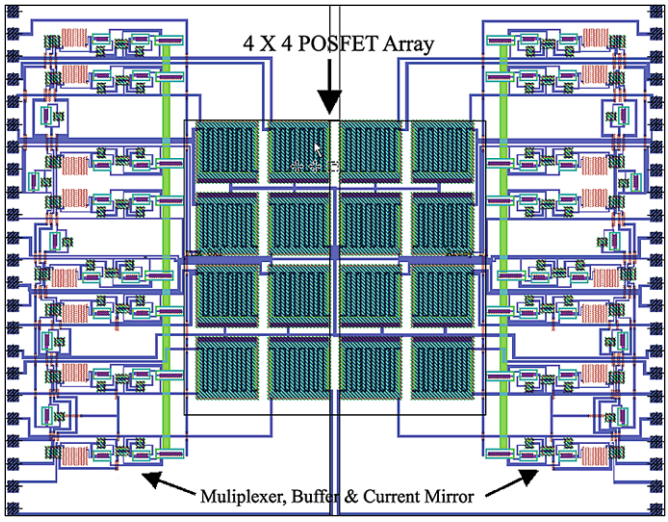

Fig. 8.14 The layout of the tactile sensing chip with integrated electronics and POSFET array

been designed and will fabricated on the same wafer. After fabrication and required optimization steps, the tactile sensing chips can be used at places like fingertips of a robot. With these advances, the POSFET devices based tactile sensing system on chip can potentially provide the much required tactile analogous of the CMOS optical array.

8.3.2 Toward Bendable Tactile Sensing Chip

The aforementioned POSFET devices based tactile sensing chips are fabricated on planar silicon. However, in Chap. 4 it is argued that any tactile sensing structure with sensors distributed in an area should be mechanically flexible so as to conform to the body parts of a robot or any 3D surface. Therefore, obtaining the mechanically flexible tactile sensing chips is an important future direction of the POSFET research. To this end, the potential alternatives include the fabrication of tactile sensing chips following the 'chip-on-flex' concept. With this approach, the bendable version of POSFET chip is obtained by first fabricating the devices on the SOI (Silicon on Insulator) wafers and then etching the oxide under the thin top silicon layer. Following this step the chip is finally transferred to flexible receiver substrates. Another interesting approach is to follow the nanostructures based route for flexible electronics. The nanostructures based route for flexible electronic systems is particularly interesting as it allows printing of electronics and sensors over unconventional substrates (e.g paper, plastic etc.) and over areas that could be larger than the wafer size. Furthermore, nanostructures can be tailored to sense different type of parameters. In

Fig. 8.15 The envisioned picture of light-weight, ultra-flexible, high-performance and cost-effective electronic skin. The devices in the picture are similar to the POSFET devices presented in this chapter

this approach, the nano-/micro structures are fabricated or synthesized (using top–down or bottom–up approach) of substrates like glass, silicon etc. These structures are then selectively transferred to large and flexible receiver substrates using elastomeric transfer stamps. Once on the receiver substrates, the arrays of nano-/micro structures can be processed to obtain the electronic devices such as TFTs (Thin Film Transistors) [14, 15]. Repeating the procedure, the integrated electronic circuits can be obtained over large areas. The POSFET like devices can also be developed after fabricating the transistors on the flexible substrates. The approach is promising for robotic tactile sensing as it will enable high-performance and cost-effective electronic skin or textile solutions, as envisioned in Fig. 8.15. Furthermore, the skin will be light-weight and ultra-flexible solutions. As an example, if an array of 100 silicon wires (assuming dimensions of each wire to be 2.5 μm × 10 μm × 1000 μm and 10 μm spacing between the wires) is used to develop an electronic or sensing component over a 50 μm thick flexible polyimide (e.g. Kapton) substrate, then the total weight of the structure will be around 7.4 mg/cm^2 (considering the densities of silicon and polyimide to be 2.33 g/cm^3 and 1.42 g/cm^3 respectively. This value is approximately 100 mg/cm^2, if the substrate thickness is considered same as that of average human skin thickness i.e. 0.7 mm. These values are much lower than the per cm^2 weight of human skin (223 mg/cm^2) presented in Chap. 3.

8.4 Summary

The design, fabrication and experimental results from the novel POSFET based tactile sensing arrays have been presented in this chapter. At first glance, the POSFET based tactile sensing arrays—in the present state, do not appear fit to be termed as 'tactile' (strictly following the definition of tactile sensing, presented in Chap. 2) as there is no local processing circuitry. However, a closer look shows that POSFET sensing elements—integral devices comprising of transducer and the electronic unit i.e. transistor, have some inherent processing (although very basic) and hence they are truly 'tactile'. The presence of temperature sensing devices, makes them multi-functional. The integral sensor unit or the POSFET device conforms very well with the 'Sense and Process at the same place' concept, presented in Chap. 4. POSFET based tactile sensing arrays are expected to be more sensitive than those obtained

with similar approaches like the extended gate approach. An argument has also been presented in this regard. The processing of polymer film on the POSFET devices has been successfully achieved, as is evident from various figures and results presented in this chapter. The relatively low melting point ($T_m \approx 150°C$) of P(VDF-TrFE) and the fact that melting point may destroy the device, places the tightest constraints on chip packaging, post-processing and assembly conditions. Certain fabrication steps like in situ polarization of the polymer film are challenging and should be performed carefully in order to ensure higher yield. It is observed that the tactile sensing array presented here have good spatial resolution ($\sim$1 mm) and a linear dynamic response over wide range of forces. The POSFET devices, in a source-follower configuration, has been tested for a wide range of input forces (0.2–5 N) and wide range of frequencies (2 Hz–2.13 kHz). It is observed that the average response of a POSFET based taxel is 49 mV/N—which can be higher if the same POSFET device is used in common-source configuration. The new version of POSFETs, with on-chip electronics, has an improved sensitivity of 102 mV/N, which is more than twice the previous value. Better spatial resolution allows the detection of contact point and contact image, more accurately, which has been demonstrated with a number of plots. The results presented here are promising and to fully exploit the advantages and capabilities of POSFET based tactile sensing arrays, more experiments—like detecting complex object shape and the ability to detect shear forces etc., are needed to be performed. The POSFET based tactile sensing chips, presented in simplest form, can be easily extended to accommodate read-out circuitry and some local processing circuitry. To this end, POSFETs with on-chip electronics have already been fabricated. The POSFET based approach provides a strong basis for having a SIP/SOC, which can potentially solve the wiring complexity also.

The POSFET tactile sensing chips are primarily meant to be used for robotic body sites such as fingertips. However, with some changes in the design and distribution of POSFETs, they can also be employed other applications such as biomedical instrumentation and wearable textiles. For instance, due to presence of piezoelectric polymers, parameters like pulse rate, heart beat and body temperature etc. can be detected with POSFETs, after some modifications. Humidity, which is known to affect the output of piezoelectric polymers, could be another parameter. Among others, the requirement of mechanical flexibility is the most important feature needed for making POSFETs suitable for these applications.

References

1. R.S. Dahiya, G. Metta, M. Valle, G. Sandini, Tactile sensing—from humans to humanoids. IEEE Trans. Robot. **26**(1), 1–20 (2010)
2. R.S. Dahiya, Human-inspired tactile sensing, in *Learning from Nature: Biologically-Inspired Sensors*, ed. by D.H.B. Wicaksono, P. French (Springer, Berlin, 2011), pp. 455–476
3. R.S. Dahiya, M. Valle, G. Metta, L. Lorenzelli, A. Adami, Design and fabrication of POSFET devices for tactile sensing, in *Proceedings of TRANSDUCERS 2009—The 15th IEEE International Conference on Solid-State Sensors, Actuators and Microsystems* (2009), pp. 1881–1884

4. R.S. Dahiya, G. Metta, M. Valle, L. Lorenzelli, A. Adami, Piezoelectric oxide semiconductor field effect transistor touch sensing devices. Appl. Phys. Lett. **95**(3), 034105 (2009)
5. R.S. Dahiya, M. Valle, L. Lorenzelli, G. Metta, S. Pedrotti, Deposition processing and characterization of PVDF-TrFE thin films for sensing applications, in *Proceedings of IEEE Sensors 2008* (2008), pp. 490–493
6. G.S. May, S.M. Sze, *Fundamentals of Semiconductor Fabrication* (Wiley, New York, 2003)
7. R.C. Jaeger, *Introduction to Microelectronic Fabrication*. Modular Series on Solid State Devices, vol. 5 (Prentice Hall, New York, 2001)
8. R.S. Dahiya, L. Lorenzelli, G. Metta, M. Valle, POSFET devices based tactile sensing arrays, in *Proceedings of 2010 IEEE International Symposium on Circuits and Systems (ISCAS)* (2010), pp. 893–896
9. H.S. Nalwa, *Ferroelectric Polymers: Chemistry, Physics, and Applications* (Marcel Dekker, Inc., New York, 1995)
10. R.S. Dahiya, M. Valle, L. Lorenzelli, SPICE model of lossy piezoelectric polymers. IEEE Trans. Ultrason. Ferroelectr. Freq. Control **56**(2), 387–396 (2009)
11. A. Adami, R.S. Dahiya, C. Collini, D. Cattin, L. Lorenzelli, POSFET touch sensor with on-chip electronic module for signal conditioning, in *The 16th International Solid-State Sensors, Actuators and Microsystems Conference (TRANSDUCERS)*, Beijing, China (2011), pp. 1982–1985
12. L. Barboni, R.S. Dahiya, G. Metta, M. Valle, Interface electronics design for POSFET devices based tactile sensing system, in *IEEE RO-MAN 2010, 19th IEEE International Symposium in Robot and Human Interactive Communication*, Viareggio, Italy (2010), pp. 1–6
13. R.S. Dahiya, A. Adami, M. Valle, L. Lorenzelli, G. Metta, CMOS implementation of POSFET tactile sensing arrays with on chip readout, in *SENSORCOMM 2010: The Fourth International Conference on Sensor Technologies and Applications*, Venice, Italy (2010), pp. 80–83
14. R.S. Dahiya, A. Adami, L. Lorenzelli, Fabrication of single crystal silicon micro-/nanowires and transferring them to flexible substrates, in *The 37th International Conference on Micro and Nano Engineering (MNE 2011)*, Berlin, Germany (2011), pp. 1–2
15. D.-H. Kim, J.-H. Ahn, W.M. Choi, H.-S. Kim, T.-H. Kim, J. Song, Y.Y. Huang, Z. Liu, C. Lu, J.A. Rogers, Stretchable and foldable silicon integrated circuits. Science **320**, 507–511 (2008)

Appendix A
Fundamentals of Piezoelectricity

Abstract The objective of this chapter is to help understand the main concepts and working of piezoelectric sensors and transducers. Accordingly, the chapter presents a simplified explanation of the piezoelectric phenomenon. The chapter begins with a brief overview of some historical milestones, such as the discovery of the piezoelectric effect and the utilization of piezoelectric materials in various applications. Various mechanisms involved in the polarization of dielectric, ferroelectric and piezoelectric materials are discussed. The piezoelectric effect has been explained with basic mathematical formulations based on the intermingling of electric and elastic phenomena. In essence, the chapter describes the basic concept of piezoelectric phenomena that one needs to know while using piezoelectric materials as transducers. For detailed theory on piezoelectric phenomenon, one may refer to standard literature on piezoelectricity (Mason in Electromechanical Transducers and Wave Filters, 1942; Mason in Physical Acoustics and the Properties of Solids, 1958; Cady in Piezoelectricity, 1946; Nalwa in Ferroelectric Polymers: Chemistry, Physics, and Applications, 1995; Ikeda in Fundamentals of Piezoelectricity, 1996).

Keywords Piezoelectricity · Dielectric · Ferroelectric · Piezoelectric · Piezoelectric effect · PVDF · PVDF-TrFE · Piezoelectric polymers · Smart materials · Sensors · Actuators

A.1 Introduction and Historical Perspective

The name "piezo" derives from the Greek, meaning "to press"; in more modern terminology, we say that the effect intermingles electric and elastic phenomena. Discovered by Curie brothers [6], the piezoelectricity rapidly grew as a new field of research in the last quarter of the nineteenth century. In 1880, Pierre and Jacques Curie found that in certain materials such as zincblende, topaz, and quartz, mechanical stresses were accompanied by macroscopic polarization and hence the production of electric surface charges. The following year, Lippmann [7], from thermodynamic considerations, predicted the converse effect: an imposed voltage produces mechanical deformations or strains the material. The piezoelectric effect remained a curiosity until the early 1920's when its presence in quartz was utilized to realize crystal resonators for the stabilization of oscillators, thereby launching the field of

R.S. Dahiya, M. Valle, *Robotic Tactile Sensing*,
DOI 10.1007/978-94-007-0579-1,

frequency control [3]. With the introduction of quartz control, timekeeping moved from the sun and stars to small, man-made sources that exceeded astronomy based references in stability. Since then the advent of the man-made piezoelectric materials widened the field of applications and devices based on piezoelectricity are used in sonar, hydrophone, microphones, piezo-ignition systems, accelerometers and ultrasonic transducers. The discovery of a strong piezoelectric effect in polyvinylidene fluoride (PVDF) polymer, by Kawai in 1969 [8], further added many applications where properties such as mechanical flexibility are desired. Today, piezoelectric applications include smart materials for vibration control, aerospace and astronautical applications of flexible surfaces and structures, sensors for robotic applications, and novel applications for vibration reduction in sports equipment (tennis racquets and snowboards). Recently, the newer and rapidly burgeoning areas of utilization are the non-volatile memory and the integral incorporation of mechanical actuation and sensing microstructures (e.g. POSFET devices) into electronic chips.

A.2 Dielectric, Ferroelectric and Piezoelectric Materials

A.2.1 Electric Polarization

One of the concepts crucial to the understanding of dielectric, ferroelectric and piezoelectric materials is their response to an externally applied electric field. When a solid is placed in an externally applied electric field, the medium adapts to this perturbation by dynamically changing the positions of the nuclei and the electrons. As a result, dipoles are created and the material is said to undergo polarization. The process of dipole formation (or alignment of already existing permanent or induced atomic or molecular dipoles) under the influence of an external electric field that has an electric field strength, E, is called polarization. There are three main types or sources of polarization: electronic, ionic, and dipolar or orientation. A fourth source of polarization is the interfacial space charge that occurs at electrodes and at heterogeneities such as grain boundaries. For an alternating electric field, the degree to which each mechanism contributes to the overall polarization of the material depends on the frequency of the applied field, as shown in Fig. A.1. Each polarization mechanism ceases to function when the applied field frequency exceeds its relaxation frequency.

Electronic polarization may be induced to one degree or another in all atoms. It results from a displacement of the center of the negatively charged electron cloud relative to the positive nucleus of an atom by the electric field, as indicated in the bottom-right of Fig. A.1. This polarization type is found in all dielectric materials, and, of course, exists only while an electric field is present. Ionic polarization occurs only in materials that are ionic. An applied field acts to displace cations in one direction and anions in the opposite direction, which gives rise to a net dipole moment. This phenomenon is illustrated in right-center of Fig. A.1. The third type, orientation polarization, is found only in substances that possess permanent dipole

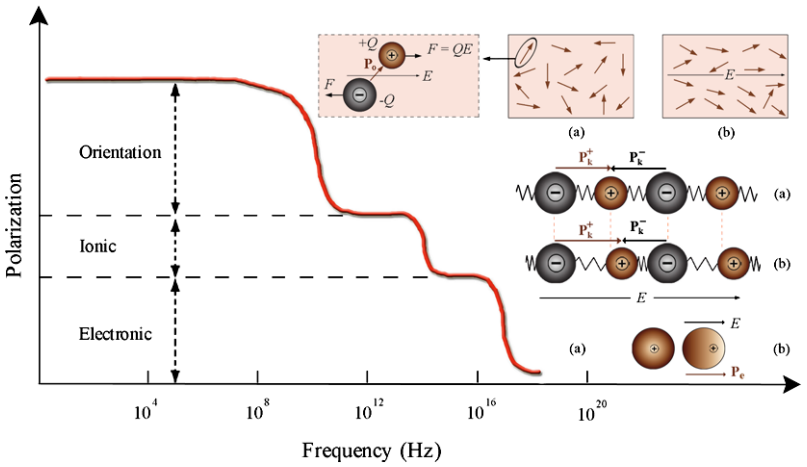

Fig. A.1 Frequency dependence of various polarization mechanisms. The electronic, ionic, and orientation polarization mechanisms are indicated

moments. Polarization results from a rotation of the permanent moments into the direction of the applied field, as represented in top-right of Fig. A.1.

The total electric polarization of a substance is equal to the sum of the electronic, ionic, and orientation (and space-charge) polarizations. It is possible for one or more of these contributions, to the total electric polarization, to be either absent or negligible in magnitude relative to the others. For example, ionic polarization will not exist in covalently bonded materials in which no ions are present. The average polarization per unit volume, $\overrightarrow{P}$, produced by N little electric dipoles (of the electric dipole moment, $\overrightarrow{p}$) which are all aligned, is given by:

$$\overrightarrow{P} = \frac{1}{Volume} \sum_{k=0}^{N} \overrightarrow{p_k} \tag{A.1}$$

A.2.2 Dielectric Materials

A dielectric material is one that is electrically insulating (nonmetallic) and exhibits or may be made to exhibit an electric dipole structure; that is, there is a separation of positive and negative electrically charged entities on a molecular or atomic level. The dielectric materials ordinarily exhibit at least one of the polarization types discussed in previous section—depending on the material and also the manner of the external field application. There are two types of dielectrics. The first type is polar dielectrics, which are dielectrics that have permanent electric dipole moments. As depicted in top-right of Fig. A.1, the orientation of polar molecules is random in the absence of an external field. When an external electric field E is present, a torque

is set up and causes the molecules to align with E. However, the alignment is not complete due to random thermal motion. The second type of dielectrics is the non-polar dielectrics, which are dielectrics that do not possess permanent electric dipole moment. Electric dipole moments can be induced by placing the materials in an externally applied electric field. Figure A.1 illustrates the state of non-polar molecules with and without an external field.

Dielectric materials are electrically insulating, yet susceptible to polarization in the presence of an electric field. This polarization phenomenon accounts for the ability of the dielectrics to increase the charge storing capability of capacitors, the efficiency of which is expressed in terms of a dielectric constant.

A.2.3 Ferroelectric Materials

Ferroelectrics are the class of dielectric materials which exhibit spontaneous polarization (polarization associated with a spontaneously formed dipole moment)—that is, polarization in the absence of an electric field. The spontaneous polarization of ferroelectric materials can be switched by applying an electric field; its expression is a typical P–E hysteresis loop similar to that shown in Fig. A.5(a). They undergo a structural phase transition from a high temperature paraelectric into a low-temperature ferroelectric phase at Curie temperature. Ferroelectric materials are the dielectric analogue of ferromagnetic materials, which may display permanent magnetic behavior. There must exist permanent electric dipoles in the ferroelectric materials. Ferroelectrics are a class of the polar piezoelectrics (e.g. polarized PZT, PVDF, and P(VDF-TrFE)) and hence all ferroelectric materials are piezoelectric.

A.2.4 Piezoelectric Materials

Piezoelectrics are the class of dielectric materials which can be polarized, in addition to an electric field, also by application of a mechanical stress (Fig. A.2). This unusual property exhibited by a few dielectric materials is called piezoelectricity, or, literally, pressure electricity. Piezoelectric materials can be divided into polar (which possess a net dipole moment) and non polar piezoelectric materials (whose dipolar moments summed in different directions give a null total moment). A detailed description of the piezoelectric effect is given in following sections.

A.3 The Piezoelectric Effect

The piezoelectric effect, explained with a simple molecular model shown in Fig. A.3, is the generation of an electric charge as a result of a force exerted on

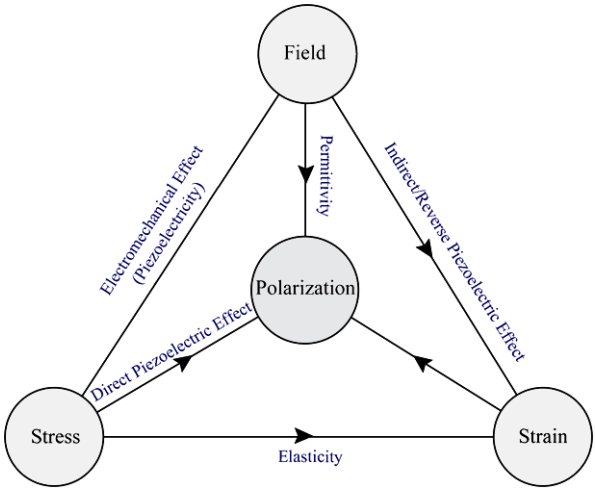

Fig. A.2 Piezoelectricity—An intermingling of electric and elastic phenomena

the material. Before subjecting the material to an external stress the centers of the negative and positive charges of each molecule coincide—resulting into an electrically neutral molecule as indicated in Fig. A.3(a). However, in presence of an external mechanical stress the internal reticular can be deformed, thus causing the separation of the positive and negative centers of the molecule and generating little dipoles as indicated in Fig. A.3(b). As a result, the opposite facing poles inside the material cancel each other and fixed charges appear on the surface. This is illustrated in Fig. A.3(c). That is to say, the material is polarized and the effect called direct piezoelectric effect. This polarization generates an electric field that can be used to transform the mechanical energy, used in the material's deformation, into electrical energy.

Figure A.4(a) shows the piezoelectric material with two metal electrodes deposited on opposite surfaces. If the electrodes are externally short circuited, with a

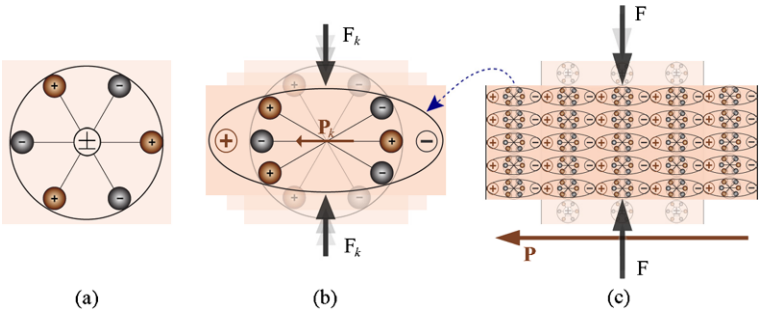

Fig. A.3 Piezoelectric effect explained with a simple molecular model: (**a**) An unperturbed molecule with no piezoelectric polarization (though prior electric polarization may exist); (**b**) The molecule subjected to an external force (F_k), resulting in to polarization (P_k) as indicated; (**c**) The polarizing effect on the surface when piezoelectric material is subjected to an external force

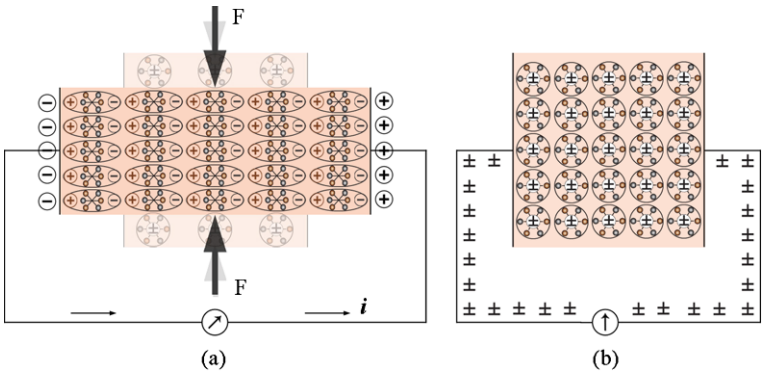

Fig. A.4 Piezoelectric phenomenon: (**a**) The neutralizing current flow when two terminal of piezoelectric material, subjected to external force, are short circuited; (**b**) The absence of any current through the short-circuit when material is in an unperturbed state

galvanometer connected to the short circuiting wire, and force is applied the surface of piezoelectric material, a fixed charge density appears on the surfaces of the crystal in contact with the electrodes. This polarization generates an electric field which in turn causes the flow of the free charges existing in the conductor. Depending on their sign, the free charges will move toward the ends where the fixed charges generated by polarization are of opposite sign. This flow of free charge continues until the free charge neutralizes the polarization effect, as indicated in Fig. A.4(a). This implies that no charge flows in the steady state or in the unperturbed state—irrespective of the presence of external force. When the force on the material is removed, the polarization too disappears, the flow of free charges reverses and finally the material comes back to its original standstill state indicated in Fig. A.4(b). This process would be displayed in the galvanometer, which would have marked two opposite sign current peaks. If short-circuiting wire is replaced with a resistance/load, the current would flow through it and hence mechanical energy would be transformed into electrical energy. This scheme is fundamental to various energy harvesting techniques that tap ambient mechanical energy such as vibrations [9] and convert it into usable electrical form.

Some materials also exhibit the reverse piezoelectric effect i.e. a mechanical deformation or strain is produced in the material when a voltage is applied across the electrodes. The strain generated in this way could be used, for example, to displace a coupled mechanical load. This way of transforming the electrical electric energy into usable mechanical energy is fundamental to the applications such as nano-positioning devices.

A.4 Piezoelectric Materials—Static Actions

The piezoelectric materials are anisotropic in nature and hence their electrical, mechanical, and electromechanical properties differ for the electrical/mechanical ex-

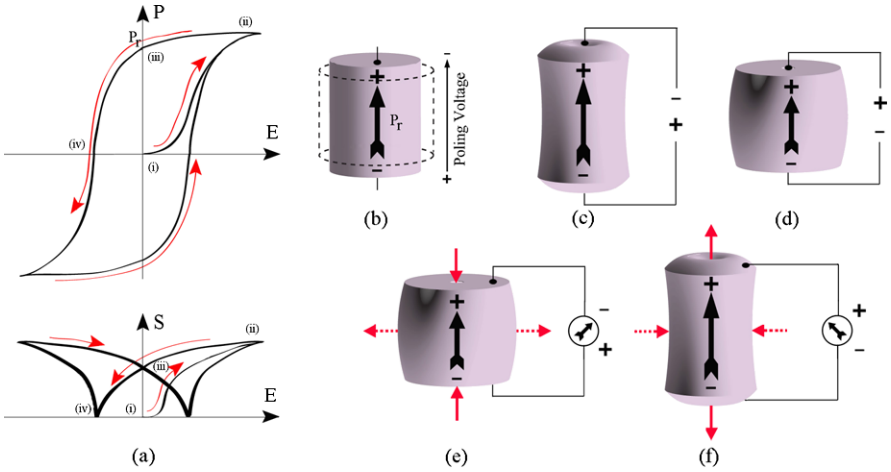

Fig. A.5 Piezoelectric material in sensing and actuating applications. (**a**) Typical P–E hysteresis plot (*top*) and the strain versus electric field plot (*bottom*) of a piezoelectric material. (**b**) The piezoelectric material before (*dotted*) and after poling, albeit change in dimension is exaggerated. The polarity of poling voltage is clearly indicated. (**c**) Material's dimension when applied voltage has polarity similar to that of poling voltage. (**d**) Material's dimension when applied voltage has polarity opposite to that of poling voltage. (**e**) The generated voltage with polarity similar to poling voltage when compressive force is applied in poling direction. (**f**) The generated voltage with polarity opposite to poling voltage when tensile force is applied in poling direction

citations along different directions. Using them in various sensing or actuating applications requires a systematic tabulation of their properties—for which, a standardized means for identifying directions is very important. That is to stay, once the piezoelectric material is chosen for a particular application, it is important to set the mechanical and electrical axes of operation. Wherever crystals are concerned, the orthogonal axes originally assigned by crystallographers are used for this purpose. A general practice to identify the axes is to assign them the numerals e.g. 1 corresponds to x axis; 2 corresponds to y axis, and 3 corresponds to z axis. These axes are set during "poling"; the process that induces piezoelectric properties in the piezoelectric material. The orientation of the DC poling field determines the orientation of the mechanical and electrical axes. The direction of the poling field is generally identified as one of the axes. The poling field can be applied in such as way that the material exhibits piezoelectric responses in various directions or combination of directions. The poling process permanently changes the dimensions of a piezoelectric material, as illustrated in Fig. A.5(b). The dimension between the poling electrodes increases and the dimensions parallel to the electrodes decrease. In some materials, the poling step is also needed for the introduction of piezoelectric effect. For example, in virgin state the piezoelectric materials such as PVDF, P(VDF-TrFE), and ceramics are isotropic and are not piezoelectric before poling. Once they are polarized, however, they become anisotropic.

After the poling process is complete, a voltage lower than the poling voltage changes the dimensions of the piezoelectric material for as long as the voltage is

applied. A voltage with the same polarity as the poling voltage causes additional expansion along the poling axis and contraction perpendicular to the poling axis, as illustrated in Fig. A.5(c). One can also notice this from the P–E and S–E plots shown in Fig. A.5(a). When a poling field, E, is applied across a piezoelectric material, the polarization as well as the mechanical strain curves follow the path (i)–(ii) on the P–E and S–E plots respectively. When the poling field is removed, the path (ii)–(iii) is followed and piezoelectric material retains certain level of polarization, called remanent polarization, P_r, and experiences permanent strain or permanent change in the dimensions. From operational point of view, the poling procedure shifts the working point from (i) to (iii). After this, whenever a voltage with the same polarity as the poling field is applied, the P–E and S–E plots will follow the curve (iii)–(ii) and hence positive strain will be developed, as indicated in Fig. A.5(a). In other words, there is expansion along the poling axis, as shown in Fig. A.5(c). Similarly, when a voltage with the polarity opposite to the poling voltage is applied the P–E and S–E plots will follow the curve (iii)–(iv), resulting in negative strain. As a result, there is contraction along the poling axis and expansion perpendicular to the poling axis, as indicated in Fig. A.5(d). In both cases, however, the piezoelectric material returns to its poled dimensions on the plots (i.e. working point (iii) on Fig. A.5(a)) when the voltage is removed from the electrodes.

If after completion of the poling process, a compressive and tensile force is applied to the piezoelectric material, a voltage is generated as shown in Fig. A.5(d), (e). With an argument similar to that presented in previous paragraph it can be shown that the generated voltage will have the same polarity as the poling field when a compressive force is applied along the poling axis or a tensile force applied perpendicular to the poling axis. This is illustrated in Fig. A.5(e). Similarly, as indicated in Fig. A.5(f), a voltage with the opposite polarity will result when a tensile force is applied along the poling axis, or when a compressive force is applied perpendicular to the poling axis.

The knowledge of the voltage polarities is very helpful before a piezoelectric material is actually put to use. Generally two or more of the above mentioned actions are present simultaneously. In some cases one type of expansion is accompanied by another type of contraction which compensate each other resulting in no change of volume. For example, the expansion of length of a plate may be compensated by an equal contraction of width or thickness. In some materials, however, the compensating effects are not of equal magnitude and net volume change does occur. In all cases, the deformations are, however, very small when amplification by mechanical resonance is not involved. The maximum displacements are on the order of a few micro-inches.

A.5 Piezoelectric Effect—Basic Mathematical Formulation

This section presents basic mathematical formulation describing the electromechanical properties of piezoelectric materials. The presentation is based on the linear the-

ory of piezoelectricity [10], according to which, piezoelectric materials have a linear profile at low electric fields and at low mechanical stress levels.[1] For the range of mechanical stresses and electrical fields used in this book, the piezoelectric materials exhibit the linear behavior.

As explained in previous sections, when a poled piezoelectric material is mechanically strained it becomes electrically polarized, producing fixed electric charge on the surface of the material. If electrodes are attached to the surfaces of the material, the generated electric charge can be collected and used. Following the linear theory of piezoelectricity [10], the density of generated fixed charge in a piezoelectric material is proportional to the external stress. In a first mathematical formulation, this relationship can be simply written as:

$$P_{pe} = d \times T \tag{A.2}$$

where P_{pe} is the piezoelectric polarization vector, whose magnitude is equal to the fixed charge density produced as a result of piezoelectric effect, d is the piezoelectric strain coefficient and T is the stress to which piezoelectric material is subjected. For simplicity, the polarization, stress, and the strain generated by the piezoelectric effect have been specified with the 'pe' subscript, while those externally applied do not have any subscript. In a similar manner, the indirect/reverse piezoelectric effect can be formulated as:

$$S_{pe} = d \times E \tag{A.3}$$

where S_{pe} is the mechanical strain produced by reverse piezoelectric effect and E is the magnitude of the applied electric field. Considering the elastic properties of the material, the direct and reverse piezoelectric effects can alternatively be formulated as:

$$P_{pe} = d \times T = d \times c \times S = e \times S \tag{A.4}$$

$$T_{pe} = c \times S_{pe} = c \times d \times E = e \times E \tag{A.5}$$

where c is the elastic constant relating the generated stress and the applied strain ($T = c \times S$), s is the compliance coefficient which relates the deformation produced by the application of a stress ($S = s \times T$), and e is the piezoelectric stress constant.

A.5.1 Contribution to Elastic Constants

The piezoelectric phenomenon causes an increase of the material's stiffness. To understand this effect, let us suppose that the piezoelectric material is subjected to a

[1] At high electric field or high mechanical stress, they may show considerable nonlinearity.

strain S. This strain will have two effects: One, it will generate an elastic stress T_e, proportional to the mechanical strain ($T_e = c \times S$); and two, it will generate a piezoelectric polarization $P_{pe} = e \times S$ according to Eq. (A.4). This polarization will create an internal electric field in the material E_{pe} given by:

$$E_{pe} = \frac{P_{pe}}{\varepsilon} = \frac{e \times S}{\varepsilon} \tag{A.6}$$

where ε is the dielectric constant of the material. Assuming a compressive stress, applied on the piezoelectric material along the poling direction, it is known from Fig. A.5(d) that the resulting electric field of piezoelectric origin will have a direction same as that of poling field. Further, it is also known from Fig. A.5(c) and related discussion in previous section that the presence of an electric field with polarity same as that of poling field results in positive strain and hence the expansion of piezoelectric material in the poling direction. That is say, the electric field (E_{pe} from Eq. (A.6)), of piezoelectric origin, produces a stress which opposes the applied external stress. This is also true if the external applied stress is tensile in nature. The stress T_{pe} ($= e \times E_{pe}$), produced by the electric field E_{pe}, as well as that of elastic origin, is against the material's deformation. Consequently, the stress generated by the strain S is:

$$T = T_e + T_{pe} = c \times S + \frac{e^2}{\varepsilon} \times S = \left(c + \frac{e^2}{\varepsilon}\right) \times S = \overline{c} \times S \tag{A.7}$$

Thus, piezoelectric effect results in an increased elastic constant or in other words, the material gets stiffened in presence of piezoelectric effect. The constant $\overline{c}$, in Eq. (A.7), is the piezoelectrically stiffened constant.

A.5.2 Contribution to Dielectric Constants

When an external electric field E is applied between two electrodes where a material of dielectric constant ε exists, an electric displacement is created toward those electrodes, generating a surface charge density $\sigma = \sigma_o + \sigma_d$, as shown in Fig. A.6. The magnitude of this electric displacement is $D = \varepsilon \times E$.[2] If the material is piezoelectric, the electric field E also produces a strain, expressed as $S_{pe} = d \times E$. This strain, of reverse piezoelectric origin, can be positive or negative depending on the direction of the external electric field with respect to the poling field. As discussed

[2]The free charge density which appears on the electrodes, will be the sum of the charge density which appears in vacuum plus the one that appears induced by the dielectric effect, i.e.:

$$\sigma = \sigma_o + \sigma_d = \varepsilon_o \times E + \chi \times E = (\varepsilon_o + \chi) \times E = \varepsilon \times E \tag{A.8}$$

where ε_o is the vacuum dielectric permittivity and χ is the dielectric susceptibility of the material.

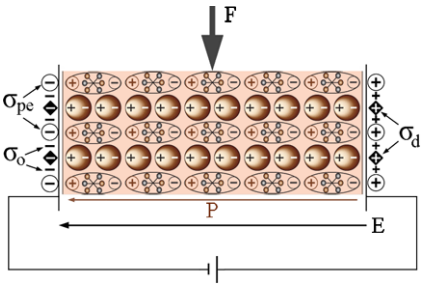

Fig. A.6 Schematic diagram indicating different electrical displacements associated with a piezoelectric and dielectric material

in previous section, if the direction of external field is same as that of poling field, the strain is positive and material undergoes expansion along the direction of poling field. This is illustrated in Fig. A.5(c). It is also evident from Fig. A.5(f) that the expansion of material along poling field (or compression perpendicular to poling field) generates a voltage having polarity opposite to that of poling field or opposite to the external applied field. The situation is similar to the one shown in Fig. A.6. In essence, this means the polarization, and hence the surface charge density, increases when the direction of applied external field is same as that of poling field. In fact, using Fig. A.5(d) and Fig. A.5(e), it can easily be shown that the surface charge density increases even if the direction of applied external field is opposite to that of the poling field. Thus, the strain, of reverse piezoelectric origin, results in polarization and therefore the surface charge density is increased by an amount $P_{pe} = e \times S_{pe} = e \times d \times E$ (Fig. A.6). If the electric field is maintained constant, the additional polarization due to piezoelectric effect increases the electric displacement of free charges toward the electrodes by the same magnitude i.e. $\sigma_{pe} = P_{pe}$. Therefore, the total electrical displacement is:

$$D = \varepsilon \times E + P_{pe} = \varepsilon \times E + e \times d \times E = \overline{\varepsilon} \times E \tag{A.9}$$

where $\overline{\varepsilon}$ is the effective dielectric constant.

A.5.3 Piezoelectric Linear Constitutive Relations

So far, the individual effect of piezoelectricity on the elastic and dielectric has been discussed. In actual practice, piezoelectricity is a cross coupling between the elastic variables, stress T and strain S, and the dielectric variables, electric charge density D and electric field E. This coupling in piezoelectric materials is discussed in this sub-section with help of commonly used linear electro-elastic constitutive equations.

According to the linear theory of piezoelectricity [10], the tensor relation to identify the coupling between mechanical stress, mechanical strain, electric field and electric displacement is given as:

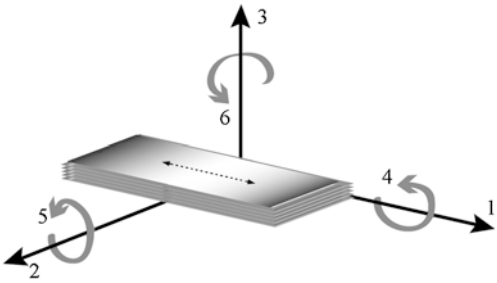

Fig. A.7 Tensor directions for defining the constitutive relations. In PVDF, *1* corresponds to the draw direction (indicated by *dotted line*), *2* to the transverse direction, and *3* to thickness (also the poling axis)

$$S_p = s^E_{pq} T_q + d_{pk} E_k \tag{A.10}$$

$$D_i = d_{iq} T_q + \varepsilon^T_{ik} E_k \tag{A.11}$$

where, s^E_{pq} is elastic compliance tensor at constant electric field, ε^T_{ik} is dielectric constant tensor under constant stress, d_{kp} is piezoelectric constant tensor, S_p is the mechanical strain in p direction, D_i is electric displacement in i direction, T_q is mechanical stress in q direction, and E_k is the electric field in k direction. The common practice is to label directions as depicted in Fig. A.7. In case of materials such as PVDF, the stretch direction is denoted as "l" and the axis orthogonal to the stretch direction in the plane of the film becomes "2". The polarization axis (perpendicular to the surface of the film) is denoted as "3". The shear planes are indicated by the subscripts "4", "5", "6" and are perpendicular to the directions "1", "2", and "3" respectively. Using these directions, Eqs. (A.1) and (A.2) can be displayed in matrix form as follows:

$$\begin{bmatrix} S_1 \\ S_2 \\ S_3 \\ S_4 \\ S_5 \\ S_6 \end{bmatrix} = \begin{bmatrix} s^E_{11} & s^E_{12} & s^E_{13} & s^E_{14} & s^E_{15} & s^E_{16} \\ s^E_{21} & s^E_{22} & s^E_{23} & s^E_{24} & s^E_{25} & s^E_{26} \\ s^E_{31} & s^E_{32} & s^E_{33} & s^E_{34} & s^E_{35} & s^E_{36} \\ s^E_{41} & s^E_{42} & s^E_{43} & s^E_{44} & s^E_{45} & s^E_{46} \\ s^E_{51} & s^E_{52} & s^E_{53} & s^E_{54} & s^E_{55} & s^E_{56} \\ s^E_{61} & s^E_{62} & s^E_{63} & s^E_{64} & s^E_{65} & s^E_{66} \end{bmatrix} \begin{bmatrix} T_1 \\ T_2 \\ T_3 \\ T_4 \\ T_5 \\ T_6 \end{bmatrix} + \begin{bmatrix} d_{11} & d_{12} & d_{13} \\ d_{21} & d_{22} & d_{23} \\ d_{31} & d_{32} & d_{33} \\ d_{41} & d_{42} & d_{43} \\ d_{51} & d_{52} & d_{53} \\ d_{61} & d_{62} & d_{63} \end{bmatrix} \begin{bmatrix} E_1 \\ E_2 \\ E_3 \end{bmatrix} \tag{A.12}$$

$$\begin{bmatrix} D_1 \\ D_2 \\ D_3 \end{bmatrix} = \begin{bmatrix} d_{11} & d_{12} & d_{13} & d_{14} & d_{15} & d_{16} \\ d_{21} & d_{22} & d_{23} & d_{24} & d_{25} & d_{26} \\ d_{31} & d_{32} & d_{33} & d_{34} & d_{35} & d_{36} \end{bmatrix} \begin{bmatrix} T_1 \\ T_2 \\ T_3 \\ T_4 \\ T_5 \\ T_6 \end{bmatrix} + \begin{bmatrix} \varepsilon_{11}^T & \varepsilon_{12}^T & \varepsilon_{13}^T \\ \varepsilon_{21}^T & \varepsilon_{22}^T & \varepsilon_{23}^T \\ \varepsilon_{31}^T & \varepsilon_{32}^T & \varepsilon_{33}^T \end{bmatrix} \begin{bmatrix} E_1 \\ E_2 \\ E_3 \end{bmatrix} \tag{A.13}$$

Another fundamental parameter used in electromechanical applications is the electromechanical coupling factor k. The electromechanical coupling factor, which measures the ability of a material to interconvert electrical and mechanical energy, is expressed as:

$$k^2 = \frac{\text{Converted Mechanical Energy}}{\text{Input Electrical Energy}} \tag{A.14}$$

or

$$k^2 = \frac{\text{Converted Electrical Energy}}{\text{Input Mechanical Energy}} \tag{A.15}$$

In many cases, processing conditions such as extrusion and the particular crystal symmetry of piezoelectric material determine which components of the dielectric constant, piezoelectric, and elastic compliance tensors are non-zero and unique. For example, for an unstretched and poled piezoelectric P(VDF-TrFE) copolymer, having 2 mm macroscopic symmetry, the matrix form of Eqs. (A.3) and (A.4) can written as:

$$\begin{bmatrix} S_1 \\ S_2 \\ S_3 \\ S_4 \\ S_5 \\ S_6 \end{bmatrix} = \begin{bmatrix} s_{11}^E & s_{12}^E & s_{13}^E & 0 & 0 & 0 \\ s_{21}^E & s_{22}^E & s_{23}^E & 0 & 0 & 0 \\ s_{31}^E & s_{32}^E & s_{33}^E & 0 & 0 & 0 \\ 0 & 0 & 0 & s_{44}^E & 0 & 0 \\ 0 & 0 & 0 & 0 & s_{55}^E & 0 \\ 0 & 0 & 0 & 0 & 0 & s_{66}^E \end{bmatrix} \begin{bmatrix} T_1 \\ T_2 \\ T_3 \\ T_4 \\ T_5 \\ T_6 \end{bmatrix} + \begin{bmatrix} 0 & 0 & d_{31} \\ 0 & 0 & d_{32} \\ 0 & 0 & d_{33} \\ 0 & d_{24} & 0 \\ d_{15} & 0 & 0 \\ 0 & 0 & 0 \end{bmatrix} \begin{bmatrix} E_1 \\ E_2 \\ E_3 \end{bmatrix} \tag{A.16}$$

Table A.1 Piezoelectric, dielectric, and elastic properties of PVDF [13–15] and P(VDF-TrFE) copolymer with 75/25 mol% [12]

Coefficient/Parameter	PVDF	P(VDF-TrFE) 75/25[a]	
		Real	Imaginary
d_{31} (pC/N)	21[b]	10.7	0.18
d_{32} (pC/N)	1.5[b]	10.1	0.19
d_{33} (pC/N)	−32.5[b]	−33.5	−0.65
d_{15} (pC/N)	−27[b]	−36.3	−0.32
d_{24} (pC/N)	−23[b]	−40.6	−0.35
s_{11}^E (10^{-10} Pa^{-1})	3.65[c]	3.32	0.1
s_{22}^E (10^{-10} Pa^{-1})	4.24[c]	3.34	0.07
s_{33}^E (10^{-10} Pa^{-1})	4.72[c]	3.00	0.07
s_{44}^E (10^{-10} Pa^{-1})	–	94.0	2.50
s_{55}^E (10^{-10} Pa^{-1})	–	96.3	2.33
s_{66}^E (10^{-10} Pa^{-1})	–	14.4	–
s_{12}^E (10^{-10} Pa^{-1})	−1.10[c]	−1.44	–
s_{13}^E (10^{-10} Pa^{-1})	−2.09[c]	−0.89	–
s_{23}^E (10^{-10} Pa^{-1})	−1.92[c]	−0.86	–
$\varepsilon_{11}^T/\varepsilon_0$	6.9[d]	7.4	0.07
$\varepsilon_{22}^T/\varepsilon_0$	8.6[d]	7.95	0.09
$\varepsilon_{33}^T/\varepsilon_0$	7.6[d]	7.9	0.09

[a]Reference [12]. [b]Reference [13]. [c]Reference [14]. [d]Reference [15]

$$\begin{bmatrix} D_1 \\ D_2 \\ D_3 \end{bmatrix} = \begin{bmatrix} 0 & 0 & 0 & 0 & d_{15} & 0 \\ 0 & 0 & 0 & d_{24} & 0 & 0 \\ d_{31} & d_{32} & d_{33} & 0 & 0 & 0 \end{bmatrix} \begin{bmatrix} T_1 \\ T_2 \\ T_3 \\ T_4 \\ T_5 \\ T_6 \end{bmatrix} + \begin{bmatrix} \varepsilon_{11}^T & 0 & 0 \\ 0 & \varepsilon_{22}^T & 0 \\ 0 & 0 & \varepsilon_{33}^T \end{bmatrix} \begin{bmatrix} E_1 \\ E_2 \\ E_3 \end{bmatrix} \tag{A.17}$$

Due to the fact that electromechanical response depends on a number of factors, including polarization conditions, stress/strain rates, temperatures, and hydrostatic pressure, the reported data for the values of various coefficients in the above equations for PVDF and P(VDF-TrFE) copolymer appear to involve certain inconsistencies. Nevertheless, it is possible to identify the typical values such as those listed in Table A.1.

The above tensor relations of Eqs. (A.5) and (A.6) are used to obtain the electromechanical response of a piezoelectric material along the same or other direction as that of stimulus. An as example, the electromechanical response of P(VDF-TrFE) copolymer, when it is used in the thickness mode i.e. both stress and electric field are along the 3-direction, as in Fig. A.7, can be expressed as [11]:

$$S_3 = s_{33}^E T_3 + d_{33} E_3 \tag{A.18}$$

$$D_3 = d_{33} T_3 + \varepsilon_{33}^T E_3 \tag{A.19}$$

The expression for longitudinal electromechanical coupling factor k_{33}, under similar conditions is:

$$k_{33}^2 = \frac{d_{33}^2}{\varepsilon_{33}^T s_{33}^E} \tag{A.20}$$

The constants d_{33}, ε_{33}^T, and s_{33}^E are frequently found in the manufacturer's data. In Eqs. (A.7) and (A.8), T_3 and E_3 are used as independent variables. If, however, D_3 and S_3 are the independent variables the above relations can also be written as:

$$T_3 = c_{33}^D S_3 - h_{33} D_3 \tag{A.21}$$

$$E_3 = -h_{33} S_3 + \beta_{33}^S D_3 = -h_{33} S_3 + \frac{D_3}{\varepsilon_{33}^S} \tag{A.22}$$

The new constants c_{33}^D, h_{33}, and ε_{33}^S are related to d_{33}, ε_{33}^T, and s_{33}^E by following mathematical relations:

$$\varepsilon_{33}^S = \varepsilon_{33}^T - \frac{d_{33}^2}{s_{33}^E} \tag{A.23}$$

$$h_{33} = \frac{d_{33}}{s_{33}^E \varepsilon_{33}^T} \tag{A.24}$$

$$c_{33}^D = h_{33}^2 \varepsilon_{33}^T + \frac{1}{s_{33}^E} \tag{A.25}$$

$$s_{33}^D = \left(1 - k_{33}^2\right) s_{33}^E \tag{A.26}$$

Depending on the independent variables chosen to describe the piezoelectric behavior, there can be two more variants of the (A.9) and (A.10), which are not discussed here. For a deeper understanding of piezoelectricity one may refer to standard literature on piezoelectricity [1–5].

References

1. W.P. Mason, *Electromechanical Transducers and Wave Filters* (Van Nostrand, New York, 1942)

2. W.P. Mason, *Physical Acoustics and the Properties of Solids* (Van Nostrand, Princeton, 1958)
3. W.G. Cady, *Piezoelectricity* (McGraw-Hill, New York, 1946)
4. H.S. Nalwa, *Ferroelectric Polymers: Chemistry, Physics, and Applications* (Marcel Dekker, Inc., New York, 1995)
5. T. Ikeda, *Fundamentals of Piezoelectricity* (Oxford University Press, New York, 1996)
6. P. Curie, J. Curie, Dévelopment, par pression, de l'électricité polaire dans les cristaux hémièdres à faces inclinées. C. R. Acad. Sci. **91**, 294–295 (1880)
7. G. Lippmann, Principe de conservation de l'électricité. Ann. Chim. Phys. **24**(5a), 145–178 (1881)
8. H. Kawai, The piezoelectricity of PVDF. Jpn. J. Appl. Phys. **8**, 975–976 (1969)
9. L. Pinna, R.S. Dahiya, M. Valle, G.M. Bo, Analysis of self-powered vibration-based energy scavenging system, in *ISIE 2010: The IEEE International Symposium on Industrial Electronics*, Bari, Italy (2010), pp. 1–6
10. ANSI/IEEE, IEEE standard on piezoelectricity. IEEE Standard 176-1987 (1987)
11. R.S. Dahiya, M. Valle, L. Lorenzelli, SPICE model of lossy piezoelectric polymers. IEEE Trans. Ultrason. Ferroelectr. Freq. Control **56**, 387–396 (2009)
12. H. Wang, Q.M. Zhang, L.E. Cross, A.O. Sykes, Piezoelectric, dielectric, and elastic properties of poly(vinylidene fluoride/trifluoroethylene). J. Appl. Phys. **74**, 3394–3398 (1993)
13. E.L. Nix, I.M. Ward, The measurement of the shear piezoelectric coefficients of polyvinylidene fluoride. Ferroelectrics **67**, 137–141 (1986)
14. V.V. Varadan, Y.R. Roh, V.K. Varadan, R.H. Tancrell, Measurement of all the elastic and dielectric constants of poled PVDF films, in *Proceedings of 1989 Ultrasonics Symposium*, vol. 2 (1989), pp. 727–730
15. H. Schewe, Piezoelectricity of uniaxially oriented polyvinylidene fluoride, in *Proceedings of 1982 Ultrasonics Symposium* (1982), pp. 519–524

Appendix B
Modeling of Piezoelectric Polymers

Abstract Piezoelectric polymers are used as transducers in many applications, including the tactile sensing presented in this book. It is valuable to use some form of theoretical model to assess, the performance of a transducer; the effects of design changes; electronics modifications etc. Instead of evaluating the transducer and conditioning electronics independently, which may not result in optimized sensor performance, it is advantageous to develop and implement the theoretical model of transducer in such a way that overall sensor (i.e. transducer + conditioning electronics) performance can be optimized. In this context, the ease with which the conditioning electronics can be designed with a SPICE like software tool, makes it important to implement the theoretical model of transducer also with a similar software tool. Moreover, with SPICE it is easier to evaluate the performance of transducer, both, in time and frequency domains. The equivalent model of piezoelectric polymers—that includes the mechanical, electromechanical and dielectric losses—and SPICE implementation of the same are presented in this chapter.

Keywords Piezoelectricity · Piezoelectric effect · PVDF · PVDF-TrFE · Piezoelectric polymers · Smart materials · Sensors · Actuators · Simulation · Modeling · Transmission line model · SPICE · Lossy piezoelectric model

B.1 Introduction

Much work has been published on transducers using piezoelectric ceramics, but a great deal of this work does not apply to the piezoelectric polymers because of their unique electrical and mechanical properties [1]. A number of attempts to model the behavior of piezoelectric materials fail to predict the behavior of piezoelectric polymers because of their lossy and dispersive dielectric properties and higher viscoelastic losses. Starting from the Redwood's transmission line version of Mason's equivalent circuit [2], a SPICE implementation of piezoelectric transducer was reported by Morris et al. [3]. Usage of negative capacitance, $-C_0$ (an unphysical electrical circuit element), by Morris et al. was avoided by Leach with the controlled source technique in an alternative SPICE implementation [4]. The models presented in both these works were verified for piezoceramics operating in the actuating mode i.e. with electrical input and mechanical output. The transducer was assumed to

R.S. Dahiya, M. Valle, *Robotic Tactile Sensing*,
DOI 10.1007/978-94-007-0579-1,

be lossless, and hence, both these implementations are insufficient for evaluating the performance of transducers with significant losses. Püttmer et al. [5] improved these piezoceramics models by involving a resistor—with value equal to that at fundamental resonance—to represent the acoustic losses in the transmission line, under the assumption that transmission line has low losses. Further, the dielectric and electromechanical losses in the transducer were assumed negligible. These assumptions worked well for piezoceramics, but modeling of lossy polymers like PVDF requires inclusion of all these losses. Keeping these facts in view, the equivalent model of piezoelectric polymers—that includes the mechanical, electromechanical and dielectric losses—was developed [6] and SPICE implementation of the same is presented in this chapter.

Following sections present the theory of the lossy model of piezoelectric polymers; its SPICE implementation and its evaluation vis-a-vis experimental results. Using the model presented in this chapter, many design issues associated with the piezoelectric polymers are also discussed.

B.2 Theory

B.2.1 Piezoelectric Linear Constitutive Relations

According to the linear theory of piezoelectricity [7], the tensor relation between mechanical stress, mechanical strain, electric field and electric displacement is:

$$S_p = s^E_{pq} T_q + d_{kp} E_k \tag{B.1}$$

$$D_i = d_{iq} T_q + \varepsilon^T_{ik} E_k \tag{B.2}$$

where, S_p is the mechanical strain in p direction, D_i is electric displacement in i direction, T_q is mechanical stress in q direction, E_k is the electric field in k direction, s^E_{pq} is elastic compliance at constant electric field, ε^T_{ik} is dielectric constant under constant stress, and d_{kp} is piezoelectric constant. In the event when polymer is used in the thickness mode, as shown in Fig. B.1, the tensor relations (B.1)–(B.2) can be written as:

$$S_3 = s^E_{33} T_3 + d_{33} E_3 \tag{B.3}$$

$$D_3 = d_{33} T_3 + \varepsilon^T_{33} E_3 \tag{B.4}$$

The constants d_{33}, ε^T_{33}, and s^E_{33} are frequently found in the manufacturer's data for polarized polymers. The analysis is simpler if the variables S_3, T_3, D_3 and E_3 are arranged in the alternate way of writing the piezoelectric relation using D_3 and S_3 as independent variables. Thus the equations representing plane compression wave propagation in the x direction (3-direction or the direction of polarization) in a piezoelectric medium are:

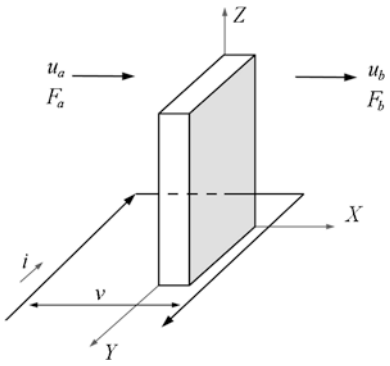

Fig. B.1 Piezoelectric polymer operating in thickness mode

$$T_3 = c_{33}^D S_3 - h_{33} D_3 \tag{B.5}$$

$$E_3 = -h_{33} S_3 + \beta_{33}^S D_3 = -h_{33} S_3 + \frac{D_3}{\varepsilon_{33}^S} \tag{B.6}$$

The new constants c_{33}^D, h_{33} and ε_{33}^S are related to the previous constants by:

$$\varepsilon_{33}^S = \varepsilon_{33}^T - \frac{d_{33}^2}{s_{33}^E} \tag{B.7}$$

$$h_{33} = \frac{d_{33}}{s_{33}^E \varepsilon_{33}^T} \tag{B.8}$$

$$c_{33}^D = h_{33}^2 \varepsilon_{33}^T + \frac{1}{s_{33}^E} \tag{B.9}$$

Based on the choice of independent variables, there can be two other variants of the (B.5) and (B.6) which are not given here. Inside polymer, the mechanical strain, mechanical stress and the electrical displacement can be written as:

$$S_3 = \frac{\partial \xi}{\partial x} \tag{B.10}$$

$$\frac{\partial T_3}{\partial x} = \rho \frac{\partial^2 \xi}{\partial t^2} \tag{B.11}$$

$$Div(D) = 0 \tag{B.12}$$

where ξ is the displacement of the particles inside polymer, ρ is the density of the polymer. Equation (B.11) is basically Newton's law and (B.12) is Gauss's law. Using (B.5) and (B.10)–(B.12), the mechanical behavior of the particles inside polymer can be described as a wave motion which is given by:

$$\frac{\partial^2 \xi}{\partial t^2} = v^2 \frac{\partial^2 \xi}{\partial x^2} \tag{B.13}$$

where, $v = \sqrt{c_{33}^D/\rho}$ is the sound velocity in the polymer and should not be confused with particle velocity ($\partial\xi/\partial t$).

B.2.2 Losses

In general, the piezoelectric polymers possess frequency dependent mechanical, dielectric and electromechanical losses. These losses can be taken into account by replacing elastic, dielectric and piezoelectric constants in (B.1)–(B.13), with their complex values [1, 8]. In other words, the mechanical/viscoelastic, dielectric and electromechanical losses are taken into account by using complex elastic constant, $c_{33}^{D^*}$; complex dielectric constant, $\varepsilon_{33}^{S^*}$ and complex electromechanical coupling coefficient, k_t^* respectively. These complex constants can be written as:

$$c_{33}^{D^*} = c_r + jc_i = c_{33}^D(1 + j\tan\delta_m) \tag{B.14}$$

$$\varepsilon_{33}^{S^*} = \varepsilon_r - j\varepsilon_i = \varepsilon_{33}^S(1 - j\tan\delta_e) \tag{B.15}$$

$$k_t^* = k_{tr} + jk_{ti} = k_t(1 + j\tan\delta_k) \tag{B.16}$$

where, the subscripts r and i stand for real and imaginary terms and $\tan\delta_m$, $\tan\delta_e$, $\tan\delta_k$ are the elastic, dielectric and electromechanical coupling factor loss tangent, respectively. The complex piezoelectric constants viz: d_{33}^* and h_{33}^*, can be obtained from electromechanical coupling constant k_t^* [7].

B.2.3 Polymer Model with Losses

It is assumed that a one-dimensional compression wave is propagating in X direction of thickness-mode piezoelectric transducer, as shown in Fig. B.1. It is also assumed that the electric field E and the electric displacement D are in the X direction. Let u $(= u_a - u_b)$ be the net particle velocity, F $(= F_a - F_b)$ be the force, and l_x, l_y, l_z are the dimensions of the polymer. Using (B.5)–(B.6) and (B.10)–(B.12), the mathematical relations for the piezoelectric polymer can be written as:

$$\frac{dF}{dx} = -\rho A_x s u \tag{B.17}$$

$$c^* \frac{d\xi}{dx} = -\frac{1}{A_x}F + h^* D \tag{B.18}$$

$$E = -h^* \frac{d\xi}{dx} + \frac{1}{\varepsilon^*}D \tag{B.19}$$

For simplicity, the subscripts have been removed from these expressions. In these equations, s $(= j\omega)$ is the Laplace variable and A_x (where $A_x = l_z \times l_y$) is the

cross-sectional area perpendicular to x axis. Complex elastic constant, piezoelectric constant and dielectric constant are represented by c^*, h^* and ε^* respectively. Numerical values of these constants are obtained from the impedance measurements, by using non linear regression technique [9], discussed in next section.

If the current flowing through the external circuit is i, then charge q on the electrodes is i/s and the electric flux density D is equal to $i/(s \times A_x)$. The particle displacement is related to particle velocity by $\xi = u/s$. From (B.12),

$$\frac{dD}{dx} = 0 \Rightarrow \frac{d(i/s)}{dx} = 0 \Rightarrow \frac{d(h^* i/s)}{dx} = 0 \tag{B.20}$$

Using (B.20) in both sides of (B.17)–(B.18), we have:

$$\frac{d}{dx}\left[F - \frac{h^*}{s} i\right] = \rho A_x s u \tag{B.21}$$

$$\frac{du}{dx} = -\frac{s}{A_x c^*}\left[F - \frac{h^*}{s} i\right] \tag{B.22}$$

$$V_{in} = \frac{h^*}{s}[u_1 - u_2] + \frac{1}{C_0^* s} i \tag{B.23}$$

where, V_{in} is the voltage at the electrical terminals of polymer and C_0^* is its lossy capacitance. Equations (B.21)–(B.22) describe the mechanical behavior and (B.23) describe the electromechanical conversion. It can be noted that (B.21)–(B.22) are similar to the standard telegraphist's equations of a lossy electrical transmission line viz:

$$\frac{dV_t}{dx} = -(L_t s + R_t) I_t \tag{B.24}$$

$$\frac{dI_t}{dx} = -(C_t s + G_t) V_t \tag{B.25}$$

where, L_t, R_t, C_t and G_t are the per unit length inductance, resistance, capacitance and conductance of the transmission line. V_t and I_t are the voltage across and current passing through the transmission line. Comparing (B.21)–(B.22) with (B.24)–(B.25), the analogy between these two sets of equations can be observed. Thus, V_t is analogous to $F - (h^*/s) \times i$; L_t is analogous to $\rho \times A_x$; R_t is zero; I_t is analogous to u; and $s/(A_x \times c^*) = C_t + G_t$. The right hand side of the last expression is a complex quantity due to complex c^*. By substituting $s = j\omega$ and then comparing coefficients on both sides, the expressions of G_t and C_t can be written as:

$$G_t = \frac{c_i \omega}{(c_r^2 + c_i^2) A_x} \tag{B.26}$$

$$C_t = \frac{c_r}{(c_r^2 + c_i^2) A_x} \tag{B.27}$$

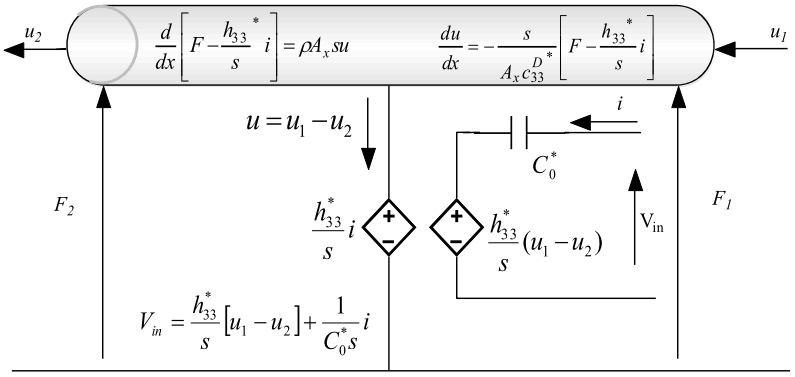

Fig. B.2 Transmission line equivalent model of piezoelectric polymer

Thus, the acoustic transmission can be represented by an analogous lossy electrical transmission line. It is the general practice to represent transmission losses by taking a non-zero R and assuming $G = 0$. But, in acoustics the difference between R and G is not that distinct [10] and it can be shown mathematically that the losses can be represented by any of the following options; (a) Both R and G are used; (b) Only G is used and $R = 0$; (c) Only R is used and $G = 0$. In the analogy presented above, $R = 0$ and $G \neq 0$ and hence the losses in the transmission can be taken into account by having a non-zero value of G. Similarly the electromechanical loss and dielectric loss are considered by using complex values of h and C_0 in (B.23). Complete analogous equivalent circuit for thickness-mode piezoelectric polymer transducer obtained by using (B.21)–(B.23), is shown in Fig. B.2. It should be noted that the model presented here does not include the time-dependence of losses. One may refer [11], for more information on viscoelastic and electromechanical energy losses, over a period of time.

B.3 Measurement of Complex Constants

The dispersive dielectric properties and the internal viscoelastic losses in piezoelectric polymers preclude the convenient use of the classical IEEE standard techniques [7] for determining dielectric and piezoelectric properties. This is due to the fact that the figure of merit, M for piezoelectric polymers is approximately 2–2.5 [1]. As mentioned in the IEEE standard, the parallel frequency, f_p, cannot be measured accurately when $M < 5$. Therefore, one should not apply the IEEE Standard's equations for k_{33} or k_t assuming that f_p and f_s are the frequencies of maximum and minimum impedance magnitude, respectively.

A technique for characterizing and modeling PVDF was first proposed by Ohigashi [8]. His approach is based on curve fitting the equation for input admittance

Table B.1 Dimensions, densities of the different samples and the electrodes used

Quantity	Symbol	PVDF-TrFE	PVDF-TrFE*	PVDF*	Lead Metaniobate*
Density (kg/m^3)	ρ	1880	1880	1780	6000
Thickness (m)	l_x	50×10^{-6}	0.408×10^{-3}	0.27×10^{-3}	1.55×10^{-3}
Width (m)	l_y	7×10^{-3}	–	–	–
Length (m)	l_z	7×10^{-3}	–	–	–
Diameter (m)	D	–	14×10^{-3}	14×10^{-3}	25.2×10^{-3}
Type of Electrode	–	Al+Cr	Au	Al	Ag
Thickness of Electrode (μm)	t_m	0.08	<0.1	<0.1	<10
Area of sample (m^2)	A_x	49×10^{-6}	154×10^{-6}	154×10^{-6}	498.7×10^{-6}

*From [9]

for an unloaded piezoelectric resonator to actual admittance measurements made over a broad frequency range that includes the fundamental half-wave resonance of the sample. To account for the lossy dispersive dielectric properties, he introduced the dielectric loss factor, $\tan\delta_e$ and to account for the internal viscoelastic losses of PVDF, he introduced the mechanical loss factor, $\tan\delta_m$. Although Ohigashi treated the elastic and dielectric constants as complex, the piezoelectric constant was still considered as real. Several other workers, including Smits [12] and Sherrit et al. [13] have introduced methods to determine the mechanical, dielectric, and piezoelectric loss constants. Smits [12] and Sherrit et al. [13] considered all the material parameters as complex, and the losses are given by the corresponding imaginary parts. A good comparison of various methods used for finding the complex constants is presented by Kwok et al. in [9]. In this work, the material parameters of PVDF, P(VDF-TrFE), PZT/epoxy 1-3 composite, and lead metaniobate are calculated from impedance data by using five methods, namely, the IEEE Std. 176 method, the methods of Smits [12] and Sherrit et al. [13], a software package "PRAP" [14], and the nonlinear regression method of authors. Kwok et al. [9] also observed that the for high loss materials like PVDF, the IEEE standard method gives much higher value of k_{33} or k_t, as compared to other methods.

The software package PRAP, which combines the methods of Smits [12] and Sherrit et al. [13], is a simple way of measuring or generating complex coefficients, if the geometry of the sample is known. In this work, PRAP is used to obtain various complex constants from the impedance and phase measurement of one of the P(VDF-TrFE) samples. The dimension, density, type and thickness of metal electrodes on the sample are given in Table B.1 and various complex constants obtained by PRAP analysis are given in Table B.2. For other samples in Tables B.1 and B.2, the data has been taken from [9]. This data was obtained with non linear regression technique, presented in [9].

Table B.2 Material constants of PVDF-TRFE, PVDF and lead metaniobate

Constant		PVDF-TrFE	PVDF-TrFE*	PVDF*	Lead Metaniobate*
k_t	Real	0.202	0.262	0.127	0.334
	Imaginary	−0.0349	0.0037	0.0055	0.0003
c_{33}^{D}* (N/m^2)	Real	1.088×10^{10}	10.1×10^{9}	8.7×10^{9}	65.8×10^{9}
	Imaginary	5.75×10^{8}	5.15×10^{8}	1.018×10^{9}	4.14×10^{9}
ε_{33}^{S}*	Real	4.64×10^{-11}	38.78×10^{-12}	55.78×10^{-12}	22.84×10^{-10}
	Imaginary	8.45×10^{-12}	4.11×10^{-12}	15.618×10^{-12}	2.033×10^{-11}
h_{33}^{*} (V/m)	Real	3.03×10^{9}	4.20×10^{9}	1.52×10^{9}	1.79×10^{9}
	Imaginary	-7.25×10^{8}	3.90×10^{8}	3.69×10^{8}	6.58×10^{7}
Q		18.78	19.60	8.54	15.87

*From [9]

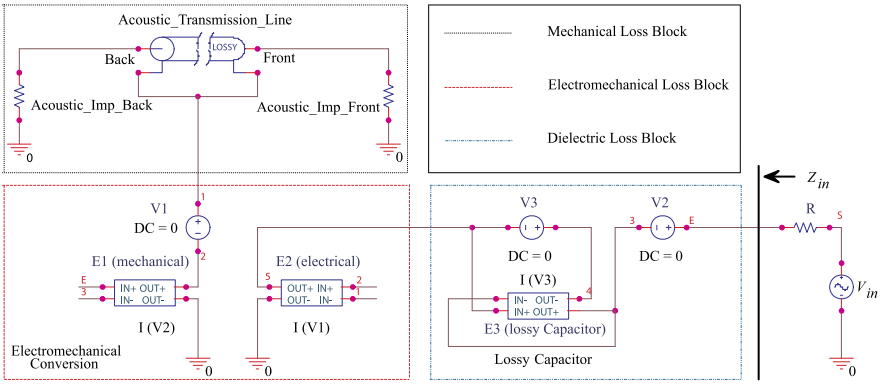

Fig. B.3 Schematic of the equivalent model of piezoelectric polymer implemented with PSpice. The model has been divided into various blocks showing the mechanical/acoustic/viscoelastic, electromechanical/piezoelectric and electric/dielectric losses

B.4 SPICE Implementation

Following the discussion above, the piezoelectric polymer model has been implemented in PSPICE circuit simulator, which is commercially available from ORCAD. Figure B.3 shows the SPICE schematic of the equivalent circuit of Fig. B.2. The mechanical, electromechanical and electrical loss blocks are clearly marked in Fig. B.3. The SPICE implementation of various blocks is explained below. The netlist for SPICE implementation is given at the end of this Appendix.

B.4.1 Mechanical Loss Block

The analogy between (B.21)–(B.22) and (B.24)–(B.25) allows the implementation of mechanical/viscoelastic behavior during acoustic transmission in polymer with a lossy transmission line, which is available in the PSPICE. It can also be implemented with lumped ladder arrangement of G_t, C_t, L_t, R_t. But, here the lossy transmission line is preferred due to the advantages—in terms of accuracy and computation time—offered by the distributed values of G_t, C_t, L_t, R_t, used in it. Further, the lossy transmission line in PSPICE allows the use of frequency dependent expression for G_t, which is desired according to (B.26). The frequency term in G_t is implemented in SPICE, by using the expression $SQRT(-s \times s)$, where, s $(= j\omega)$ is the Laplace operator. The parameters of transmission line viz: G_t, C_t and L_t are obtained by using complex elastic constant i.e. c^* in the analogous expression obtained from the analogy between acoustic wave propagation and the lossy electrical transmission line. For various sample parameters in Tables B.1 and B.2, the transmission line parameters are given in Table B.2. While G_t and C_t are obtained from (B.26)–(B.27); L_t is given by $\rho \times A_x$ and the length, l_x, of the transmission line is equal to the thickness of the sample. As shown in Fig. B.3, the lossy transmission line is terminated into the acoustic impedance of the mediums on two sides of the polymer—which is given by, $Z_m = \rho_m \times v_m \times A_x$. In this expression, ρ_m is the density of medium, v_m is the velocity of sound in medium and A_x is the area of sample. In this work air is present on both sides of samples, hence using, $\rho_m = 1.184\ \text{kg/m}^3$, $v_m = 346$ m/s and A_x from Table B.1, the acoustic impedances of front and backside are given in Table B.3. In a multilayer transducer, the acoustic impedances on both sides can be replaced by transmission lines having parameters (acoustic impedance and time delay etc.) corresponding to the mediums on each side.

B.4.2 Electromechanical Loss Block

The electromechanical conversion is analogous to the transformer action. It is implemented with the behavioral modeling of controlled sources, i.e. with the 'ELAPLACE' function in PSPICE. The currents passing through the controlled sources *E1(mechanical)* and *E2(electrical)*; are h^*/s times the currents passing through *V2* and *V1* respectively. The gain term i.e. 'h^*/s' used in the controlled sources *E1(mechanical)* and *E2(electrical)*—of PSPICE schematic in Fig. B.3—are given in Table B.2. In SPICE, the current in any branch can be measured by using a zero value DC voltage source in that branch. The voltage sources *V1* and *V2*, shown in Fig. B.3, have zero DC values and are thus used to measure the current passing through them. The complex piezoelectric constant, h^* ensures the inclusion of piezoelectric losses in the model. The complex number operator 'j' in the expression of h^* is implemented in PSPICE by using the expression $-s/abs(s)$.

Table B.3 Value/expression of parameters used in the SPICE equivalent model

Parameter	PVDF-TrFE	PVDF-TrFE*	PVDF*	Lead Metaniobate*
L_t (H)	0.0921	0.2894	0.274	2.993
G_t	$9.8958 \times 10^{-8} \times \sqrt{(-s \times s)}$	$3.271 \times 10^{-8} \times \sqrt{(-s \times s)}$	$8.61 \times 10^{-8} \times \sqrt{(-s \times s)}$	$1.912 \times 10^{-9} \times \sqrt{(-s \times s)}$
C_t (F)	1.8705×10^{-6}	6.415×10^{-7}	7.39×10^{-7}	3.035×10^{-8}
l_x (m)	50×10^{-6}	0.408×10^{-3}	0.27×10^{-3}	1.55×10^{-3}
Z_m (Ω)	0.020	0.063	0.063	0.204
C_0 (F)	4.545×10^{-11}	14.63×10^{-12}	31.81×10^{-12}	735.05×10^{-12}
h^*/s	$(3.03 \times 10^9 - j7.25 \times 10^8)/s$	$(4.2 \times 10^9 + j3.9 \times 10^8)/s$	$(1.52 \times 10^9 + j3.69 \times 10^8)/s$	$(1.79 \times 10^9 + j6.58 \times 10^7)/s$
Gain of *E3*	$1/(s \times (4.54 \times 10^{-11} + j8.28 \times 10^{-12}))$	$1/(s \times (14.63 \times 10^{-12} + j1.55 \times 10^{-12}))$	$1/(s \times (31.81 \times 10^{-12} + j8.91 \times 10^{-12}))$	$1/(s \times (735 \times 10^{-12} + j6.54 \times 10^{-12}))$

*From [9]

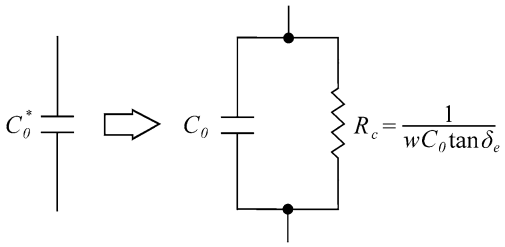

Fig. B.4 Equivalent representation of lossy capacitor

B.4.3 Dielectric Loss Block

This block consists of the lossy capacitance of polymer connected to the external voltage source or load. The use of complex permittivity i.e. ε^*, ensures the inclusion of dielectric losses. The lossy capacitor obtained by using ε^*, is equivalent to a lossless capacitor, $C_0 = \varepsilon A_x / l_x$ connected in parallel with the frequency dependent resistor $R_0 = 1/(\omega C_0 \tan\delta_e)$ as shown in Fig. B.4, where, C_0 is the static lossless capacitance of polymer. The voltage across the equivalent lossy capacitor is given as:

$$V_c = \frac{I_c}{sC_0 + \omega C_0 \tan\delta_e} \tag{B.28}$$

The SPICE circuit simulators allow only constant values of resistors and capacitors. To implement the lossy capacitor—which has the frequency dependent resistor—the behavior modeling of controlled voltage source is used here. The controlled source *E3(lossy capacitor)* is implemented with the 'ELAPLACE' function of PSPICE. As per (B.28), the voltage across *E3(lossy capacitor)*, is proportional to the current flowing through itself and measured by the zero value DC source *V3*, as shown in Fig. B.3.

The expressions of the gain terms used in the controlled source *E3(lossy capacitor)*, are given in Table B.3. Again, ω is implemented with the expression $SQRT(-s \times s)$. The netlist for the SPICE implementation shown in Fig. B.3—generated with PSPICE—is given at the end of Appendix B.

B.5 Experiment Versus Simulation

B.5.1 Evaluation of Lossless Model

Since it is difficult to apply forces over wide range of frequencies (∼MHz) by any mechanical arrangement, the piezoelectric polymer model in sensing mode was evaluated by using the same SPICE model of the polymer in actuating mode. The arrangement, as shown in Fig. B.5, is similar to the standard pulse-echo method, explained in [7]. The actuating mode component of the whole arrangement produces the force needed as the input in sensing component of the SPICE model of

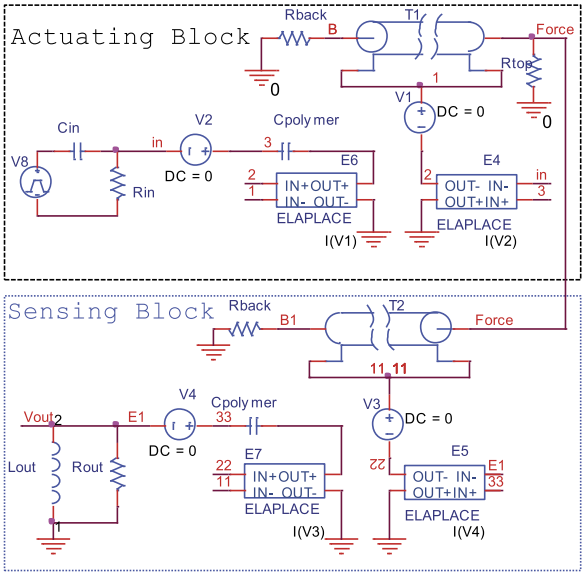

Fig. B.5 SPICE implementation of the standard Pulse-echo method for evaluating the SPICE model of piezoelectric polymer

piezoelectric polymer. The performance of polymer model in sensing mode was evaluated by comparing the simulated response with experiment results reported in [15]. For the purpose of comparison only, the electrical impulse input to the transmitting stage; the load at the output terminal of sensing stage; and various constants were kept same as that used in [15]. The input to the actuating stage is a voltage impulse (300 V, fall time 100 ns) generated by $R_{in} = 100\ \Omega$ and $C_{in} = 2$ nF. The output of the sensing stage is terminated in to a load, comprising of a resistance ($R_{out} = 100\ \Omega$) and inductance ($L_{out} = 4.7\ \mu$H)—connected in parallel. The losses could not be considered in this comparative study as the constants used in [15] are real numbers. Figure B.6 shows that the simulated outputs of the polymer, both in sensing and actuating mode, are in good agreement with the experiment results, presented in [15].

B.5.2 Evaluation of Lossy Model

The SPICE model presented in earlier section has been evaluated by comparing the simulated impedance and phase plots with the corresponding plots obtained from the measured data of PVDF, P(VDF-TrFE) and lead metaniobate. As mentioned earlier, the approximate lossy models developed for piezoceramic transducers are insufficient for evaluating the behavior of piezoelectric polymers. Keeping this in view, a comparison has also been made with the impedance and phase plots obtained by Püttmer's approach for lossy piezoceramics [5]. Using the PSPICE schematic of Fig. B.3, the simulated impedance, Z_{in}, for all the samples is obtained by dividing

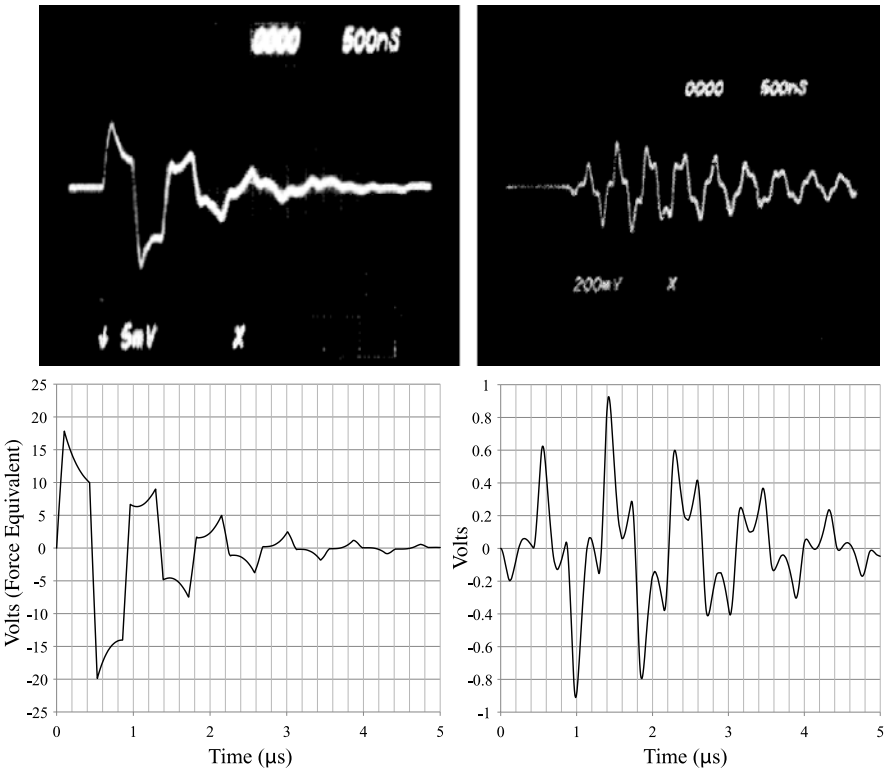

Fig. B.6 (*top-left*) Force generated by piezoelectric material (actuating component) in the pulse-echo arrangement, reproduced from [15]; (*top-right*) Voltage output of piezoelectric material (sensing component) in the pulse-echo arrangement, reproduced from [15]; (*bottom-left*) Simulated force obtained from SPICE model of piezoelectric material (actuating component) (*bottom-right*) Simulated voltage obtained from SPICE model of piezoelectric material (sensing component)

the voltage at node E (Fig. B.3) with the current passing through this node. For these simulations, the transmission line was terminated into the acoustic impedance of air on both sides and the effect of electrodes present on both sides of polymer was assumed to be negligible due to their negligible small thickness in comparison to that of test samples.

In the case of 50 μm thick P(VDF-TrFE) polymer film, the impedance and phase measurements were obtained with HP4285 LCR meter. The measured impedance and phase plots for other samples, viz: PVDF, P(VDF-TrFE) (0.408 mm thick) and lead metaniobate, used here, are same as those used in [9]. The physical dimensions, calculated complex constants and various parameters of SPICE model for all these samples are given in Tables B.1–B.2.

The impedance and phase plots of lead metaniobate sample, obtained by the SPICE model presented in this work has been compared in Fig. B.7 with those obtained by Püttmer's approach [5] and measured data. The lead metaniobate sam-

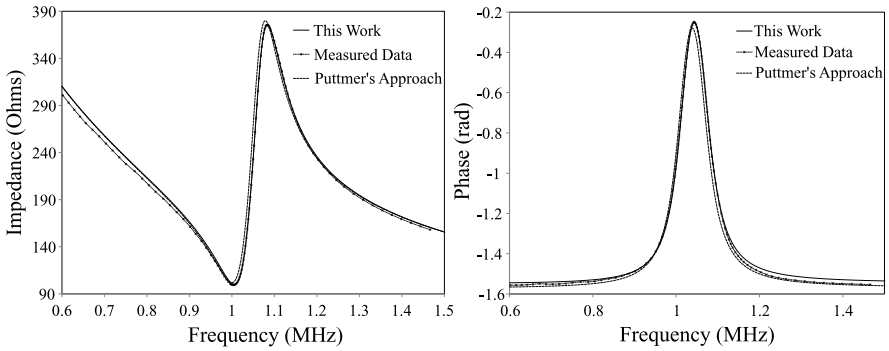

Fig. B.7 Comparison of Impedance (*left*) and Phase (*right*) plots of lead metaniobate sample, with the corresponding plots obtained by the Püttmer's approach and from the measured impedance data of [9]

ple is chosen here because the model in [5], was evaluated for lead metaniobate. The netlist of the SPICE model using Püttmer's approach is given in Appendix B. Püttmer's approach considers the losses in the transmission line only and dielectric and piezoelectric losses are assumed to be negligible. Other difference between Püttmer's approach and the work presented here is the use of R_t and G_t respectively, to represent the losses in the transmission line. In Püttmer's approach, L_t is given by $\rho \times A_x$; C_t is given by $1/(c_r \times A_x)$ and a simplified expression of R_t was obtained by assuming the transmission line to be having low loss. The value of R_t was given by $(L_t/Q) \times SQRT(-s \times s)$, where Q is the mechanical quality factor obtained by dividing real part of elastic constant with its imaginary part. It can be observed from Fig. B.7, that the impedance and phase plots of piezoceramics—obtained with the SPICE model presented in this work—are in good agreement with the measured plots and the plots obtained Püttmer's approach presented in [5]. The agreement between these plots is in line with the observations on the equivalence of using R_t or G_t to represent losses in the acoustic transmission [10].

The impedance and phase plots of two different P(VDF-TrFE) samples, obtained by the SPICE model presented in this work has been compared in Fig. B.8 and Fig. B.9 with those obtained by Püttmer's approach [5] and from the measured data. The plots in Fig. B.8 correspond to the thin 50 μm film and those in Fig. B.9 correspond to that of 0.408 mm thick film.

An additional plot obtained by considering the transmission losses only, in the SPICE model presented in this work, is also shown in Fig. B.8. It can be observed that the plots obtained with the approach presented here are in good agreement with the measured data. The difference between the approach presented here and that of Püttmer's approach is more evident in case of thinner polymer film (Fig. B.8) and more so in case of phase plots of both samples. Thus, in case of polymers, Püttmer's approach leads to a significant deviation from the measured plots.

The comparison of the impedance and phase plots for PVDF is given in Fig. B.10. In case of PVDF, it can be observed that—although an improvement over past

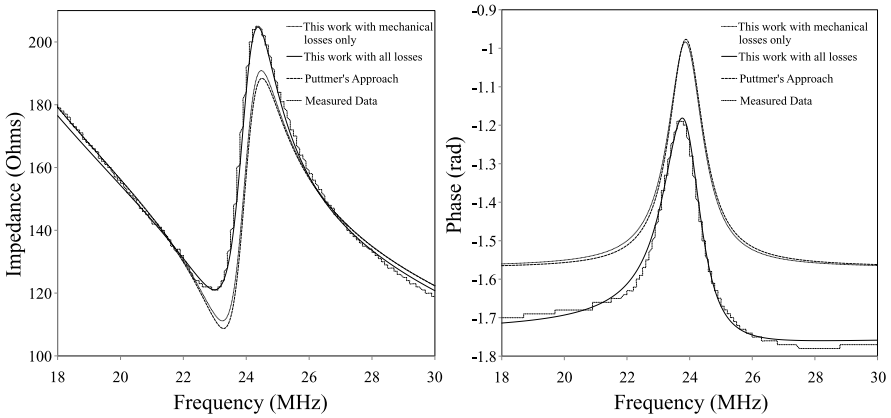

Fig. B.8 Comparison of Impedance (*left*) and Phase (*right*) plots of 50 μm thick PVDF-TrFE polymer film with the corresponding plots obtained by the Püttmer's approach and from the measured impedance data. The plots obtained by taking the transmission loss only in the SPICE model presented here, has also been shown. In principle, taking only transmission loss only in the model presented here is same as that of Püttmer's work

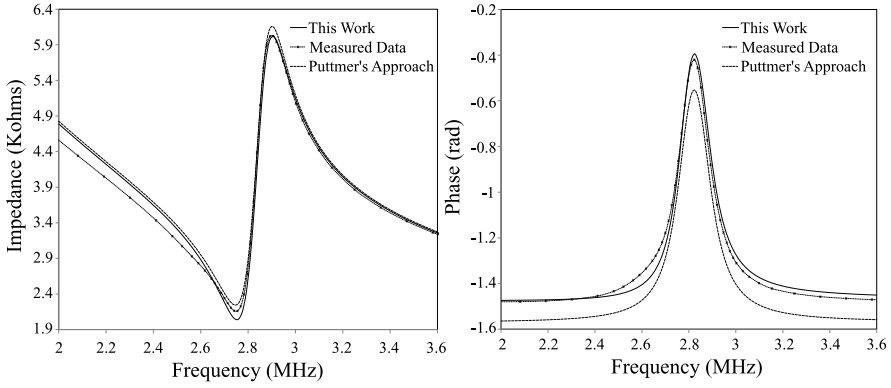

Fig. B.9 Comparison of Impedance (*left*) and Phase (*right*) plots of 0.408 mm thick PVDF-TrFE film with the corresponding plots obtained by the Püttmer's approach and from the measured impedance data of [9]

approach—the plots obtained with the approach presented in this work still have some discrepancies with the plots obtained from the measured data. The discrepancies are especially higher in the region outside resonance. This can be attributed to the frequency dependence of material parameters [9], which were assumed to be independent of frequency for these simulations. For a piezoelectric transducer the

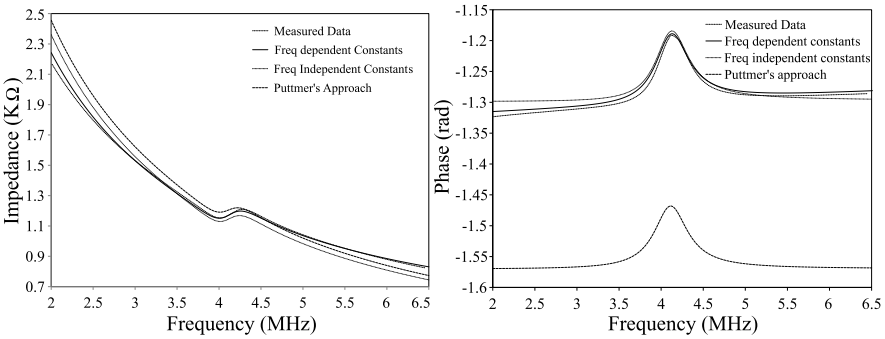

Fig. B.10 Comparison of Impedance (*left*) and Phase (*right*) plots PVDF film with the corresponding plots obtained by the Püttmer's approach and from the measured impedance data of [9]. The plots obtained by using first order frequency dependence of ε_{33}^{S} and $\tan\delta_e$ are also shown

electrical impedance at thickness extensional resonance is given by:

$$Z(f) = \frac{l_x}{i2\pi f \varepsilon_{33}^{S*} A_x}\left[1 - k_t^{2*}\frac{\tan(\pi f l_x\sqrt{\rho/c_{33}^{D*}})}{\pi f l_x\sqrt{\rho/c_{33}^{D*}}}\right] \tag{B.29}$$

where, f is the frequency. It can be noticed from (B.29) that outside resonance the impedance depends on ε_{33}^{S*} and hence on the ε_{33}^{S} and $\tan\delta_e$ and hence as a first approximation, taking into account the frequency dependence of ε_{33}^{S} and $\tan\delta_e$ should improve the simulation results. Following Kwok's approach, presented in [9], we obtained values of ε_{33}^{S} and $\tan\delta_e$ at various frequencies of the measured impedance data. It was observed that these constants vary with frequency. Considering the data values of ε_{33}^{S} and $\tan\delta_e$ at frequencies outside resonance, a first order frequency dependence of ε_{33}^{S} and $\tan\delta_e$ was obtained by linear fit of the ε_{33}^{S} and $\tan\delta_e$ versus frequency plots. Using these frequency dependent constants in the SPICE model, the impedance and phase plots were obtained. As shown in Fig. B.10, this improves the match between the simulated plots and plots from the measured data. The matching can be further improved—albeit, at the cost of computation power—by using a higher order frequency dependence of ε_{33}^{S} and $\tan\delta_e$ and also the frequency dependence of other material constants viz: c_{33}^{D*} and k_t^*.

B.6 Relative Contribution of Various Losses

Having presented the model with all the losses, the next question that comes to mind is—what is their relative contribution? If the contribution of a particular loss component far outweighs others, then such an argument can be a basis for using a simplified model. To evaluate the role of various loss components, the SPICE model was used to simulate impedance and phase under various combinations of losses. Impedance

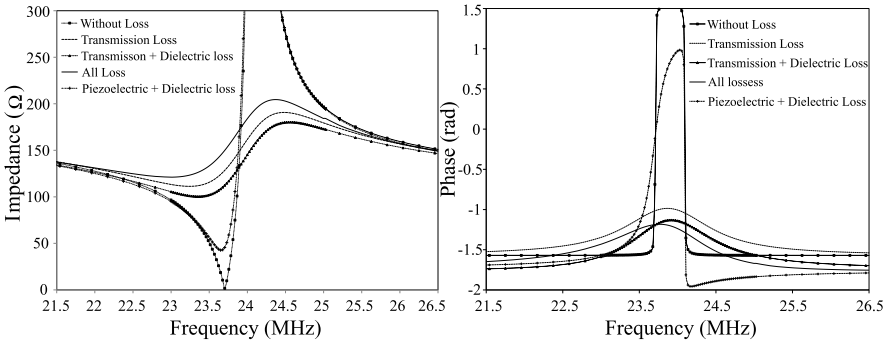

Fig. B.11 Impedance (*left*) and Phase (*right*) plots comparing the relative contribution of various losses. Simulations were performed under assumption of different combinations of losses

and phase plots so obtained are shown in Fig. B.11. It can be noticed that inclusion of only acoustic/transmission losses gives a first approximation of the impedance and phase, which is further improved by the dielectric and piezoelectric losses.

B.7 Design Issues Associated with Piezoelectric Polymer Film

The model developed for piezoelectric polymers can be used to study the effect of various parameters used in the model, which ultimately helps in optimizing their response. Various factors that influence the response of polymer are its thickness, material on front and back of the polymer, area of the polymer film, and type of electrodes [1]. The open circuit voltage of a piezoelectric polymer, when a step force is applied on top is:

$$\begin{aligned} V_{polymer} = -\frac{h_{zz} \times F_{in} \times (1 - R_{fp})}{Z_{ap}} \Bigg[& t - (1 + R_{pb}) \times \left(t - \frac{Z}{v} \right) \times u\left(t - \frac{Z}{v} \right) \\ & + R_{pb} \times (1 + R_{fp}) \times \left(t - \frac{2Z}{v} \right) \times u\left(t - \frac{2Z}{v} \right) \\ & - R_{fb} \times R_{pb} \times (1 + R_{pb}) \\ & \times \left(t - \frac{3Z}{v} \right) \times u\left(t - \frac{3Z}{v} \right) + \ldots \Bigg] \end{aligned} \tag{B.30}$$

where, $R_{fp} = (Z_p - Z_f)/(Z_p + Z_f)$ represent the reflection coefficient at front-polymer interface and $R_{pb} = (Z_p - Z_b)/(Z_p + Z_b)$ at polymer-back faces. Z_p, Z_f, and Z_b are the acoustic impedances of polymer, and the material on the front and back (silicon in the present case) sides respectively. Z is the thickness of the polymer, v is the wave velocity in polymer and $u(\cdot)$ is the step function. It can be noted from (7.2) that the open circuit voltage of the polymer depends on the thickness of the polymer, the reflection coefficients at the two faces, internal parameters

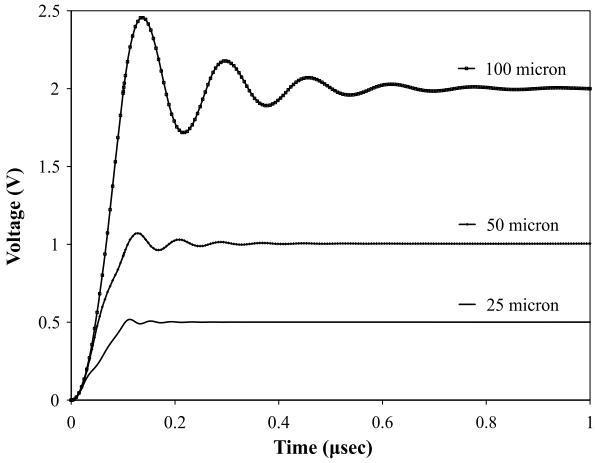

Fig. B.12 Simulated open circuit voltage of 25, 50 and 100 μm thick polymer film. A step force of 0.1 N was applied

like piezoelectric constant and elastic constant (acoustic impedance). In addition to these, the capacitance of polymer is also involved when the polymer is connected with a load.

In (B.30), the term outside brackets represents the net mechanical to electrical conversion and the terms inside the bracket are combination of incident and reflected force waves. It can be observed from the first term inside brackets that the voltage is a ramp function. If the thickness of the polymer is increased, the step function terms are further delayed (delay time increases as Z is increased). Thus the open circuit voltage keeps on increasing linearly until first delay term contributes to the net voltage. Thus, the open circuit voltage in general increases with the thickness of the polymer film. This thickness effect of polymer film can also be noted from the simulation result shown in Fig. B.12. Apart from above discussed factors, the response of polymer also depends on its area, which depends on sensor configuration.

The internal properties like piezoelectric constant depend on the way the polymer is made. Uniform thin films of piezoelectric polymers like P(VDF-TrFE), can be obtained by spin coating the polymer solution and annealing it at around 100° [16]. In order to have piezoelectric properties, the piezoelectric polymer needs to be poled at a rate of (∼100 V/μm). The intrinsic properties of polymers depend on the way the films are processed.

The materials on the front and back of the polymer offer different acoustic impedances to the force waves. The response of polymer with different materials under polymer, simulated with the SPICE model, is shown in Fig. B.13. It can be noticed that the polymer has higher sensitivity when a stiff material is used on the back side. For stiffer materials, the reflection coefficient R_{pb} is high and the device operates in $\lambda/4$ mode. For piezoelectric polymer based sensors realized on silicon wafers, the back side is made of silicon whose acoustic impedance is approximately five times that of P(VDF-TrFE). Thus, the reflection coefficient, R_{pb}, is 0.66. This means that piezoelectric polymer based sensors having silicon under the polymer, have high sensitivity.

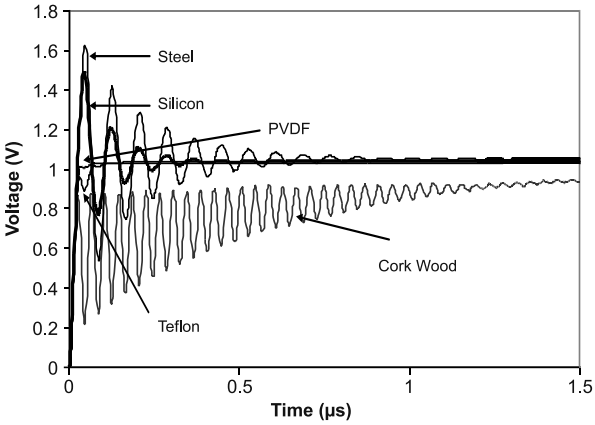

Fig. B.13 Response of polymer with different backside materials. Acoustic impedance of steel, silicon, PVDF, teflon and wood are 9, 3.8, 0.8, 0.6 and 0.02 MRayl respectively. A step force of 0.01 N was applied

B.8 SPICE Netlist of Piezo-Polymer Model

* source LOSSY PIEZO POLYMER

E_E3(Lossy_Capacitor) 3 4 LAPLACE{I(V_V3)} = $1/(s \times (C_0 - C_0 \times \tan(\delta_e) \times (s/abs(s))))$
R_Acoustic_Imp_back 0 BACK Z_m
T_Acoustic_Transmission_Line BACK 1 FRONT 1 LEN=l_x R=0 L=L_t G=G_t C=C_t
V_V3 4 5 DC 0 AC 0 0
V_V2 E 3 DC 0 AC 0 0
E_E2(electrical) 5 0 LAPLACE I(V_V1) = h^*/s
V_V1 1 2 DC 0 AC 0 0
V_Vin S 0 DC 0Vdc AC 1Vac
R_Acoustic_Imp_Front 0 FRONT Z_m
E_E1(mechanical) 2 0 LAPLACE{I(V_V2)} = h^*/s
R_R 5 E 1n

* source PIEZO LOSSY MODEL OF PUTTMER

V_V1 S 0 DC 0Vdc AC 1Vac
V_V2 E 3 DC 0 AC 0 0
T_T1 Back 1 Front 1 LEN=l_x R=$(L_t/Q) * SQRT(-1 * (s) * (s))$ L=L_t G=0 C=C_t
E_E1 2 0 LAPLACE I(V_V2) = h/s
R_Acoustic_Imp_back 0 BACK Z_m
X_F1 1 2 0 3 SCHEMATIC1_F1
R_Acoustic_Imp_Front 0 FRONT Z_m
C_C0 0 3 C_0
R_R S E 1n
.subckt SCHEMATIC1_F1 1 2 3 4
F_F1 3 4 VF_F1 $h \times C_0$

```
VF_F1 1 2 0V
.ends SCHEMATIC1_F1
```

B.9 Summary

The SPICE model for piezoelectric polymers presented in this chapter, for the first time, incorporates all losses namely: viscoelastic, piezoelectric and dielectric. It has been shown that, the model provides a good match between simulated and measured data and that the past approaches, developed mainly for piezoceramics, are not suitable for piezoelectric polymers. By comparing the contribution of various losses in the model, the viscoelastic losses have been found to have a major role. Perhaps, this is one reason why past approaches tried to model the viscoelastic losses only. The discussion on design issues associated with piezoelectric polymers, when they are used as transducer, provide good insight into their behavior under various conditions. Around low frequencies ($\sim$1 kHz), such a model can be approximated with a capacitor in series with a voltage source, as discussed in following chapters. Thus, the model presented in this chapter can be used to evaluate the performance of POSFET based tactile sensing devices, discussed in Chaps. 7 and 8, over a wide range of frequencies and can be used to explore the utility of such devices to applications other than tactile sensing as well. The successful implementation of the transducer model in SPICE, has made it convenient to evaluate the performance of transducer, both, in time and frequency domains. This implementation will greatly help in designing and evaluating the sensor system i.e., transducer and conditioning electronics, all together.

References

1. L.F. Brown, Design consideration for piezoelectric polymer ultrasound transducers. IEEE Trans. Ultrason. Ferroelectr. Freq. Control **47**, 1377–1396 (2000)
2. M. Redwood, Transient performance of piezoelectric transducers. J. Acoust. Soc. Am. **33**, 527–536 (1961)
3. S.A. Morris, C.G. Hutchens, Implementation of Mason's model on circuit analysis programs. IEEE Trans. Ultrason. Ferroelectr. Freq. Control **33**, 295–298 (1986)
4. W.M. Leach, Controlled-source analogous circuits and SPICE models for piezoelectric transducers. IEEE Trans. Ultrason. Ferroelectr. Freq. Control **41**, 60–66 (1994)
5. A. Püttmer, P. Hauptmann, R. Lucklum, O. Krause, B. Henning, SPICE models for lossy piezoceramics transducers. IEEE Trans. Ultrason. Ferroelectr. Freq. Control **44**, 60–66 (1997)
6. R.S. Dahiya, M. Valle, L. Lorenzelli, SPICE model of lossy piezoelectric polymers. IEEE Trans. Ultrason. Ferroelectr. Freq. Control **56**(2), 387–396 (2009)
7. ANSI/IEEE, IEEE standard on piezoelectricity. IEEE Standard 176-1987 (1987)
8. H. Ohigashi, Electromechanical properties of polarized polyvinylidene fluoride films as studied by the piezoelectric resonance method. J. Appl. Phys. **47**, 949–955 (1976)
9. K.W. Kwok, H.L.W. Chan, C.L. Choy, Evaluation of the material parameters of piezoelectric materials by various methods. IEEE Trans. Ultrason. Ferroelectr. Freq. Control **44**, 733–742 (1997)

10. J. Wu, G. Du, Analogy between the one-dimensional acoustic waveguide and the electrical transmission line for cases with loss. J. Acoust. Soc. Am. **100**, 3973–3975 (1996)
11. A.M. Vinogradov, V.H. Schmidt, G.F. Tuthill, G.W. Bohannan, Damping and electromechanical energy losses in the piezoelectric polymer PVDF. Mech. Mater. **36**, 1007–1016 (2004)
12. J.G. Smits, Iterative method for accurate determination of the real and imaginary parts of the materials coefficients of piezoelectric ceramics. IEEE Trans. Sonics Ultrason. **SU-23**, 393–402 (1976)
13. S. Sherrit, H.D. Wiederick, B.K. Mukherjee, Non-iterative evaluation of the real and imaginary material constants of piezoelectric resonators. Ferroelectrics **134**, 111–119 (1992)
14. TASI Technical Software Inc. Ontario, Canada (2007). Available at: http://www.tasitechnical.com/
15. G. Hayward, M.N. Jackson, Discrete-time modeling of the thickness mode piezoelectric transducer. IEEE Trans. Sonics Ultrason. **SU-31**(3), 137–166 (1984)
16. R.S. Dahiya, M. Valle, G. Metta, L. Lorenzelli, S. Pedrotti, Deposition processing and characterization of PVDF-TrFE thin films for sensing applications, in *IEEE Sensors: The 7th International Conference on Sensors*, Lecce, Italy (2008), pp. 490–493

Appendix C
Design of Charge/Voltage Amplifiers

Abstract The designs of three stage charge and voltage amplifiers, to read the taxels on piezoelectric polymer—MEA based tactile sensing chip, are presented here. Piezoelectric polymers is approximately represented as a voltage source in series with the static capacitance of the polymer. Due to the presence of capacitance, piezoelectric polymers have very high output impedance. Thus, to measure the charge/voltage generated due to applied forces, an amplifier with very high input impedance (e.g. CMOS input based) is required.

C.1 Charge Amplifier

The independence of amplifier output from the cable capacitances and the minimization of the charge leakage through the stray capacitance around the sensor, make charge amplifier a preferred choice especially when long connecting cables are present. The schematic of the charge amplifier is given in Fig. C.1. The amplifier consists of three stages. The differential charge amplifier in the first stage is followed by differential to single ended amplifier, which is then followed by a second order Sallen–Key low pass filter and a low pass RC filter. In the first stage FET input based OPA627 operational amplifiers are used. These are low noise op-amps with typical input bias current of 2 pA. In the second and third stage TL082 op-amp is used. The gain of second stage is 5 and that of third stage is 4. Overall gain of the amplifier is set by value of feedback capacitances in the first stage with respect to the static polymer capacitance. The circuit has been designed to have a frequency range of 2 Hz–200 kHz.

C.2 Voltage Amplifier

The voltage amplifiers are preferred if the ambient temperature variation is high, since they exhibit less temperature dependence and hence useful for measuring the piezoelectric polymer film response. This is due to the fact that piezoelectric polymer's voltage sensitivity (g-constant) variation over temperature is smaller than the charge sensitivity (d-constant) variation. The schematic of voltage amplifier is

R.S. Dahiya, M. Valle, *Robotic Tactile Sensing*,
DOI 10.1007/978-94-007-0579-1,

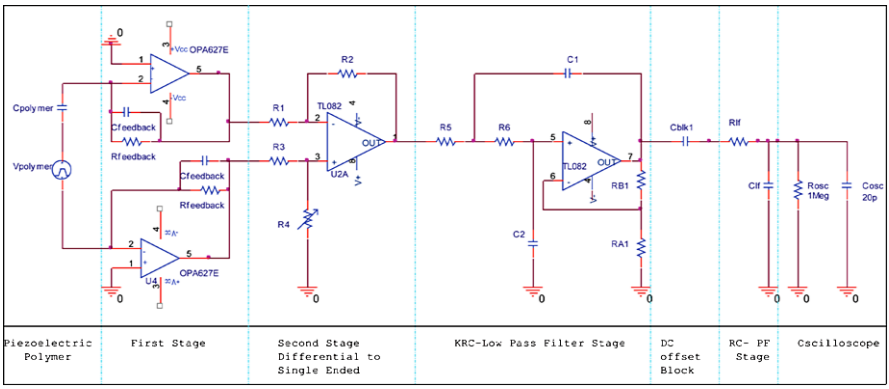

Fig. C.1 Schematic of three stage charge amplifier

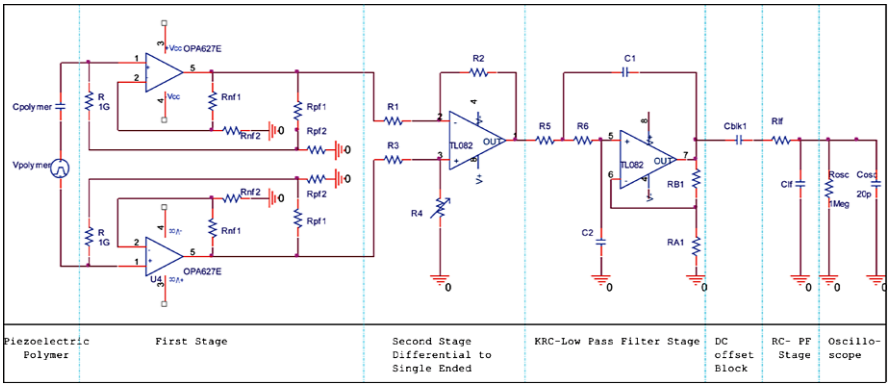

Fig. C.2 Schematic of three stage voltage amplifier

shown in Fig. C.2. It also comprises of three stages. Except first stage, remaining two stages are same as that of the charge amplifier. Since the source capacitance in the present case is ∼1 pF, the low frequency response can be brought down to ∼5 Hz by keeping the circuit loading effect as minimum as possible. This was obtained by providing a resistive load of 1 GΩ in the first stage. This value appears 3–5 times higher to the polymer, due to the bootstrapping technique adopted by using positive feedback. Use of resistors with resistances more than 1 GΩ is not recommended as higher values are prone to noise due to humidity, dust, temperature variation etc. With the adoption of this technique the voltage amplifier has a gain of 46 dB in the frequency range of 8 Hz–200 kHz.

Index

R.S. Dahiya, M. Valle, *Robotic Tactile Sensing*,
DOI 10.1007/978-94-007-0579-1,